DIN 67SD4300
20 JUNE 1967

N68-19376

ACCELERATION HODOGRAPH ANALYSIS TECHNIQUES FOR POWERED ORBITAL TRAJECTORIES

(FINAL REPORT — PHASE 3)

PREPARED
BY
SAMUEL P. ALTMAN

UNDER
CONTRACT NAS8-20360
CONTROL NO. DCN1-6-75-00050 (1F)

GENERAL ELECTRIC
SPACECRAFT DEPARTMENT
A Department of the Missile and Space Division
Valley Forge Space Technology Center
P. O. Box 8555 • Philadelphia, Penna. 19101

FOREWORD

This report was prepared by the Spacecraft Department of the General Electric Missile and Space Division under Contract NAS8-20360 on "Derivation of Analytical Methods Which Give Rapid Convergence to the Solution of Optimized Trajectories" for the George C. Marshall Space Flight Center of the National Aeronautics and Space Administration. The work was administered under technical direction of Resources Management Office, Aero-Astrodynamics Laboratory, George C. Marshall Space Flight Center with D. Chandler acting as project manager.

During the course of the study program, interim work reports were issued which comprise the sections of this Phase Final Report. The sections corresponding to the Phase Work Reports are as follows:

Section	Phase Work Report
1	III A-1
2	III A-2
3	III B-1
4	III B-2
5	III B-3
6	III B-4
7	III B-5
8	III B-6

TABLE OF CONTENTS

TABLE OF CONTENTS (Cont'd)

LIST OF ILLUSTRATIONS

LIST OF ILLUSTRATIONS (Cont'd)

LIST OF ILLUSTRATIONS (Cont'd)

LIST OF TABLES

SECTION 1

FORMAL PRESENTATION OF THE HODOGRAPHIC EQUATIONS OF MOTION

AUTHORS: SAMUEL P. ALTMAN
AND
CARLOS R. CAVOTI

SECTION 1

FORMAL PRESENTATION OF THE HODOGRAPHIC EQUATIONS OF MOTION

The primary objective of the Phase III study is development of the synthesis and analysis techniques for powered orbital trajectories in acceleration vector space. Phase IIIB is concerned directly with this conceptual approach to the trajectory formulation and computational procedures. As discussed in Section 3 (see Table 3-2), the analysis procedures will employ a space variable (i.e., the true anomaly $\emptyset$) as the independent variable rather than time t. That is, a formal treatment in acceleration vector space together with the trajectory loci in time and mass state spaces, will be developed. However, the hodographic equations of motion (see Table 3-1, Section 3) with time as the independent variable, define the complete dynamic state of the spacecraft. Consequently, this latter set of equations may be used for trajectory synthesis and analysis. Work Phase IIIA is directed to this hodographic formulation with time as the independent variable.

This formulation can be extremely useful in the following ways:

a. As a complete demonstration of the development of the hodographic equations of motion in accordance with one formal procedure of classical mechanics

b. As a parametric formulation of the trajectory dynamics problem, to provide an intermediate set of equations which might assist relative appraisal of the conventional and vector space formulations

c. As an alternative formulation for trajectory optimization and guidance theory development, which lends itself immediately to the use of conventional optimization and control techniques.

Aside from the formal demonstration noted in (a) above, the original derivations (Reference 1) of the equations of motion are also valid and provide the same results (upon correlation of notation conventions). The parametric nature of the hodographic formulation (noted in b above) will be quite valuable in demonstrating the advantages which may be realized from a parametric analysis of trajectory dynamics. Within the last few years, considerable interest and research activity in this direction has increased (Reference 2).

It should be noted that this Phase IIIA formulation with time as independent variable does not utilize the transformation functions between the solution trajectory in the vector space of analysis, and the corresponding state trajectories in other vector (or state) spaces of engineering interest and utility. That is, the time-dependent hodographic formulation would utilize formal integration for solution (i.e., soluble by quadratures). In essence, the transforms are the invariant forms of the operations carried out by formal integration. In later application work, it may prove useful to compare the relative merits of the time-dependent versus space-variable-dependent formulations, in terms of computation programming and solution (e.g., total running time, solution errors, convergence, etc.).

Finally, this IIIA formulation may be used directly for trajectory optimization by the use of the variational calculus. Also, the conventional control techniques (such as differential correction) presently in practice may be easily applied to the formulation, with the least conceptual difficulty by analysts trained in conventional guidance methods. At this point, it is noted that the IIIB formulation will be directly suitable for application of the geodesics theory of curves and surfaces, of the differential geometry (Reference 3) for trajectory optimization. Consequently, the use of the variational calculus with the IIIA formulation can then be correlated and compared with the use of the geodesics theory with the IIIB formulation. Aside from the resulting knowledge of the tradeoff advantages and mechanization requirements for each procedure in guidance computation, further knowledge and insight into the yet unsolved problems of trajectory optimization might then become available.

1.1 NOTATION CONVENTIONS

A uniform set of notation conventions will be employed in this and subsequent sections. As noted in Section 4, these conventions are consistent with the conventions of the complex variable theory. In this way, correlation between IIIA and IIIB formulations and analysis techniques should be facilitated. The conventions of aerodynamics, celestial mechanics, guidance and control technologies will all be of interest and use in technical applications of this theory. Consequently, best judgement and agreement of the research team members has been employed to provide a definitive set of notation conventions for this vector space theory of Newtonian mechanics. The notation conventions represent, necessarily, a hybrid of the cherished conventions of each older field of specialization.

- The definitive nomenclature is compiled in Table 1-1. The related graphical descriptions of the defined terms are shown in Figures 1-1 through 1-5. As noted in Figures 1-1 and 1-2, four coordinate systems are available:

  a. Cartesian Inertial System ($\mathbf{X}$, $\mathbf{Y}$, Z)

  b. Cartesian Plane-Imbedded System (X, Y, Z)

  c. Rotating Cartesian System (x, y, z)

  d. Polar System (r, ν)

1.2 NONPARAMETRIC DYNAMICS FOR A BALLISTIC TRAJECTORY

The nonparametric dynamics for a ballistic trajectory are reviewed here, for motion in two-dimensional space only. That is, all motion considered here lies in an inertially-fixed orbital plane, solely for convenience of analysis and development in this work phase. Extension to three-dimensional space can later be accomplished as required.

For each unit of mass, the equations of motion due to an inverse-square attracting force center are

$$\ddot{X} = -\left(\frac{\mu}{r^3}\right)X \qquad (1\text{-}1)$$

$$\ddot{Y} = -\left(\frac{\mu}{r^3}\right)Y \quad . \qquad (1\text{-}2)$$

The momentum and energy integrals respectively are:

$$X\dot{Y} - Y\dot{X} = \text{constant} = \ell/m \qquad (1\text{-}3)$$

$$V^2 - \frac{2\mu}{r} = \text{constant} = h/m \quad . \qquad (1\text{-}4A)$$

Table 1-1. Definitive Nomenclature

A	scalar magnitude of the acceleration vector $\overline{A}$
a	semimajor axis of a conic
b	semiminor axis of a conic
C	scalar magnitude of the velocity parameter vector $\overline{C}$
¢	real component of the complex variable q (= ¢ + id) which represents the acceleration
d	imaginary component of the complex variable q (= ¢ + id) which represents the acceleration
E	total point-mass potential and kinetic energy of orbital motion
e	eccentricity of a conic
h	constant of the energy integral, defined as = (2E/m)
h'	constant of the energy integral, defined as = (E/m) = (h/2)
i	unit vector of the imaginary component of a complex variable (i.e., of z, w or q)
J	first coupling constant of the spherical harmonic expansion for the gravitational potential of the celestial body, described as an oblate spheroid.
$\overline{\iota}_{(\,)}$	unit vector of the ( )-component vector
k^2	gravitational constant of the celestial body
ℓ	scalar magnitude of the angular momentum vector $\overline{\ell}$ of point-mass motion
m	mass of the orbital spacecraft
n	mean angular velocity of the spacecraft in orbit
P, P', P''	corresponding points in position, velocity (or CV-) and acceleration vector spaces respectively
q	the complex variable which represents the acceleration (= ¢ + id)
R	scalar magnitude of the velocity parameter vector $\overline{R}$
r	scalar magnitude of the radius of position vector $\overline{r}$ (= z)
s	path length along a trajectory or locus curve
T	scalar magnitude of the thrust vector $\overline{T}$
t	time
u	real component of the complex variable w (=u + iv) which represents the velocity
V	scalar magnitude of the velocity vector $\overline{V}$
V_e	velocity of exhaust gases of combustion for propulsion
v	imaginary component of the complex variable w (= u + iv) which represents the velocity
v'	slope of a trajectory in velocity vector space
w	the complex variable which represents the velocity (= u + iv)
Ξ, Υ, Z	the Cartesian inertial system of coordinates with origin identical with the force center, and Ξ Υ lying in the equatorial plane, of the attracting celestial body
X, Y, Z	the Cartesian system of coordinates fixed in the instantaneous (or given) orbital plane, with X-axis identical with the line-of-nodes in the $\Xi\Upsilon$-plane
x, y, z	the Cartesian system of coordinates fixed in the instantaneous (or given) orbit of the trajectory, with X-axis identical with the apsidal line

y'	slope of a trajectory in position vector space
z	the complex variable which represents the position ($= x + iy$)
γ	direction angle referring the thrust vector $\bar{T}$ to the $\bar{J}_{\mathcal{V}}$-vector direction (i.e., to the local horizon)
$\Delta_{(\,)}$	determinant of ( )
δ	second invariant of the two-fixed-center problem
ϵ	rate of mass loss due to propulsion ($= -\dot{m}$)
ζ	angle of intersection between two orbital planes
η	angular difference between the apsidal lines of two orbits at perigee passage
θ	angle between the velocity vector and the local horizon in position vector space (i.e., the flight path angle)
θ'	angle between the tangent to the orbital acceleration hodograph and the perpendicular to the acceleration polar, in acceleration vector space
ι	the incidence angle between the instantaneous (or given) orbital plane and the equatorial plane of the attracting celestial body
κ	curvature of the moving trihedron
λ	torsion of the moving trihedron
μ	gravitational constant of the celestial body ($= k^2$)
ν	direction angle referring the radius vector $\bar{r}$ to the line-of-nodes (or X-axis)
ρ	polar of a trajectory
σ	angular difference between two radius vectors (i.e., the central angle)
ϕ	true anomaly of the vehicle in the instantaneous (or given) orbit
Ψ	direction angle of the apsidal line at perigee passage for an instantaneous (or given) orbit, referred to the line-of-nodes
Ω	direction angle of the line-of-nodes for an instantaneous (or given) orbital plane, referred to the X-axis

SUBSCRIPTS

b	ballistic
C, R	in the $\bar{C}$- or $\bar{R}$-direction, respectively
e	in the $\bar{e}$-direction (i.e., parallel to apsidal line)
f	final
i	initial
p	powered
q, w, z	in the acceleration, velocity or position vector space, respectively
r	radial
T	in the $\bar{T}$-direction
t	at time t
x, y, z	in the x, y or z coordinate, respectively
κ	in the direction of the center-of-curvature
ν	in the normal coordinate (i.e., perpendicular to the radius vector, in the orbital plane)

(Ξ, Υ, Ζ)	CARTESIAN INERTIAL SYSTEM
(X, Y, Z)	CARTESIAN PLANE-IMBEDDED SYSTEM
(x, y, z)	ROTATING CARTESIAN SYSTEM

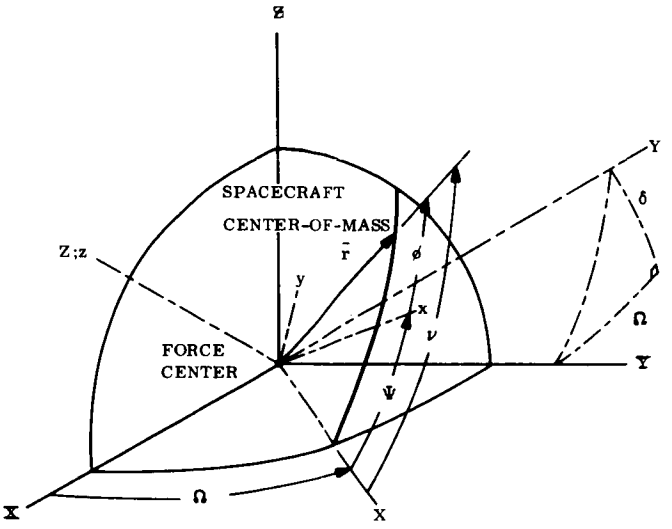

Figure 1-1. Coordinate Systems for Orbit Orientation in Three-Dimensional Space

(X, Y)	CARTESIAN PLANE-IMBEDDED SYSTEM
(x, y)	ROTATING CARTESIAN SYSTEM
(r, ν)	POLAR SYSTEM

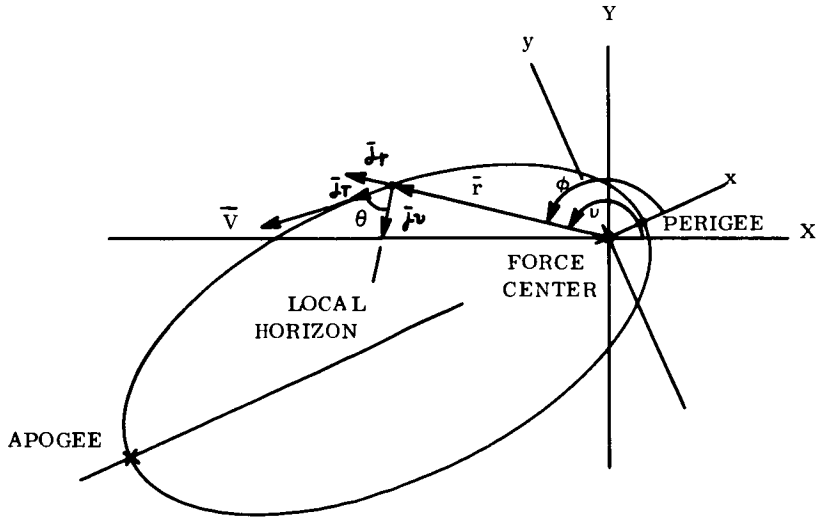

Figure 1-2. Coordinate Systems for Two-Dimensional Space Only

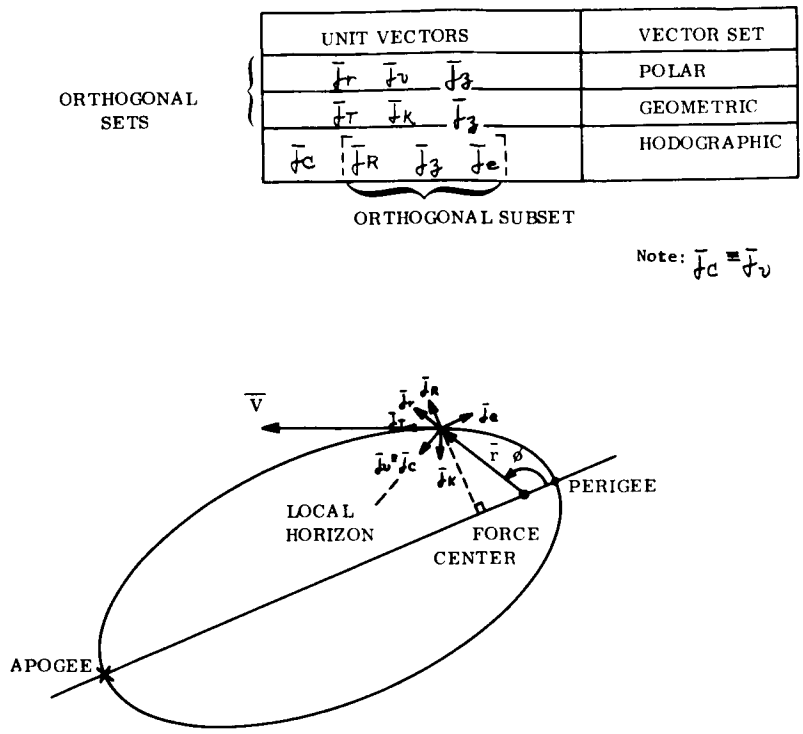

Figure 1-3. Alternative Vector Sets in Two-Dimensional Space Only

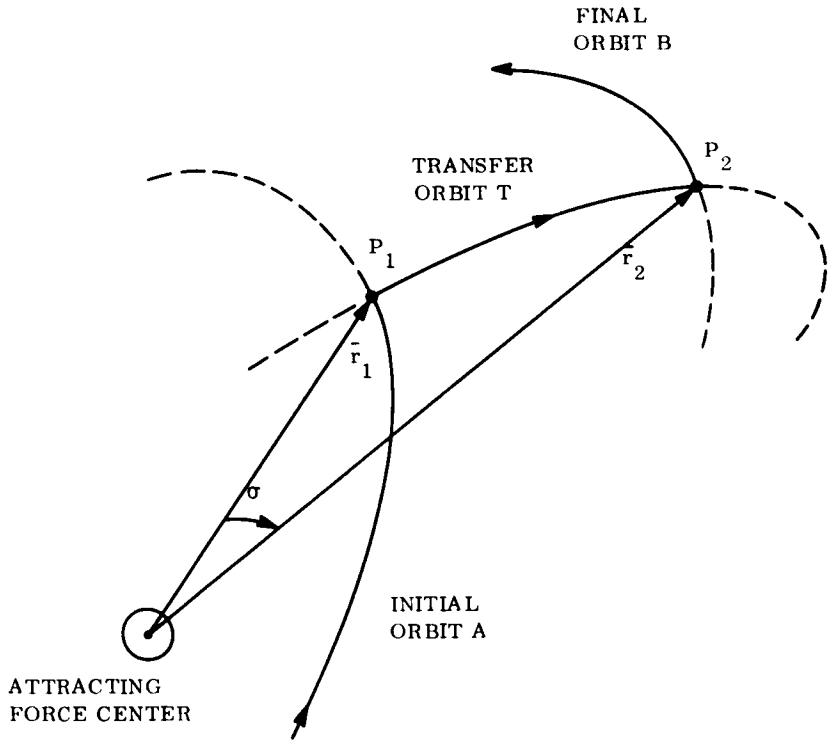

Figure 1-4. Schematic Illustration of Orbital Transfer in Three-Dimensional Space

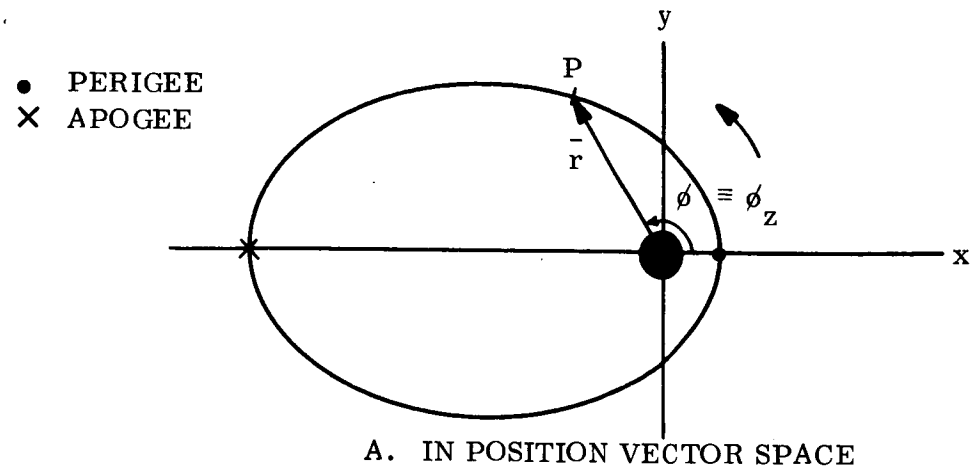

A. IN POSITION VECTOR SPACE

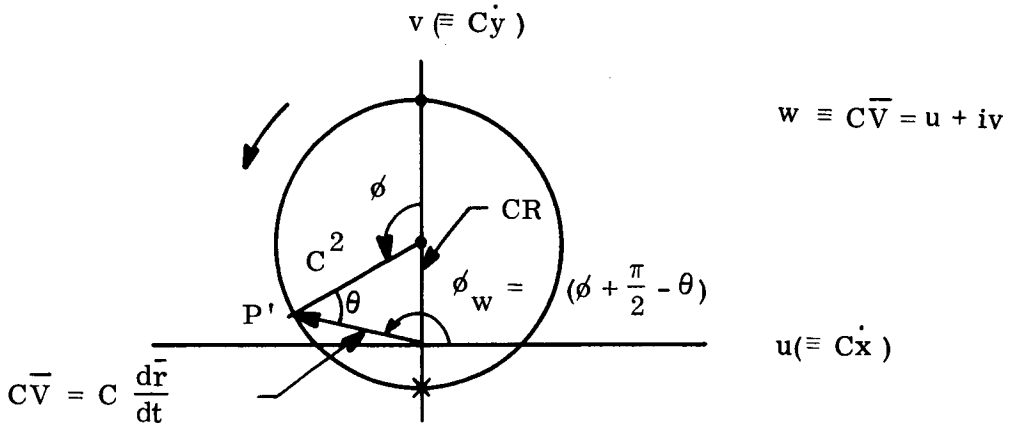

B. IN VELOCITY (OR POTENTIAL) VECTOR SPACE

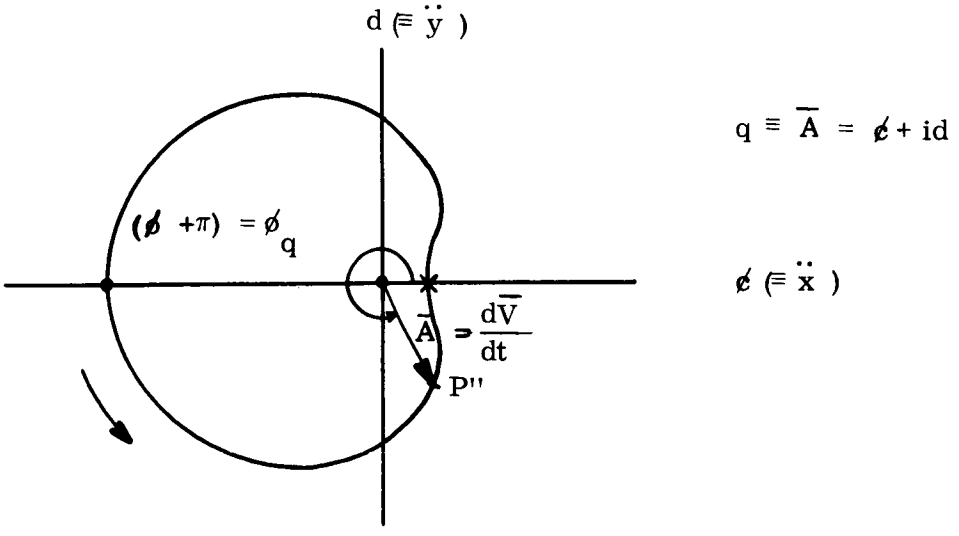

C. IN ACCELERATION VECTOR SPACE

Figure 1-5. Vector Space Maps of an Orbit

Since

$$X = r \cos \upsilon \tag{1-5}$$

$$Y = r \sin \upsilon \quad , \tag{1-6}$$

then

$$r^2 \dot{\upsilon} = \text{constant} = \ell/m \quad . \tag{1-7A}$$

In polar coordinates, the velocity vector is defined by

$$\bar{V} = (V_r)\bar{\jmath}_r + (V_\upsilon)\bar{\jmath}_\upsilon \tag{1-8A}$$

where

$$V_r = \dot{r} \tag{1-9}$$

$$V_\upsilon = r\dot{\upsilon} \quad . \tag{1-10}$$

In polar coordinates, the acceleration vector is defined by

$$\bar{A} = (A_r)\bar{\jmath}_r + (A_\upsilon)\bar{\jmath}_\upsilon \tag{1-11}$$

where

$$A_r = \ddot{r} - r\dot{\upsilon}^2 = \dot{V}_r - \frac{V_\upsilon^2}{r} \tag{1-12}$$

$$A_\upsilon = \frac{1}{r}\frac{d}{dt}(r^2\dot{\upsilon}) = 2\dot{r}\dot{\upsilon} + r\ddot{\upsilon} \tag{1-13A}$$

or

$$A_\upsilon = \dot{V}_\upsilon + \frac{V_r V_\upsilon}{r} \quad . \tag{1-13B}$$

1.3 VELOCITY HODOGRAPH

The velocity hodograph may be defined either in the Cartesian coordinate systems (X, Y or x, y) or the polar coordinate system (r, ν). The former is called the classical velocity hodograph, whereas the latter is called the special (or polar) velocity hodograph. In the polar coordinate system,

$$V_r^2 + V_\nu^2 - \frac{2\mu}{r} = h/m \tag{1-4B}$$

$$rV_\nu = \ell/m \tag{1-7B}$$

so that

$$V_r^2 + (V_\nu - C)^2 = (h/m) + C^2 \tag{1-4C}$$

or

$$V_r^2 + (V_\nu - C)^2 = R^2 \tag{1-4D}$$

where

$$C = \frac{\mu}{(\ell/m)} = \frac{\mu m}{\ell} \tag{1-14}$$

$$R = \sqrt{(h/m) + C^2} \quad . \tag{1-15}$$

In terms of the conic parameters for the orbital trajectory in position vector space,

$$e = \sqrt{1 + \frac{(\ell/m)^2 (h/m)}{\mu^2}} = \frac{R}{C} \tag{1-16}$$

and

$$r = \frac{(\frac{\ell}{m})^2/\mu}{1 + e\cos(\nu - \Psi)} = \frac{\mu/C^2}{1 + (\frac{R}{C})\cos\phi} \tag{1-17}$$

so that

$$\cos\phi = \frac{V_\nu - C}{R} \quad . \tag{1-18}$$

Then

$$\boxed{V_r = R\sin\phi} \tag{1-19}$$

$$\boxed{V_\nu = C + R\cos\phi} \quad . \tag{1-20}$$

Note that Equations 1-19 and 1-20 can be deduced directly from Equation 1-4D, recognizing this equation as the algebraic equation of a circle with radius of R, and center fixed at +C on the $\bar{J}_v$-axis, as shown in Figure 1-6. That is, the displacement of the circle center from the $\bar{J}_r$-$\bar{J}_v$ origin is the velocity parameter vector $\bar{C}$ and the radius is the velocity parameter vector $\bar{R}$. As shown in Figure 1-6, the vectors are referred to a rotating coordinate system, so that the correct vector orientation in the vector spaces (both position and velocity) can only be identified by reference to the radius vector in inertial coordinates. This will be demonstrated shortly.

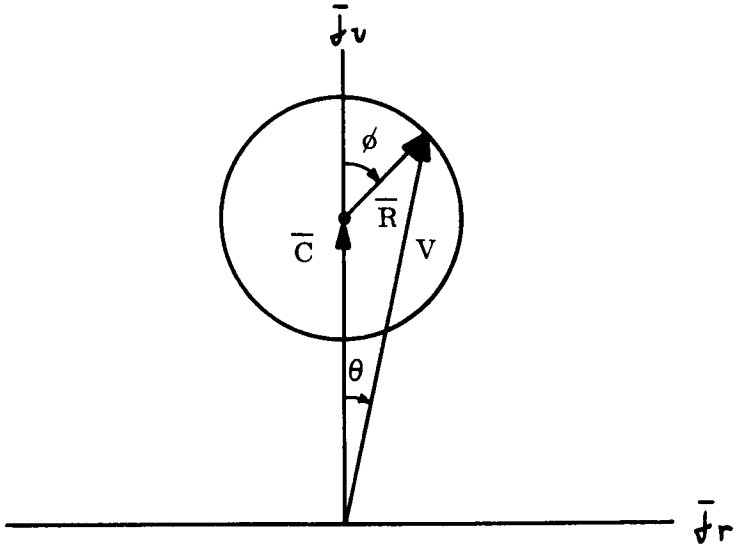

Figure 1-6. Polar Velocity Hodograph

In the Cartesian inertial coordinate system,

$$\bar{V} = (\dot{X})\bar{J}_X + (\dot{Y})\bar{J}_Y \qquad (1\text{-}8B)$$

But

$$\begin{Bmatrix} \bar{J}_r \\ \bar{J}_v \end{Bmatrix} = \begin{bmatrix} \cos v & \sin v \\ -\sin v & \cos v \end{bmatrix} \begin{Bmatrix} \bar{J}_X \\ \bar{J}_Y \end{Bmatrix} \qquad (1\text{-}21)$$

so that

$$\dot{X} = V_r \cos v - V_v \sin v \qquad (1\text{-}22)$$

$$\dot{Y} = V_r \sin v + V_v \cos v \quad . \qquad (1\text{-}23)$$

Consequently,

$$\dot{X} = -R \sin \Psi - C \sin (\phi + \Psi) \qquad (1\text{-}24A)$$

$$\dot{Y} = R \cos \Psi + C \cos (\phi + \Psi) \; . \qquad (1\text{-}25A)$$

Introducing the Cartesian coordinate system (x, y) with unit vectors $\bar{J}_x, \bar{J}_y$ and rotation matrix

$$\begin{Bmatrix} \bar{J}_x \\ \bar{J}_y \end{Bmatrix} = \begin{bmatrix} \cos \Psi & \sin \Psi \\ -\sin \Psi & \cos \Psi \end{bmatrix} \begin{Bmatrix} \bar{J}_X \\ \bar{J}_Y \end{Bmatrix} \qquad (1\text{-}26)$$

we obtain

$$x = X \cos \Psi + Y \sin \Psi \qquad (1\text{-}27)$$

$$y = -X \sin \Psi + Y \cos \Psi \; . \qquad (1\text{-}28)$$

When $\Psi = 0$, then $x = X$, $y = Y$ and consequently

$$\boxed{\dot{x} = -C \sin \phi} \qquad (1\text{-}29)$$

$$\boxed{\dot{y} = R + C \cos \phi} \; . \qquad (1\text{-}30)$$

Since the (x, y) coordinates are inertial in this instance,

$$\bar{V} = (\dot{x})\bar{J}_x + (\dot{y})\bar{J}_y \qquad (1\text{-}31)$$

and

$$\dot{x}^2 + \dot{y}^2 - \frac{2\mu}{r} = h/m \qquad (1\text{-}32A)$$

$$r = \frac{\ell/m}{V_v} = \frac{\ell/m}{C + R \cos \phi} \qquad (1\text{-}33)$$

so that

$$\dot{x}^2 + \dot{y}^2 - 2C^2 - 2R(\dot{y} - R) = h/m \qquad (1\text{-}32B)$$

yielding

$$\dot{x}^2 + (\dot{y} - R)^2 = C^2 \,. \qquad (1\text{-}32C)$$

The inertial (or classical) velocity hodograph is shown in Figure 1-7, for $\Psi = 0$.

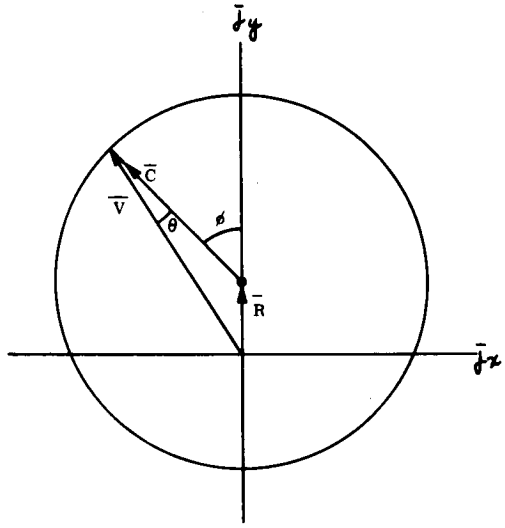

Figure 1-7. Inertial Velocity Hodograph

The vectorial inter-relation between the polar and inertial velocity hodographs is illustrated in the schematic diagram of Figure 1-8. It is obvious that the velocity parameter vector $\bar{R}$ is fixed in inertial space, while the velocity parameter vector $\bar{C}$ rotates with the true anomaly ϕ. Referring to the representation of the vector $\bar{R}$ in the polar velocity hodograph, it is clear that $\bar{R}$ must always remain perpendicular to $\bar{j}_x$ for all points in orbit.

1.4 HODOGRAPHIC EQUATIONS OF MOTION IN ACCELERATION VECTOR SPACE

To obtain the hodographic equations of motion in rotating coordinates, the following definitive equations of the preceding section are used:

$$\bar{V} = (V_r)\bar{j}_r + (V_v)\bar{j}_v$$

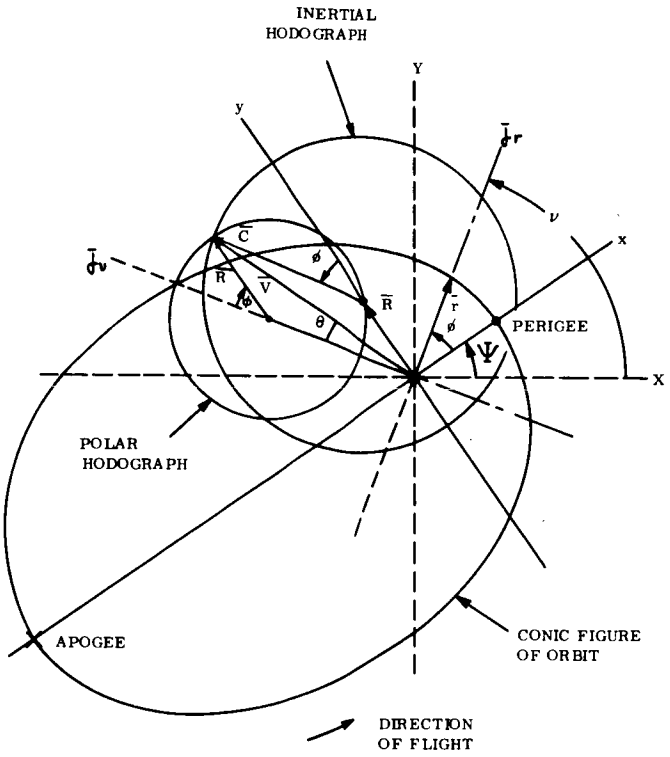

Figure 1-8. Polar and Inertial Velocity Hodographs for an Elliptic Figure of Orbital Trajectory

where

$$V_r = \dot{r}$$

$$V_v = r\dot{v}$$

and the rotation matrix

$$\begin{Bmatrix} \bar{\jmath}_r \\ \bar{\jmath}_v \end{Bmatrix} = \begin{bmatrix} \cos v & \sin v \\ -\sin v & \cos v \end{bmatrix} \begin{Bmatrix} \bar{\jmath}_X \\ \bar{\jmath}_Y \end{Bmatrix}$$

Now

$$\bar{A} = \frac{d\bar{\bar{V}}}{dt} = (\dot{V}_r)\bar{\jmath}_r + (\dot{V}_v)\bar{\jmath}_v + (V_r)\dot{\bar{\jmath}}_r + (V_v)\dot{\bar{\jmath}}_v \quad (1\text{-}34A)$$

and

$$\dot{\bar{\jmath}}_r = \frac{d\bar{\jmath}_r}{dt} = \left(\frac{d\bar{\jmath}_r}{d\upsilon}\right)\dot{\upsilon} = \left(\bar{\jmath}_\upsilon\right)\dot{\upsilon} \qquad (1\text{-}35)$$

$$\dot{\bar{\jmath}}_\upsilon = \frac{d\bar{\jmath}_\upsilon}{dt} = \left(\frac{d\bar{\jmath}_\upsilon}{d\upsilon}\right)\dot{\upsilon} = \left(-\bar{\jmath}_r\right)\dot{\upsilon} \qquad (1\text{-}36)$$

so that

$$\bar{A} = \overbrace{\left(\dot{V}_r - V_\upsilon\dot{\upsilon}\right)}^{A_r}\bar{\jmath}_r + \overbrace{\left(\dot{V}_\upsilon + V_r\dot{\upsilon}\right)}^{A_\upsilon}\bar{\jmath}_\upsilon \qquad (1\text{-}34B)$$

or

$$A_r = \dot{V}_r - \frac{V_\upsilon^2}{r} \qquad (1\text{-}37A;\ \text{also } 1\text{-}12)$$

$$A_\upsilon = \dot{V}_\upsilon + \frac{V_r V_\upsilon}{r} \quad . \qquad (1\text{-}38A;\ \text{also } 1\text{-}13B)$$

Since

$$V_r = R\sin\phi$$

$$V_\upsilon = C + R\cos\phi$$

then

$$\dot{V}_r = \dot{R}\sin\phi + R\cos\phi\,(\dot{\phi}) \qquad (1\text{-}39)$$

$$\dot{V}_\upsilon = \dot{C} + \dot{R}\cos\phi - R\sin\phi\,(\dot{\phi}) \quad . \qquad (1\text{-}40)$$

Consequently,

$$A_r = \dot{R}\sin\phi + R\cos\phi\,(\dot{\phi}) - (C + R\cos\phi)\dot{\upsilon} \qquad (1\text{-}37B)$$

or

$$\boxed{A_r = \dot{R}\sin\phi - R\dot{\Psi}\cos\phi - C\dot{\upsilon}} \qquad (1\text{-}37C)$$

and

$$A_v = \dot{C} + \dot{R}\cos\phi - R\sin\phi\,(\dot{\phi}) + R\sin\phi\,(-\dot{v}) \qquad (1\text{-}38B)$$

or

$$\boxed{A_v = \dot{C} + \dot{R}\cos\phi + R\dot{\Psi}\sin\phi} \quad . \qquad (1\text{-}38C)$$

In the preceding section, it was shown (see Equations 1-19 and 1-20 or Figures 1-6 and 1-7) that the hodographic figure of the orbital trajectory is a circle either in inertial or polar velocity coordinates. By use of Equations 1-37C and 1-38C, the hodographic figure of any trajectory may be obtained in polar acceleration coordinates. From Equations 1-37C and 1-38C, respectively,

$$A_r + C\dot{v} = \dot{R}\sin\phi - R\dot{\Psi}\cos\phi \qquad (1\text{-}39)$$

$$A_v - \dot{C} = \dot{R}\cos\phi + R\dot{\Psi}\sin\phi \qquad (1\text{-}40)$$

or

$$(A_r + C\dot{v})^2 = \dot{R}^2\sin^2\phi - 2R\dot{R}\dot{\Psi}\sin\phi\cos\phi + (R\dot{\Psi})^2\cos^2\phi \qquad (1\text{-}41)$$

$$(A_v - \dot{C})^2 = \dot{R}^2\cos^2\phi + 2R\dot{R}\dot{\Psi}\sin\phi\cos\phi + (R\dot{\Psi})^2\sin^2\phi \qquad (1\text{-}42)$$

so that

$$(A_r + C\dot{v})^2 + (A_v - \dot{C})^2 = \dot{R}^2 + (R\dot{\Psi})^2 \qquad (1\text{-}43)$$

defines the acceleration hodograph figure. If the spacecraft is subject only to the gravitational force field, then $\dot{C} = \dot{R} = \dot{\Psi} = 0$ so that $A_v = 0$ and

$$A_r = -C\dot{\phi} \quad . \qquad (1\text{-}44)$$

Consequently, the acceleration hodograph of an orbital trajectory in polar acceleration coordinates is a straight line segment on the negative A_r-axis, with periodic motion along it in accordance with

$$A_r = -\frac{C^2}{\mu}(C + R\cos\phi)^2 \quad . \tag{1-45}$$

To obtain the hodographic equations of motion in Cartesian coordinates, let

$$\bar{V} = (\alpha)\bar{I}_x + (\beta)\bar{I}_y \tag{1-46}$$

where α and β are the velocity components referred to the Cartesian rotating system (x, y). Now

$$\bar{A} = \frac{d\bar{V}}{dt} = (\dot{\alpha})\bar{I}_x + (\dot{\beta})\bar{I}_y + (\alpha)\dot{\bar{I}}_x + (\beta)\dot{\bar{I}}_y \tag{1-34C}$$

and

$$\dot{\bar{I}}_x = \frac{d\bar{I}_x}{dt} = \left(\frac{d\bar{I}_x}{d\Psi}\right)\dot{\Psi} \tag{1-47A}$$

$$\dot{\bar{I}}_y = \frac{d\bar{I}_y}{dt} = \left(\frac{d\bar{I}_y}{d\Psi}\right)\dot{\Psi} \quad . \tag{1-48A}$$

Referring to Equation 1-26, we see that

$$\frac{d\bar{I}_x}{d\Psi} = (-\sin\Psi)\bar{I}_X + (\cos\Psi)\bar{I}_Y \tag{1-49}$$

$$\frac{d\bar{I}_y}{d\Psi} = (-\cos\Psi)\bar{I}_X + (-\sin\Psi)\bar{I}_Y \tag{1-50}$$

so that

$$\dot{\bar{I}}_x = (\bar{I}_y)\dot{\Psi} \tag{1-47B}$$

$$\dot{\bar{I}}_y = (-\bar{I}_x)\dot{\Psi} \quad . \tag{1-48B}$$

Also,

$$\alpha = \dot{x} - (\dot{\Psi})y = -C\sin\phi \tag{1-51}$$

$$\beta = \dot{y} + (\dot{\Psi})x = R + C\cos\phi \tag{1-52}$$

so that

$$\dot{\alpha} = \ddot{x} - (\ddot{\Psi})y - (\dot{\Psi})\dot{y} = -\dot{C}\sin\phi - (C\cos\phi)\dot{\phi} \tag{1-53}$$

$$\dot{\beta} = \ddot{y} + (\ddot{\Psi})x + (\dot{\Psi})\dot{x} = \dot{R} + \dot{C}\cos\phi - (C\sin\phi)\dot{\phi} \ . \tag{1-54}$$

Then

$$\bar{A} = [-\dot{C}\sin\phi - (C\cos\phi)\dot{\phi}]\bar{I}_x + [\dot{R} + \dot{C}\cos\phi - (C\sin\phi)\dot{\phi}]\bar{I}_y +$$

$$+[(-C\sin\phi)\dot{\Psi}]\bar{I}_y + [-(R + C\cos\phi)\dot{\Psi}]\bar{I}_x \tag{1-34D}$$

or

$$\bar{A} = [-\dot{C}\sin\phi - R\dot{\Psi} - (C\cos\phi)(\dot{\phi} + \dot{\Psi})]\bar{I}_x +$$

$$+[\dot{R} + \dot{C}\cos\phi - (C\sin\phi)(\dot{\phi} + \dot{\Psi})]\bar{I}_y \tag{1-34E}$$

or finally,

$$\bar{A} = [-\dot{C}\sin\phi - R\dot{\Psi} - Ci\cos\phi]\bar{I}_x +$$

$$+[\dot{C}\cos\phi + \dot{R} - Ci\sin\phi]\bar{I}_y \tag{1-34F}$$

so that

$$\boxed{A_x = -\dot{C}\sin\phi - R\dot{\Psi} - Ci\cos\phi} \tag{1-55}$$

$$\boxed{A_y = \dot{C}\cos\phi + \dot{R} - Ci\sin\phi} \tag{1-56}$$

The acceleration components (A_x, A_y) in the Cartesian inertial coordinates may be obtained by use of the rotation matrix of Equation 1-26, with Equations 1-55 and 1-56.

From Equations 1-55 and 1-56 respectively,

$$A_x + R\dot{\Psi} = -\dot{C}\sin\phi - C\dot{v}\cos\phi \tag{1-57}$$

$$A_y - \dot{R} = \dot{C}\cos\phi - C\dot{v}\sin\phi \tag{1-58}$$

or

$$(A_x + R\dot{\Psi})^2 = \dot{C}^2\sin^2\phi + 2C\dot{C}\dot{v}\sin\phi\cos\phi + (-C\dot{v})^2\cos^2\phi \tag{1-59}$$

$$(A_y - \dot{R})^2 = \dot{C}^2\cos^2\phi - 2C\dot{C}\dot{v}\sin\phi\cos\phi + (-C\dot{v})^2\sin^2\phi \tag{1-60}$$

so that

$$(A_x + R\dot{\Psi})^2 + (A_y - \dot{R})^2 = \dot{C}^2 + (-C\dot{v})^2 \tag{1-61}$$

defines the acceleration hodograph figure. If the spacecraft is subject only to the gravitational force field, then $\dot{C} = \dot{R} = \dot{\Psi} = 0$ so that

$$A_x^2 + A_y^2 = A^2 = (C\dot{\phi})^2 \tag{1-62}$$

or

$$A = C\dot{\phi} \tag{1-63}$$

and

$$A = \frac{C^2}{p}(C + R\cos\phi)^2 \quad . \tag{1-64}$$

Noting that the polar equation for the geometric figure of Pascal's limaçon is

$$\rho = k_1 + k_2\cos\phi \tag{1-65}$$

the acceleration hodograph of an orbital trajectory in inertial acceleration coordinates is a geometric figure (as shown in Figure 1-5C) which resembles Pascal's limaçon, except that the acceleration polar is the square of the limaçon polar (Reference 4).

Brief consideration of the hodograph equations of motion, Equations 1-37C, 1-38C or 1-55, 1-56, from the physical viewpoint reveals that only two degrees of freedom occur here, whether expressed in terms of thrust control variables (T, γ) or in terms of the hodographic variables (C, R, Ψ). That is, only two of the three hodographic variables can be free, with the third variable a dependent function of the other two. This basic equation will be derived here, for $\dot{\Psi}$ as a function of $\dot{C}$ and $\dot{R}$. From Equations 1-7B and 1-14,

$$C = \frac{\mu}{r V_v} \tag{1-66}$$

so that

$$r = \frac{\mu}{C V_v} = \mu \left(C^2 + CR\cos\phi \right)^{-1} . \tag{1-67}$$

Then

$$\dot{r} = -\mu \left(C^2 + CR\cos\phi \right)^{-2} \left(2C\dot{C} + \dot{C}R\cos\phi + C\dot{R}\cos\phi - CR\dot{\phi}\sin\phi \right) \tag{1-68A}$$

or

$$V_r = -\mu \left(CV_v \right)^{-2} \left[\dot{C}\left(2C + R\cos\phi \right) + \dot{R}\left(C\cos\phi \right) - \dot{\phi}\left(CR\sin\phi \right) \right] . \tag{1-68B}$$

But

$$\dot{\phi} = \dot{v} - \dot{\Psi} \tag{1-69}$$

so that

$$V_r \left(CV_v \right)^2 = -\mu \left[\dot{C}\left(2C + R\cos\phi \right) + \dot{R}\left(C\cos\phi \right) - CV_r \left(\dot{v} - \dot{\Psi} \right) \right] . \tag{1-70A}$$

From Equations 1-10 and 1-66,

$$C\dot{v} = \frac{\left(CV_v \right)^2}{\mu} \tag{1-71}$$

so that

$$V_r(CV_v)^2 = V_r(CV_v)^2 - \mu\left[\dot{C}(2C+R\cos\phi)+\dot{R}(C\cos\phi)+\dot{\Psi}(CV_r)\right]. \quad (1\text{-}70B)$$

Then

$$-(CV_r)\dot{\Psi} = \dot{C}(2C+R\cos\phi)+\dot{R}(C\cos\phi), \quad (1\text{-}72A)$$

$$-R\dot{\Psi} = \dot{C}\left(\frac{2C+R\cos\phi}{C\sin\phi}\right)+\dot{R}(\cot\phi) \quad (1\text{-}72B)$$

or

$$\boxed{-\dot{\Psi} = \frac{\dot{C}}{C}\left(\frac{V_v+C}{V_r}\right)+\frac{\dot{R}}{R}\left(\frac{V_v-C}{V_r}\right)}. \quad (1\text{-}72C)$$

1.5 HODOGRAPHIC EQUATIONS OF MOTION IN THE PRESENCE OF A GENERALIZED THRUST

A generalized thrust applied to an orbital spacecraft can be simply expressed by a thrust vector $\overline{T}$ with vector direction defined by the direction angle γ referred to the $\overline{J}_v$-vector direction (i.e., to the local horizon in the orbital plane), as shown in Figure 1-9.

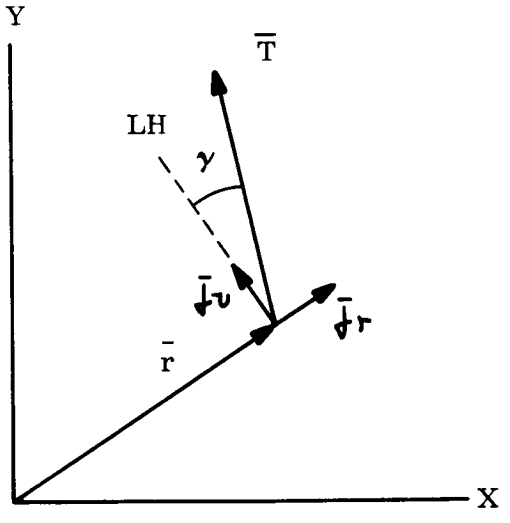

Figure 1-9. Definition of the Thrust Vector, $\overline{T}$

Then, referring to Equations 1-37C and 1-38C respectively,

$$mA_r = m\left(\dot{R}\sin\phi - R\dot{\Psi}\cos\phi - C\dot{v}\right) = -\left(\frac{\mu m}{r^2}\right)+T\sin\tau \quad (1\text{-}73)$$

and

$$m A_v = m\left(\dot{C} + \dot{R}\cos\phi + R\dot{\Psi}\sin\phi\right) = T\cos\gamma \quad . \tag{1-74}$$

Since

$$C\dot{v} = \frac{\mu}{r^2} \quad , \tag{1-75}$$

$$\dot{R}\sin\phi \qquad - R\dot{\Psi}\cos\phi = \frac{T\sin\gamma}{m} \tag{1-76}$$

$$\dot{R}\cos\phi + \dot{C} + R\dot{\Psi}\sin\phi = \frac{T\cos\gamma}{m} \quad . \tag{1-77}$$

Also, from Equation 1-72B,

$$\dot{R}C\cos\phi + \dot{C}(2C + R\cos\phi) + R\dot{\Psi}(C\sin\phi) = 0 \tag{1-78}$$

whereas

$$\dot{v} = \frac{C(C + R\cos\phi)^2}{\mu} \quad . \tag{1-79}$$

Equations 1-76 through 1-79 comprise a set of four equations in four hodographic differentials ($\dot{R}$, $\dot{C}$, $\dot{\Psi}$, $\dot{v}$), which may be presented as functions of the hodographic variables (R, C, ϕ) and thrust control variables (T, γ, m). This system of four equations in four differentials of the hodographic variables is summarized in Table 1-2, and recast in matrix form in Table 1-3, prior to reduction to an equivalent set of equations with only one differential in each.

Table 1-2. System of Hodographic Equations of Motion

	$\dot{R}$	$\dot{C}$	$\dot{\Psi}$	$\dot{\nu}$	"FORCING FUNCTION"
radial	$\dot{R}\sin\phi$		$-R\dot{\Psi}\cos\phi$		$= \frac{T}{m}\sin\gamma$ (1-76)
normal	$\dot{R}\cos\phi$	$+\dot{C}$	$+R\dot{\Psi}\sin\phi$		$= \frac{T}{m}\cos\gamma$ (1-77)
coordinate rotation	$-\dot{R}(C\cos\phi)$	$-\dot{C}(2C+R\cos\phi)$	$-R\dot{\Psi}(C\sin\phi)$		$= 0$ (1-78)
anomaly rotation				$\dot{\nu}$	$= \frac{C(C+R\cos\phi)^2}{\mu}$ (1-79)

Table 1-3. Matrix Form of the System of Hodographic Equations

$$\begin{bmatrix} \sin\phi & 0 & -R\cos\phi & 0 \\ \cos\phi & 1 & +R\sin\phi & 0 \\ -C\cos\phi & -(2C+R\cos\phi) & -CR\sin\phi & 0 \\ 0 & 0 & 0 & 1 \end{bmatrix} \begin{bmatrix} \dot{R} \\ \dot{C} \\ \dot{\Psi} \\ \dot{v} \end{bmatrix} = \begin{bmatrix} \left(\frac{T}{m}\right)\sin\gamma \\ \left(\frac{T}{m}\right)\cos\gamma \\ 0 \\ \frac{C(C+R\cos\phi)^2}{\mu} \end{bmatrix} \tag{1-80}$$

In order to solve for the differentials, the determinants of the system matrix in Table 1-3 . will be used. The determinant of the coefficient matrix is

$$\Delta = \begin{bmatrix} \sin\phi & 0 & -R\cos\phi & 0 \\ \cos\phi & 1 & +R\sin\phi & 0 \\ -C\cos\phi & -(2C+R\cos\phi) & -CR\sin\phi & 0 \\ 0 & 0 & 0 & 1 \end{bmatrix} \tag{1-81A}$$

so that

$$\Delta = \sin\phi\left[-CR\sin\phi + R\sin\phi(2C+R\cos\phi)\right] - R\cos\phi\left[-\cos\phi(2C+R\cos\phi) + C\cos\phi\right] \tag{1-81B}$$

or

$$\Delta = R(C+R\cos\phi) = RV_v \quad . \tag{1-81C}$$

For solution of $\dot{R}$,

$$\Delta_{\dot{R}} = \begin{bmatrix} \frac{T\sin\tau}{m} & 0 & -R\cos\phi & 0 \\ \frac{T\cos\tau}{m} & 1 & +R\sin\phi & 0 \\ 0 & -(2C+R\cos\phi) & -CR\sin\phi & 0 \\ \frac{C(C+R\cos\phi)^2}{\mu} & 0 & 0 & 1 \end{bmatrix} \tag{1-82A}$$

so that

$$\Delta_{\dot{R}} = \frac{T\sin\gamma}{m}\left[-CR\sin\phi + R\sin\phi\,(2C+R\cos\phi)\right] -$$

$$-R\cos\phi\left[-\frac{T\cos\gamma}{m}(2C+R\cos\phi)\right] \qquad (1\text{-}82B)$$

or

$$\Delta_{\dot{R}} = \frac{TR}{m}\left[(C+R\cos\phi)\cos(\phi-\gamma)+C\cos\phi\cos\gamma\right]. \qquad (1\text{-}82C)$$

Consequently,

$$\dot{R} = \frac{\Delta_{\dot{R}}}{\Delta} = \frac{T}{m}\left[\cos(\phi-\gamma)+\left(\frac{C}{C+R\cos\phi}\right)\cos\phi\cos\gamma\right]. \qquad (1\text{-}83)$$

For solution of $\dot{C}$,

$$\Delta_{\dot{C}} = \begin{bmatrix} \sin\phi & \frac{T\sin\gamma}{m} & -R\cos\phi & 0 \\ \cos\phi & \frac{T\cos\gamma}{m} & +R\sin\phi & 0 \\ -C\cos\phi & 0 & -CR\sin\phi & 0 \\ 0 & \frac{C(C+R\cos\phi)^2}{\mu} & 0 & 1 \end{bmatrix} \qquad (1\text{-}84A)$$

so that

$$\Delta_{\dot{C}} = \sin\phi\left[-\frac{T\cos\gamma}{m}(CR\sin\phi)\right] +$$

$$+\frac{T\sin\gamma}{m}\left[-\cos\phi(CR\sin\phi)+R\sin\phi(C\cos\phi)\right] - \qquad (1\text{-}84B)$$

$$-R\cos\phi\left[\frac{T\cos\gamma}{m}(C\cos\phi)\right]$$

or

$$\Delta_{\dot{C}} = -\frac{TCR}{m}(\cos\gamma) \quad . \tag{1-84C}$$

Consequently,

$$\dot{C} = \frac{\Delta_{\dot{C}}}{\Delta} = -\frac{TC}{m(C+R\cos\phi)}\cos\gamma \, . \tag{1-85}$$

For solution of

$$\Delta_{\dot{\Psi}} = \begin{bmatrix} \sin\phi & 0 & \frac{T\sin\gamma}{m} & 0 \\ \cos\phi & 1 & \frac{T\cos\gamma}{m} & 0 \\ -C\cos\phi & -(2C+R\cos\phi) & 0 & 0 \\ 0 & 0 & \frac{C(C+R\cos\phi)^2}{\mu} & 1 \end{bmatrix} \tag{1-86A}$$

so that

$$\Delta_{\dot{\Psi}} = \sin\phi\left[\frac{T\cos\gamma}{m}(2C+R\cos\phi)\right] +$$

$$+\frac{T\sin\gamma}{m}\left[-\cos\phi(2C+R\cos\phi)+C\cos\phi\right] \tag{1-86B}$$

or

$$\Delta_{\dot{\Psi}} = \frac{T}{m}\left[C\sin\phi\cos\gamma + (C+R\cos\phi)\sin(\phi-\gamma)\right] \, . \tag{1-86C}$$

Consequently,

$$\dot{\Psi} = \frac{\Delta_{\dot{\Psi}}}{\Delta} = \frac{T}{mR}\left[\frac{C}{C+R\cos\phi}\sin\phi\cos\gamma + \sin(\phi-\gamma)\right] \, . \tag{1-87}$$

The terms (ϵV_e) represents the thrust force due to propulsion, in the vector direction of $\overline{T}$, so that

$$T = -\epsilon V_e \quad . \tag{1-88}$$

The complete set of six hodographic equations of motion in six variables (R, C, ν, Ψ, ϕ, m) is summarized in Table 1-4. The equivalent set of five equations in five variables (R, C, ν, ϕ, m) is summarized in Table 1-5.

1.6 REDUCTION OF THE HODOGRAPHIC EQUATIONS IN THE PRESENCE OF IMPULSIVE THRUST

Impulsive thrust is an analytic idealization of an applied thrust, such that the time of duration is instantaneous. Since such thrust is active only at one point in space, the necessary result is an instantaneous change in the velocity vector scalar and direction only. This idealization is invaluable in establishing ideal (although physically unrealizable) design limits, and as a simpler feasibility analysis technique in preliminary trajectory design. In the presence of impulsive thrust, the hodographic equations reduce to provide

$$\frac{dR}{d(Lg\, m)} = -V_e \left[\cos(\phi - \gamma) + \frac{C}{(C + R\cos\phi)} \cos\phi \cos\gamma \right] \tag{1-96}$$

$$\frac{d(Lg\, C)}{d(Lg\, m)} = V_e \left[\frac{\cos\gamma}{(C + R\cos\phi)} \right] \tag{1-97}$$

$$\frac{d\Psi}{d(Lg\, m)} = \frac{V_e}{R} \left[\frac{C}{(C + R\cos\phi)} \sin\phi \cos\gamma + \sin(\phi - \gamma) \right] \tag{1-98}$$

$$\nu = \text{constant} \quad . \tag{1-99}$$

Table 1-4. System of Hodographic Equations with Separate Differentials

$$(R, C, v, \Psi, \phi, m)$$

$$\dot{R} - \frac{\epsilon V_e}{m}\left[\cos(\phi-\gamma) + \frac{C}{(C+R\cos\phi)}\cos\phi\cos\gamma\right] = 0 \qquad (1\text{-}89)$$

$$\dot{C} + \frac{\epsilon V_e}{m}\left[\frac{C}{(C+R\cos\phi)}\cos\gamma\right] = 0 \qquad (1\text{-}90)$$

$$\dot{\Psi} - \frac{\epsilon V_e}{mR}\left[\frac{C}{(C+R\cos\phi)}\sin\phi\cos\gamma + \sin(\phi-\gamma)\right] = 0 \qquad (1\text{-}91)$$

$$\dot{v} - \frac{C(C+R\cos\phi)^2}{\mu} = 0 \qquad (1\text{-}92)$$

$$\dot{m} + \epsilon = 0 \qquad (1\text{-}93)$$

$$v - \phi - \Psi = 0 \qquad (1\text{-}94)$$

Table 1-5. System of Hodographic Equations with Separate Differentials

$$(R, C, v, \phi, m)$$

$$\dot{R} \qquad - \frac{\epsilon V_e}{m}\left[\cos(\phi-\gamma) + \frac{C}{(C+R\cos\phi)}\cos\phi\cos\gamma\right] = 0 \qquad (1\text{-}89)$$

$$\dot{C} \qquad + \frac{\epsilon V_e}{m}\left[\frac{C}{(C+R\cos\phi)}\cos\gamma\right] = 0 \qquad (1\text{-}90)$$

$$\dot{\phi} \quad - \frac{C(C+R\cos\phi)^2}{\mu} + \frac{\epsilon V_e}{mR}\left[\frac{C}{(C+R\cos\phi)}\sin\phi\cos\gamma + \sin(\phi-\gamma)\right] = 0 \qquad (1\text{-}95)$$

$$\dot{v} \quad - \frac{C(C+R\cos\phi)^2}{\mu} \qquad = 0 \qquad (1\text{-}92)$$

$$\dot{m} \qquad + \epsilon \qquad = 0 \qquad (1\text{-}93)$$

1.7 PHYSICAL SIGNIFICANCE OF THE PARAMETRIC NATURE OF THE HODOGRAPHIC FORMULATION

Parametric equations have been employed for some of the most powerful treatments in celestial mechanics, as presented in the variation-of-parameters method of analysis (Reference 5). The hodographic formulation presents the complete equations of motion in terms of the natural parameters (or hodographic variables). It has been shown that all accelerations due either to conservative force field, applied thrust, or perturbations can thus be expressed as complete differentials of the velocity hodograph parameters. Consequently, trajectory synthesis and analysis may be carried out with hodographic formulation, either in traditional form by means of formal integration (as covered by Work Phase IIIA) or in acceleration vector space by use of differential geometry and transformations between vector and state spaces (as covered by Work Phase IIIB). In any case, the physical significance of the parametric nature of the hodographic formulation is extremely desirable, for both heuristic and pedagogical purposes.

When the spacecraft experiences an applied acceleration due to a propulsion thrust force, the spacecraft mass is then variable in accordance with

$$\ddot{X} = -\left(\frac{\mu}{r^3}\right)X + \frac{T_x}{m} \tag{1-100}$$

$$\ddot{Y} = -\left(\frac{\mu}{r^3}\right)Y + \frac{T_y}{m} \tag{1-101}$$

where

$$\bar{r} = (X)\bar{J}_X + (Y)\bar{J}_Y \tag{1-102}$$

$$\bar{T} = (T_x)\bar{J}_X + (T_y)\bar{J}_Y \tag{1-103}$$

and

$$\bar{V} = \dot{\bar{r}} = (\dot{X})\bar{J}_X + (\dot{Y})\bar{J}_Y \quad . \tag{1-104}$$

Consequently

$$X\ddot{Y} - Y\ddot{X} = \frac{1}{m}(XT_Y - YT_X) \ , \tag{1-105}$$

$$m\frac{d}{dt}(X\dot{Y} - Y\dot{X}) = XT_Y - YT_X \ , \tag{1-106}$$

$$m\frac{d}{dt}(\bar{r} \times \bar{V}) = \bar{r} \times \bar{T} \tag{1-107}$$

and finally, the "Areal Integral":

$$\boxed{\bar{r} \times \bar{V} = \int_{t_0}^{t} \frac{\bar{r} \times \bar{T}}{m}\, dt + \bar{K}_0} \ . \tag{1-108}$$

When $\bar{T} = 0$ (as for the ballistic trajectory covered in Subsection 1.2),

$$\bar{r} \times \bar{V} = \text{constant} = \bar{K} \ . \tag{1-109}$$

That is, Equation 1-109 is the vector equation for which Equation 1-7A defines the scalar $|\bar{K}|$, so that

$$|\bar{K}| = \ell/m \ . \tag{1-110}$$

Also,

$$2(\dot{X}\ddot{X} + \dot{Y}\ddot{Y}) = -\left(\frac{\mu}{r^3}\right)\frac{d(r^2)}{dt} + \frac{2}{m}(\dot{X}T_X + \dot{Y}T_Y) \tag{1-111}$$

so that

$$\frac{d(V^2)}{dt} = 2\mu\frac{d}{dt}\left(\frac{1}{r}\right) + \frac{2}{m}(\bar{T} \cdot \bar{V}) \tag{1-112}$$

and finally, the 'Energy Integral":

$$\boxed{\frac{V^2}{2} - \frac{\mu}{r} = \int_{t_0}^{t} \frac{\bar{T}\cdot\bar{V}}{m}\,dt + \frac{h_0}{2}} \quad . \tag{1-113}$$

When $\bar{T} = 0$ (as for the ballistic trajectory covered in Subsection 1.2),

$$\frac{V^2}{2} - \frac{\mu}{r} = \frac{h}{2} = \text{constant} \quad . \tag{1-114}$$

Let us carry forth the expository analysis in polar coordinates. Then

$$X = r\cos v$$

$$Y = r\sin v$$

so that

$$X\dot{Y} - Y\dot{X} = \bar{r}\times\bar{V} = (r\bar{\jmath}_r)\times(V_r\bar{\jmath}_r + V_v\bar{\jmath}_v) \tag{1-115A}$$

$$X\dot{Y} - Y\dot{X} = (rV_v)\bar{\imath}_z \quad . \tag{1-115B}$$

Since

$$\bar{r}\times\bar{T} = (r\bar{\jmath}_r)\times(T_r\bar{\jmath}_r + T_v\bar{\jmath}_v) = (rT_v)\bar{\imath}_z \;, \tag{1-116}$$

then Equation 1-108 provides the scalar

$$\boxed{rV_v = K_0 + \int_{t_0}^{t} \frac{rT_v}{m}\,dt = K(t)} \quad . \tag{1-117}$$

Since

$$\bar{T}\cdot\bar{V} = \dot{X}T_X + \dot{Y}T_Y = T_r V_r + T_v V_v \qquad (1\text{-}118A)$$

$$\bar{T}\cdot\bar{V} = T_r \dot{r} + T_v r\dot{v} \quad , \qquad (1\text{-}118B)$$

then Equation 1-113 provides

$$\boxed{(V_r^2 + V_v^2) - \frac{2\mu}{r} = h_0 + 2\int_{t_0}^{t} \frac{T_r V_r + T_v V_v}{m}\,dt = h(t)} \qquad (1\text{-}119)$$

Differentiating Equation 1-119,

$$V_r \dot{V}_r + V_v \dot{V}_v + \left(\frac{\mu}{r^2}\right)\dot{r} = \frac{1}{m}\left(T_r V_r + T_v V_v\right) . \qquad (1\text{-}120A)$$

Since, according to Equations 1-37A and 1-38A respectively,

$$\dot{V}_r = A_r + \frac{V_v^2}{r} \qquad (1\text{-}37D)$$

$$\dot{V}_v = A_v - \frac{V_r V_v}{r} \quad , \qquad (1\text{-}38D)$$

then

$$\left(V_r A_r + \frac{V_r V_v}{r}\right) + \left(V_v A_v - \frac{V_r V_v}{r}\right) + \left(\frac{\mu}{r^2}\right)\dot{r} = \frac{1}{m}\left(T_r V_r + T_v V_v\right) \qquad (1\text{-}120B)$$

or

$$V_r\left(A_r + \frac{\mu}{r^2}\right) + V_v A_v = \frac{T_r V_r + T_v V_v}{m} . \qquad (1\text{-}120C)$$

Differentiating Equation 1-117,

$$\dot{r} V_v + r \dot{V}_v = \frac{r T_v}{m} \tag{1-121A}$$

so that, by use of Equation 1-38D,

$$\cancel{\dot{r} V_v} + (r A_v - \cancel{V_r V_v}) = \frac{r T_v}{m} \tag{1-121B}$$

or

$$\boxed{A_v = \frac{T_v}{m}} \tag{1-121C}$$

Consequently, Equations 1-120C and 1-121C provide

$$V_r \left(A_r + \frac{k}{r^2} \right) = \frac{T_r V_r}{m} \tag{1-122A}$$

or

$$\boxed{A_r = -\frac{k}{r^2} + \frac{T_r}{m}} \tag{1-122B}$$

When thrust is zero ($\overline{T} = 0$), then

$$\boxed{A_{vb} = 0} \tag{1-123}$$

$$\boxed{A_{rb} = -\frac{k}{r^2}} \tag{1-124}$$

1.7.1 POLAR VELOCITY HODOGRAPH

Let us consider the polar velocity hodograph for powered flight (or subarcs of a complete trajectory), in order to demonstrate the quasi-steady or parametric nature of the hodograph formulations. Let

$$C(t) = \frac{\mu}{K(t)} \tag{1-125}$$

in which K (t) is defined by Equation 1-114 so that, by use of Equation 1-119,

$$V_r^2 + V_v^2 - 2C(t)V_v = h(t) \tag{1-126A}$$

or

$$V_r^2 + [V_v - C(t)]^2 = h(t) + [C(t)]^2 = [R(t)]^2 \tag{1-126B}$$

where

$$R(t) = \sqrt{h(t) + [C(t)]^2}\ , \tag{1-127}$$

so that

$$\boxed{V_r = R(t)\sin\phi} \tag{1-128}$$

$$\boxed{V_v = C(t) + R(t)\cos\phi}\ . \tag{1-129}$$

It is obvious that the instantaneous velocity hodographs of powered flight are also circles, as shown in Figure 1-10. At each successive instant of time, the velocity hodographs change from the preceding, unless thrust ceases. While C(t), R(t), $\Psi(t)$ may increase or decrease with increasing t, the true anomaly $\phi(t)$ can only increase also. Each velocity hodograph represents the instantaneous orbit at that instant of time. Consequently, the velocity hodographs will define the complete powered subarc or trajectory in velocity vector space. For example, the complete powered flight trajectory in position vector space is the locus of successive points on the osculating ellipses which are the instantaneous orbits, as shown in Figure 1-11. The corresponding velocity hodograph of the powered flight trajectory is the locus of successive points on the hodograph circles which are the instantaneous orbital velocity hodographs, as shown in Figure 1-12.

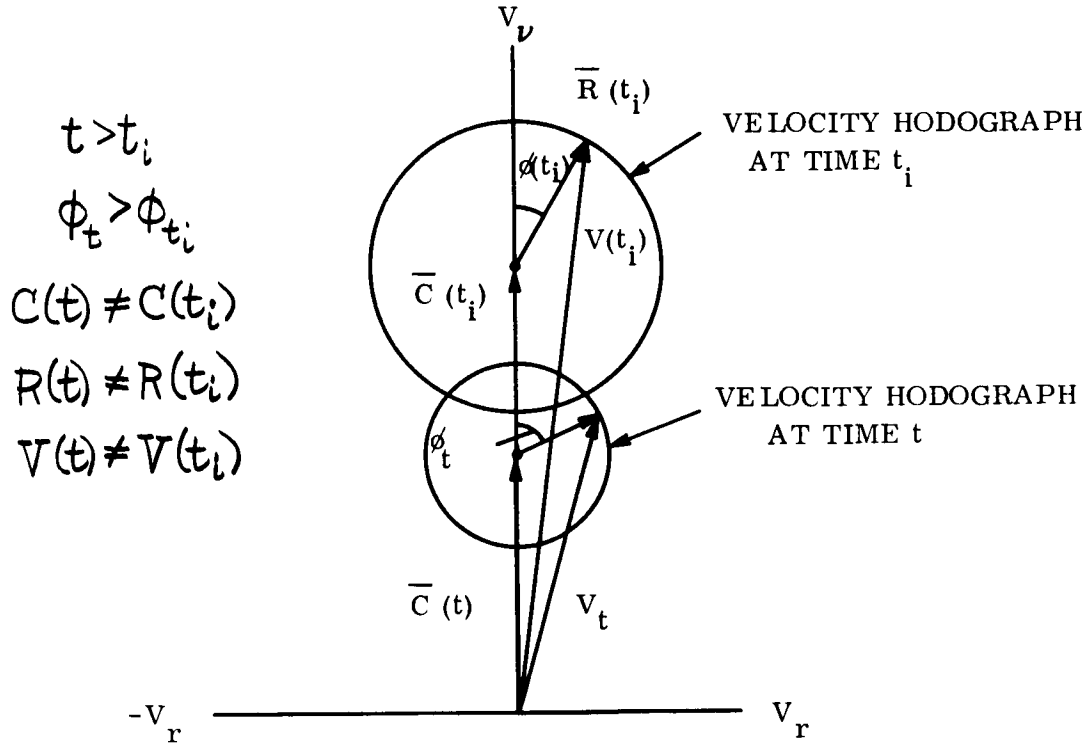

Figure 1-10. Successive Velocity Hodographs of Powered Flight

If the complete trajectory consists of powered and coasting (or ballistic) subarcs, the thrust, mass, angular momentum and energy will vary with time as shown in the characteristic diagrams of Figures 1-13 or 1-14. The thrust discontinuity may occur due to fuel cutoff as shown in Figure 1-13, or due to staging as shown in Figure 1-14.

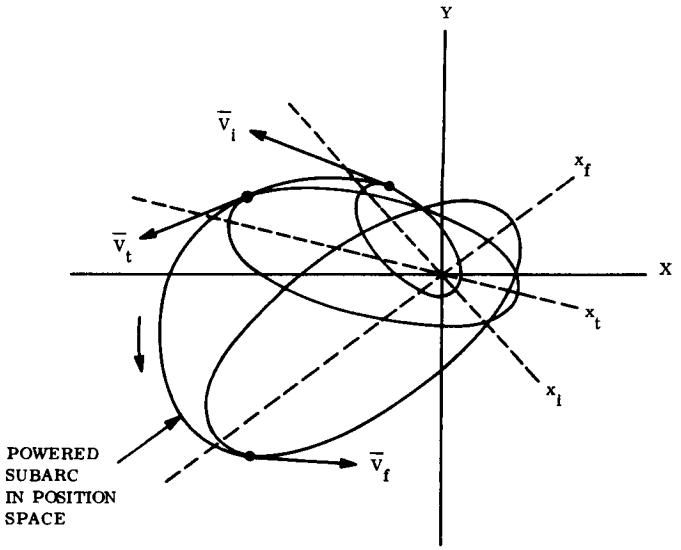

Figure 1-11. Powered Subarc and Its Osculating Ellipses in Position Vector Space

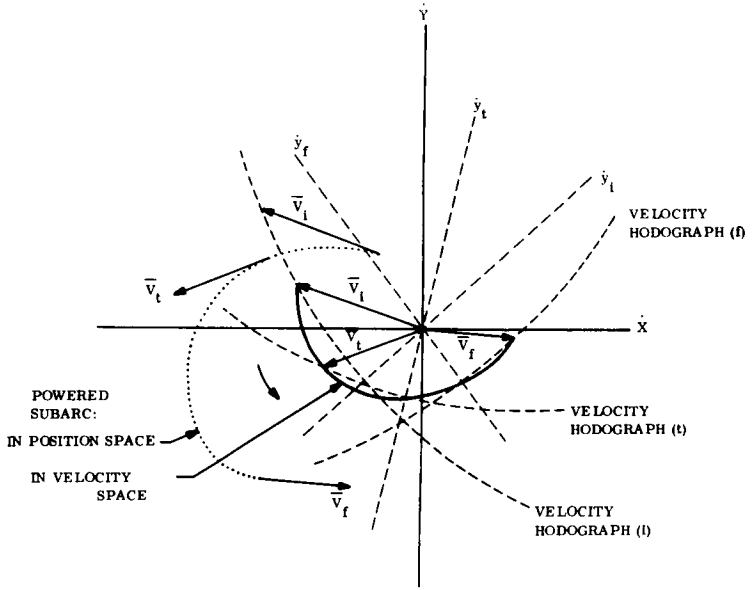

Figure 1-12. Powered Subarc and its Velocity Hodographs (for the Osculating Ellipses) in Velocity Vector Space

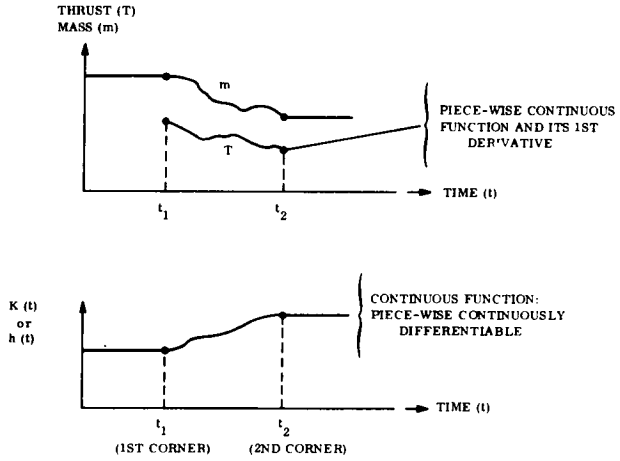

Figure 1-13. Effect of Thrust Discontinuities at Corners

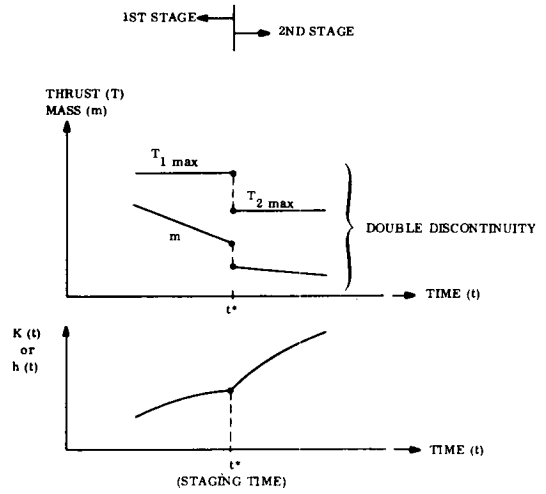

Figure 1-14. Effect of Staging (with Discontinuous Thrust through Staging)

1.7.2 VELOCITY HODOGRAPH IN ROTATING CARTESIAN COORDINATES

In Subsection 1.3 the rotation matrix (Equation 1-26) provided

$$x = X\cos\Psi + Y\sin\Psi$$

$$y = -X\sin\Psi + Y\cos\Psi$$

so that

$$\dot{x} = \dot{X}\cos\Psi - X\dot{\Psi}\sin\Psi + \dot{Y}\sin\Psi + Y\dot{\Psi}\cos\Psi \qquad (1\text{-}130)$$

$$\dot{y} = -\dot{X}\sin\Psi - X\dot{\Psi}\cos\Psi + \dot{Y}\cos\Psi - Y\dot{\Psi}\sin\Psi \; . \qquad (1\text{-}131)$$

But, as shown in Figure 1-15,

$$\dot{X} = -R(t)\sin\Psi - C(t)\sin[\phi+\Psi] \qquad (1\text{-}24B)$$

$$\dot{Y} = R(t)\cos\Psi + C(t)\cos[\phi+\Psi] \qquad (1\text{-}25B)$$

and

$$X = x\cos\Psi - y\sin\Psi \qquad (1\text{-}132)$$

$$Y = x\sin\Psi + y\cos\Psi \qquad (1\text{-}133)$$

so that

$$\dot{x} = -C(t)\sin\phi + y\dot{\Psi} \qquad (1\text{-}134)$$

$$\dot{y} = R(t) + C(t)\cos\phi - x\dot{\Psi} \; . \qquad (1\text{-}135)$$

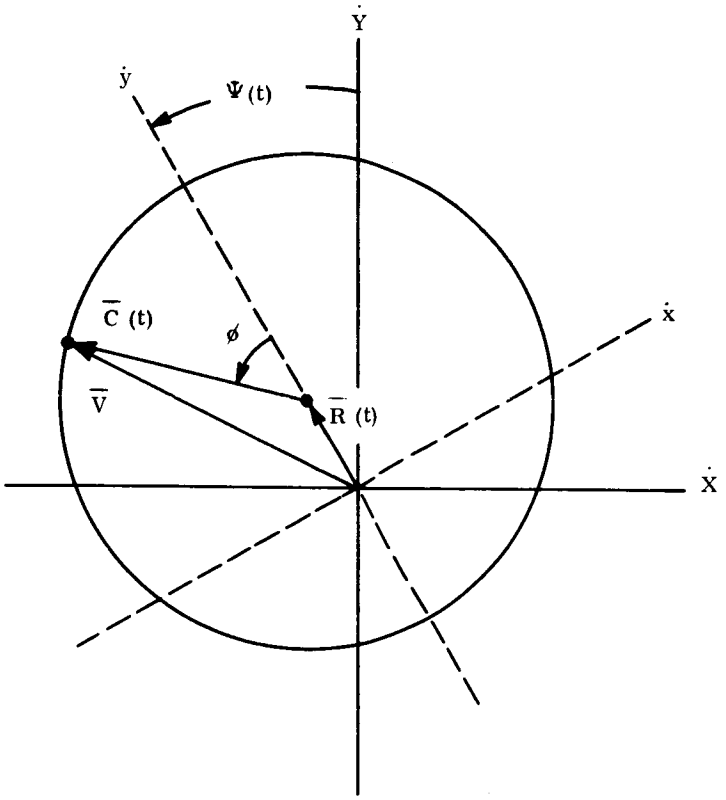

Figure 1-15. Velocity Hodograph with Hodograph Parameters as Functions of Time

Since

$$\bar{V} = (\alpha)\bar{I}_x + (\beta)\bar{I}_y$$

where

$$\alpha = \dot{x} - (\dot{\Psi})y$$

$$\beta = \dot{y} + (\dot{\Psi})x \quad ,$$

then

$$V^2 - \frac{2k}{r} = \alpha^2 + \beta^2 - \frac{2k}{r} = h(t) \qquad (1\text{-}136)$$

and

$$r = \frac{K(t)}{V_v} = \frac{K(t)}{C(t) + R(t)\cos\phi} \quad . \tag{1-137}$$

Therefore

$$\alpha^2 + \beta^2 - 2\left[C(t)\right]^2 - 2C(t)R(t)\cos\phi = h(t) \tag{1-138A}$$

and

$$\cos\phi = \frac{\beta - R(t)}{C(t)} \tag{1-139}$$

according to Equations 1-52 and 1-138, so that

$$\alpha^2 + \beta^2 - 2\left[C(t)\right]^2 - 2R(t)\left[\beta - R(t)\right] = h(t) \tag{1-138B}$$

or

$$\alpha^2 + \left[\beta - R(t)\right]^2 = \left[C(t)\right]^2 \tag{1-138C}$$

and

$$V_x(t) = \alpha(t) = -C(t)\sin\phi \tag{1-140}$$

$$V_y(t) = \beta(t) = R(t) + C(t)\cos\phi \quad . \tag{1-141}$$

References

1. S. P. Altman, Orbital Hodograph Analysis, Vol. 3, AAS Science and Technology Series, Western Periodicals 1965, Chapter 3.

2. S. Ross, "Optimal Ascent Into Orbit -- A New Look at an Old Problem," Proceedings of the XVth International Astronautical Congress, Vol. I, 1964, pp. 347-361.

3. D. J. Struik, Differential Geometry, Addison-Wesley Publishing Co., Reading, Massachusetts, 1961, 2nd edition.

4. S. P. Altman, "The Hodographic Theory of Newtonian Mechanics," Recent Developments in Space Flight Mechanics, Vol. 9, AAS Science and Technology Series, 1966.

5. F. R. Moulton, Differential Equations, Dover Publications, New York, 1958, pp. 60-70.

SECTION 2

OPTIMUM TRAJECTORIES FOR HODOGRAPHIC EQUATIONS OF MOTION IN A CENTRAL GRAVITATIONAL FIELD

AUTHOR: CARLOS R. CAVOTI

SECTION 2

OPTIMUM TRAJECTORIES FOR HODOGRAPHIC EQUATIONS OF MOTION IN A CENTRAL GRAVITATIONAL FIELD

A generalized variational problem in orbit mechanics is formulated, using the hodographic equations of motion in an inverse square gravitational field about one force center. The object of this study is to present the variational formulation assuming a general form for the function to be minimized as well as for the boundary conditions. Thus, generalized necessary conditions are derived that apply to the variety of variational problems which may be obtained as particular cases of the one treated here. As an example, a particular case is discussed in the last section to show a specific application of the conditions obtained. The example presented shows the nonexistence of intermediate-thrust subarcs for the class of problems considered.

The treatment of other specific problems and the methods of numerical solution should be the object of further work.

2.1 VARIATIONAL FORMULATION OF THE EQUATIONS OF MOTION

In general, the equations of motion written in generalized coordinates will be assumed given by a set of first order nonlinear differential equations of the form (see Table 2-1 for nomenclature):

$$\psi_j \equiv \dot{q}_j - f_j(q_i, t) = 0 \,, \qquad \begin{matrix} j = 1, .., n \\ i = 1, .., m \\ m > n \end{matrix} \tag{2-1}$$

This form of the equations of motion corresponds with that obtained in our previous report (Section 1) for the motion of a particle in a central force field in terms of hodographic coordinates. Thus, in the specific problem to be considered here, q is an m -dimensional vector of coordinates $[q_1, q_2, .., q_7] \equiv [R, C, \phi, \nu, m, \gamma, \epsilon]$. Consequently, in Equation 2-1, the subindex ranges are; j = 1 , ... , 5 and i = 1 , . . . , 7, because the equations of motion specifically considered are:

Table 2-1. Definitive Nomenclature

q	generalized coordinate
t	time
ψ	differential constraint
R, C, ϕ, ν	hodograph variables
m	mass
δ	direction angle of vector thrust
ϵ	mass flow rate ($= -\dot{m}$)
V_e	velocity of the exhaust gases at the exit section of the rocket nozzle
$\mathcal{I}$	function to be minimized
X_s	terminal constraints (i.e., boundary conditions)
μ_s	constant Lagrange multiplier
Π	Euler-Lagrange sum
λ_j	variable Lagrange multiplier
τ_j	canonical influence function
H	Hamiltonian

Superscripts and Subscripts

$(\cdots)_F$	final condition
$(\cdots)_I$	initial condition
$\dot{(\cdots)} = \frac{d}{dt}$	

$$\psi_1 \equiv \dot{R} - \frac{\epsilon V_e}{m}\left[\cos(\phi-\gamma) + \frac{C}{C+R\cos\phi}\cos\phi\cos\gamma\right] = 0 \,, \tag{2-2}$$

$$\psi_2 \equiv \dot{C} + \frac{\epsilon V_e C}{m(C+R\cos\phi)}\cos\gamma = 0 \,, \tag{2-3}$$

$$\psi_3 \equiv \dot{\phi} - \frac{C(C+R\cos\phi)^2}{\mu} + \frac{\epsilon V_e}{mR}\left[\frac{C}{C+R\cos\phi}\sin\phi\cos\gamma + \sin(\phi-\gamma)\right] = 0 \,, \tag{2-4}$$

$$\psi_4 \equiv \dot{\nu} - \frac{C(C+R\cos\phi)^2}{\mu} = 0 \,, \tag{2-5}$$

$$\psi_5 \equiv \dot{m} + \epsilon = 0 \,. \tag{2-6}$$

Any solution of Equations 2-2 through 2-6 is expressed in terms of the state-variable functions R(t), C(t), ϕ(t), ν(t), m(t) and the control-variable functions γ(t) and ϵ(t). The control variables determine the magnitude and direction of the vector thrust. In the following, it will be assumed that the thrust direction γ(t) is unbounded, whereas the thrust magnitude is bounded by

$$0 \leq \epsilon(t) \leq \epsilon_{max.} \,, \quad t_I \leq t \leq t_F \,. \tag{2-7}$$

To the extent of treating a generalized variational problem, we propose to derive the necessary conditions for an extremal such that the function

$$\Upsilon = \Upsilon\left(q_{j_I}, q_{j_F}, t_I, t_F\right) \,, \quad j = 1,..,n=5, \tag{2-8}$$

is minimized subject to the arbitrary boundary conditions

$$X_s\left(q_{j_I}, q_{j_F}, t_I, t_F\right) = 0, \quad s = 1,..,r \,, \quad r \leq 2n+1. \tag{2-9}$$

The subindexes I and F indicate an initial or a final value, respectively. Clearly, the problem proposed is general and the necessary conditions thus derived will apply to a variety of optimal problems which can be obtained as particular cases of Equation 2-8. For example, if

$$\Upsilon = t_F - t_I = \Delta t = min.,$$

we specify the minimum time problem (provided t_F or t_I, or both, are not given by Equation 2-9). If

$$\Upsilon = -q_{5_F} = -m_F = min.,$$

we propose the minimum fuel consumption problem (assuming - as is commonly the case-that m_I is given by Equation 2-9). And, to give a further example, if

$$\Upsilon = \left[\Delta\left(q_1^2 - q_2^2\right)\right]^{-1} = \left[\left(R^2 - C^2\right)_F - \left(R^2 - C^2\right)_I\right]^{-1} = min.,$$

the optimum transfer with maximum total energy increment is treated. The latter problem is of interest in general, for studies in which the available propellant is known from Equation 2-9 (i.e., $\Delta m = m_F - m_I$ is fixed).

The problem of minimizing the function Υ subject to the equations of constraint $\Psi_j = 0$, $j = 1, \ldots, 5$ (Equations 2-2 to 2-6) and the boundary conditions $X_s = 0$, $s = 1, \ldots, r \leq 2n + 1$, is expressed analytically as the problem of minimizing the function of Bolza's form

$$J = \mu_o \Upsilon + \mu_s X_s + \int_{t_I}^{t_F} \Pi\left(\dot{q}_j, q_i, \lambda_j, t\right) dt , \qquad (2\text{-}10)$$

in the class D^1 (piece-wise continuously differentiable) of arcs $q_j(t)$, $j = 1, \ldots, 5$, and D^0 (piece-wise continuous functions which may present finite discontinuities or jumps) of arcs $q_6(t)$ and $q_7(t)$. The admissible discontinuous functions of the latter class are called control functions (i.e., in our problem, $q_6(t) = \gamma(t)$ and $q_7(t) = \epsilon(t)$). In Equation 2-10 the μ's are constant multipliers while the λ's are variable Lagrange multipliers used to form the fundamental function $\Pi = \sum_{j=1}^{n} \lambda_j \psi_j$. Since in the present study, we will assume that the extremal arc is normal,* we can therefore take $\mu_o = 1$.

2.1.1 FORMULATION IN TERMS OF CANONICAL VARIABLES

The problem formulated in Paragraph 2.1 in terms of the variables (t, q_i, q_j, λ_j), $j=1, \ldots, 5$; $i = 1, \ldots, 7$, may be expressed in terms of the canonical variables $(t, q_j, q_6, q_7, \tau_j)$, introducing the Legendre transformation

$$\tau_j = \frac{\partial \Pi}{\partial \dot{q}_j} \quad , \quad \tau_j \dot{q}_j - \Pi = H \quad . \tag{2-11}$$

The variables $\tau_j(t)$, $j = 1, \ldots, 5$, are called canonical influence functions while H is called the Hamiltonian of the system.

The variational problem is formulated in canonical form introducing the fundamental function

(See next page)

*An extremal arc is said to be normal if there is no set of constants and multipliers $(\mu_o = 0, \mu_s, \lambda_j)$ with which it satisfies the Transversality Condition and the Euler equations. The set of multipliers satisfying a normal extremal $(\mu_o \neq 0, \mu_s, \lambda_j)$ is unique and therefore it can always be reduced to the set $(1; \tilde{\mu}_s = \mu_s/\mu_o; \tilde{\lambda}_j = \lambda_j/\mu_o)$.

$$\Lambda(t, q_j, q_6, q_7, \tau_j) = \tau_j \frac{dq_j}{dt} - H. \quad * \qquad (2\text{-}12)$$

The method of Lagrange multipliers leads to the transformation considered here which, in general, permits us to express the extremal by means of a set of first-order differential equations instead of the second-order Euler equations.

In fact, from the first variation problem (References 1, 2), it follows that the first necessary conditions for an extremal, in canonical form, lead to the following "canonical differential equations of the extremals":

$$\frac{d\tau_j}{dt} + \frac{\partial H}{\partial q_j} = 0 \quad , \quad j = 1, .., 5 \quad , \qquad (2\text{-}13)$$

$$\frac{dq_j}{dt} - \frac{\partial H}{\partial \tau_j} = 0 \quad , \qquad (2\text{-}14)$$

$$\frac{dH}{dt} - \frac{\partial H}{\partial t} = 0 \quad . \qquad (2\text{-}15)$$

Equations 2-13 through 2-15 are obtained as the equations of variation of the fundamental function Λ (Equation 2-12) assuming unrestricted variations of the state variables q_j and the canonical functions τ_j. Equation 2-14, as can be easily recognized, corresponds to the equations of motion.

---

* According to the implicit function theorems (Reference 1), there is a neighborhood N of $(t, q_j, q_6, q_7, \tau_j) \in E$ (E = extremal) in which the equations $\psi_j = 0$ and $\tau_j = \partial\Pi/\partial\dot{q}_j$ have, in general, solutions $\dot{q}_j = \dot{q}_j\,(t, q_j, q_6, q_7, \tau_j)$, $\lambda_j = \lambda_j\,(t, q_j, q_6, q_7, \tau_j)$ which reduce to $(\dot{q}_j, \lambda_j) \in E$ for $(t, q_j, q_6, q_7, \tau_j) \in E$. For this reason, we can express Λ as a function of $(t, q_j, q_6, q_7, \tau_j)$ in Equation 2-12.

In addition to Equations 2-13 through 2-15, any extremal arc must satisfy the equations of variation associated with admissible variations of the control variables $q_6 = \gamma$ and $q_7 = \epsilon$. Because γ is unbounded, unrestricted variations $\delta\gamma \gtrless 0$ are admissible, thus leading to the necessary condition

$$\frac{\partial H}{\partial q_{f_6}} = \frac{\partial H}{\partial \gamma} = 0 \ , \tag{2-16}$$

along any subarc forming the extremal. However, due to the boundedness of the control variable ϵ (i.e., $0 \leqq \epsilon \leqq \epsilon_{max.}$) unrestricted as well as restricted (or one-sided) variations are admissible. Correspondingly, the following necessary conditions are derived:

$$\frac{\partial H}{\partial q_{f_7}} = \frac{\partial H}{\partial \epsilon} = 0 \quad , \quad \delta\epsilon \gtrless 0 \quad \therefore \quad 0 < \epsilon < \epsilon_{max.} \ , \tag{2-17}$$

$$H_{q_{f_7}} = \frac{\partial H}{\partial \epsilon} \geqq 0 \quad , \quad \delta\epsilon \leqq 0 \quad \therefore \quad \epsilon = \epsilon_{max.} \ , \tag{2-18}$$

$$H_{q_{f_7}} = \frac{\partial H}{\partial \epsilon} \leqq 0 \quad , \quad \delta\epsilon \geqq 0 \quad \therefore \quad \epsilon = \epsilon_{min.} = 0 \ . \tag{2-19}$$

Furthermore, an important necessary condition associated with the terminal differentials $d_{q_{j_F}}$, $d_{q_{j_I}}$, dt_F, dt_I, may be derived from the first-variation problem. This necessary condition requires that the $\left[(r+1) \times (2n+2)\right]$ matrix

$$\left\| \begin{matrix} \dfrac{\partial \Upsilon}{\partial q_{j_{f_I}}} - \tau_{j_I} & \dfrac{\partial \Upsilon}{\partial q_{j_{f_F}}} + \tau_{j_F} & \dfrac{\partial \Upsilon}{\partial t_I} + H_I & \dfrac{\partial \Upsilon}{\partial t_F} - H_F \\ \dfrac{\partial X_s}{\partial q_{j_{f_I}}} & \dfrac{\partial X_s}{\partial q_{j_{f_F}}} & \dfrac{\partial X_s}{\partial t_I} & \dfrac{\partial X_s}{\partial t_F} \end{matrix} \right\| \tag{2-20}$$

must be of rank $R < (r+1)$.

In view of the fact that not all the (r × r) determinants which may be formed out of the $\left[r \times (2n \times 2) \right]$ matrix

$$\left\| \frac{\partial X_s}{\partial q_{j_I}} \quad \frac{\partial X_s}{\partial q_{j_F}} \quad \frac{\partial X_s}{\partial t_I} \quad \frac{\partial X_s}{\partial t_F} \right\| \tag{2-21}$$

may vanish (so there is no linear dependence between the boundary conditions), this preceding condition on the matrix 2-20 implies

$$\frac{\partial \Upsilon}{\partial q_{j_I}} - \tau_{j_I} + \mu_s \frac{\partial X_s}{\partial q_{j_I}} = 0 , \tag{2-22}$$

$$\frac{\partial \Upsilon}{\partial q_{j_F}} + \tau_{j_F} + \mu_s \frac{\partial X_s}{\partial q_{j_F}} = 0 , \tag{2-23}$$

$$\frac{\partial}{\partial t_I} \left[\Upsilon + \mu_s X_s \right] + H_I = 0 , \tag{2-24}$$

$$\frac{\partial}{\partial t_F} \left[\Upsilon + \mu_s X_s \right] - H_F = 0 . \tag{2-25}$$

The fact that the matrix 2-20 must have rank R< (r+1) is referred to as the matrix form of the Transversality condition. Thus, Equations 2-22 through 2-25 which derive from this condition, are called subconditions of transversality.

The previous necessary conditions derived from the first-variation problem lead to the following theorem: "Any arc E, which satisfies Equations 2-1 and 2-9 with a set of constants and multipliers consistent with the canonical Equations 2-13 through 2-19 and the transversality conditions in Equations 2-22 through 2-25 is an extremal which satisfies the Multiplier Rule."

The first necessary conditions implied by the Multiplier Rule will be specifically applied to the problem with side conditions given by Equations 2-2 through 2-6, in the following. However, it is opportune to point out that, to the extent of applying the Transversality Condition, it is convenient to express it independently of the constant multipliers μ_s. This can be achieved upon noting that Equations 2-22 through 2-25 imply that

$$d\mathcal{T}(q_{j_F}, q_{j_I}, t_F, t_I) + \left[\tau_j\, dq_j - H\, dt\right]_I^F \equiv 0 \quad , \qquad (2\text{-}26)$$

for any set of admissible differentials ($d_{q_{j_F}}$, $d_{q_{j_I}}$, dt_F, dt_I) which satisfy the following equations of variations of the boundary conditions:

$$\frac{\partial X_s}{\partial q_{j_F}}\, dq_{j_F} + \frac{\partial X_s}{\partial q_{j_I}}\, dq_{j_I} + \frac{\partial X_s}{\partial t_F}\, dt_F + \frac{\partial X_s}{\partial t_I}\, dt_I \equiv 0. \qquad (2\text{-}27)$$

In the following section, these necessary conditions are applied to our specific set of equations of motion in hodographic variables.

2.2 CANONICAL EQUATIONS OF THE EXTREMALS IN TERMS OF THE HODOGRAPHIC STATE VARIABLES

Using the hodographic equations of motion given by Equations 2-2 through 2-6, and definition of the Hamiltonian (Equation 2-11), we obtain for the specified problem formulation considered here:

$$H = \tau_1 \frac{\epsilon V_e}{m}\left[\cos(\phi-\gamma)+\frac{C}{C+R\cos\phi}\cos\phi\cos\gamma\right]-$$

$$-\tau_2\frac{\epsilon V_e C\cos\gamma}{m(C+R\cos\phi)}+\tau_3\left\{\frac{C(C+R\cos\phi)^2}{\mu}-\frac{\epsilon V_e}{mR}\left[\frac{C}{C+R\cos\phi}\sin\phi\cos\gamma+\right.\right.$$

$$\left.\left.+\sin(\phi-\gamma)\right]\right\}+\tau_4\frac{C(C+R\cos\phi)^2}{\mu}-\tau_5\epsilon\,. \qquad (2\text{-}28)$$

Consequently, the canonical equations of the extremals given by Equation 2-13 require that the set of canonical influence functions (also called adjoint variables) $\tau_j(t)$, $j=1,\ldots,5$, satisfy the following differential equations

$$\dot{\tau}_1=\frac{\epsilon V_e C}{m(C+R\cos\phi)^2}\cos\gamma\cos\phi\left[\tau_1\cos\phi-\tau_2-\tau_3\frac{\tan\phi}{R^2}(C+2R\cos\phi)\right]-$$

$$-\tau_3\frac{\epsilon V_e\sin(\phi-\gamma)}{mR^2}-\frac{2C}{\mu}(C+R\cos\phi)\cos\phi(\tau_3+\tau_4)\,, \qquad (2\text{-}29)$$

$$\dot{\tau}_2=\frac{\epsilon V_e\cos\gamma R}{m(C+R\cos\phi)^2}\cos\phi\left[-\tau_1\cos\phi+\tau_2+\tau_3\frac{\sin\phi}{R}\right]-$$

$$-\frac{3C^2+4CR\cos\phi+R^2\cos^2\phi}{\mu}(\tau_3+\tau_4)\,, \qquad (2\text{-}30)$$

$$\dot{\tau}_3=\frac{\epsilon V_e}{m}\left\{\tau_1\left[\sin(\phi-\gamma)+\frac{C^2\cos\gamma\sin\phi}{(C+R\cos\phi)^2}\right]+\tau_2\frac{CR\cos\gamma\sin\phi}{(C+R\cos\phi)^2}+\right.$$

$$\left.+\frac{\tau_3}{R}\left[\frac{C\cos\gamma(R+C\cos\phi)}{(C+R\cos\phi)^2}+\cos(\phi-\gamma)\right]\right\}+\frac{2C}{\mu}(C+R\cos\phi)R\sin\phi(\tau_3+\tau_4)\,, \qquad (2\text{-}31)$$

$$\dot{\tau}_4 = 0 \quad , \quad \therefore \quad \tau_4 = K_4 = const. \, , \tag{2-32}$$

$$\dot{\tau}_5 = \frac{\epsilon V_e}{m^2} \left\{ \tau_1 \left[\cos(\phi - \gamma) + \frac{C}{C + R\cos\phi} \cos\phi \cos\gamma \right] - \tau_2 \frac{C}{C + R\cos\phi} \cos\gamma - \right.$$

$$\left. - \tau_3 \frac{1}{R} \left[\frac{C}{C + R\cos\phi} \sin\phi \cos\gamma + \sin(\phi - \gamma) \right] \right\} . \tag{2-33}$$

The necessary condition associated with variations $\delta\gamma \gtreqless 0$ (Equation 2-16) leads to

$$\frac{\epsilon V_e}{m} \left\{ \tau_1 \left[\sin(\phi - \gamma) - \frac{C}{C + R\cos\phi} \cos\phi \sin\gamma \right] + \tau_2 \frac{C}{C + R\cos\phi} \sin\gamma \right.$$

$$\left. + \frac{\tau_3}{R} \left[\frac{C}{C + R\cos\phi} \sin\phi \sin\gamma + \cos(\phi - \gamma) \right] \right\} = 0 . \tag{2-34}$$

The previous equations constitute a set of first necessary conditions which must be satisfied by the extremal between the initial and final points (I and F respectively); that is, along any subarc. Furthermore, it is important to notice that, due to the fact that $\frac{\partial H}{\partial t} = 0$, Equation 2-15 leads to the first integral

$$\frac{\epsilon V_e}{m} \left\{ \tau_1 \left[\cos(\phi - \gamma) + \frac{C}{C + R\cos\phi} \cos\phi \cos\gamma \right] - \tau_2 \frac{C}{C + R\cos\phi} \cos\gamma - \right.$$

$$\left. - \frac{\tau_3}{R} \left[\frac{C}{C + R\cos\phi} \sin\phi \cos\gamma + \sin(\phi - \gamma) \right] - \frac{m \tau_5}{V_e} \right\} + \tag{2-35}$$

$$+ \frac{C}{\mu} (C + R\cos\phi)^2 (\tau_3 + \tau_4) = K = const.$$

which must be satisfied along the extremal.

2.2.1 SUBARCS THAT MAY FORM THE EXTREMAL

From Equation 2-28, it follows that

$$\frac{\partial H}{\partial \epsilon} = \frac{V_e}{m}\left\{\tau_1\left[\cos(\phi-\gamma)+\frac{C}{C+R\cos\phi}\cos\phi\cos\gamma\right]-\tau_2\frac{C}{C+R\cos\phi}\cos\gamma\right.$$

$$\left.-\frac{\tau_3}{R}\left[\frac{C}{C+R\cos\phi}\sin\phi\cos\gamma+\sin(\phi-\gamma)\right]\right\}-\tau_5 \ . \qquad (2\text{-}36)$$

Consequently, Equations 2-17 through 2-19 and Equation 2-36 give the necessary condition explicitly which must be satisfied along every subarc which may form part of the extremal arc.

In particular, along <u>zero-thrust subarcs</u> (i.e., $\epsilon = 0$), it follows from Equations 2-2 through 2-6 that

$$R = \text{const.}\ , \qquad C = \text{const.}\ , \qquad m = \text{const.}\ , \qquad (2\text{-}37)$$

$$\dot{\phi} = \dot{\gamma} = \frac{C(C+R\cos\phi)^2}{\mu}\ , \qquad (2\text{-}38)$$

while the adjoint variables must satisfy

$$\dot{\tau}_1 = -\frac{2C}{\mu}(C+R\cos\phi)\cos\phi(\tau_3+\tau_4)\ , \qquad (2\text{-}39)$$

$$\dot{\tau}_2 = -\frac{2C(C+R\cos\phi)+(C+R\cos\phi)^2}{\mu}(\tau_3+\tau_4)\ , \qquad (2\text{-}40)$$

$$\dot{\tau}_3 = \frac{2C}{\mu}(C+R\cos\phi)R\sin\phi(\tau_3+\tau_4)\ , \qquad (2\text{-}41)$$

$$\tau_4 = K_4 = \text{const.}\ , \qquad (2\text{-}42)$$

$$\tau_5 = K_5 = \text{const.} \qquad (2\text{-}43)$$

The Hamiltonian function in Equations 2-28 and 2-35 leads to the further necessary condition

$$\frac{C}{\mu}(C+R\cos\phi)^2(\tau_3+\tau_4) = K = const., \tag{2-44}$$

which together with Equation 2-42 leads to

$$\tau_3 = K\frac{\mu}{C(C+R\cos\phi)^2} - K_4 \quad . \tag{2-45}$$

From the previous equations, eliminating the independent variable t, we can obtain the multipliers as functions of the true anomaly ϕ as follows:

$$\tau_1(\phi) = -\frac{2K\mu}{C}\int_{\phi_0}^{\phi}\frac{d\sin\phi}{(C+R\cos\phi)^3} + \tau_{1_0} \quad , \tag{2-46}$$

$$\tau_2(\phi) = -\frac{K\mu}{C}\int_{\phi_0}^{\phi}\left[\frac{2}{(C+R\cos\phi)^3} + \frac{1}{C(C+R\cos\phi)^2}\right]d\phi + \tau_{2_0} \quad . \tag{2-47}$$

The multiplier $\tau_3(\phi)$ is obtained from Equation 2-45 while τ_4 and τ_5 are constants. This set of multipliers must satisfy the necessary condition given in Equation 2-19 when replaced in Equation 2-36.

The determination of these multipliers along the subarc considered is of particular interest in order to conduct error propagation and perturbation analysis. In fact, the influence coefficients replace the array of partial derivatives commonly used in such studies, with many advantages. These aspects, however, are beyond the scope of this work and will not be considered here.

2.3 CONDITIONS ALONG VARIABLE THRUST SUBARCS

The study of subarcs along which $0 < \epsilon < \epsilon_{max.}$ is of special interest in variational problems. In fact, in our specific problem, the matter of whether or not it is convenient to use the propulsive device at an intermediate level is of relevant importance. Clearly, this matter has definite practical as well as theoretical interest. From the point of view of engine design, obviously, the effect of this matter on the associated technological aspects is fundamental. On the other hand, from the theoretical point of view of the properties of such extremal subarcs, it is equally important to analyze the relative gains obtained when comparing such extremals with other admissible solutions flown with a different control program.

Although a complete and exhaustive treatment of these various aspects falls beyond the scope of this study, we will, however, analyze in this subsection the necessary conditions as well as the properties of such subarcs in some detail. Such analysis provides the very foundations upon which must be based any detailed study of the existence and admissibility of such subarcs.

In the following, we will identify the intermediate-thrust subarc by "I. T. S" or "$\epsilon_{var.}$ subarc". From Equations 2-17 and 2-36, we derive that the τ_5 multiplier is expressed by

$$\tau_5 = \frac{V_e}{m}\left\{\tau_1\left[\cos(\phi-\gamma) + \frac{C}{C+R\cos\phi}\cos\phi\cos\gamma\right] - \tau_2\frac{C}{C+R\cos\phi}\cos\gamma \right. \\ \left. - \frac{\tau_3}{R}\left[\frac{C}{C+R\cos\phi}\sin\phi\cos\gamma + \sin(\phi-\gamma)\right]\right\}. \tag{2-48}$$

Consequently, Equations 2-33, 2-48, and 2-6 lead to

$$\dot{\tau}_5 = -\frac{\dot{m}}{m}\tau_5 \quad , \quad \therefore \quad \tau_5 = \frac{K_5}{m} \, . \tag{2-49}$$

The latter equation and Equation 2-48 provide

$$\tau_1\left[\cos(\phi-\gamma)+\frac{C}{C+R\cos\phi}\cos\phi\cos\gamma\right]-\tau_2\frac{C}{C+R\cos\phi}\cos\gamma$$

$$-\frac{\tau_3}{R}\left[\frac{C}{C+R\cos\phi}\sin\phi\cos\gamma+\sin(\phi-\gamma)\right]=\frac{K_5}{V_e}=K_6=\text{const.} \tag{2-50}$$

Rearranging terms in the expression of the Hamiltonian (Equation 2-28), we see that it can be written

$$H=\epsilon\left\{\tau_1\frac{V_e}{m}\left[\cos(\phi-\gamma)+\frac{C}{C+R\cos\phi}\cos\phi\cos\gamma\right]-\tau_2\frac{V_e}{m}\frac{C}{C+R\cos\phi}\cos\gamma\right.$$

$$\left.-\tau_3\frac{V_e}{mR}\left[\frac{C}{C+R\cos\phi}\sin\phi\cos\gamma+\sin(\phi-\gamma)\right]-\tau_5\right\} \tag{2-51}$$

$$+\frac{C}{\mu}(C+R\cos\phi)^2(\tau_3+\tau_4)=K=\text{const.}$$

Thus, from Equations 2-36 and 2-51 follows that the Hamiltonian may be written

$$H=\epsilon\frac{\partial H}{\partial\epsilon}+\frac{C}{\mu}(C+R\cos\phi)^2(\tau_3+\tau_4)=K. \tag{2-52}$$

Since along the I. T. S., $H_\epsilon = 0$ (from Equation 2-17), then we obtain

$$\frac{C}{\mu}(C+R\cos\phi)^2(\tau_3+\tau_4)=K=\text{const.} \tag{2-53}$$

And therefore, from Equations 2-32 and 2-53,

$$\tau_3=K\frac{\mu}{C(C+R\cos\phi)^2}-K_4. \tag{2-54}$$

Note that since along the I. T. S, $\epsilon \neq 0$, Equation 2-34 implies

$$\tau_1\left[\sin(\phi-\gamma) - \frac{C}{C+R\cos\phi}\cos\phi\sin\gamma\right] + \tau_2\frac{C}{C+R\cos\phi}\sin\gamma + \frac{\tau_3}{R}\left[\frac{C}{C+R\cos\phi}\sin\phi\sin\gamma + \cos(\phi-\gamma)\right] = 0 \,. \tag{2-55}$$

Consequently, solving the preceding system of nonhomogeneous, algebraic equations for τ_1 and τ_2 (Equations 2-50 and 2-55) we can derive

$$\tau_1 = \frac{1}{R\tan\phi}\left[K_4 - \frac{\mu K}{C(C+R\cos\phi)^2}\right] + K_6\frac{\sin\gamma}{\sin\phi} \,, \tag{2-56}$$

$$\tau_2 = \frac{1}{R\sin\phi}\left[K_4 - \frac{\mu K}{C(C+R\cos\phi)^2}\right]\left[1 + \frac{C+R\cos\phi}{C}\right] - K_6\left\{\cos\gamma\,\frac{C+R\cos\phi}{C} - \frac{\cos\phi\sin\gamma}{\sin\phi}\left[1 + \frac{C+R\cos\phi}{C}\right]\right\} \,. \tag{2-57}$$

The preceding set of equations determines the multipliers $\tau_1, \ldots, \tau_5$ explicitly in terms of the state and control variables. It is interesting to note that the set of multipliers is independent of the control variable ϵ. The multipliers are determined along the I. T. S. once we know the control function $\gamma(t)$ and the initial (or "corner" values) of the constants K, K_4, and K_6.

2.4 FURTHER NECESSARY CONDITIONS: WEIERSTRASS CONDITION, MAXIMALITY PRINCIPLE AND LEGENDRE - CLEBSCH CONDITION

In addition to the previous necessary conditions, there are other necessary conditions which must be satisfied along any subarc forming the extremal. These conditions are: the Weierstrass condition and the Legendre-Clebsch Condition. The former is equivalent to the Maximality Principle of Pontryagin's. This principle can be readily derived from the Weierstrass condition upon introducing the Legendre transformation of the variational problem in canonical form.

The Weierstrass condition, using the canonical variables $(t, q_j, q_6, q_7, \tau_j)$, $j = 1, \ldots, 5$, requires that

$$W \equiv \Pi(t, q_j, q_6, q_7, \tau_j) - \Pi(t, q_j, q_6^*, q_7^*, \tau_j) - (\dot{q}_j - \dot{q}_j^*)\tau_j \geqq 0 \qquad (2\text{-}58)$$

at any point $(t, q_j, q_6^*, q_7^*, \tau_j) \in E$ (E = extremal) for any set $(t, q_j, q_6, q_7, \tau_j)$ pertaining to a differentiable admissible arc. Thus, Equation 2-58 implies a comparison between an admissible arc and the extremal E at a common point of coordinates (t, q_j, τ_j) which may be reached by both arcs with different controls. Along the admissible neighboring arc, $q_6 = q_6^* + \Delta q_6$, and $q_7 = q_7^* + \Delta q_7$. The increments used in Equation 2-58 may be arbitrary, provided the controls are admissible (i.e., between bounds if it is bounded). The increments Δq_j in Equation 2-58 are obtained from the "incremental equations" $\Delta\psi_j = 0 = \Delta\dot{q}_j - \Delta f_j$ (see Equation 2-1). Thus, the $\Delta\dot{q}_j$ are admissible for admissible control increments Δq_6, Δq_7 (i.e., $\Delta\gamma$, $\Delta\epsilon$). Note now that, introducing the Legendre transformation given by Equation 2-11, we can immediately express Equation 2-58 as the necessary condition

$$\Delta H \equiv H(t, q_j, q_6, q_7, \tau_j) - H(t, q_j, q_6^*, q_7^*, \tau_j) \leqq 0 . \qquad (2\text{-}59)$$

Equation 2-59 expresses Pontryagin's Maximum Principle which says that the optimum controls q_6^*, q_7^* maximize the Hamiltonian (for given t, q_j, τ_j).

The expansion of Equation 2-59 in Taylor series upon introducing $q_6 = \gamma$, $q_7 = \epsilon$ is written

$$\Delta H = \sum_{i=1}^{n} \frac{1}{i!} \left(\frac{\partial}{\partial\gamma} \Delta\gamma + \frac{\partial}{\partial\epsilon} \Delta\epsilon \right)^i H \Big|_{\gamma^*, \epsilon^*} \leqq 0 , \qquad (2\text{-}60)$$

which, expanded up to second order terms (i.e., assuming small variations $\Delta\gamma \to \delta\gamma$, $\Delta\epsilon \to \delta\epsilon$) implies the necessary condition of Legendre-Clebsch

$$\delta H = H_\gamma\,\delta\gamma + H_\epsilon\,\delta\epsilon + \frac{1}{2}H_{\gamma\gamma}(\delta\gamma)^2 + \frac{1}{2}H_{\epsilon\epsilon}(\delta\epsilon)^2 + H_{\gamma\epsilon}\,\delta\gamma\delta\epsilon \leqq 0. \quad (2\text{-}61)$$

Note now that, from Equations 2-16 through 2-19, we obtain that $H_\gamma = 0$, while $H_\epsilon\,\delta\epsilon \leqq 0$ in any case (i.e., for control interior or on the boundaries of the domain of admissible control). Thus, to investigate the character of the extremum, we need to examine the quadratic form in $\delta\gamma$, $\delta\epsilon$ in Equation 2-61.

From the theory of quadratic forms, it follows that the necessary and sufficient conditions for such forms to be definite negative for any set of control variations $(\delta\gamma, \delta\epsilon) \neq (0, 0)$ are

$$\begin{vmatrix} \frac{\partial^2 H}{\partial\gamma^2} & \frac{\partial^2 H}{\partial\gamma\partial\epsilon} \\ \frac{\partial^2 H}{\partial\epsilon\partial\gamma} & \frac{\partial^2 H}{\partial\epsilon^2} \end{vmatrix} < 0 \quad , \quad \frac{\partial^2 H}{\partial\gamma^2} < 0 \, . \quad (2\text{-}62)$$

The previous determinant is a symmetric Hessian since $H_{\gamma\epsilon} = H_{\epsilon\gamma}$. Calculating the necessary partial derivatives, we find

$$\frac{\partial^2 H}{\partial\epsilon^2} = 0 \, , \quad (2\text{-}63)$$

$$\frac{\partial^2 H}{\partial\epsilon\,\partial\gamma} = \frac{V_e}{m}\left\{\tau_1\left[\sin(\phi-\gamma) - \frac{C}{C+R\cos\phi}\cos\phi\sin\gamma\right] + \tau_2\frac{C}{C+R\cos\phi}\sin\gamma + \right.$$

$$\left. + \frac{\tau_3}{R}\left[\frac{C}{C+R\cos\phi}\sin\phi\sin\gamma + \cos(\phi-\gamma)\right]\right\} \, , \quad (2\text{-}64)$$

$$\frac{\partial^2 H}{\partial \gamma^2} = \frac{\epsilon V_e}{m}\left\{-\tau_1\left[\cos(\phi-\gamma)+\frac{C}{C+R\cos\phi}\cos\phi\cos\gamma\right]+\tau_2\frac{C}{C+R\cos\phi}\cos\gamma+\right.$$

$$\left.+\frac{\tau_3}{R}\left[\frac{C}{C+R\cos\phi}\sin\phi\cos\gamma+\sin(\phi-\gamma)\right]\right\}. \qquad (2\text{-}65)$$

Equation 2-63 vanishes because in our problem ϵ is a linear control. Equation 2-64, in view of Equation 2-34, leads to

$$H_{\epsilon\gamma} = \frac{H_\gamma}{\epsilon} = 0, \qquad (2\text{-}66)$$

while Equation 2-65, accounting for Equation 2-36, reduces to

$$H_{\gamma\gamma} = -\epsilon\left(H_\epsilon + \tau_5\right). \qquad (2\text{-}67)$$

Consequently, in our case, Equations 2-62, 2-63, 2-66, and 2-67 lead to the results

$$H_{\gamma\gamma}H_{\epsilon\epsilon} - \left(H_{\gamma\epsilon}\right)^2 = 0, \qquad (2\text{-}68)$$

and

$$H_{\gamma\gamma} \leq 0 \quad \text{if} \quad \left(H_\epsilon + \tau_5\right) \geq 0, \quad 0 < \epsilon \leq \epsilon_{max.}. \qquad (2\text{-}69)$$

As a result of the preceding analysis, we derive the following conclusions:

a. Control interior to the region of admissible control ($0 < \epsilon < \epsilon_{max.}$):

In this case (which corresponds to the I. T. S.), we have $H_\epsilon = 0$ and Equation 2-61 reduces to the quadratic terms in $\delta\gamma$, $\delta\epsilon$ only. In view of the fact that the Hessian vanishes, no statement on the type of extremum attained can be made. However, the inequality in Equation 2-69 still provides an important necessary condition which

must be satisfied along I. T. S. Along such subarcs, Equations 2-17 and 2-69 require

$$\zeta_5 \geq 0 \ . \tag{2-70}$$

Consequently, in accordance with Equations 2-49 and 2-50, it follows that

$$K_5 \geq 0 \quad , \quad K_6 \geq 0 \ . \tag{2-71}$$

Furthermore, since -- from Equations 2-33 and 2-36

$$\dot{\zeta}_5 = \frac{\epsilon}{m}\left(H_\epsilon + \zeta_5\right) \ , \tag{2-72}$$

we conclude, by use of Equations 2-69 and 2-72, that

$$\dot{\zeta}_5 \geq 0 \ . \tag{2-73}$$

b. Control on the Boundaries of admissible control (i.e., $\epsilon = 0$ or $\epsilon = \epsilon_{max.}$):

In this case, if $H_\epsilon = 0$ (weak form of Equations 2-18 and 2-19), then the immediately preceding conditions apply here also. However, if $H_\epsilon \neq 0$ (i.e., Equations 2-18 and 2-19 are satisfied in their strong form), then we will have a relative minimum along the boundaries of control. That is, there will exist a suitably small positive number $\rho > 0$ such that $H(\gamma^* + \delta\gamma\ ;\ \epsilon^* + \delta\epsilon) > H(\gamma^*,\ \epsilon^*)$ for any set of admissible variations $\delta\gamma$, $\delta\epsilon$ satisfying $(\delta\gamma)^2 + (\delta\epsilon)^2 < \rho$.

2.5 TREATMENT OF SPECIFIC PROBLEMS

As indicated in Section 2.4 the equations derived previously imply general necessary conditions because they have been obtained for the problem of minimizing a generalized function $\Upsilon(q_{j_I},\ q_{j_F},\ t_I,\ t_F)$ where $j = 1, \ldots,\ n=5$, subject to an arbitrary set of boundary conditions $X_s(q_{j_I},\ q_{j_F},\ t_I,\ t_F) = 0$ where $s = 1, \ldots,\ r \leq 2n + 1$.

For the treatment of specific problems, the previous necessary conditions are accordingly specialized once the function Υ and the boundary conditions X_s are given a definite form. In essence, this implies the determination of the particular values taken by the constants K, K_4 and K_6 which are fundamental in order to determine the adjoint functions along the I. T. S. and to study other subarcs. Also, stipulation of the Υ-function considered as well as the pertinent boundary conditions enables the development of further expressions, from those

already obtained, which apply specifically to the problem at hand and simplify its treatment.

Consequently, as a specific example, we will now consider the problem of optimal transfer with minimum fuel consumption between given terminal points where the central angle and the time of transfer are left unspecified.

2.5.1 MINIMUM FUEL CONSUMPTION, FREE-CENTRAL ANGLE, FREE-TIME

For this problem, the function Υ is written

$$\Upsilon = -m_F \quad , \tag{2-74}$$

and the boundary conditions are assumed to be of the form

$$\begin{aligned} X_1 &\equiv R_I - a = 0 \quad , & X_5 &\equiv m_I - e = 0, \\ X_2 &\equiv C_I - b = 0 \quad , & X_6 &\equiv t_I - f = 0, \\ X_3 &\equiv \phi_I - c = 0 \quad , & X_7 &\equiv R_F - g = 0, \\ X_4 &\equiv \nu_I - d = 0 \quad , & X_8 &\equiv C_F - h = 0, \\ X_9 &\equiv \phi_F - l = 0 \quad , & (a,b,c,..,l) &= const. \end{aligned} \tag{2-75}$$

As indicated in Section 1, this problem in hodographic terms implies a transfer between the points I and F which are located on the initial and final circles (C_I, R_I) and (C_F, R_F), respectively.

From the transversality condition and the equations of variation of the terminal conditions (Equations 2-26 and 2-27), we obtain the following subconditions of transversality for this case:

$$\left(\tau_{5_F} - 1\right) d m_F = 0 \ , \quad d m_F \neq 0 \quad \therefore \quad \tau_{5_F} = 1 \ , \tag{2-76}$$

$$\tau_{4_F} \, d \nu_F = 0 \ , \quad d \nu_F \neq 0 \ \therefore \ \tau_{4_F} = 0 \ , \ \tau_4 = K_4 = const. = 0 , \tag{2-77}$$

$$H_F \, d t_F = 0 \ , \quad d t_F \neq 0 \ \therefore \ H_F = 0 \ , \quad H = K = const. = 0 . \tag{2-78}$$

Since we are particularly interested in the conditions along the I. T. S. (or $\epsilon_{var.}$ subarc), we will restrict our attention to such a subarc in this subsection. Consequently, Equation 2-77 is applicable in our case (i.e., $H_\epsilon = 0$). Equations 2-54, 2-77, and 2-78 lead to

$$\tau_3(t) = 0 \ , \tag{2-79}$$

along I. T. S. Furthermore, Equations 2-56 and 2-57 reduce (due to Equations 2-77 and 2-78) to the set

$$\tau_1 = K_6 \ \frac{\sin \gamma}{\sin \phi} \ , \tag{2-80}$$

$$\tau_2 = - K_6 \left\{ \cos \gamma \, \frac{C + R \cos \phi}{C} - \frac{\cos \phi \sin \gamma}{\sin \phi} \left(1 + \frac{C + R \cos \phi}{C} \right) \right\} =$$

$$= K_6 \ \frac{C \cos \phi \sin \gamma - (C + R \cos \phi) \sin (\phi - \gamma)}{C \sin \phi} \ . \tag{2-81}$$

Upon substituting these values of τ_1, τ_2 and τ_3 into Equation 2-33, we obtain

$$\dot{\tau}_5 = \frac{\epsilon V_e}{m^2}\left\{K_6 \frac{\sin\gamma}{\sin\phi}\left[\cos(\phi-\gamma)+\frac{C}{C+R\cos\phi}\cos\phi\cos\gamma\right]-\right.$$
$$\left.-K_6\frac{C}{C+R\cos\phi}\cos\gamma\left[\frac{C\cos\phi\sin\gamma-(C+R\cos\phi)\sin(\phi-\gamma)}{C\sin\phi}\right]\right\}=$$
$$= K_6\frac{\epsilon V_e}{m^2}\,, \qquad (2\text{-}82)$$

since the terms between the key reduce to K_6. Equation 2-82 may also be readily obtained from Equations 2-6, 2-49, and 2-50, which lead to

$$\dot{\tau} = -\frac{\dot{m}}{m}\tau_5 = \frac{\epsilon}{m}\tau_5\,,$$
$$\tau_5 = \frac{K_5}{m} = \frac{K_6 V_e}{m} \quad \therefore \quad \dot{\tau}_5 = K_6\frac{\epsilon V_e}{m^2}\,. \qquad (2\text{-}83)$$

Equations 2-77, 2-79, 2-80, 2-81 and 2-83 form a set of equations defining the multipliers along the I. T. S. This particular set exhibits an important property: namely, that if K_6 vanishes, all the multipliers vanish and therefore no I. T. S. may exist. Thus, this condition implies the requirement that the necessary conditions derived in Equations 2-70, 2-71 and 2-73 must be satisfied in their strong forms: $\tau_5 > 0$, $\tau_5 > 0$, $K_6 > 0$, along the I. T. S. of the given problem. This finding points out clearly, as previously mentioned, the importance of the necessary condition of Equation 2-69. Note that, since $\tau_3 = 0 =$ const. along the I. T. S., Equation 2-31 and the preceding equations of this section lead to the necessary condition

$$\tau_1\left[\sin(\phi-\gamma)+\frac{C^2\cos\gamma\sin\phi}{(C+R\cos\phi)^2}\right]+\tau_2\frac{CR\cos\gamma\sin\phi}{(C+R\cos\phi)^2} =$$

$$\frac{\sin\gamma}{\sin\phi}\left[\sin\phi\cos\gamma-\cos\phi\sin\gamma+\frac{C^2\cos\gamma\sin\phi}{(C+R\cos\phi)^2}\right]- \tag{2-84}$$

$$-\frac{CR\cos\gamma\sin\phi}{(C+R\cos\phi)^2}\left[\cos\gamma\,\frac{C+R\cos\phi}{C}-\frac{\cos\phi\sin\gamma}{\sin\phi}\left(1+\frac{C+R\cos\phi}{C}\right)\right]=0\,,$$

which is obtained upon assuming that K_6 =const. $\neq 0$.

Upon subsequent reduction, Equation 2-84 provides the control variable γ (t) explicitly along I. T. S. as

$$\tan\gamma=\tan\phi\left[1\pm\sqrt{\frac{C}{C+R\cos\phi}}\right] \tag{2-85}$$

On the other hand, as seen from our previous equations, the control variable program ϵ (t) does not appear to be of any significant influence in our solutions. Since such control appears to be ineffective, the variable ϵ subarc (I. T. S.) appears to be of doubtful existence as a whole. This situation can be explicitly shown by noting that the set of multipliers can be dissociated into two noninteracting sets. In effect, from Equations 2-77, 2-79 2-80, 2-81 and 2-83, we find that the multipliers have the following functional dependence

$$\begin{aligned}
\tau_1&=\tau_1(K_6,\gamma,\phi)\,,\\
\tau_2&=\tau_2(K_6,\gamma,\phi,C,R)\,,\\
\tau_3&=\tau_4=0\,,\\
\tau_5&=\tau_5(K_6,m)=\frac{K_6\,V_e}{m}\,.
\end{aligned} \tag{2-86}$$

Only τ depends on m, which implies an indirect dependence on the mass-flow history.

The set ($\tau_1, \ldots, \tau_4$) is not interrelated with τ_5, which controls the thrust program, since its slope is related to ϵ by Equation 2-83. The indirect relation between the multipliers $\tau_1, \ldots, \tau_4$ and ϵ is only established through Equations 2-2 through 2-4. In view of the preceding conditions, the problem originally considered in accordance with Equation 2-74 may be equivalently posed as that of minimizing $\left|K_6 V_e\right|$ (since $\tau_{5_F} = 1$) along the $\epsilon_{var.}$ subarc.

Since, $\epsilon \neq 0$ along this subarc, then $V_e \neq 0$ and, consequently, the absolute minimum is obtained for $K_6 = 0$. However, as pointed out before, such a condition implies the non-existence of the I. T. S. for the present problem. Consequently, in our case, no I. T. S. may form part of the extremal.

The preceding application has been presented with the object of showing the treatment of one specific case as well as to demonstrate the use of the general conditions derived in the previous paragrpahs. Each minimal problem with given boundary conditions will require a similar analysis in order to determine the existence, admissibility, sequence and number of sub-arcs which may form the extremal solution.

References

1. Bliss, G. A., "Lectures on the Calculus of Variations", University of Chicago Press, Chicago, Illinois, 1946.

2. Cavoti, C. R., "The Calculus of Variations Approach To Systems Optimization", Journal für die reine and angew. Mathematik, Band 217, Seite 1 bis 48, 1965.

3. Cicala, P., "An Engineering Approach to the Calculus of Variations", Libreria Editrice Universitaria Levrotto & Bella, Torino, Italy, 1957.

4. Bolza, O., "Lectures on the Calculus of Variations", New York, Stechert-Hafner, Inc., 1946.

5. Lawden, D. F., "Optimal Intermediate-Thrust Arcs In A Gravitational Field", Astronautica Acts, Vol. VIII, Fasc, 2-3, 1962.

6. Lawden, D. F., "Optimal Powered Arcs in An Inverse Square Law Field", ARS Journal, April 1961.

7. Altman, S.P., and C.R. Cavoti, Phase Work Report IIIA-1, "Formal Presentation of the Hodographic Equations of Motion", January 1967.

8. Boltyanskii, V.G., R.V. Gamkrelidze, and L.S. Pontryagin, "The Theory of Optimum Control Processes, I: The Maximum Principle", Izvest. Akad. Nauk. SSR, Ser. Mat. 24, No. 1, (1960), pp. 3-42. Amer. Math. Soc. Transl. (2), 18 (1961), pp. 341-382.

SECTION 3

GENESIS OF THE PROBLEM
(ACCELERATION HODOGRAPH ANALYSIS OF POWERED ORBITAL TRAJECTORIES)

AUTHOR: SAMUEL P. ALTMAN

SECTION 3

GENESIS OF THE PROBLEM

(ACCELERATION HODOGRAPH ANALYSIS OF POWERED ORBITAL TRAJECTORIES)

3.1 ABSTRACT

The hodographic analysis of orbital trajectories subject to essentially impulsive thrust which provides instantaneous changes in the orbital velocity vector has been accomplished in velocity vector space. This general and unified treatment of all such orbital trajectories (i.e., for all conic sections and orbital energies in the presence of one force center) is achieved because an orbital hodograph in a given vector space presents directly, by means of line elements and angles, explicit and geometrically inter-related data not only on the trajectory vectors in that given vector space, but also on the vectors in all lower orders of vector space. For example, the orbital velocity hodograph shown in Figure 3-1 defines all orbital velocity components at each point of the orbit, and also the scalar magnitude and direction of the position or radius vector $\bar{r}$ defining that point in inertial space. Since an orbital trajectory is completely determined by the position and velocity states at each point of the trajectory*, the complete analysis may be accomplished in velocity vector space.

When the applied thrust is not essentially impulsive (i.e., of finite time-duration with varying thrust vector direction and magnitude), then hodographic analysis in velocity vector space is not well-defined, but approximate at best. However, the acceleration vector space is ideally suited for such analysis, especially since the acceleration due to applied thrust can be decomposed into differentials of the velocity hodograph parameters (C, R). This characteristic property of the acceleration hodograph is shown schematically by Figures 3-2 and 3-3, and analytically by the following equations of motion in two-dimensional space.+

---

* As a theoretical alternative, the orbital trajectory can be determined by the velocity and acceleration states at each point. However, most contemporary engineering applications work with sensor data on position and velocity state variables.

\+ The discussion is restricted to two-dimensional space only for convenience in discussion.

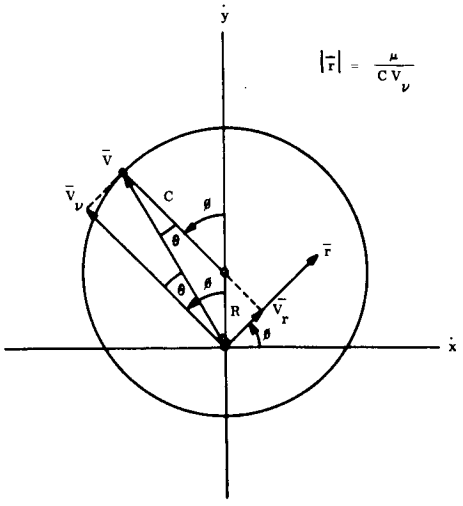

Figure 3-1. Hodographic Definition of Position and Velocity Vectors of an Orbit, in Velocity Vector Space

instantaneous ballistic acceleration — instantaneous applied acceleration

$$\ddot{x} = -C\dot{\upsilon}\cos\phi - \dot{C}\sin\phi - R\dot{\Psi} \tag{3-1}$$

$$\ddot{y} = -C\dot{\upsilon}\sin\phi + \dot{C}\cos\phi + \dot{R} \tag{3-2}$$

$$\ddot{x} = \ddot{x}_{ballistic} + \Delta\ddot{x} \tag{3-3}$$

$$\ddot{y} = \ddot{y}_{ballistic} + \Delta\ddot{y} \tag{3-4}$$

$$\Delta\ddot{x} = -\dot{C}\sin\phi - R\dot{\Psi} \tag{3-5}$$

$$\Delta\ddot{y} = \dot{C}\cos\phi + \dot{R} \tag{3-6}$$

$$-R\dot{\Psi} = \frac{\dot{C}}{C}\left(\frac{2C + R\cos\phi}{\sin\phi}\right) + \dot{R}\cot\phi \tag{3-7}$$

$$\dot{\upsilon} = \dot{\phi} + \dot{\Psi} \tag{3-8}$$

$$\dot{x} = -C\sin\phi \tag{3-9}$$

$$\dot{y} = R + C\cos\phi \tag{3-10}$$

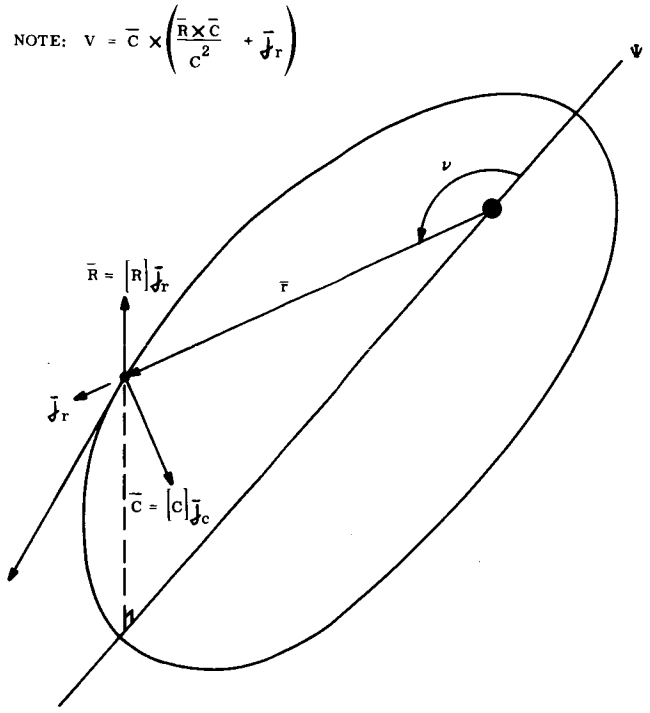

Figure 3-2. Schematic Diagram of Orbital Velocity Vectors in Vector Space

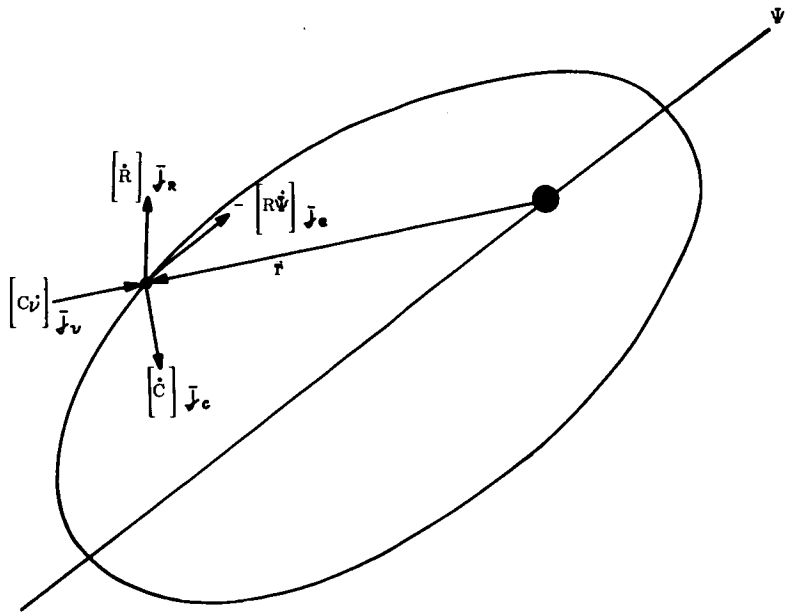

Figure 3-3. Schematic Diagram of Orbital and Applied Acceleration Vectors in Acceleration Vector Space

At this point, attention is directed to an outstanding feature of the methods of solution in advanced dynamics, which is consistently employed in many of the most difficult problems. In the initial formulation of a physical problem in rigid-body dynamics, time appears as the independent variable; that is, the differential or finite difference variation of significant state variables of solution (upon change in the value of the time) is determined. However, time is truly only a parameter, not an independent variable, since- in nonrelativistic mechanics, at least - time cannot be arbitrarily selected or varied. As a consequence, time may be eliminated from the complete equations of motion in many problems, i.e., when time is not explicitly evident. The analytical procedures and conditions of such a reduction in the dynamics equations are well-known in the classical literature, and extensively applied in many vital problems (References 1 and 2).

Moreover, time may be treated as a complex variable, rather than a real variable, as demonstrated by Kovalevskaya (Reference 3) in the problem of motion of a rigid body about a fixed point. In this treatment, time is arbitrarily selected in the complex plane so that "under some conditions, the complete integration of the differential equations, whose integrals have removable poles and have no other irregular points in the finite part of the plane of the independent variable, can be carried out quite independently of whether the problem reduces to quadratures or not."

Returning to the general orbital trajectory problem of space mechanics with one force center, the hodographic formulation of a powered orbital trajectory in acceleration vector space provides equations of motion by which time may be eliminated as the independent variable. Then the independent variable may be a convenient space variable which provides the most amenable analytic reduction for solution. This procedure can best be described by reference to Equations 3-5 and 3-6, in which the applied acceleration (i.e., due to sources other than the force center) is expressed in terms of the hodograph parameters (C, R) and the space variables (Ψ, ϕ), with time as the independent variable. Also, let us assume the applied acceleration is provided by thrust force alone* so that

* Other physical sources of applied acceleration, such as lift and drag forces during atmospheric passage, may be comparably treated.

$$\ddot{\Delta x} \equiv \frac{T_x}{m} \tag{3-11}$$

$$\ddot{\Delta y} \equiv \frac{T_y}{m} \tag{3-12}$$

where

$$T_x = T \sin(\nu + \gamma) = T \sin(\phi + \Psi + \gamma) \tag{3-13}$$

$$T_y = T \cos(\nu + \gamma) = T \cos(\phi + \Psi + \gamma) \tag{3-14}$$

since

$$\nu = \phi + \Psi \ , \tag{3-15}$$

and γ = angle between ordinate axis y and thrust vector $\overline{T}$.

Then

$$-\dot{C} \sin \phi - R \dot{\Psi} = (T/m) \sin(\phi + \Psi + \gamma) \tag{3-16}$$

$$\dot{C} \cos \phi + \dot{R} = (T/m) \cos(\phi + \Psi + \gamma) \tag{3-17}$$

where

$$-R\dot{\Psi} = \frac{\dot{C}}{C}\left(\frac{2C + R\cos\phi}{\sin\phi}\right) + \dot{R}\cot\phi \ .$$

Also,

$$\dot{\nu} = C\,(C + R\cos\phi)^2/\mu \ . \tag{3-18}$$

Let us assume that thrust is due to one propellant class* so that

$$T = -V_e \dot{m} \tag{3-19}$$

---

* This condition is imposed only for convenience in discussion. The use of fuels of different specific impulse, or different propulsion designs is not excluded in this general treatment.

$$\frac{T}{m} = -V_e\left(\frac{\dot{m}}{m}\right) \tag{3-20}$$

$$m = m_0 + \int \dot{m}\, dt = m_0 + \int dm \tag{3-21}$$

$$\frac{T}{m} = -V_e\left[\dot{m} / (m_0 + \int dm)\right] \tag{3-22}$$

where V_e is the velocity of the exhaust gases at the exit section of the rocket nozzle. The complete set of trajectory equations in terms of differentials with respect to time are summarized in Table 3-1.

Table 3-1. Hodographic Equations of Motion, As Functions of Time

Variables of Dynamic State: $C, R\ ;\ \Psi, \phi, v$

Control Variables: τ, m

Independent Variable: t

$$\dot{C}\cos\phi + \dot{R} = -V_e \cos(v+\tau)\left[\dot{m} / (m_0 + \int_{m_t} dm)\right] \quad \text{A}$$

$$\dot{C}\sin\phi + R\dot{\Psi} = V_e \sin(v+\tau)\left[\dot{m} / (m_0 + \int_{m_t} dm)\right] \quad \text{B}$$

$$-R\dot{\Psi} = \frac{\dot{C}}{C}\left(\frac{2C + R\cos\phi}{\sin\phi}\right) + \dot{R}\cot\phi \quad \text{C}$$

$$\dot{v} = C(C + R\cos\phi)^2/\mu \quad \text{D}$$

$$v = \Psi + \phi \quad \text{E}$$

First, note that the five equations and the initial conditions or values of the dynamic state variables define the trajectory completely in acceleration vector space. The velocity space state is determined, point for point, by Equations 3-9 and 3-10, and the position space state by the equation

$$r = \mu / C(C + R\cos\phi) \quad . \tag{3-23}$$

Consequently, the trajectory is completely defined in all state spaces by this set of five equations for acceleration vector space.

Equations A through D of Table 3-1 are transformed into Equations A through D of Table 3-2, respectively, upon multiplying each equation by $(dt/d\emptyset)$. Consequently, in acceleration vector space, the trajectory variation with respect to the space variable $\emptyset$, rather than time t, is defined by Equations A, B, C, and E only (of Table 3-2). Note that the instantaneous ballistic acceleration

$$a_b = -C\dot{v} \tag{3-24}$$

(reference Equations 3-1 and 3-2) is now defined by

$$a_b = -Cv' (d\phi/dt) \quad . \tag{3-25}$$

The physical significance of this vector or state space formulation cannot be effectively conceived without visualization and treatment of time and mass as state spaces.

Table 3-2. Hodographic Equations of Motion, as Functions of Space Variable

Variables of Dynamic State: $C, R ; \Psi, v ; t$

Control Variables: τ, m

Independent Variable: ϕ

$( )'$ denotes $\frac{d( )}{d\phi}$

$$C' \cos\phi + R' = -V_e \cos(v+\tau)\left[m'/(m_0 + \int_{m_\phi} dm)\right] \quad \text{A}$$

$$C' \sin\phi + R\Psi' = V_e \sin(v+\tau)\left[m'/(m_0 + \int_{m_\phi} dm)\right] \quad \text{B}$$

$$-R\Psi' = \frac{C'}{C}\left(\frac{2C + R\cos\phi}{\sin\phi}\right) + R'\cot\phi \quad \text{C}$$

$$t' = \mu/C(C + R\cos\phi)^2 \quad \text{D}$$

$$v = \Psi + \phi \quad \text{E}$$

3.2 TRAJECTORY LOCUS IN TIME STATE SPACE

The previous hodographic theory of trajectory analysis in state spaces has shown that an orbital trajectory is defined by its states at any given point in which the spacecraft may be located. An instant of time, referred to a given initial reference time, is only a parameter which enables the ordering of admissible state points defining the trajectory, in accordance with the equations of motion. Actually, a space variable, such as the central angle referred to a given inertially-fixed line through the force center, may be employed for this ordering of points comprising the trajectory. Then time is only significant or useful as a means of relating the state points of the trajectory (i.e., position, velocity, etc.) to other state points of the spacecraft (such as attitude orientation, thermal state, etc.), or to the corresponding state points of another orbital body, such as in interplanetary flight or earth rendezvous operations*.

---

* Note that many other states, such as thermal, are often direct functions of space variables rather than time.

Considering time as a state, a unique point in the time state space must correspond with the trajectory points in the other state spaces*, as a function of the space variable selected as the independent variable. Moreover, the locus of such points, defined as the time locus+ of the trajectory, should be obtainable from the trajectory locus (or hodograph) in any other state space (or vector space) by means of a geometric transformation. Let us consider the circular orbit, as shown in Figure 3-4A.

Assuming $t_o = 0$ when the orbit crosses the positive x-axis (i.e., at the circled point), the points $P_{\pi/2}$, P_{π}, $P_{3\pi/2}$, $P_{2\pi}$, ... which occur successively at central angle increments of $\pi/2$ will occur at equally spaced time intervals since the orbital velocity in inertial space is constant (i.e., $t_{\pi} = 2t_{\pi/2}$, $t_{3\pi/2} = 3t_{\pi/2}$, $t_{2\pi} = 4t_{\pi/2}$, ...). As shown in Figure 3-4B, plot the time locus for each trajectory point with scalar length proportional to the referenced time and directed identically with the corresponding trajectory point in position vector space (i.e., identical central angle). Then the set of these trajectory points in time state space is the time locus. The time locus for a circular orbit, shown in Figure 3-4B, is the Archimedes' spiral

$$t = [k, \phi] \exp(i\phi) \quad . \tag{3-26}$$

Note that the original and coordinate axes (t_x, t_y) of the time state space are respectively coincident with the origin and coordinate axes (x, y) of the position vector space. Consequently, the time state space definition of an orbital trajectory is never ambiguous since the time locus will always spiral outward from the origin, without closure or intersection.

---

* Hereafter, time will be referred to the time state space, rather than time vector space. The logic of the operations in time state space are significantly different from those of the usual vector analysis and yet to be comprehensively explored and understood. The term vector space will be reserved exclusively to describe the Newtonian vector spaces of position, velocity, acceleration....

+ The trajectory in time state space is defined as the time locus rather than the time hodograph, since hodograph refers to the locus of vectors.

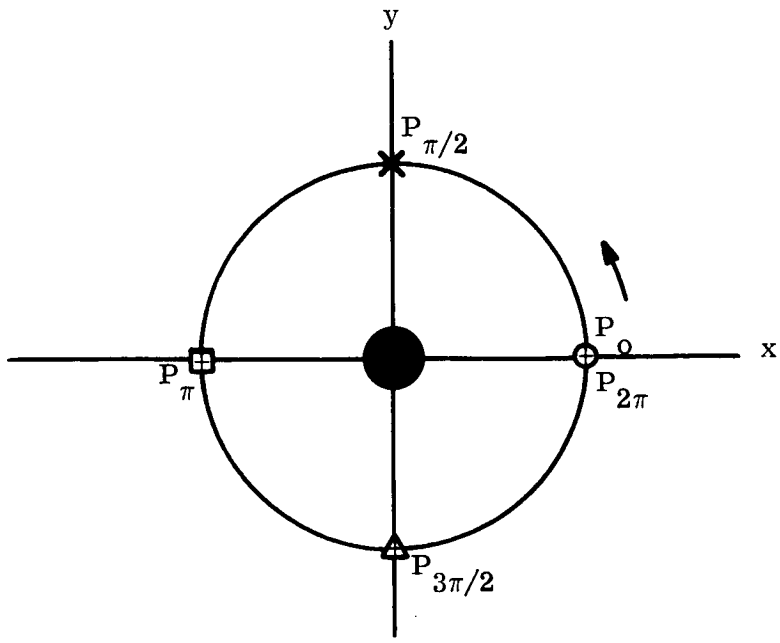

A. THE ORBIT IN POSITION VECTOR SPACE

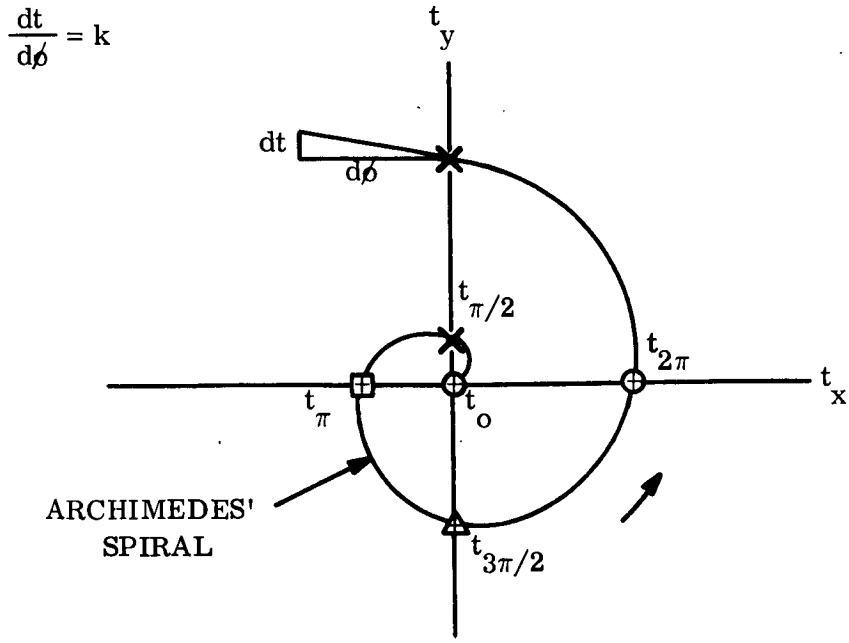

B. IN TIME STATE SPACE

Figure 3-4. The Time Locus of a Circular Orbit

The time locus of an elliptical orbit is shown schematically in Figure 3-5, compared with that for the circular orbit of equal period.

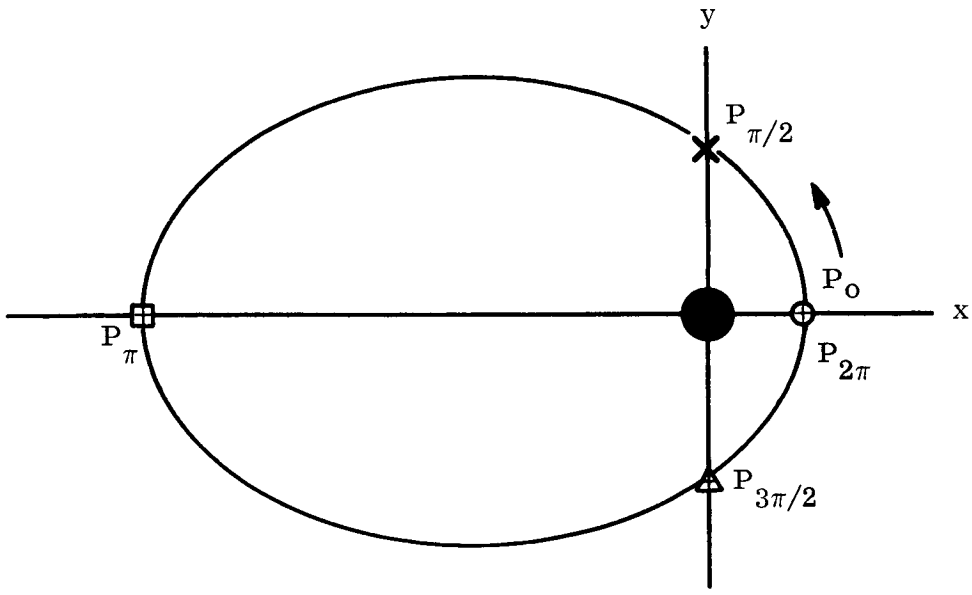

A. ORBIT IN POSITION VECTOR SPACE

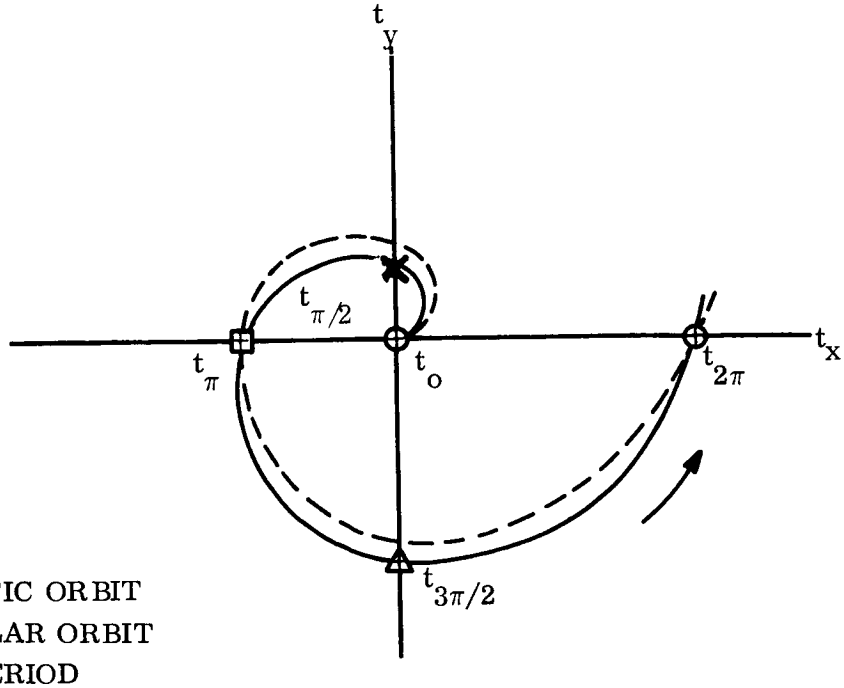

—— FOR ELLIPTIC ORBIT
--- FOR CIRCULAR ORBIT OF SAME PERIOD

B. IN TIME STATE SPACE

Figure 3-5. The Time Locus of an Elliptical Orbit

The time locus for any orbital trajectory must be obtainable upon transformation from any one Newtonian vector space. One task of this work phase is development of the direct and inverse transforms between the time locus in time state space and the trajectory hodograph in any one vector space. Consequently, corresponding points will be mapped conformally by geometric transformation.

The time locus is necessary for dynamics problems in which time constraints are imposed (rendezvous, interplanetary flight, etc).

3.3 TRAJECTORY LOCUS IN MASS STATE SPACE

Referring to Equations A and B of Table 3-2, it is apparent that the vehicle mass m may vary with the space variable $\emptyset$. Since the mass is defined at each value of this space variable, a trajectory locus in mass state space can be generated, dependent upon the functional law or control process governing mass expenditure*. If the mass expenditure is principally due to fuel consumption for propulsion, then the engine control laws will identify the mass loss function with high fidelity.

If the mass is constant, as in ballistic flight, the mass locus will be a circle as shown in Figure 3-6. All trajectories with mass loss will approach the origin as the vehicle proceeds along its trajectory. For example, a constant rate of mass loss will cause a continuous locus of spiral-like form to be generated, as shown schematically in Figure 3-6. Note that this mass locus would be an Archimedes' spiral if the point-mass dynamics were not consequently affected.+ For mass loss occurring with applied thrust affecting the point-mass motion, the space variable $\emptyset$ will be altered from that for ballistic motion.

---

* Theoretically, the vehicle mass may be increased rather than decreased, by natural as well as synthetic means. However, only mass loss is anticipated as an engineering condition within the immediate future.

\+ If the constant mass loss is due to propulsion for attitude orientation control only, then the mass locus would be an Archimedes' spiral.

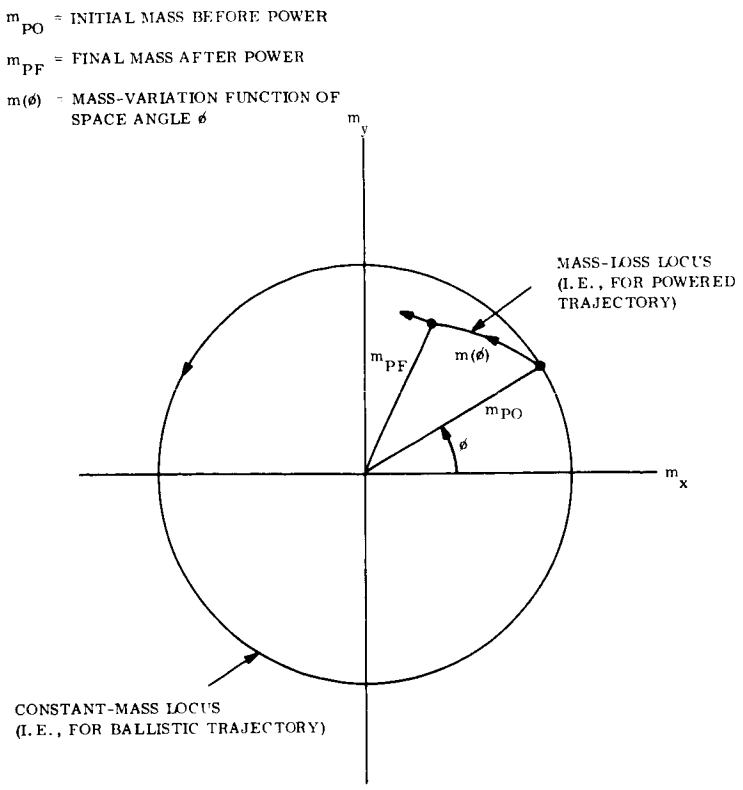

Figure 3-6. The Mass Locus of an Orbit or Trajectory

The trajectory is uniquely determined by the time locus since all hodographs in the Newtonian vector spaces could then be generated from it. Joint use of the mass and the functional law of mass loss can also provide complete trajectory determination. For a given mass loss law, the trajectory in any other vector or state space must be obtainable from the mass locus by transformation, point-by-point. One task of this work phase is development of the direct and inverse transforms between the mass locus in mass state space and the trajectory hodograph (or locus) in any one vector space (or state space). The transforms will be geometric transformations. Note that the mass state space is so described rather than as the mass vector space for the same reason as for the time state space (see footnote on page 3-9).

The mass locus can be extremely valuable in maximum effective use of existing propulsion control systems, or the advanced design of new propulsion controls. That is, propulsion thrust can be monitored by the use of control loop command inputs as direct functions of the space variable ($\emptyset$), rather than programming the control loop performance as a function of time.

3.4 SYNTHESIS OF THE ACCELERATION HODOGRAPH FOR A POWERED TRAJECTORY

Ballistic trajectories may be analyzed in position, velocity or acceleration vector spaces. Whenever the interdependence of trajectory states becomes crucial in a trajectory problem (such as in orbit determination or guidance sensor error prediction), then analysis in velocity or acceleration vector space becomes eminently desirable. For powered trajectories in which velocity vector changes are provided by essentially impulsive thrust, velocity space analysis has proven most suitable; the greatest part of preceding hodographic analysis techniques has been directed to this vector space. In such analysis, the mass changes need not be treated immediately but deferred until the complete trajectory is synthesized or defined in terms of its position and velocity states. Also, time constraints can be treated in the velocity vector space directly* (Reference 4). Consequently, such velocity vector space analysis can be carried out in two successive steps:

a. Synthesize the required or desired trajectory in velocity vector space;

b. Synthesize the propulsion design (and consequently, the mass loss law) which will provide the trajectory of Step (a) preceding.

If the mass loss law is a direct function of time, then the time locus in time state space (or any equivalent analytical treatment) must be used or the mass loss law transformed into a function of the space variable for analysis in the mass state space. That is, Step (a) synthesis is carried out in velocity vector space and Step (b) synthesis in mass state space.

---

* Further development of the analysis techniques in velocity vector space, with time constraints, is possible and desirable. The projected task on time state space should prove useful in such development work.

Referring to Table 3-2, it can be seen that the preceding methodology of velocity vector space analysis can be extended, in analogous fashion, to acceleration vector space analysis of powered trajectories subject to thrust forces which may be of finite time duration, and variable in magnitude and vector direction. Noting that the control variables (γ, m) are freely selectable, Equations (A), (B), (C) and (E) of Table 3-2 show that trajectory analysis (as in Step (a) above) can be completely carried out in the acceleration vector space whenever time constraints are not imposed. If time constraints are present, then both the acceleration vector space and time state space must be concurrently used in Step(a) analysis, unless direct representation of time in the acceleration vector space is available (as for velocity vector space). In either case, Step(b) may then be carried out as noted previously.

Two alternative aerospace system design problems must be solvable by any complete methodology of trajectory analysis, for effective and versatile engineering utility:

A. Assuming complete freedom of propulsion design, select an applied acceleration history which will generate a trajectory fulfilling specified constraints on the states, then develop the propulsion design (consequently, the mass loss law) which will fulfill the trajectory requirements.

B. Given the performance characteristics of a propulsion design (consequently, the mass loss law), determine the classes of trajectories which may be attainable, and the conditions upon the dynamic states (i.e., position, velocity and acceleration) and time state. Finally, provide or identify criteria for ranking and choice of the propulsion/trajectory design alternatives.

In essence, the design problem defined in Step (B) is the converse (or inversion) of design problem given in Step (A). Consequently, the analytical techniques for each procedure are different in detail, although functionally related throughout. This work phase will develop the acceleration state space techniques of analysis for the design problem in Step (A). One outstanding task is the analytical generation of a powered trajectory hodograph*, given the

* A powered trajectory hodograph is defined as the locus curve of successive points on the instantaneous orbital acceleration hodographs of the continuum (or set) of hodographs for the complete powered trajectory.

initial ballistic trajectory hodograph and an arbitrarily specified applied acceleration history (as a function of time, or of a space variable). In the initial study phase, the applied acceleration history is assumed to be available as a function of space variable ν. This problem is illustrated schematically in Figure 3-7.

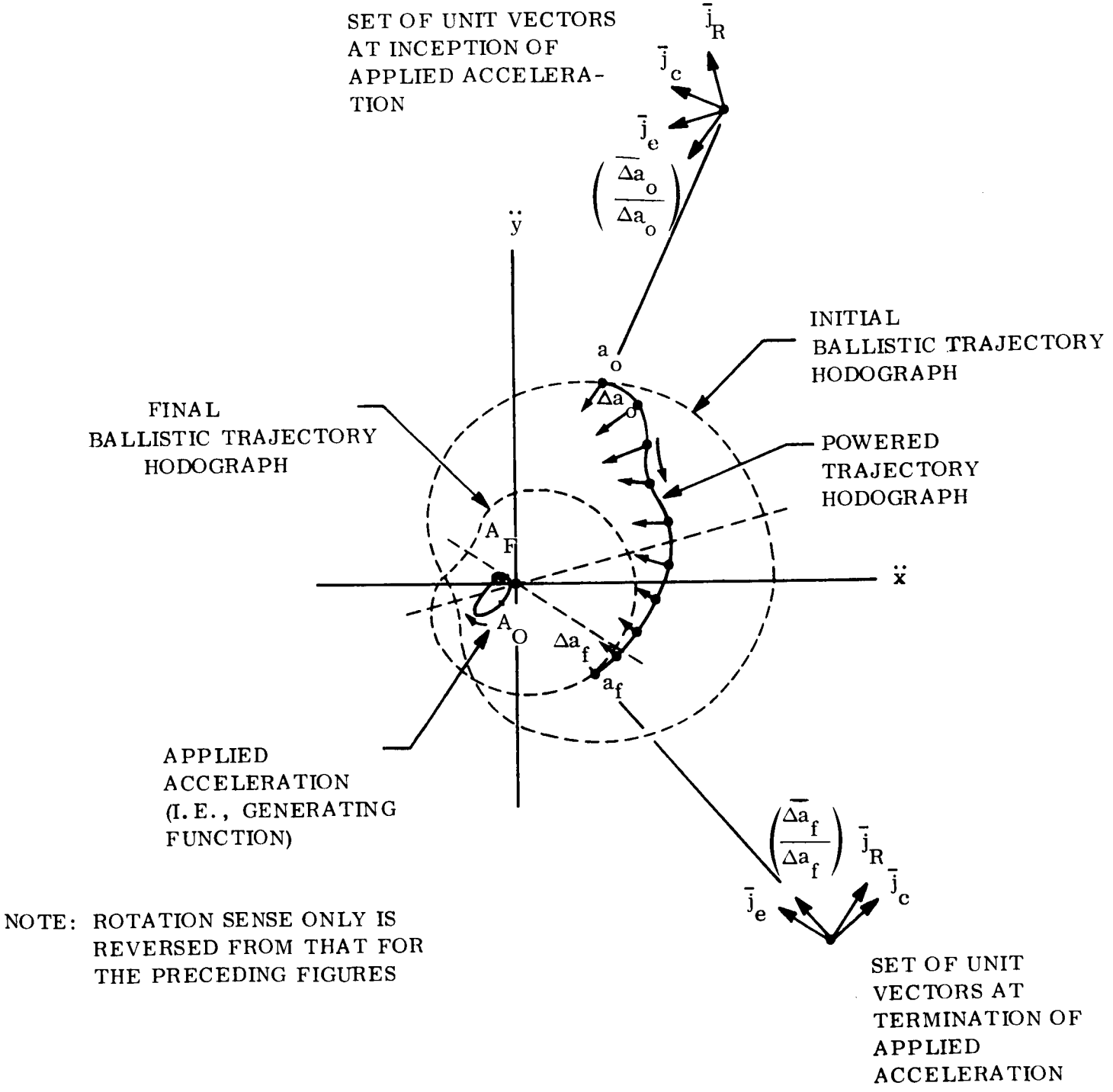

NOTE: ROTATION SENSE ONLY IS REVERSED FROM THAT FOR THE PRECEDING FIGURES

Figure 3-7. The Acceleration Hodograph of a Powered Trajectory

At the point or time of thrust inception (A_o), the unit vectors of the acceleration per unit mass are orientated relative to the initial ballistic trajectory hodograph, as shown. Consequently, the applied acceleration vector ($\bar{\Delta q}_o$) can be decomposed into its constituent vectors $\left[\dot{R}\right], \bar{i}_R, \left[\dot{C}\right], \bar{i}_C, \left[R\,\Psi\right], \bar{i}_e$ which define the differential change in the instantaneous hodograph. The terminal vector of applied acceleration ($\bar{\Delta q}_f$) can also be decomposed into its constituent vectors $\left[\dot{R}\right], \bar{i}_R \left[\dot{C}\right], \bar{i}_C, \left[R\ \dot{\Psi}\right], \bar{i}_e$. As the result of the complete history of applied acceleration ($\Delta q_o \rightarrow \Delta q_f$) or ($A_o \rightarrow A_f$), the powered trajectory hodograph will be the locus of successive points on instantaneous ballistic trajectory hodographs. Consequently, any point on the powered trajectory hodograph and the tangent line to that hodograph at that point define the acceleration hodograph of the instantaneous ballistic trajectory. As shown in Figure 3-8, the instantaneous acceleration hodograph provides the velocity and position data which define the instantaneous velocity hodograph and conic section of orbit. As an alternative, the hodograph inverse transforms may be used for point-to -point transformation by means of algebraic functions (Reference 4).

The second phase of the design problem in Step (B), aboverequires development of the mass and time loci. Finally, the necessary and sufficient conditions upon the trajectory will be developed for various optimization criteria (e. g., minimum fuel, least time, etc.).

Since the powered trajectory hodograph in acceleration vector space can be generated by a differential process, as shown upon reference to Table 3-2 and Figures 3-7 and 3-8, it appears most promising to employ the methods of differential geometry (Reference 5). In the differential geometry, the Serret-Frenet vector formulae

$$\left.\begin{aligned} \frac{d\bar{j}_T}{ds} &= \kappa \bar{j}_\kappa \\ \frac{d\bar{j}_\kappa}{ds} &= -\kappa \bar{j}_T + \lambda \bar{j}_z \\ \frac{d\bar{j}_z}{ds} &= -\lambda \bar{j}_\kappa \end{aligned}\right\} \qquad (3\text{-}27)$$

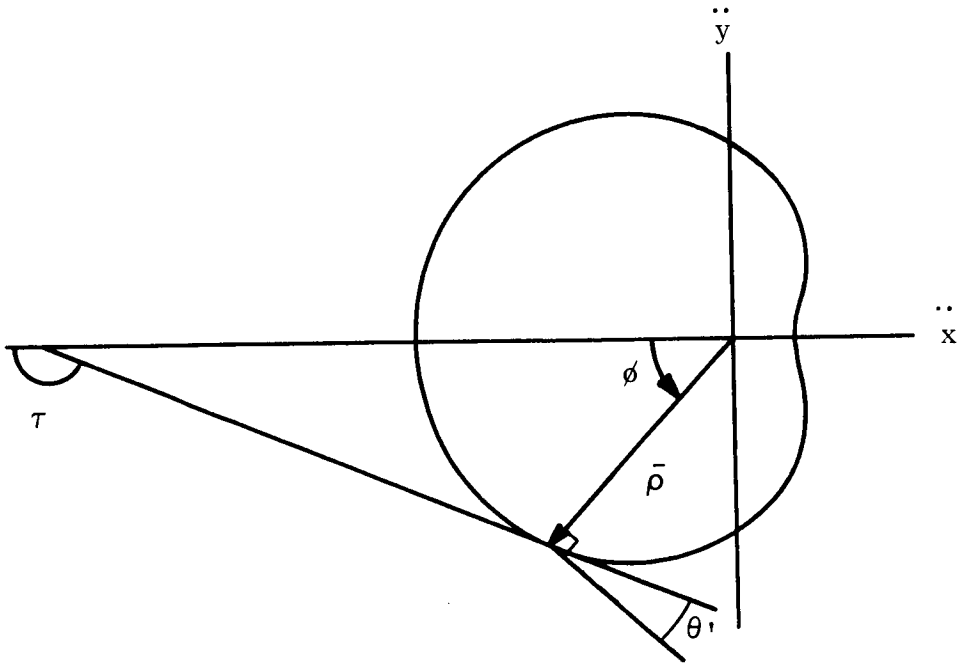

		ACCELERATION		VELOCITY		POSITION
MODULUS	$\left[\bar{\rho}\right]$	=	$\frac{(CV_\nu)^2}{\mu}$	=	$\frac{\mu}{r^2}$
ARGUMENT	$\left[\bar{\rho}\right]$	=	$\phi_w + \frac{\pi}{2} + \theta$	=	$\phi + \pi$
	θ'	=	$\arctan\left(\frac{2V_r}{V_\nu}\right)$	=	$\arctan(2\tan\theta)$

Figure 3-8. An Orbital Acceleration Hodograph, and Its Equivalent Definition in Other Vector Spaces

define the vector motion of the "moving trihedron" along a three-dimensional space curve. The tangent vector $\bar{j}_T$, principal normal vector $\bar{j}_k$ and binormal vector $\bar{j}_z$ are an orthogonal set which define the osculating plane $(\bar{j}_T, \bar{j}_k)$, the normal plane $(\bar{j}_k, \bar{j}_z)$, and the rectifying plane $(\bar{j}_z, \bar{j}_T)$. The scalars of Equation 3-27 are the curvature K and the torsion λ. For the two-dimensional problem, the torsion λ is zero so that the Serret-Frenet vector formulae for the acceleration hodograph are

$$\left.\begin{aligned} \frac{d\bar{j}_T}{ds} &= \kappa \bar{j}_\kappa \\ \frac{d\bar{j}_\kappa}{ds} &= -\kappa \bar{j}_T \end{aligned}\right\} \qquad (3\text{-}28)$$

where the curvature is

$$K = \frac{d\tau}{ds} = \frac{\cos^3\theta'}{\rho}\left(1 + \cot\phi \tan\theta' + \frac{3}{2}\tan^2\theta'\right) . \qquad (3\text{-}29)$$

Initial study will be directed to use of the Serret-Frenet vector formulation, together with the parametric resolution (or decomposition) of applied acceleration $\Delta\bar{A}$ into the acceleration hodograph differentials C', R', RΨ'. Noting that the vectors $(\bar{j}_c, \bar{j}_R, \bar{j}_e)$ comprise a nonorthogonal set, the use of this nonorthogonal set in lieu of the orthogonal set $(\bar{j}_T, \bar{j}_\kappa, \bar{j}_z)$ might nevertheless prove advantageous; in any case, it appears that transformation between these vector sets may be essential in development of the required synthesis techniques.

An outstanding attraction in use of the differential geometry for hodograph analysis is the potential use of geodesics theory of curves and surfaces to obtain the necessary and sufficient conditions for optimization criteria.

References

1. H.C. Plummer, An Introductory Treatise on Dynamical Astronomy, Dover Publications, New York, 1960.

2. C.G.J. Jacobi, Vorlesungen über Dynamik, 2nd revised edition, G. Reiner, Berlin, 1884, 21st lecture.

3. V.V. Golubev, Lectures on Integration of the Equations of Motion of a Rigid Body About a Fixed Point, Moscow, 1953 (Translation from Russian under OTS 60-21163, Monson, Jerusalem, 1960).

4. S.P. Altman, Orbital Hodograph Analysis, Vol. 3, AAS Science and Technology Series, Western Periodicals 1965, Chapter 3.

5. D.J. Struik, Differential Geometry, Addison-Wesley, Reading, Mass., 1961.

SECTION 4

TRANSFORMATION FUNCTIONS OF THE ORBITAL HODOGRAPHS

AUTHORS: SAMUEL P. ALTMAN
JOSEF S. PISTINER

SECTION 4

TRANSFORMATION FUNCTIONS OF THE ORBITAL HODOGRAPHS

It has been shown (Reference 1) that the orbital hodographs in Newtonian vector spaces (position, velocity, acceleration, etc.) may be mapped point-by-point, from any one vector space into another. That is, the dynamic constraints of the equations of motion produce unique classes of geometric curves (in the Newtonian vector spaces) which define the orbital trajectory completely. These geometric curves are conformal maps which are related by hodograph transformations. With the coordinates and curve slope at any one trajectory state point, all other corresponding state points are directly obtainable by use of the algebraic function of the hodograph transform, without quadrature (or formal integration).

The hodograph transformations are key analytical tools for use in both Work Phases II and III. Moreover, they should be invaluable in future development of large-scale computer programs founded upon the hodographic formulation of the trajectory equations of motion.

Some notation conventions employed in Reference 1 are inconsistent with the conventions of complex variable theory. Also, the real and imaginary components of some transform functions are in error. Consequently, this section presents a complete revision of the hodograph transformation functions - direct and inverse.

4.1 NOTATION CONVENTIONS

The positive inertial coordinate axes (i.e., $x, \dot{x}, \ddot{x}; y, \dot{y}, \ddot{y}$) referred to the space coordinate origin are directed to the right or up, respectively. The positive rotating coordinate axes (i.e., $r, V_r, A_r; r\phi, V_\nu, A_\nu$) referred to the satellite center-of-mass are directed outward from the space coordinate origin or transverse to the radius in the orbital plane in the sense of orbital flight, respectively. All central angles (e.g., ν, ϕ, Ψ) are defined as positive for counterclockwise rotation. Consequently, a typical set of orbital hodographs in position, velocity and acceleration vector spaces will appear as shown schematically in Figure 4-1. Note that the apsidal line in position vector space is coincident with the positive x-axis, and apogee passage at orbit intersection with the negative x-axis.

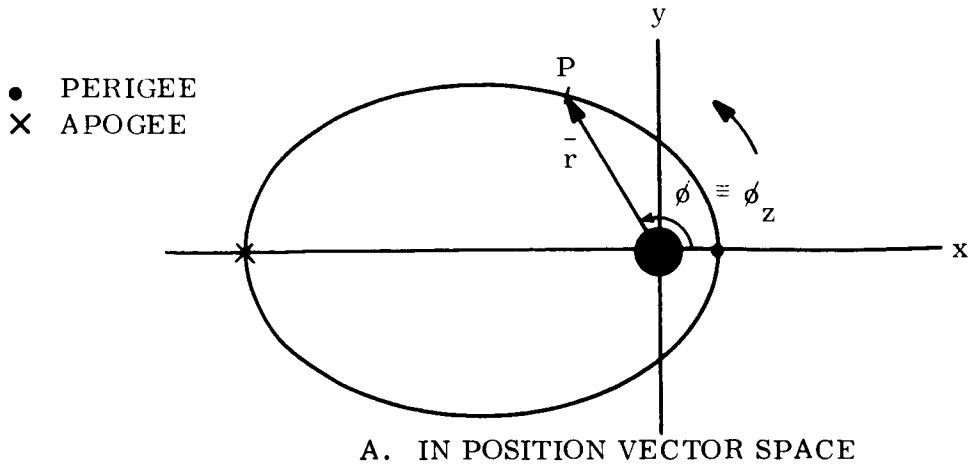

A. IN POSITION VECTOR SPACE

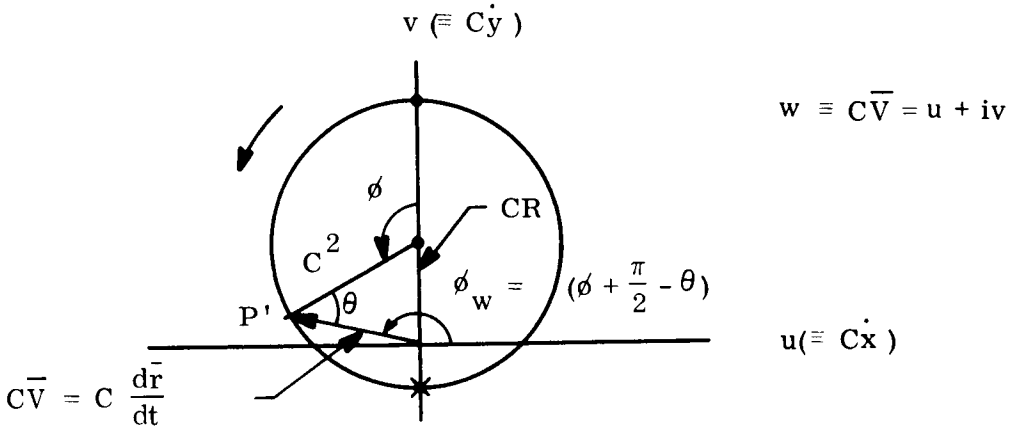

B. IN VELOCITY (OR POTENTIAL) VECTOR SPACE

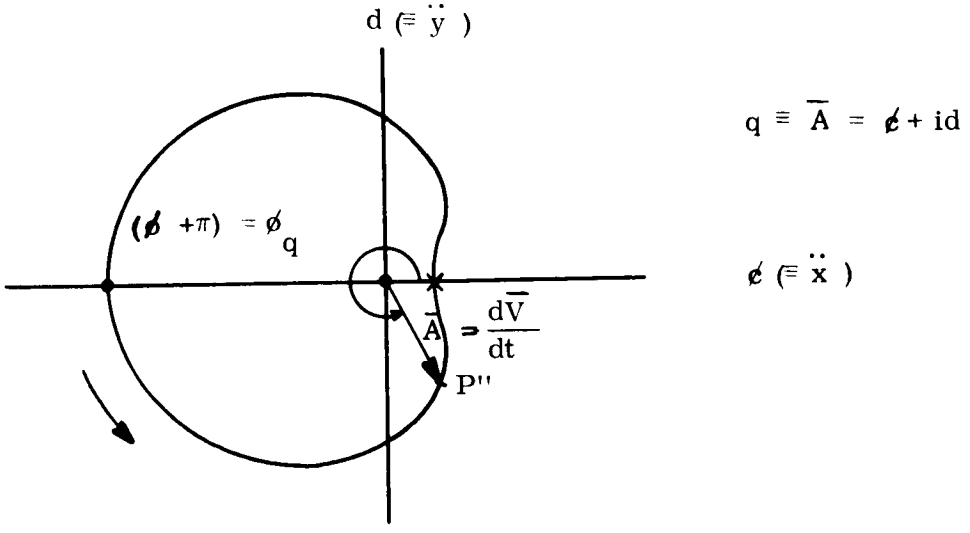

C. IN ACCELERATION VECTOR SPACE

Figure 4-1. Vector Space Maps of an Orbit

4.2 ORBITAL HODOGRAPHS

4.2.1 POSITION

Let $$z \equiv \bar{r} = x + iy \tag{4-1}$$

or $$z = r \exp(i\phi_z) \ . \tag{4-2}$$

Since

$$C = \frac{r}{\mu V_\nu} \tag{4-3}$$

and

$$V_\nu = C + R \cos \phi \ , \tag{4-4}$$

$$x = r \cos \phi = \frac{\mu \cos \phi}{C(C + R \cos \phi)} \tag{4-5}$$

$$y = r \sin \phi = \frac{\mu \sin \phi}{C(C + R \cos \phi)} \tag{4-6}$$

or

$$z = \left[\frac{\mu}{C(C + R \cos \phi)} \right] \exp(i\phi_z) \ . \tag{4-7}$$

Also,

$$\tan \phi_z = \frac{\sin \phi}{\cos \phi} = \tan \phi \tag{4-8}$$

so that

$$\phi_z \equiv \phi \ . \tag{4-9}$$

4.2.2 VELOCITY

Let $$w = u + iv = CV_x + iCV_y \ . \tag{4-10}$$

But

$$CV_x = -C^2 \sin \phi \tag{4-11}$$

$$CV_y = CR + C^2 \cos \phi \tag{4-12}$$

so that

$$w = -C^2 \sin\phi + i\,(CR + C^2\cos\phi) \tag{4-13}$$

$$w = C^2(-\sin\phi + i\cos\phi) + i(CR) \tag{4-14}$$

$$w = C^2 \exp\left[i\left(\phi + \tfrac{\pi}{2}\right)\right] + i(CR) \tag{4-15}$$

or

$$w = [CV]\exp(i\phi_w) \tag{4-16}$$

where

$$V = \sqrt{V_x^2 + V_y^2} \quad . \tag{4-17}$$

Now

$$\tan\theta = \frac{V_r}{V_v} = \frac{R\sin\phi}{C + R\cos\phi} \tag{4-18}$$

so that

$$\tan(\phi - \theta) = \frac{\tan\phi - \tan\theta}{1 + \tan\phi\tan\theta} \tag{4-19}$$

$$\tan(\phi - \theta) = \frac{C\sin\phi}{R + C\cos\phi} \quad . \tag{4-20}$$

But

$$\tan\phi_w = \frac{R + C\cos\phi}{-C\sin\phi} \tag{4-21}$$

so that

$$\tan(\phi - \theta) = -\cot\phi_w \tag{4-22}$$

or

$$\phi_w = \frac{\pi}{2} + (\phi - \theta) = \phi_z + \left(\frac{\pi}{2} - \theta\right) . \tag{4-23}$$

4.2.3 ACCELERATION

Let

$$q = \phi + id = A_x + iA_y \,. \tag{4-24}$$

But

$$A_x = -C\dot{v}\cos\Phi \tag{4-25}$$

$$A_y = -C\dot{v}\sin\Phi \tag{4-26}$$

where

$$\dot{v} = \dot{\Phi} + \dot{\Psi} \tag{4-27A}$$

so that

$$q = \left[C\dot{v}\right]\exp\left[i(\Phi+\pi)\right] \tag{4-28}$$

or

$$q = \left[C\dot{v}\right]\exp(i\Phi_q) \tag{4-29}$$

where

$$\dot{v} = \frac{C}{\mu}(C+R\cos\Phi)^2 \quad , \tag{4-27B}$$

$$C\dot{v} = \frac{\mu}{r^2} \quad , \tag{4-30}$$

and

$$\Phi_q = \Phi + \pi \equiv \Phi_z + \pi \quad . \tag{4-31A}$$

4.3 DIRECT HODOGRAPH TRANSFORMATIONS

A direct hodograph transformation is defined as the function which operates upon a trajectory state point in a lower order of Newtonian vector space, in order to obtain the corresponding trajectory state point in any higher order of Newtonian vector space. For example, to obtain a velocity or acceleration hodograph point directly from the coordinates and curve slope at a trajectory state point in position vector space (that is, P' or P'' from P in Figure 4-1).

Given the position, velocity and acceleration hodographs as defined by Equations 4-1 through 4-31, the direct transformations will be developed here. As noted in Chapter 2 of Reference 1, the geometric properties of the hodographs were vital in identifying the basic geometric transformation for this synthesis - the pedal transformation (Reference 2).

4.3.1 (DT1) POSITION → VELOCITY:

$$x = \frac{\mu \cos\phi}{C(C+R\cos\phi)}$$

and

$$y = \frac{\mu \sin\phi}{C(C+R\cos\phi)} \quad .$$

Since

$$y' = \frac{dy}{dx} = \frac{\dot{y}}{\dot{x}} = \frac{V_y}{V_x} = \frac{R+C\cos\phi}{-C\sin\phi} \quad , \tag{4-32A}$$

then

$$y - xy' = \frac{\mu \sin\phi}{C(C+R\cos\phi)} + \frac{\mu\cos\phi}{C(C+R\cos\phi)} \cdot \frac{R+C\cos\phi}{C\sin\phi} \tag{4-33A}$$

$$= \frac{\mu}{C^2 \sin\phi} = \frac{\mu}{-CV_x} \quad . \tag{4-33B}$$

But

$$u = CV_x \tag{4-34A}$$

so that

$$y - xy' = -\frac{\mu}{u} \tag{4-33C}$$

or

$$u = -\frac{\mu}{y - xy'} \quad . \tag{4-34B}$$

Also,

$$v = CV_y \tag{4-35A}$$

and

$$y' = \frac{v}{u} \tag{4-32B}$$

or

$$v = u y' \tag{4-35B}$$

so that

$$v = -\frac{\mu y'}{y - x y'} \quad . \tag{4-35C}$$

Consequently

$$w = u + iv = -\frac{\mu}{y - x y'} - i\frac{\mu y'}{y - x y'} \tag{4-36A}$$

$$= \frac{\mu}{y - x y'}(-1 - i y') \tag{4-36B}$$

$$w = \left[\frac{\mu}{y - x y'}\sqrt{1 + y'^2}\right] \exp(i\phi_w) \tag{4-36C}$$

or

$$w = \left[\frac{\mu}{y - x y'}\sqrt{1 + y'^2}\right] \exp\left[i\left(\frac{\pi}{2} + \phi_z - \theta\right)\right] \quad . \tag{4-36D}$$

4.3.2 (DT2) VELOCITY → ACCELERATION:

Since

$$v' = \frac{dv}{du} = \frac{\dot{v}}{\dot{u}} = \frac{A_y}{A_x} = \tan\phi \tag{4-37}$$

then

$$v - u v' = C V_y - C V_x \tan\phi \tag{4-38A}$$

$$= C(R + C\cos\phi) - C(-C\sin\phi)\tan\phi \tag{4-38B}$$

$$= CR + C^2\cos\phi + C^2\left(\frac{\sin^2\phi}{\cos\phi}\right) \tag{4-38C}$$

$$= CR + C^2\sec\phi \tag{4-38D}$$

$$v - u v' = \frac{C(C + R\cos\phi)}{\cos\phi} \tag{4-38E}$$

so that

$$(v-uv')^2 = \frac{C^2(C+R\cos\phi)^2}{\cos^2\phi} \quad . \tag{4-39A}$$

Referring to Equation 4-27B, it is seen that

$$(v-uv')^2 = \frac{C(\mu\dot{v})}{\cos^2\phi} \quad . \tag{4-39B}$$

Also,

$$1+v'^2 = 1+\tan^2\phi = \sec^2\phi \tag{4-40}$$

or

$$(1+v'^2)^{\frac{3}{2}} = \sec^3\phi \tag{4-41}$$

so that

$$-\frac{(v-uv')^2}{\mu(1+v'^2)^{3/2}} = -C\dot{v}\cos\phi \tag{4-42}$$

or

$$\phi' = -\frac{(v-uv')^2}{\mu(1+v'^2)^{3/2}} \quad . \tag{4-43}$$

Referring to Equation 4-37, it is seen that

$$-\frac{v'(v-uv')^2}{\mu(1+v'^2)^{3/2}} = \tan\phi\,(-C\dot{v}\cos\phi) \tag{4-44A}$$

$$= -C\dot{v}\sin\phi \tag{4-44B}$$

so that

$$d = -\frac{v'(v-uv')^2}{\mu(1+v'^2)^{3/2}} \quad . \tag{4-45}$$

Consequently,

$$q = \ddot{\xi} + i\ddot{d} = -\left[\frac{(v-uv')^2}{\mu(1+v'^2)^{3/2}}\right] - i\left[\frac{v'(v-uv')^2}{\mu(1+v'^2)^{3/2}}\right] \tag{4-46A}$$

$$= \frac{(v-uv')^2}{\mu(1+v'^2)^{3/2}}(-1-iv') \tag{4-46B}$$

$$q = \left[\frac{(v-uv')^2}{\mu(1+v'^2)}\right]\exp(i\phi_q) \tag{4-46C}$$

or

$$q = \left[\frac{(v-uv')^2}{\mu(1+v'^2)}\right]\exp\left[i\left(\frac{\pi}{2}+\phi_w+\theta\right)\right] \quad . \tag{4-46D}$$

4.3.3 (DT3) POSITION → ACCELERATION:

Referring to Equations 4-30, 4-25, and 4-26, it is seen that

$$\ddot{\xi} \equiv \ddot{A}_x = -\frac{\mu}{r^2}\cos\phi \tag{4-47A}$$

$$\ddot{d} \equiv \ddot{A}_y = -\frac{\mu}{r^2}\sin\phi \quad . \tag{4-48A}$$

Since, referring to Equations 4-5 and 4-6,

$$\cos\phi = \frac{x}{r} \tag{4-49}$$

and

$$\sin\phi = \frac{y}{r} \quad , \tag{4-50}$$

then

$$\ddot{\xi} = -\frac{\mu x}{r^3} = -\frac{\mu x}{(x^2+y^2)^{3/2}} \tag{4-47B}$$

$$\ddot{d} = -\frac{\mu y}{r^3} = -\frac{\mu y}{(x^2+y^2)^{3/2}} \tag{4-48B}$$

so that

$$q = \phi + i\delta = -\left[\frac{\mu x}{(x^2+y^2)^{3/2}}\right] - i\left[\frac{\mu y}{(x^2+y^2)^{3/2}}\right] \tag{4-51A}$$

$$= \frac{\mu}{(x^2+y^2)^{3/2}}(-x-iy) \tag{4-51B}$$

$$q = \left[\frac{\mu}{(x^2+y^2)}\right]\exp(i\phi_q) \tag{4-51C}$$

or

$$q = \left[\frac{\mu}{r^2}\right]\exp\left[i(\phi_z+\pi)\right]. \tag{4-51D}$$

4.4 INVERSE HODOGRAPH TRANSFORMATIONS

An inverse hodograph transformation is defined as the function which operates upon a trajectory state point in a higher order of Newtonian vector space, in order to obtain the corresponding trajectory state point in any lower order of Newtonian vector space (e.g., P from P'' or P' in Figure 4-1). Consequently, an inverse transform is the operational inverse of the corresponding direct transform (as will be shown later, in the functional network of Figure 4-2). Obviously, the direct transform functions are used for derivation of the inverse transforms, as developed here.

4.4.1 (IT3) ACCELERATION → POSITION:

Referring to Equations 4-47B and 4-51D, it is seen that

$$x = -\frac{\phi r^3}{\mu} \tag{4-52A}$$

and

$$|q| = \frac{\mu}{r^2} \tag{4-53}$$

so that

$$x = -\left[\frac{\mu}{|q|}\right]^{\frac{3}{2}} \cdot \frac{\ell}{\mu} \quad ; \tag{4-52B}$$

similarly,

$$y = -\left[\frac{\mu}{|q|}\right]^{\frac{3}{2}} \cdot \frac{d}{\mu} \quad . \tag{4-54A}$$

But

$$|q| = \frac{\ell}{\cos\phi_q} = \frac{d}{\sin\phi_q} \tag{4-55, 4-56}$$

so that

$$x = -\left[\frac{\mu\cos\phi_q}{\ell}\right]^{\frac{3}{2}} \cdot \frac{\ell}{\mu} \tag{4-52C}$$

and

$$y = -\left[\frac{\mu\sin\phi_q}{d}\right]^{\frac{3}{2}} \cdot \frac{d}{\mu} \quad , \tag{4-54B}$$

or

$$x = -\left[\frac{\mu\cos^3\phi_q}{\ell}\right]^{\frac{1}{2}} \tag{4-52D}$$

and

$$y = -\left[\frac{\mu\sin^3\phi_q}{d}\right]^{\frac{1}{2}} \quad . \tag{4-54C}$$

Consequently,

$$z = x + iy = -\left[\frac{\mu\cos^3\phi_q}{\ell}\right]^{\frac{1}{2}} - i\left[\frac{\mu\sin^3\phi_q}{d}\right]^{\frac{1}{2}} \tag{4-57A}$$

or

$$z = \left[\left(\frac{\mu}{|q|}\right)^{\frac{1}{2}}\right] \exp(i\phi_z) \quad . \tag{4-57B}$$

But

$$\phi_z = \phi_q - \pi \qquad (4\text{-}31B)$$

so that, finally,

$$z = \left[\left(\frac{\mu}{|q|}\right)^{\frac{1}{2}}\right] \exp\left[i(\phi_q - \pi)\right] \quad ; \qquad (4\text{-}57C)$$

also

$$x = -\left[\frac{\mu}{|q|}\right]^{\frac{1}{2}} \cos\phi_q \qquad (4\text{-}52E)$$

and

$$y = -\left[\frac{\mu}{|q|}\right]^{\frac{1}{2}} \sin\phi_q \quad . \qquad (4\text{-}54D)$$

4.4.2 (IT2) ACCELERATION → VELOCITY:

From Section 4.3.1,

$$u = -\frac{\mu}{y - xy'}$$

$$y' = \frac{v}{u} = \tan\phi_w \quad ; \qquad (4\text{-}58)$$

from Section 4.2.2,

$$\phi_w = \frac{\pi}{2} + (\phi - \theta)$$

so that

$$\phi_w = \phi_q - \left(\frac{\pi}{2} + \theta\right) \quad ; \qquad (4\text{-}59)$$

from Section 4.4.1,

$$x = -\left[\frac{\mu}{|q|}\right]^{\frac{1}{2}} \cos\phi_q$$

$$y = -\left[\frac{\mu}{|q|}\right]^{\frac{1}{2}} \sin\phi_q \quad ;$$

consequently

$$u = -\frac{\mu}{-\left[\frac{\mu}{|q|}\right]^{\frac{1}{2}} \sin\phi_q + \left[\frac{\mu}{|q|}\right]^{\frac{1}{2}} \cos\phi_q \tan\left[\phi_q - \left(\frac{\pi}{2}+\theta\right)\right]} \tag{4-60A}$$

$$= -\frac{\sqrt{\mu|q|}}{-\sin\phi_q + \cos\phi_q \tan\left[-\frac{\pi}{2} + (\phi_q - \theta)\right]} \quad . \tag{4-60B}$$

But

$$\tan\left[-\frac{\pi}{2} + (\phi_q - \theta)\right] = -\cot(\phi_q - \theta) = -\frac{\cot\phi_q + \tan\theta}{1 - \cot\phi_q \tan\theta} \tag{4-61}$$

so that

$$u = \sqrt{\mu|q|}\,(\sin\phi_q - \cos\phi_q \tan\theta) \tag{4-60C}$$

or

$$u = \sqrt{\mu|q|}\,\sec\theta \sin(\phi_q - \theta) \quad . \tag{4-60D}$$

Also,

$$\tan\theta' = 2\tan\theta \tag{4-62}$$

so that

$$u = -\frac{\sqrt{\mu|q|}}{2}(-2\sin\phi_q + \cos\phi_q \tan\theta') \tag{4-60E}$$

or

$$u = \frac{\sqrt{\mu|q|}}{2}\left[\sin\phi_q + \sec\theta' \sin(\phi_q - \theta')\right] \quad . \tag{4-60F}$$

Referring again to Equations 4-35C and 4-58,

$$v = -\frac{\mu \tan \phi_w}{y - x \tan \phi_w} \tag{4-63A}$$

$$= -\frac{\mu}{\frac{y}{\tan \phi_w} - x} \tag{4-63B}$$

Referring again to Equations 4-61 and 4-62,

$$v = -\frac{\mu}{\frac{\left[\frac{\mu}{|q|}\right]^{\frac{1}{2}} \sin \phi_q \left(2 - \cot \phi_q \tan \theta'\right)}{2 \cot \phi_q + \tan \theta'} + \left[\frac{\mu}{|q|}\right]^{\frac{1}{2}} \cos \phi_q} \tag{4-63C}$$

so that

$$v = -\frac{\sqrt{\mu |q|}}{2} \left(2 \cos \phi_q + \sin \phi_q \tan \theta'\right) \tag{4-63D}$$

or

$$v = -\frac{\sqrt{\mu |q|}}{2} \left[\cos \phi_q + \sec \theta' \cos \left(\phi_q - \theta'\right)\right] . \tag{4-63E}$$

Then

$$w = u + iv = \left[\frac{1}{2} \sqrt{\mu |q| \left(4 + \tan^2 \theta'\right)}\right] \exp \left(i \phi_w\right) . \tag{4-64A}$$

But

$$\phi_w = \phi_q - \left(\frac{\pi}{2} + \theta\right) = \phi_q - \frac{\pi}{2} - \text{arc tan} \left(\frac{\tan \theta'}{2}\right)$$

so that, finally,

$$w = \left[\frac{1}{2} \sqrt{\mu |q| \left(4 + \tan^2 \theta'\right)}\right] \exp \left\{i \left[\phi_q - \frac{\pi}{2} - \text{arc tan} \left(\frac{\tan \theta'}{2}\right)\right]\right\} . \tag{4-64B}$$

4.4.3 (IT1) VELOCITY → POSITION:

$$x = \frac{\mu \cos\phi}{C(C + R\cos\phi)}$$

and

$$v - uv' = \frac{C(C + R\cos\phi)}{\cos\phi}$$

so that

$$x = \frac{\mu}{v - uv'} \quad . \tag{4-65}$$

Also,

$$y = \frac{\mu \sin\phi}{C(C + R\cos\phi)}$$

and

$$v' = \tan\phi$$

so that

$$y = \frac{\mu v'}{v - uv'} \quad . \tag{4-66}$$

Then

$$z = x + iy = \frac{\mu}{v - uv'} + i\,\frac{\mu v'}{v - uv'} \tag{4-67A}$$

or

$$z = \left[\frac{\mu}{v - uv'}\left(1 + v'^2\right)^{\frac{1}{2}}\right] \exp\left(i\phi_z\right) \quad . \tag{4-67B}$$

But

$$\phi_z = \phi_w + \theta - \frac{\pi}{2} \tag{4-68}$$

so that,

$$z = \left[\frac{\mu}{v - uv'}\left(1 + v'^2\right)^{\frac{1}{2}}\right] \exp\left[i\left(\phi_w + \theta - \frac{\pi}{2}\right)\right] \quad . \tag{4-67C}$$

4.5 SUMMARY

The functional network of hodograph transformations developed in the preceding sections is shown in Figure 4-2. The basic equations for the orbit hodographs in position, velocity and acceleration vector spaces, the direct transformations from lower to higher order vector space, and the inverse transformations from higher to lower order vector space are compiled in Tables 4-1 to 4-3 respectively.

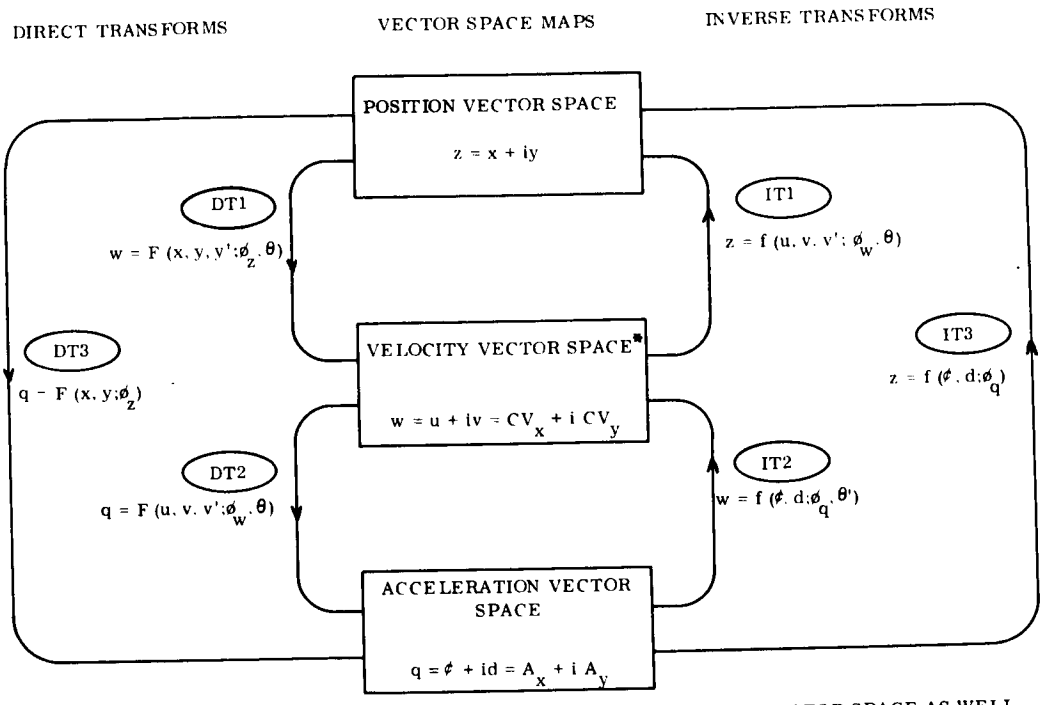

*NOTE: THIS VECTOR SPACE CAN BE REFERRED TO AS A "POTENTIAL" VECTOR SPACE AS WELL AS A "VELOCITY" VECTOR SPACE, WITH EQUAL JUSTIFICATION. THE SIGNIFICANCE OF THIS PHYSICAL INTERPRETATION HAS YET TO BE FULLY EXPLORED AND UNDERSTOOD.

Figure 4-2. Functional Network of Orbital Hodograph Transformations

The inputs to each transformation function are variables which are directly available in the initial vector space. Moreover, all such variables are geometrically measurable and defined explicitly in the given vector space. Note that the inverse transforms IT2 and IT3 are functions of the Cartesian metrics (¢, d) and argument metrics (ϕq, θ') - without the use of the curve slope variable d'. Upon brief contemplation, it is apparent that all the transformation functions - not only transforms IT2 and IT3 - may be completely expressed in terms of Cartesian metrics and two argument metrics without recourse to the curve slope (y', v' or d'). However, the form of the tabulated functions is deemed most amenable to computation

Table 4-1. Complex Function Equations of the Vector Space Maps of an Orbit

POSITION	$z = x + iy = \left[\frac{\mu}{C(C+R\cos\phi)}\right]\exp(i\phi_z)$ $x = \frac{\mu\cos\phi}{C(C+R\cos\phi)}$ $y = \frac{\mu\sin\phi}{C(C+R\cos\phi)}$
VELOCITY	$w = CV_x + iCV_y = C^2\exp\left[i\left(\phi+\frac{\pi}{2}\right)\right] + iCR$ $CV_x = -C^2\sin\phi$ $CV_y = CR + C^2\cos\phi$
ACCELERATION	$q = \ell + id = \left[C\dot{v}\right]\exp(i\phi_q)$ $\ell = -C\dot{v}\cos\phi$ $d = -C\dot{v}\sin\phi$
ADDITIONAL DEFINITIVE RELATIONS	$\phi \equiv \phi_z = \phi_w + \theta - \frac{\pi}{2} = \phi_q - \pi$ $\dot{v} = \frac{C}{\mu}(C+R\cos\phi)^2$

Table 4-2. Direct Transforms of the Orbital Hodographs

DT1 POSITION ↓ VELOCITY	$W = \left[\frac{\mu}{y-xy'}\sqrt{1+y'^2}\right]\exp\left[i\left(\frac{\pi}{2}+\phi_z-\theta\right)\right]$ $u = -\frac{\mu}{y-xy'}$ $v = -\frac{\mu y'}{y-xy'}$
DT2 VELOCITY ↓ ACCELERATION	$q = \left[\frac{(v-uv')^2}{\mu(1+v'^2)}\right]\exp\left[i\left(\frac{\pi}{2}+\phi_w+\theta\right)\right]$ $\mathcal{L} = -\frac{(v-uv')^2}{\mu(1+v'^2)^{3/2}}$ $d = -\frac{v'(v-uv')^2}{\mu(1+v'^2)^{3/2}}$
DT3 POSITION ↓ ACCELERATION	$q = \left[\frac{\mu}{r^2}\right]\exp\left[i(\phi_z+\pi)\right]$ $\mathcal{L} = -\frac{\mu x}{r^3}$ $d = -\frac{\mu y}{r^3}$

Table 4-3. Inverse Transforms of the Orbital Hodographs

IT1 VELOCITY ↓ POSITION	$$z = \left[\frac{\mu}{v - uv'}\sqrt{1+v'^2}\right]\exp\left[i\left(\phi_w + \theta - \frac{\pi}{2}\right)\right]$$ $$x = \frac{\mu}{v - uv'}$$ $$y = \frac{\mu v'}{v - uv'}$$
IT2 ACCELERA- TION ↓ VELOCITY	$$w = \left[\frac{1}{2}\sqrt{\mu\lvert q\rvert(4+\tan^2\theta')}\right]\exp\left\{i\left[\phi_q - \frac{\pi}{2} - \arctan\left(\frac{\tan\theta'}{2}\right)\right]\right\}$$ $$u = -\frac{\sqrt{\mu\lvert q\rvert}}{2}(-2\sin\phi_q + \cos\phi_q \tan\theta')$$ $$v = -\frac{\sqrt{\mu\lvert q\rvert}}{2}(2\cos\phi_q + \sin\phi_q \tan\theta')$$
IT3 ACCELERA- TION ↓ POSITION	$$z = \left[\sqrt{\frac{\mu}{\lvert q\rvert}}\right]\exp\left[i(\phi_q - \pi)\right]$$ $$x = -\sqrt{\frac{\mu\cos^3\phi_q}{\ell}}$$ $$y = -\sqrt{\frac{\mu\sin^3\phi_q}{d}}$$

or graphical use, since all variables within the modulus of the complex variable functions are Cartesian metrics, and all variables within the argument are angles. Consequently, the modulus (i.e., scalar) can be directly generated geometrically, by use of inversion, pedal scaling. This functional form of the transform equations may prove especially suitable for computation by means of geometry routines, or solution on analogue or DDA machine computers.

4.6 RESEARCH NOTES

Attention is called to potential areas of further research and advanced development in orbital trajectory synthesis and analysis, stemming from the presence and availability of the hodograph maps and transforms.

First, this vector space theory and formulation should be formally unified within the body of the Hamiltonian theory of dynamics. Noting that the hodograph transforms are contact transformations (Reference 1), it is clear that they are truly (as would be suspected on intuitive grounds or by broad logic) in conformance with the classical theory. The formal unification of this vector space theory within the classical theory may indicate fruitful extensions of the Hamiltonian principles, which might otherwise not be obvious.

Second, analytical extension of this theory to higher order vector spaces appears desirable and theoretically feasible. In particular, a general tensor form of the complete class of hodograph transformations between Newtonian vector spaces would be eminently desirable. In any case, the further development of transformation to the next higher order of vector space (i.e., for the space of vectors defined by $d^3 \bar{r}/dt^3$) could conceivably prove useful in engineering applications. This vector space would present state data analogous to the so-called "jerk" functions which are utilized by the electrical engineer in control engineering.

Third, further study of the physical interpretation of w-space as a "potential" rather than a "velocity" vector space appears quite promising and useful, especially in extension of the state or vector space theory to trajectories in the presence of more than one force center.

Fourth and finally, new and valuable computation aids - mechanical, electromechanical or electronic - may be developed, based upon the hodograph maps and transforms, for system application in:

a. Trajectory design solutions in system feasibility studies.

b. Backup navigation procedures and equipment.

c. Heuristic or educational devices for orbital dynamics.

It should be noted that the general hodographic theory is not restricted to one class of force center, such as the current subject of the inverse-square attracting gravitational field. Characteristic maps and transforms which occur in the presence of other theoretical field functions (e.g., direct inverse attracting) or due to other physical sources (such as electromagnetic field) may be developed as encountered or required, by following the basic logical procedures of the vector space (or hodographic) theory.

References

1. S. P. Altman, Orbital Hodograph Analysis, Vol. 3, AAS Science and Technology Series, Western Periodicals, 1965, Chapter 2.

2. F. S. Woods, Higher Geometry, Dover Publications, New York, 1961, pages 120 to 137.

SECTION 5

COMPLEX TIME LOCUS OF AN ORBITAL TRAJECTORY IN TIME STATE SPACE

AUTHORS: SAMUEL P. ALTMAN
AND
WILLIAM F. MACKEY

SECTION 5

COMPLEX TIME LOCUS OF AN ORBITAL TRAJECTORY IN TIME STATE SPACE

The vector space (or hodographic) theory of orbital trajectory analysis for either ballistic or powered flight has shown that an orbital trajectory is defined by its states at any given point in which the spacecraft may be located (References 1 and 2). Moreover, in parametric form, a powered trajectory is rigorously conceived and treated as a continuum of successive states of the spacecraft (or mass-body). Each point of the continuum provides complete definition of the spacecraft orbital motion, by establishing all states in the state spaces of Newtonian mechanics (as differentiated, for example, from thermal state). Knowledge of one state point (such as in velocity vector space) immediately provides explicit definition of all other states germane to the Newtonian motion, by means of the transformations between the state or vector spaces. Also, if the transitional effects, such as thrust producing an applied acceleration, were removed or ceased, then the set of state variable points describing the spacecraft orbital state of the event (rather than the time) of discontinuity of thrust would define all subsequent motion; that is, the ballistic flight or orbit subsequent to the event of thrust cutoff (References 1, 3, 4). The term "transition" is employed rather than "perturbation" in order to emphasize the conceptual break with the conventions and nomenclature of the classical mechanics.

There are compelling reasons for this new vector space concept and consequent formulation of the Newtonian mechanics. Although this concept is new to Newtonian mechanics as a formal methodology suitable for engineering application*, it has proven extremely powerful in other sciences (such as quantum mechanics) and technologies (such as control theory of electrical engineering). Moreover, the vector space theory has roots in various historical phases of classical mechanics (Reference 4).

However, the most outstanding motivation for a new concept of time in Newtonian mechanics is the overdue need and timeliness of a unified treatment of time in order to explain and relate

*The use of vector notation and analysis in current astrodynamics use is only a partial and incomplete aspect of the complete vector space theory.

the various specialized analyses in which time, upon apparently arbitrary manipulation by the mathematician, is eliminated, or employed in other than the traditional (or intuitive) sense. Of course, relativistic mechanics (Reference 5, 6) has shown that time must be treated as a variable, in order to provide a unified relativity theory. It appears reasonable that a new definition for formal treatment of time in Newtonian mechanics should offer hope of greater consistency between the deterministic theory of classical mechanics and the probabilistic theory of quantum mechanics. In general, the analytical use and treatment of time in orbital mechanics has changed but little from Kepler's era.

As the result of previous research study, it became clear that time must necessarily be treated as a state space. Although this concept is alien to our usual intuitive feeling or visualization, the time state space and the time trajectory (i.e., locus) in it is essential for complete and rigorous formulation of the vector space theory of mechanics. Moreover, the formulation and treatment of the time locus of the spacecraft trajectory is feasible and extremely valuable for engineering use. Consequently, this report presents study results on the orbital trajectory locus in time state space in five following subsections:

5.1 The Concept of Time State and Locus.

5.2 The Time Locus Transformation.

5.3 Parameter Determination From A Given Time Locus.

5.4 Perimetric Time Curve.

5.5 Potential Applications.

5.1 CONCEPT OF TIME STATE AND LOCUS

The fundamental concepts of mechanics are: space, time, mass and force. The state variables which are treated as vectors are defined in terms of these concepts; for example, position, velocity and acceleration. In the usual formulations of physical problems in rigid-body dynamics, time appears as the "independent" variable; in fact, time is a parameter which, due to the clock references which have become available, has been obvious

and convenient in simpler observational methods and test procedures. However, many of the more difficult problems of advanced dynamics have repeatedly become tractable to solution only by the elimination of time from the complete definitive set of equations, or by the treatment of time as a complex variable (References 7, 8, 9, 10). As shown by Kovalevskaya, certain cases of the problem of motion of a rigid body about a fixed point became solvable only by use of time as a complex variable, described in Reference 9 by the following excerpt:

> "This remarkable progress in solving the problem of the motion of a rigid body about a fixed point resulted from the application of the general methods of the theory of complex variables to a problem of mechanics. In the investigations of Euler, Lagrange and Poisson, just as in all studies in mechanics until the work of S. V. Kovalevskaya, time was considered as a variable taking only real values. Even in the investigations of Jacobi, who applied the theory of elliptic functions developed by himself and Abel to the problem of integration of the equations of motion of a rigid body about a fixed point, we shall find no hint about the application of the complex variable, or about the theory of elliptic functions created by him. Thus S. V. Kovalevskaya's study represents a remarkable extension of the mechanical problem: she was the first to consider time as a variable, taking arbitrary values in the complex plane. Such an extension of the mechanical problem allowed her to apply to it the thoroughly worked out apparatus of the theory of the complex variable.
>
> S. V. Kovalevskaya's work is of no lesser importance from the point of view of mathematics. The point is that under some conditions the complete integration of the differential equations, whose integrals have removable poles and have no other irregular points in the finite part of the plane of the independent variable, can be carried out quite independently of whether the problem reduces to quadratures or not."

It has been proven (References 2, 4) that an orbit in any one vector space corresponds, point for point, with its trajectory in all other vector spaces, as shown graphically in Figure 5-1. Consequently, any trajectory of the orbit in other vector spaces can be generated by the hodograph transformations between these vector space maps. The hodograph transformations are geometric transforms which are conformal, and algebraic in form. Note that time does not appear explicitly in any way; time is present only implicitly, as embodied within the basic definitions of the state vectors: position, velocity

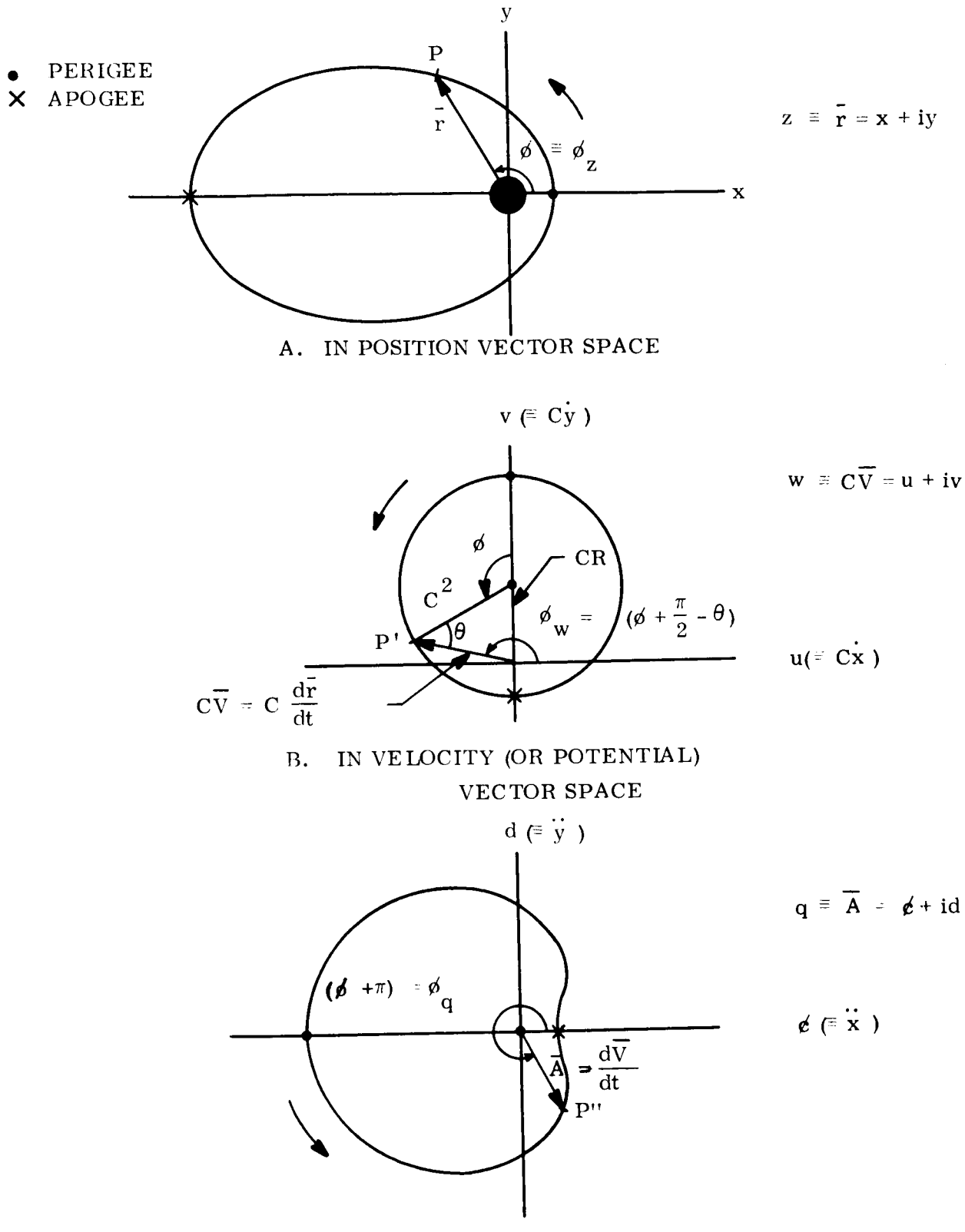

Figure 5-1. Vector Space Maps of an Orbit

and acceleration. Consequently, a complete analysis of the trajectory is possible without recourse to or the presence of time (Reference 1). In these cases, time is "free" or "open"; however, if time is constrained, how can such constraints be treated formally? Such formal treatment requires the definition and use of time as a state variable, with the essential properties and valid operations in the time state space consistent with the dynamics of mass motion.

Time is defined and treated as a state variable, such that a given point in the time space* must correspond, point for point, with the trajectory points in the other state or vector spaces, in accordance with a given logic. Also, the coordinates of the time state space must be defined so that direct and unique functional relations between time and the other state spaces for the spacecraft orbital state may be derived. That is, the locus of such points, defined as the time locus**of the trajectory, should be obtainable from the trajectory locus (or hodograph) in any other state space (or vector space) by means of a mapping or geometric transformation.

The equations for elapsed time along an orbital trajectory are well-known (References 4, 11) and can be expressed in terms of either the true anomaly ϕ or the eccentric anomaly E. The true anomaly ϕ and the eccentric anomaly E may be generated either in position or velocity vector space. In position vector space, the eccentric anomaly E is generated from the true anomaly ϕ by use of the "auxiliary circle," a well-known classical technique, as shown in Figure 5-2A. Several techniques of geometric generation in velocity vector space are available (References 4, 12, 13). However, the generating technique in inertial velocity vector space , shown in Figure 5-2B and newly derived in Subsection 5.6, has special merit and use in the time transformation. Note that the classical technique of mapping ϕ and E requires translation of the coordinate origin from the attracting force center O to the geometric center of the orbital ellipse and the auxiliary circle. However, the velocity

* Hereafter, time will be referred to the "time state space," rather than "time vector space." The logic of the operations in (or algorithm of) time state space are significantly different from those of the usual "vector analysis" and yet to be comprehensively explored and understood. The term "vector space" will be reserved exclusively to describe the Newtonian vector spaces of position, velocity, acceleration.....

**The trajectory in time state space is defined as the "time locus" rather than the "time hodograph," since "hodograph" refers to the locus of vectors in the sense described in the footnote preceding.

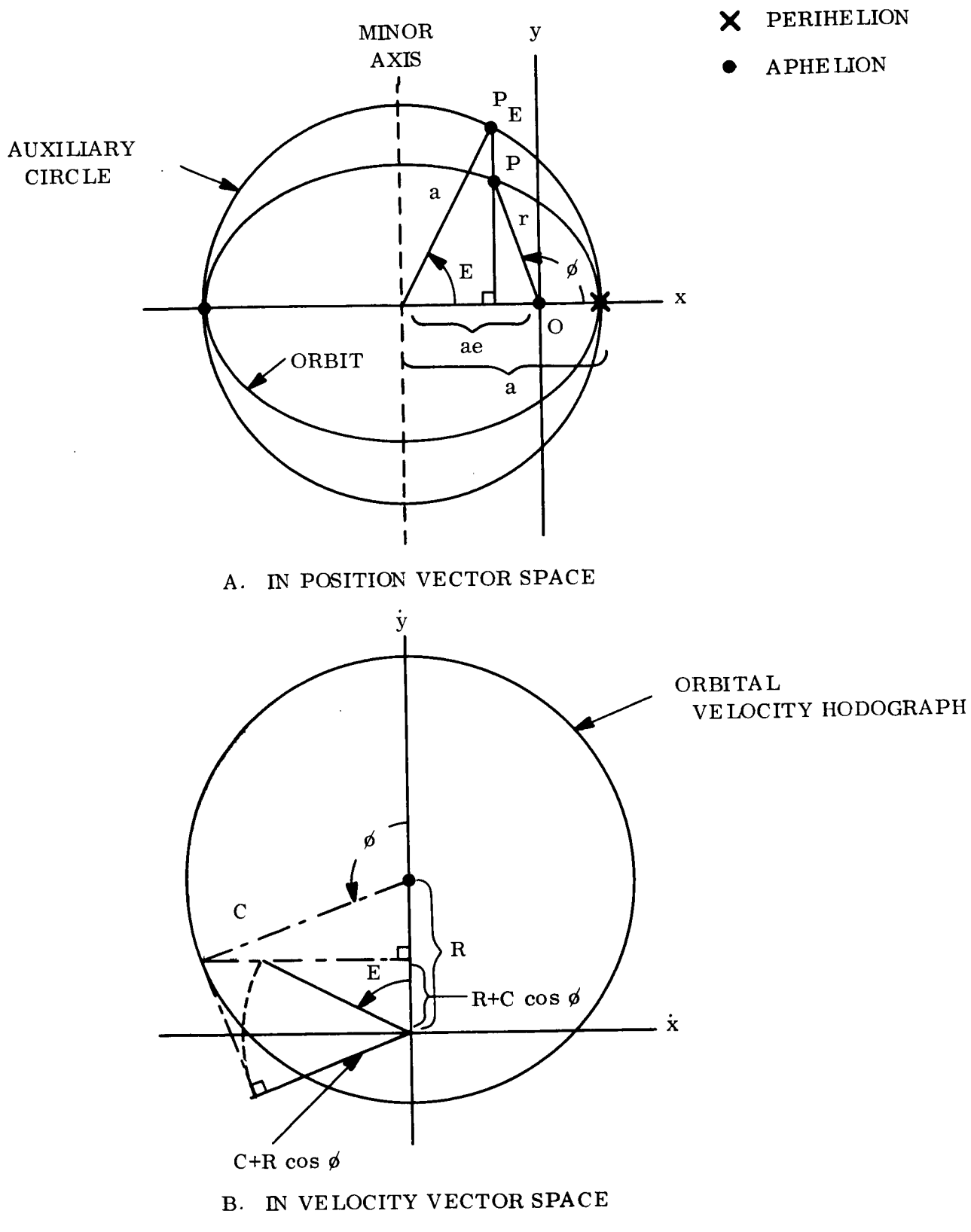

Figure 5-2. Geometric Generation of the Eccentric Anomaly

hodograph technique of mapping ϕ into E provides translation of the reference center for the anomaly ϕ into the coordinate origin for the anomaly E, identical with origin of the vector spaces. This property of the mapping transformation from ϕ to E has outstanding merit in developing a time transformation between a vector space and the time state space. Equations for orbital elapsed time, in position and velocity vector spaces, are presented in Table 5-1. Note that the velocity vector space formulation (Equations 5-3 and 5-5) is valid for all orbits (i.e., for all eccentricities) whereas the position vector space formulation (Equations 5-1 and 5-2) is valid only for circular and elliptic orbits (i.e., for $0 \leq e < 1$). The orbital trajectory (or locus) in time state space will be the geometric representation of these equations. That is, analytic transformation between the orbital trajectory in position or velocity vector space and the orbital locus in time state space must fulfill the equations listed in Table 5-1. Since the transformations between position, velocity, and acceleration vector spaces are already known (Reference 2), only transformation between one such vector space and time state space is unknown; the remaining transforms are then immediately derivable.

In order to postulate a time state space, with properties which enable us to develop the desired formal methodology, let us consider a circular orbit as shown in Figure 5-3A. Defining the epoch at $t_o = 0$ when the orbit crosses the positive x-axis (i.e., at the circled point), the points $P_{\pi/2}$, P_{π}, $P_{3\pi/2}$, $P_{2\pi}$, ... which occur successively at central angle increments of $\pi/2$ will occur at equally spaced time intervals since the orbital velocity in inertial space is constant (i.e., $t_{\pi} = 2t_{\pi/2}$, $t_{3\pi/2} = 3t_{\pi/2}$, $t_{2\pi} = 4t_{\pi/2}$, ...). The origin of the time state space is selected as coincident with the origins of the other vector spaces, and Cartesian coordinate axes (t_x, t_y) coincident with the corresponding vector space coordinate axes (i.e., x, y; $\dot{x}$, $\dot{y}$; $\ddot{x}$, $\ddot{y}$). As shown in Figure 5-3B, plot the time scalar for each trajectory point, with its length proportional to the elapsed time relative to a time reference point and directed identically with the corresponding trajectory point in position vector space (i.e., identical central angle). Then the set of these trajectory points in time state space is the time locus. The time locus for the circular orbit, as shown in Figure 5-3B, is the Archimedes' spiral (References 14-16) defined by

$$\rho = k_a \phi, \tag{5-6}$$

Table 5-1. Orbital Time In Position and Velocity Vector Spaces

In Position Vector Space

$$t = \frac{\left[a(1-e^2)\right]^{3/2}}{(1-e^2)\sqrt{\mu}} \left[\frac{2}{\sqrt{1-e^2}} \arctan\left(\sqrt{\frac{1-e}{1+e}} \tan\frac{\phi}{2}\right) - e\left(\frac{\sin\phi}{1+e\cos\phi}\right)\right] \tag{5-1}$$

or

$$t = \frac{a^{3/2}}{\sqrt{\mu}} \left[E - e\sin E\right] \tag{5-2}$$

In Velocity Vector Space

$$t = \frac{\mu}{C(C^2-R^2)} \left[\frac{2C}{\sqrt{C^2-R^2}} \arctan\left(\sqrt{\frac{C-R}{C+R}} \tan\frac{\phi}{2}\right) - R\left(\frac{\sin\phi}{C+R\cos\phi}\right)\right] \tag{5-3}$$

where

$$R\left(\frac{\sin\phi}{C+R\cos\phi}\right) = \frac{V_r}{V_v} \tag{5-4}$$

or

$$t = \frac{\mu}{(C^2-R^2)^{3/2}} \left[E - \left(\frac{R}{C}\right)\sin E\right] \tag{5-5}$$

$$\left[\text{NOTE: } T = \frac{2\pi a^{3/2}}{\mu^{1/2}} = \frac{2\pi\mu}{(C^2-R^2)^{3/2}}\right]$$

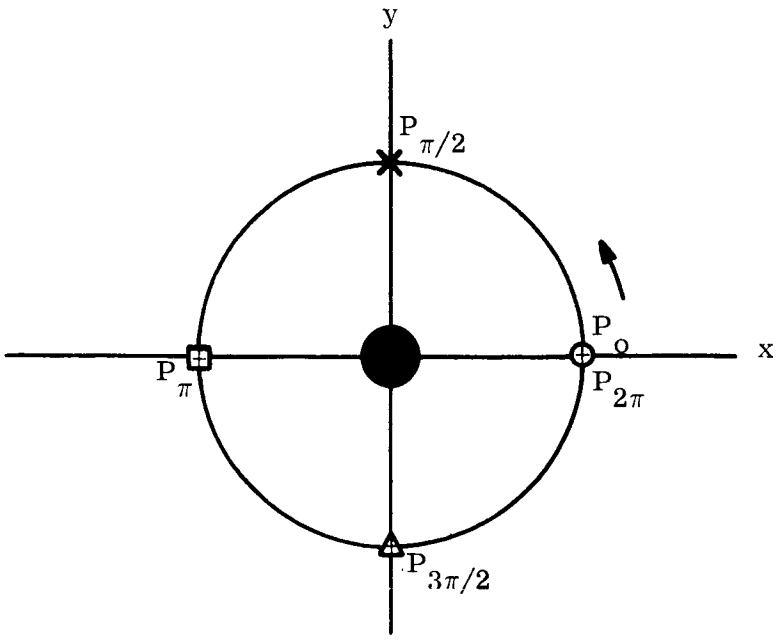

A. THE ORBIT IN POSITION VECTOR SPACE

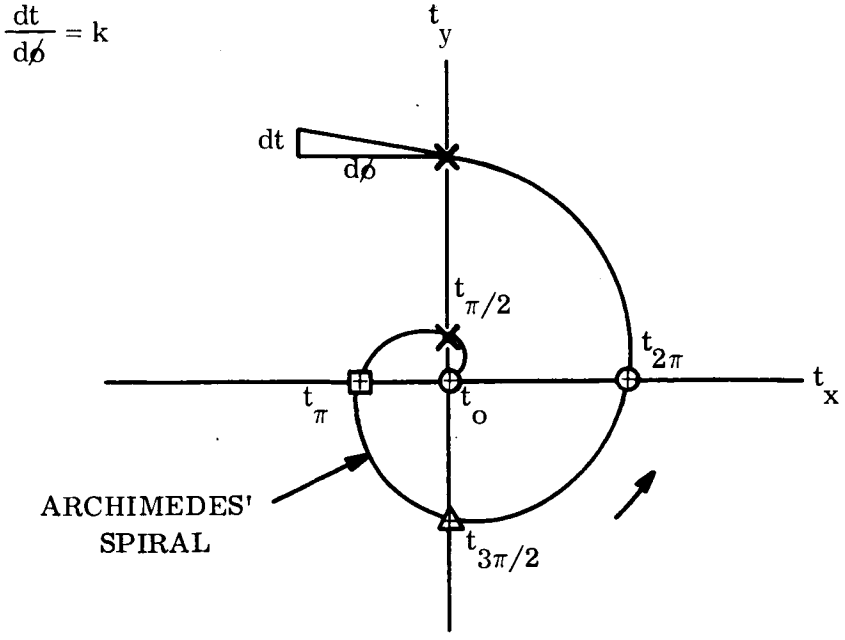

B. IN TIME STATE SPACE

Figure 5-3. Time Locus of a Circular Orbit

since the polar ρ (i.e., the time t) is proportional to the argument (i.e., the true anomaly ϕ). The Archimedes' spiral has many unique properties, some of which are vital to the transformation of an orbital trajectory from the vector spaces to the time state space. Now, at any point on the spiral, the tangent of the angle α between the tangent line and the perpendicular to the polar ρ (such as shown in Figure 5-3B, and defined here as the "polar slope") is

$$\frac{d\rho}{d\phi} = k_a = \text{constant} \quad , \tag{5-7}$$

so that

$$\frac{dt}{d\phi} = k = \text{constant} \tag{5-8}$$

for the time locus of a circular orbit. As shown in Reference 3, Equations 5-63 and 5-64,

$$C\dot{\phi} = \frac{(CV_v)^2}{\mu} = \frac{C^2(C+R\cos\phi)^2}{\mu} \tag{5-9}$$

so that

$$\frac{dt}{d\phi} = \frac{\mu}{CV_v^2} = \frac{\mu}{C(C+R\cos\phi)^2} \tag{5-10}$$

for any orbit in the presence of one force center. Since R = 0 for a circular orbit, then

$$\frac{dt}{d\phi} = \frac{\mu}{C^3} = k \tag{5-11}$$

in this case. With this definition of the time state space, the time locus of any trajectory is never ambiguous since the time locus will always spiral outward from the origin, without closure upon or intersection with itself.

The time locus of an elliptical orbit is shown schematically in Figure 5-4, compared with that for the circular orbit of equal period. Here, the time reference (or epoch) is at perigee passage shown at the orbital intersection with the positive x-axis in position vector space (Figure 5-4A). Then the elliptical orbit locus from perigee to apogee (i.e., for the true anomaly ϕ from 0 to π, or from $n\pi$ to $(n+1)\pi$ for n = even number) lies inside the time locus of the equal-period circular orbit, and outside from apogee to successive perigee (i.e., for the true anomaly ϕ from π to 2π, or from $m\pi$ to $(m+1)\pi$ for m = odd number). The polar slope of the time locus at any point is defined by Equation 5-10.

For a powered orbital trajectory, the time locus will be the continuum of successive points on the time loci for the instantaneous orbits, corresponding, point by point, with the powered trajectory hodographs in position, velocity and acceleration vector spaces (see Figures 11A and 11B of Reference 3, and Figure 7 of Reference 1, respectively). A powered trajectory in position vector space, and its corresponding time locus in time state space are illustrated in Figure 5-5A and 5-5B respectively. The time origin or epoch is defined arbitrarily as time $\bar{t}_i = 0$ at point P_i. Then the complex time $\bar{t}_t$ corresponds with any one point P_t until, finally, the complex time t_f corresponding with the terminal point P_f is reached. If the time state space with the trajectory time locus were superimposed upon the position vector space, with its trajectory position locus, so that origin and coordinate axes coincided (i.e., t_x -axis $\equiv$X-axis, t_y -axis $\equiv$Y -axis), then corresponding complex times $\bar{t}_{(\ )}$ and points $P_{(\ )}$ would lie on identical radial lines or polars. Note that, although the time locus of a powered trajectory (as for any real trajectory) must "spiral out" or diverge from the time origin, the geometric figure of the time locus will no longer be simply described by a classical or simply-described form of spiral.

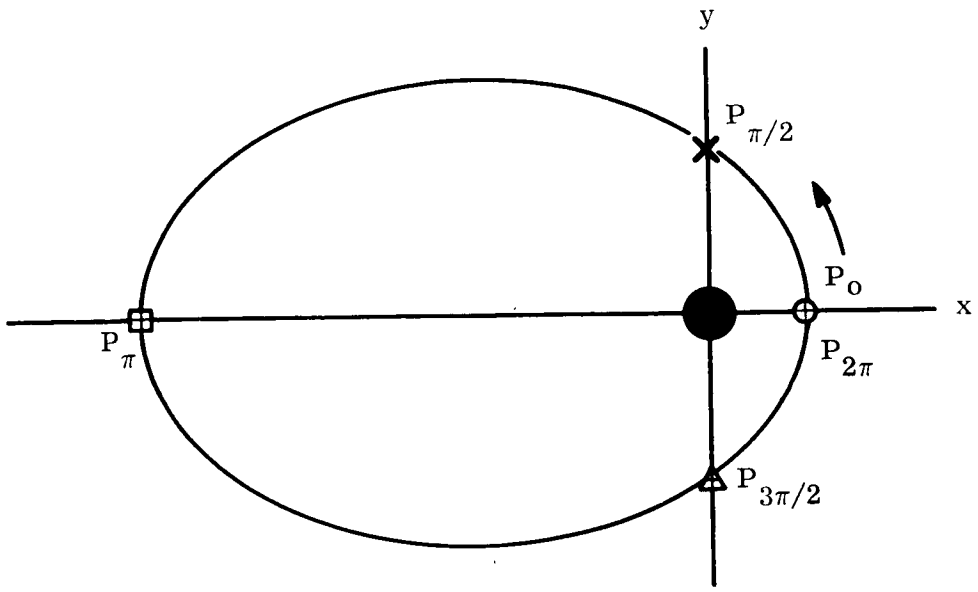

A. ORBIT IN POSITION VECTOR SPACE

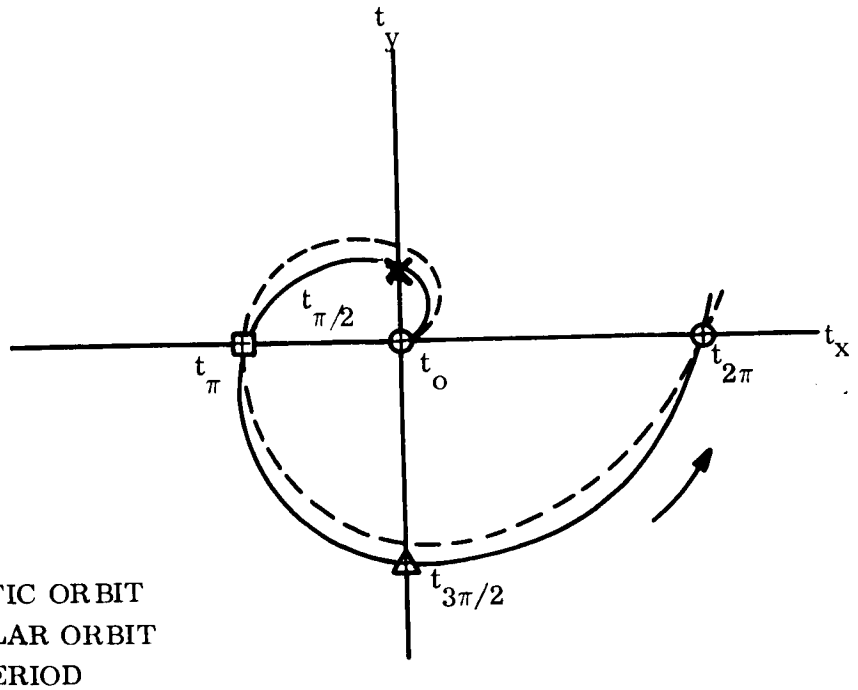

—— FOR ELLIPTIC ORBIT
– – – FOR CIRCULAR ORBIT OF SAME PERIOD

B. IN TIME STATE SPACE

Figure 5-4. Time Locus of an Elliptical Orbit

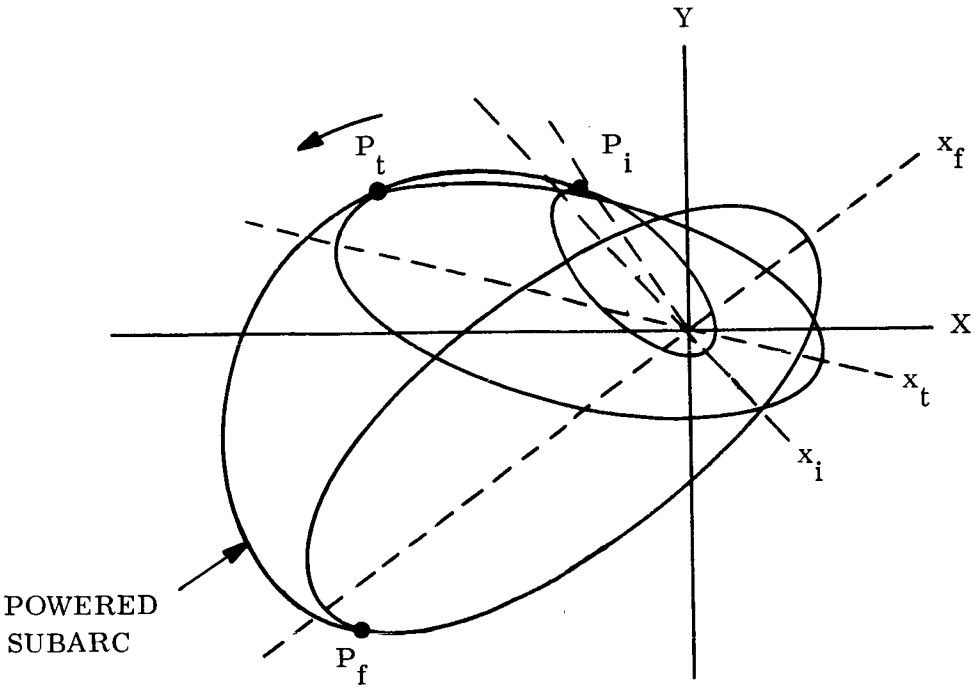

A. IN POSITION VECTOR SPACE

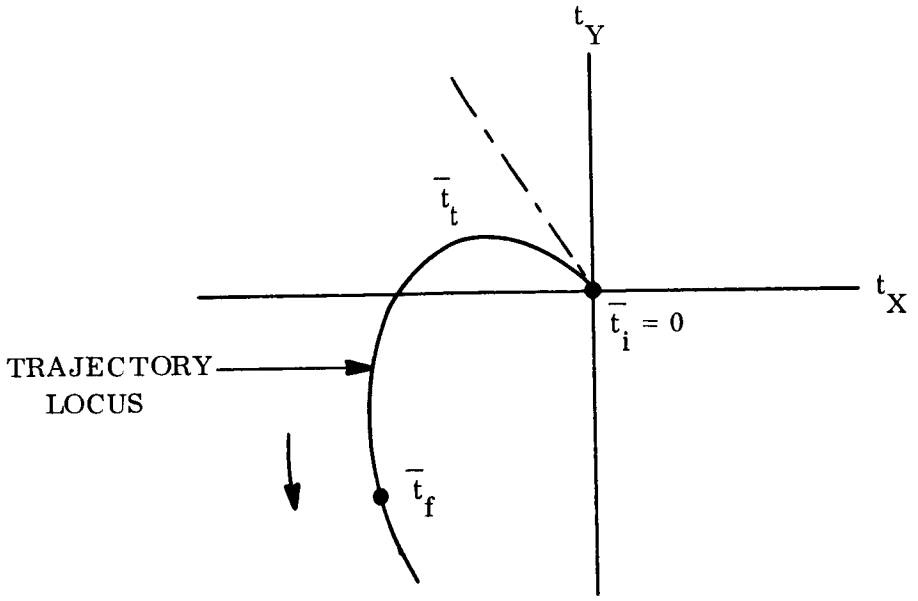

B. IN TIME STATE SPACE

Figure 5-5. State Loci of a Powered Trajectory

Although the time reference or epoch may be selected at convenience for the intended application and the consequent formulation, the epoch will always be located at the origin of the time state space and consequently coincident with the force center. Also, the direction of the successive time polars or trajectory "time-lines" in time state space are dependent upon the direction of the corresponding position vectors in position vector space (shown in Figure 5-5A). The length of the trajectory time-line is dependent upon the anomaly ($\emptyset$ or E) and the parameters of the instantaneous orbit (e.g., C, R, Ψ), and the time-line of the preceding locus point. That is, time is a state variable which is completely defined by knowledge of the trajectory hodograph in any one vector space. Conversely, given the time locus, the corresponding hodograph in any one vector space is defined. This latter case is directly useful for analysis whenever various possible constraints upon time are to be imposed.

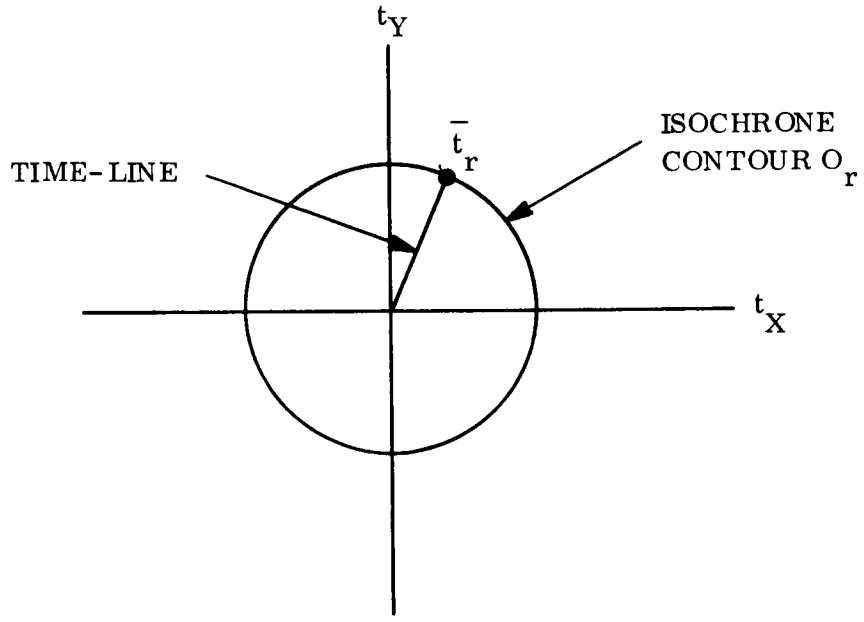

Figure 5-6. Isochrone Contour

The logical operations for analysis of an orbital trajectory (ballistic or powered) in time state space have yet to be derived and studied, for use in complete trajectory analysis and synthesis. However, some basic definitions are presented here for discussion of the potential applications of the trajectory time locus. Referring to Figure 5-6, a point in

time state space is denoted as the complex time t_r. The polar from the origin to the complex time t_r is the time-line* at the given trajectory point. The circle O_r with center at the origin is denoted as an isochrone contour. (Note that an isochrone contour cannot be a realizable or admissible trajectory). The intersections of a given isochrone contour, by admissible trajectories, are identically those trajectory points which are t_r following the epoch; that is, the concurrent or alternative points which the spacecraft will occupy at a time following the reference time. Consequently, the central angle between such intersection points for any two given trajectories in position vector space is shown directly as the angle between the respective time-lines in time state space.

A brachistochrone is an admissible trajectory which provides transition from an initial to a final given state in the shortest possible time, for a given class of such admissible trajectories. As shown in Figure 5-7, a brachistochrone trajectory is that one (of the given class) of such admissible trajectories, which is bounded by the minimal (or thinnest ring) isochrone annulus; that is, $(t_f - t_i)$ = minimal. In general, any realizable or admissible trajectory must lie within (i.e., be bounded by) its isochrone annulus defined by the endpoint time-lines. Within the given class of admissible trajectories, the central angle between time-lines $\bar{t}_i$ and $\bar{t}_f$ for the brachistochrone may be free (unless specified by other constraints or criteria than time); that is,

$$\arg(\bar{t}_{f1}) - \arg(\bar{t}_{i1}) \neq \text{fixed} .$$

The same minimum-time condition may also be fulfilled in a region of different ranges of complex time, as shown in Figure 5-7B. In Figure 5-7B,

$$t_{f2} - t_{i2} = t_{f1} - t_{i1}$$

*The term "time-line" will always be used in trajectory analysis, in this sense, unless otherwise stated. In process analysis of system engineering, a chain of events is often described by a "time-line" on a symbolic diagram.

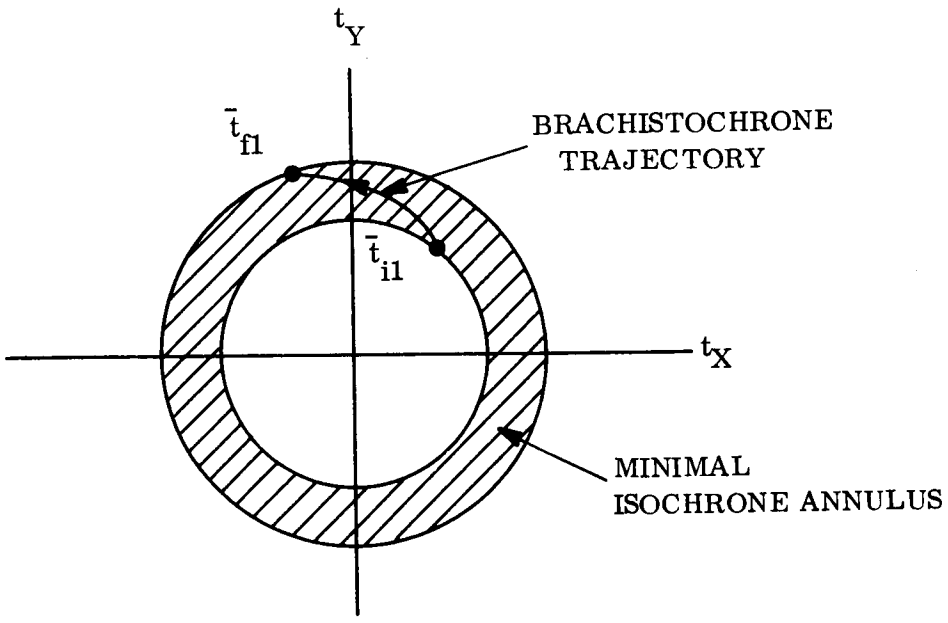

A. BRACHISTOCHRONE WITH ENDPOINT COMPLEX TIMES $\bar{t}_{i1}$, $\bar{t}_{f1}$

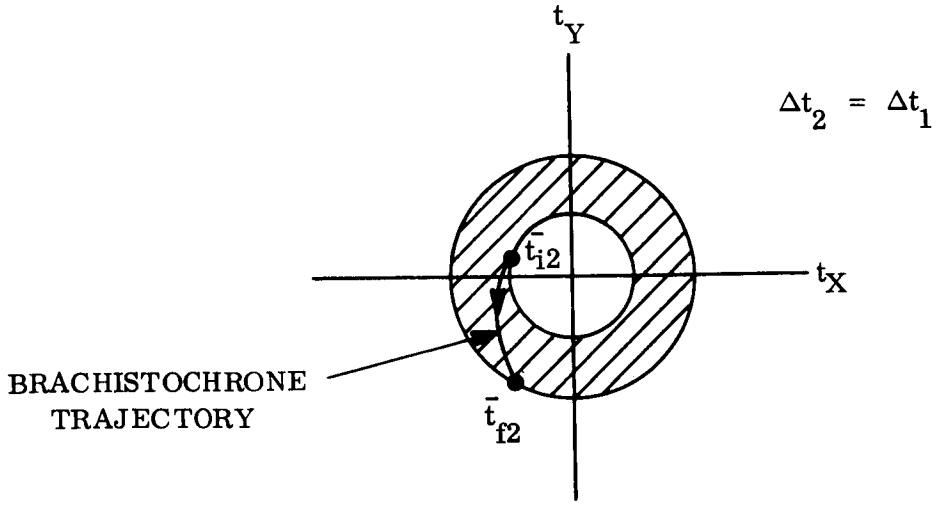

B. BRACHISTOCHRONE WITH EQUAL ELAPSED TIME
(BUT DIFFERENT ENDPOINT COMPLEX TIMES)

Figure 5-7. Brachistochrone Trajectories

solely for pedogogical purposes. If both the brachistochrone trajectories shown in Figure 5-7 were time-extremals for a given problem statement, then these brachistochrones would also be tautochrones.

A tautochrone is one (of two or more) admissible trajectories which require the same time for transition from an initial to a final given state, for a given class of such admissible trajectories. As shown in Figure 5-8A, the endpoint time-lines for the tautochrone trajectories may be coincident or noncoincident, dependent only upon other constraints or criteria than time. For tautochrone trajectories the elapsed time for trajectory flight is fixed; that is,

$$t_{f2} - t_{i2} = t_{f1} - t_{i1} \quad = \text{fixed (or specified).}$$

The same fixed-time condition may also be fulfilled in a region of different ranges of complex time, as shown in Figure 5-8B, provided that the scalar difference between the endpoint time-lines is the same; that is,

$$t_{f3} - t_{i3} = t_{f2} - t_{i2} = t_{f1} - t_{i1} = \text{fixed.}$$

These definitions for orbital time loci are only a partial description of the geometric properties of a trajectory in time state space. Further research beyond the reported work of this section would enable complete analysis of orbital trajectories in time state space, if required or convenient. The utility of these definitions in problem applications will be discussed later, in Subsection 5.5. It is stressed that such definitions are not merely convenient illustrations of the problem for ease of visualization, but are analytically rigorous representations of the trajectory dynamics in terms of the differential geometry. The following analysis and discussion of the time locus transformation should demonstrate this point most effectively.

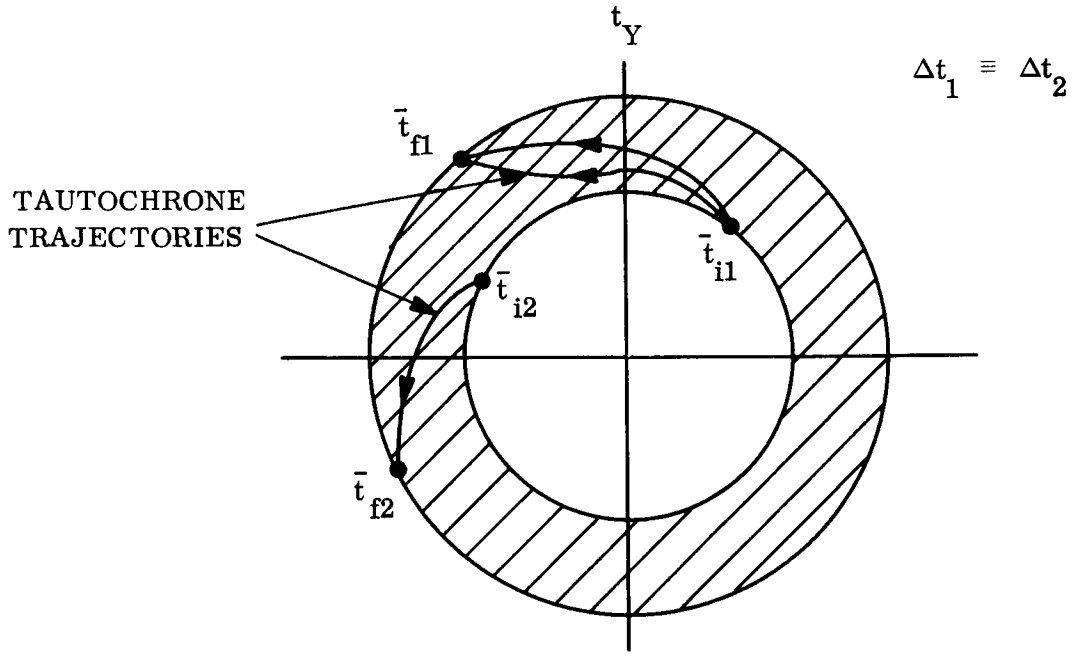

A. TAUTOCHRONES WITH IDENTICAL COMPLEX TIMES AT ENDPOINTS

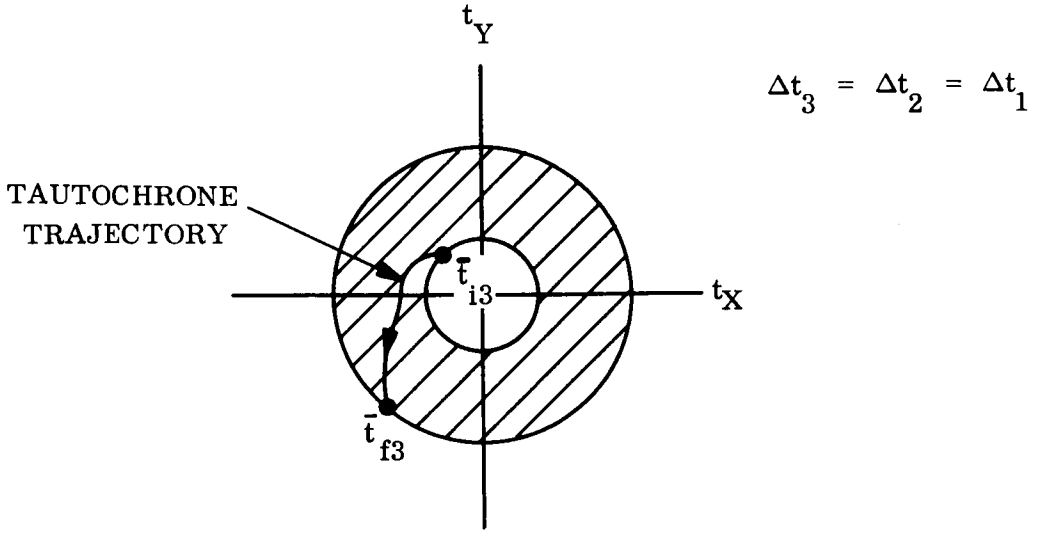

B. TAUTOCHRONE WITH EQUAL ELAPSED TIME
(BUT DIFFERENT ENDPOINT COMPLEX TIMES)

Figure 5-8. Tautochrone Trajectories

Although the work of this report is developed for trajectories in two-dimensional space (i.e., in one plane), the basic definitions and theory can be directly extended to three-dimensional problems without analytic revision. For example, the brachistochrone and tautochrone must then lie within (i.e., be bounded by) a spherical shell rather than an annulus. Also, all the transform properties utilized in Subsection 5.2 are valid in the same sense. In general, the hodographs (or loci) in vector (or state) spaces, and the transforms between these spaces, are analytic about the origin, throughout the region of admissible solution.

5.2 TIME LOCUS TRANSFORMATION

The hodograph (or state) locus of a trajectory in a vector (or state) space can enable analysis of ballistic or powered orbital trajectories, by use of the inherently parametric formulation of a trajectory problem. As discussed in References 1 and 3, this parametric formulation and analysis provides the orbits (for ballistic flight problems) or the continuum of instantaneous orbits (for powered flight problems) in the state space of analysis, with subsequent use of the hodograph transformations to obtain the other corresponding states, as required. These transformations are valid for ballistic (i.e., orbital) hodographs.

The previously described logic of parametric analysis can be extended to time state space. Consequently, the time locus transformations, which relate the orbital time locus to the vector spaces, should be available in a complete, formal methodology of vector space theory of Newtonian mechanics. Although this subsection demonstrates this by developing one form of such transformation, further study is required along several promising avenues of research extension. Not only are other direct transformations possible, but the inverse transforms have yet to be developed. However, further time locus study has been deferred to complete the techniques development of hodographic analysis in acceleration vector space.

In complex notation, the orbital time locus is defined as

$$\bar{t} = [f\phi]\, e^{i\phi} \tag{5-12}$$

in which

$$f = Cr^2/\mu \tag{5-13A}$$

or

$$f = \mu/CV_v^2 \tag{5-13B}$$

or

$$f = C/A \quad . \tag{5-13C}$$

in position, velocity and acceleration vector spaces, respectively. The required transformations from vector to state space will fulfill these analytic relations by means of geometric mapping operations. While Equations 5-12 and 5-13 alone are sufficient for computational use with the respective vector space formulations, a formal transformation is desired. Immediately, the question arises: which vector space should be used as the starting point in developing one of the required transformations? Since the hodograph transforms and basic differential geometric foundations are still new and not completely understood (nevertheless complete and rigorous), the "best" approach was not obvious. However, one vital clue was perceived: namely, that the Archimedes' spiral can be generated as the pedal of an involute of a circle, with the pedal point located at the circle center. This generation or transformation is illustrated schematically in Figure 5-9, in which Figure 5-9B shows the pedal curve (i.e., the Archimedes' spiral) obtained subsequently from the involute generated in Figure 5-9A. The pedal of a basis curve is the locus of the foot of a perpendicular from a fixed point, the pedal point, upon the tangent to any point of the basis curve (e.g., see Figure 5-9B). The involute of a basis curve is the

A. INVOLUTE OF THE BASIS CURVE
(BASIC CURVE = CIRCLE)

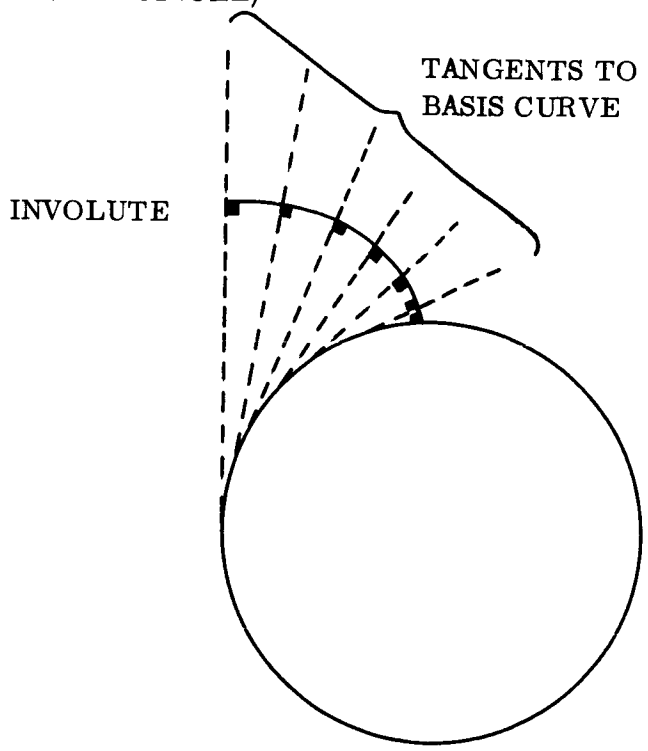

B. PEDAL OF THE INVOLUTE
(PEDAL POINT = CIRCLE CENTER)

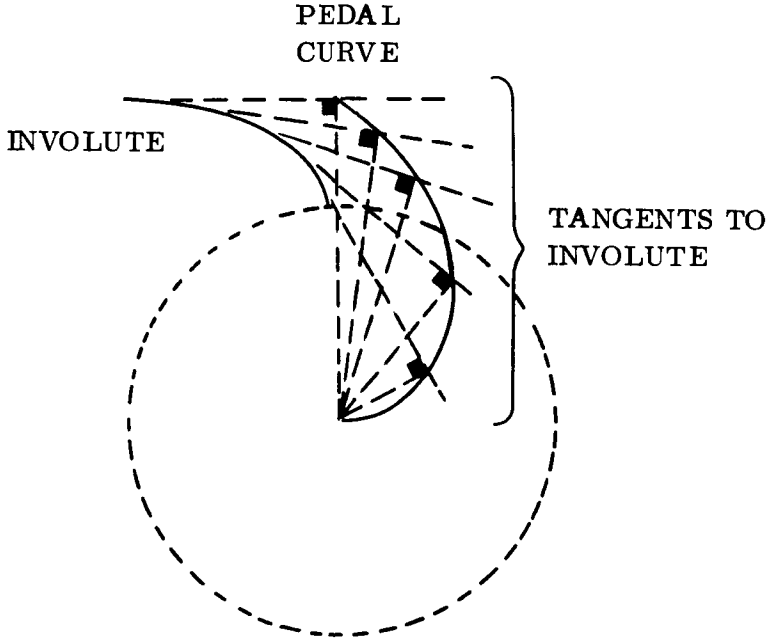

Figure 5-9. Geometric Generation of an Archimedes' Spiral

path described by the end of a flexible, non-extendable cord lying along the basis curve, when unwound so that the cord remains taut and tangent to the curve (e.g., see Figure 5-9A). The involute of a general curve is briefly described in Subsection 5.7, in complex notation.

The major difficulty in extending this mapping transformation to the other orbital time loci (i.e., for e and $R \neq 0$) is that the hodographs of a circular orbit in all orders of vector space (position, velocity, acceleration, ...) are themselves circles, as shown in Figure 5-10. It is not apparent which hodograph is the "best" map to use with this basic mapping transformation. Moreover, the transformation underlined above may be considered a reduced or degenerate form of a more general form of transformation: namely, that the Archimedes' spiral can be generated as the pedal of the involute of the caustic of a circle, with both the radiant point and the pedal point located at the circle center. In this special case of the circular orbit, the "caustic transformation" reduces to the underlined, simpler transform, since here the caustic of the circle is itself a concentric circle. In general, the caustic of a curve is not itself an identical curve, so that the more general (albeit more complex) form of the caustic transform could have been used to generate the time loci of elliptic, parabolic or hyperbolic orbits. However, this more complex analysis was unnecessary, as shown by the work results covered by this report.

Refering to Figure 5-2 and Table 5-1, at least two choices in transform development are available:

a. Direct use of the orbital trajectory either in position or velocity vector space, as the initial map.

b. Direct use either of the true anomaly $\emptyset$ or the eccentric anomaly E as one of the time parameters.

Because of its simplicity of geometric figure, the velocity hodograph -- always a circle -- was used in this initial approach. The basic vector components of the velocity hodographs, in inertial and in polar coordinates, are recapitulated in Figure 5-11.

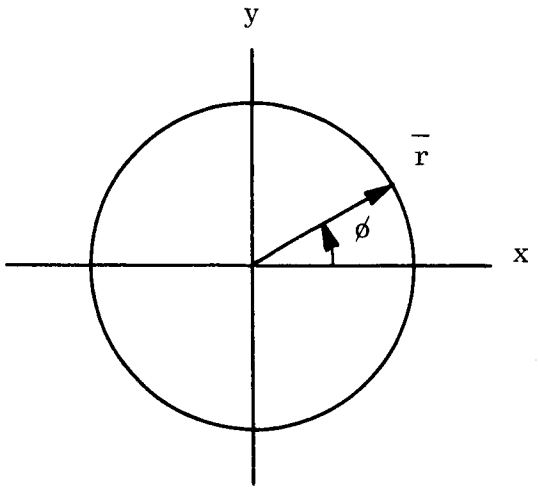

A. IN POSITION VECTOR SPACE (e = 0)

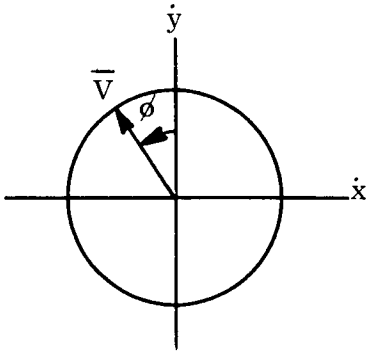

B. IN VELOCITY VECTOR SPACE (R = 0)

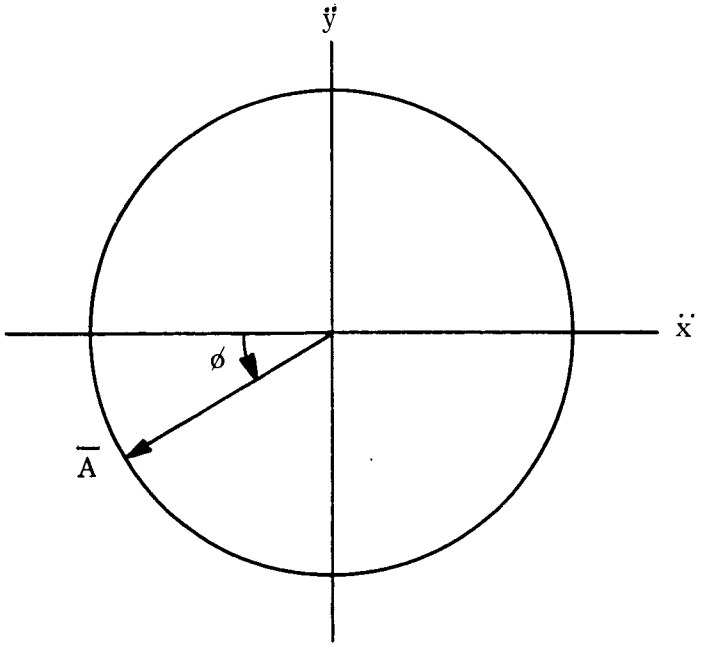

C. IN ACCELERATION VECTOR SPACE

Figure 5-10. Circular Orbit in the Vector Spaces

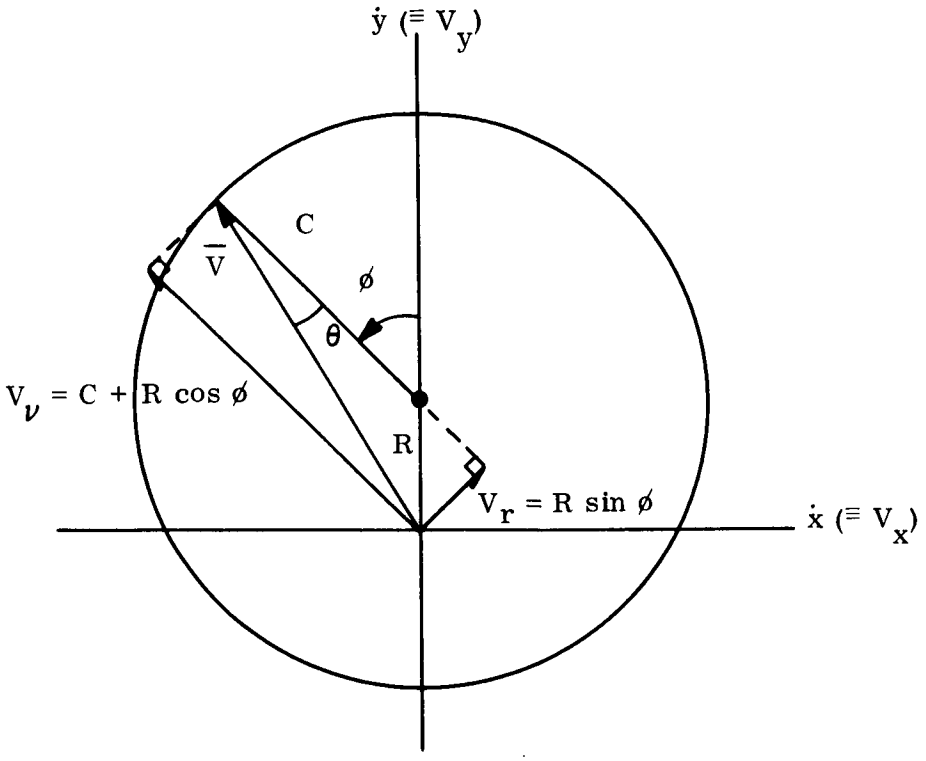

A. IN INERTIAL COORDINATES

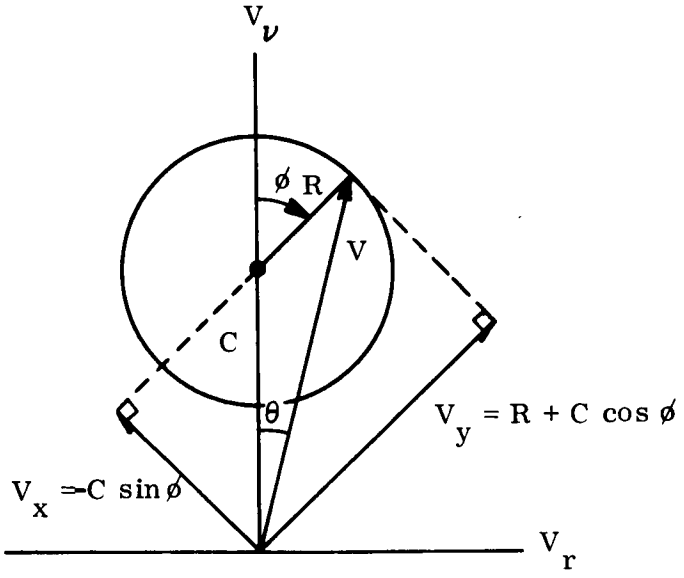

B. IN POLAR COORDINATES

Figure 5-11. Orbital Velocity Hodograph

(Note that the use of the acceleration hodograph or the time equation in terms of the acceleration hodograph parameters has not been discussed. Although more definitive work in this area is still required, some significant and relevant data and observations on this point are presented in the next section.)

Upon studying the equations in Table 5-1, it is apparent that the simpler form of the equations as functions of E (rather than $\emptyset$) lend themselves directly to geometric interpretation. Consequently, attention was focussed upon the use of E for the required time transformation. Although the time locus consists of complex time points with direction defined by the true anomaly $\emptyset$, the transformation by use of the eccentric anomaly E is completely acceptable and valid as a rigorous demonstration of the analytic validity of the trajectory locus in time state space. For engineering applications, Equations 5-12 and 5-13 are complete and sufficient for the use of and conventional computation upon complex time $\overline{t}$.

The basic transform operations which enable development of the time locus transformation are the involute and the pedal. In this development, three conditions for involution must be determined:

a. The basis curve for the involute.

b. The point of initiation for the involute.

c. The direction (i.e., clockwise or counterclockwise) of generation.

Also, two conditions for the pedal must be selected:

A. The basis curve for the pedal (not necessarily the above involute itself).

B. The pedal point for generation.

Since the velocity hodograph for all orbits is a circle, it appears that the basis curve might be a circle also (although not necessarily the velocity hodograph itself). The parameters

of the basis curve to be determined are defined as: C_B, R_B, ϕ_B and Ψ_B. However, since the velocity hodograph center can only be located somewhere on the $\dot{y}$-axis, let us constrain the possible location of the basis circle center to the $\dot{y}$-axis only (i.e., $\Psi_B = e^{i\pi/2}$). At this point, let this basis circle center be located at the origin so that $R_B = O$, and the radius scalar C_B be equal to the hodograph parameter C (i.e., $C_B = C$) of the velocity hodograph for the given orbit. Note that C_B will -- in general -- be a function f (C, R) and the radial angle ϕ_B (referred to the positive $\dot{y}$-axis) be a function g (C, R, ϕ) of the velocity hodograph. Since $\phi_B = O$ is defined as located on the positive $\dot{y}$-axis, the complex form of the basis curve (See a)

$$\bar{\zeta}_B = (C_B e^{i\phi_B}) e^{i(\pi/2)} = (iC_B) e^{i\phi_B} . \qquad (5\text{-}14)$$

The parameters C_B and ϕ_B must now be determined (if possible with the assumed conditions for R_B and Ψ_B), in order to fulfill the orbital time Equation 5-5.

Let us define the involute of this hypothetical basis curve as generated by counterclockwise involution, starting at $\phi_B = O$ so that $\bar{z}_{BO} = iC_B$ (See b and c). In accordance with Subsection 5-7,

$$\bar{\zeta}_I = \bar{\zeta}_B + \bar{\zeta}_{TA} \qquad (5\text{-}15)$$

where

$$\bar{\zeta}_{TA} = -s_B \left(\frac{d\bar{\zeta}_B}{ds_B} \right) \qquad (5\text{-}70B)$$

Since

$$\frac{d\bar{\zeta}_B}{d\phi_B} = -\left[C_B \right] e^{i\phi_B} \qquad (5\text{-}16)$$

so that

$$\left| \frac{d\bar{z}_B}{d\phi_B} \right| = C_B \tag{5-17}$$

and then (by use of Equation 5-70B)

$$s_B = \int_0^{\phi_B} (C_B)\, d\phi_B = C_B \phi_B \quad , \tag{5-18}$$

finally

$$\frac{d\bar{z}_B}{ds_B} = \left(\frac{d\bar{z}_B}{d\phi_B}\right)\left(\frac{d\phi_B}{ds_B}\right) = -e^{i\phi_B} \quad . \tag{5-19}$$

Consequently,

$$\bar{z}_{TA} = \left[C_B \phi_B\right] e^{i\phi_B} \tag{5-20}$$

so that the involute vector can be shown as

$$\bar{z}_I = (C_B \phi_B + iC_B) e^{i\phi_B} \tag{5-21A}$$

by use of Equations 5-14, 5-15 and 5-20. Noting that the parenthetical term $(C_B \phi_B + iC_B)$ is itself complex, the argument of $\bar{z}_I$ cannot be ϕ_B. Since

$$e^{i\phi_B} = \cos\phi_B + i \sin\phi_B \tag{5-22}$$

and

$$\bar{z}_I = u + iv \quad , \tag{5-23}$$

then

$$\bar{z}_I = \left[z_I\right] e^{i\beta_B} \tag{5-21B}$$

where the modulus is

$$\left|\bar{z}_I\right| = \left[\bar{z}_I\,\bar{z}_I^{*}\right]^{\frac{1}{2}} = C_B\left[1+\phi_B^2\right]^{\frac{1}{2}} \qquad (5\text{-}24)$$

and the argument is

$$\beta = \arctan\left(v/u\right) = \arctan\left[\frac{\cos\phi_B + \phi_B \sin\phi_B}{\phi_B\cos\phi_B - \sin\phi_B}\right]. \qquad (5\text{-}25)$$

The involute (Equation 5-21) of the tentative basis curve (Equation 5-14) is now employed as the basis curve for the pedal (see A). The last condition is selection of the pedal point, from which the pedal curve is generated. Noting that the pedal point for generating the Archimedes' spiral was the center of the original basis curve (i.e., a circle) as shown in Figure 5-9B, it is not unreasonable to speculate that the required pedal point must lie somewhere along the $\dot{y}$-axis, so that the location of the pedal point for the Archimedes' spiral generation is the limit or bound of the field of pedal points for generation of the time trajectories for all orbits (for all eccentricities e or velocity parameter R). Moreover, the upper bound for the pedal location on the $\dot{y}$-axis must be iC_B, since any pedal points located above $\bar{z} = iC_B$ will not generate spirals. Consequently, the pedal will be located at some one point $\tilde{P}$ on the line segment of the $\dot{y}$-axis (Figure 5-12). Note that $\tilde{P}$ must be determined as a function of the hodograph parameters (C, R). Then the desired final curve should be obtained -- upon judicious assignment of C_B as a function of the hodograph parameters (C, R) -- either by translation of the pedal curve, or by concurrent translation of both the involute $\bar{z}_I$ and the pedal point $\tilde{P}$, through the distance $\tilde{P}$ parallel to the $\dot{y}$-axis. That is, the transformation property of translation is required, in addition to involution and pedal. Since, as shown in Subsection 5-6, geometric generation of the eccentric anomaly E from the velocity hodograph and true anomaly ϕ defines the anomaly E at the origin, it is most convenient to translate both the involute and pedal prior to generation of the required time trajectory.

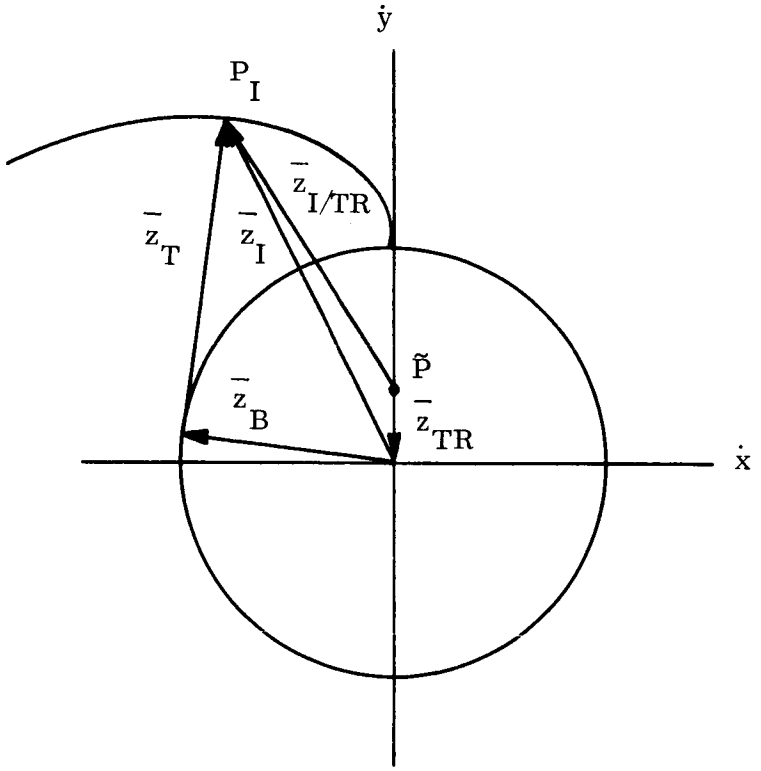

Figure 5-12. Pedal Point of the Basis Curves (or Translation of the Involute)

Let the pedal point $\tilde{P}$, yet to be determined, be defined in complex notation by

$$\bar{z}_{TR} = -i\tilde{P} \tag{5-26}$$

Then the involute, relative to the pedal point $\tilde{P}$ is defined by

$$\bar{z}_{I/TR} = \bar{z}_I + \bar{z}_{TR} \tag{5-27}$$

so that

$$\bar{z}_{I/TR} = -i\tilde{P} + (C_B\phi_B + iC_B)e^{i\phi_B} \; . \tag{5-28}$$

The pedal of a given curve is definable (Reference 15) by

$$\bar{\zeta}_P = \frac{1}{2} \frac{\bar{\zeta}_{I/TR}\, \dot{\bar{\zeta}}_{I/TR}^{\,*} - \bar{\zeta}_{I/TR}^{\,*}\, \dot{\bar{\zeta}}_{I/TR}}{\dot{\bar{\zeta}}_{I/TR}^{\,*}} \quad . \tag{5-29}$$

Since

$$\bar{\zeta}_{I/TR} = -i\tilde{P} + (C_B \phi_B + i C_B) e^{i\phi_B} \quad , \tag{5-30}$$

$$\dot{\bar{\zeta}}_{I/TR} = i C_B \phi_B e^{i\phi_B} \tag{5-31}$$

and

$$\bar{\zeta}_{I/TR}^{\,*} = i\tilde{P} + (C_B \phi_B - i C_B) e^{-i\phi_B} \quad , \tag{5-32}$$

$$\dot{\bar{\zeta}}_{I/TR}^{\,*} = -i C_B \phi_B e^{-i\phi_B} \quad , \tag{5-33}$$

then, upon substitution of Equations 5-30 through 5-33 into Equation 5-29,

$$\bar{\zeta}_{\tilde{P}} = (C_B \phi_B - \tilde{P} \sin \phi_B) e^{i\phi_B} \tag{5-34}$$

defines the class of spirals generated as described to this point of development. Note that this spiral reduces to an Archimedes' spiral when $\tilde{P} = 0$.

In Equation 5-34, the basis curve parameters (C_B, ϕ_B) and the pedal point translation scalar $\tilde{P}$ must be suitably selected functions of the given orbital velocity hodograph parameters (C, R, ϕ or E). Referring to Equation 5-5 of Table 5-1, it can be shown that

$$t = \frac{\tau}{2\pi C} (C\mathcal{E} - R \sin \mathcal{E}) \tag{5-35}$$

where the orbital period τ is defined by

$$\tau = \frac{2\pi\mu}{(C^2-R^2)^{3/2}} \quad . \tag{5-36}$$

Comparing the modulus of Equation 5-34 with 5-35, the functional similitude requires that

$$\phi_B = \mathcal{E} \tag{5-37}$$

and

$$C_B = \frac{\mu}{(C^2-R^2)^{3/2}} \tag{5-38}$$

$$\tilde{P} = \frac{\mu}{(C^2-R^2)^{3/2}}\left(\frac{R}{C}\right) = C_B\left(\frac{R}{C}\right) . \tag{5-39}$$

Then the time trajectory in terms of the velocity hodograph parameters (C, R) and eccentric anomaly E would be

$$\bar{t} = \left[\frac{\mu}{C(C^2-R^2)^{3/2}}(C\mathcal{E} - R\sin\mathcal{E})\right]e^{i\mathcal{E}} \tag{5-40A}$$

as required. However, a far more useful similitude of geometric convenience and physical significance is the employment of a scale factor (or magnification) of

$$k = \frac{\mu}{(C^2-R^2)} \tag{5-41A}$$

so that

$$C_B^* = \sqrt{C^2-R^2} \tag{5-42A}$$

and

$$P^* = \frac{R}{C}\sqrt{C^2-R^2} = C_B^*\left(\frac{R}{C}\right) . \tag{5-43A}$$

Then

$$\bar{t} = \left[k(C_B^*\mathcal{E} - P^*\sin\mathcal{E})\right]e^{i\mathcal{E}} \quad . \tag{5-40B}$$

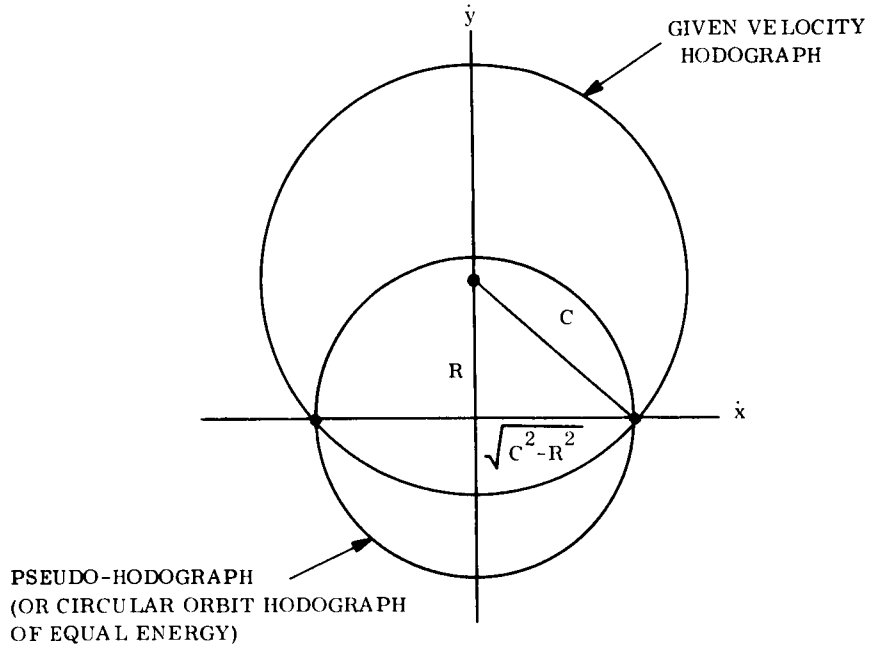

Figure 5-13. Pseudo-Hodograph

Note that the terms k, C_B^* and P* may be expressed in position space parameters, as follows

$$k = a^2/\mu \tag{5-41B}$$

$$C_B^* = \sqrt{\mu/a} \tag{5-42B}$$

$$P^* = e\sqrt{\mu/a} = C_B^* e \quad . \tag{5-43B}$$

Noting that $R_B^* = 0$ and $C_B^* \sqrt{C^2 - R^2}$, it can be shown that these parameters define a pseudo-hodograph which has the same orbital energy as the given orbit, as shown in Figure 5-13. Since the $\dot{x}$-axis intercept of the velocity hodograph is $\sqrt{C^2 - R^2}$, the family of all velocity hodographs with this intercept represents all orbits of the same orbital energy and coincident apsidal lines. Since the original orbital hodograph provides the eccentric anomaly E (Subsection 5.6), then the intersection of an E-line with the pseudo-hodograph (Figure 5-14) defines the hodograph map of a point on the auxiliary circle (Figure 5-2A). In fact, Figures 5-13 and 5-14 are hodographic maps of an orbit and its auxiliary circle from position vector space. Consequently, motion around the pseudo-hodograph as a

spacecraft proceeds in orbit occurs at a constant (or mean) speed n (just as on the auxiliary circle). Also the pedal point P* can be defined in terms of this pseudo-hodograph, as shown in Equation 5-43A. Consequently, the basic spiral shape of the time trajectory can be directly generated without use of the scale factor k.

The complete transformation from the orbital velocity hodograph in velocity vector space to the time trajectory in time state space is summarized in Figure 5-15.

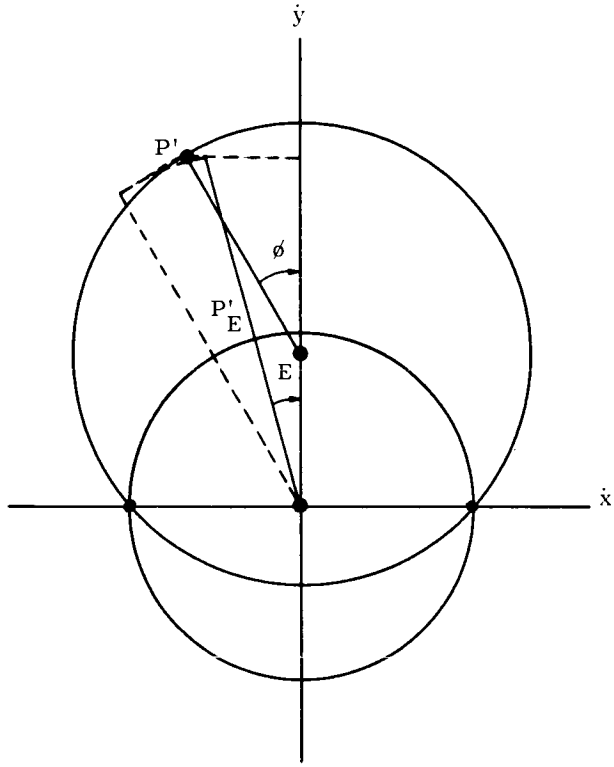

Figure 5-14. Eccentric Anomaly of the Pseudo-hodograph

5.3 HODOGRAPH DETERMINATION FROM A GIVEN TIME LOCUS

If a time locus for an orbital trajectory is arbitrarily given or specified*, then the hodograph parameters of the trajectory or its hodograph in any one vector space (position, velocity or acceleration) are required for complete analysis. Certainly, the inverse transformation from time state space to velocity vector space should be available. In essence, the inverse operations of those discussed in the preceding section will provide the required transformation. For example, the evolute is the inverse of the involute, whereas the negative pedal is the inverse of the pedal.

However, the properties of the time locus, as defined for an orbital trajectory by Equations 5-6 through 5-13, enable direct determination of the complete set of hodograph parameters of

*The synthesis of a trajectory by means of its time locus has not been completely developed. However, further study based upon the analytical results and discussion of this report will provide such synthesis techniques.

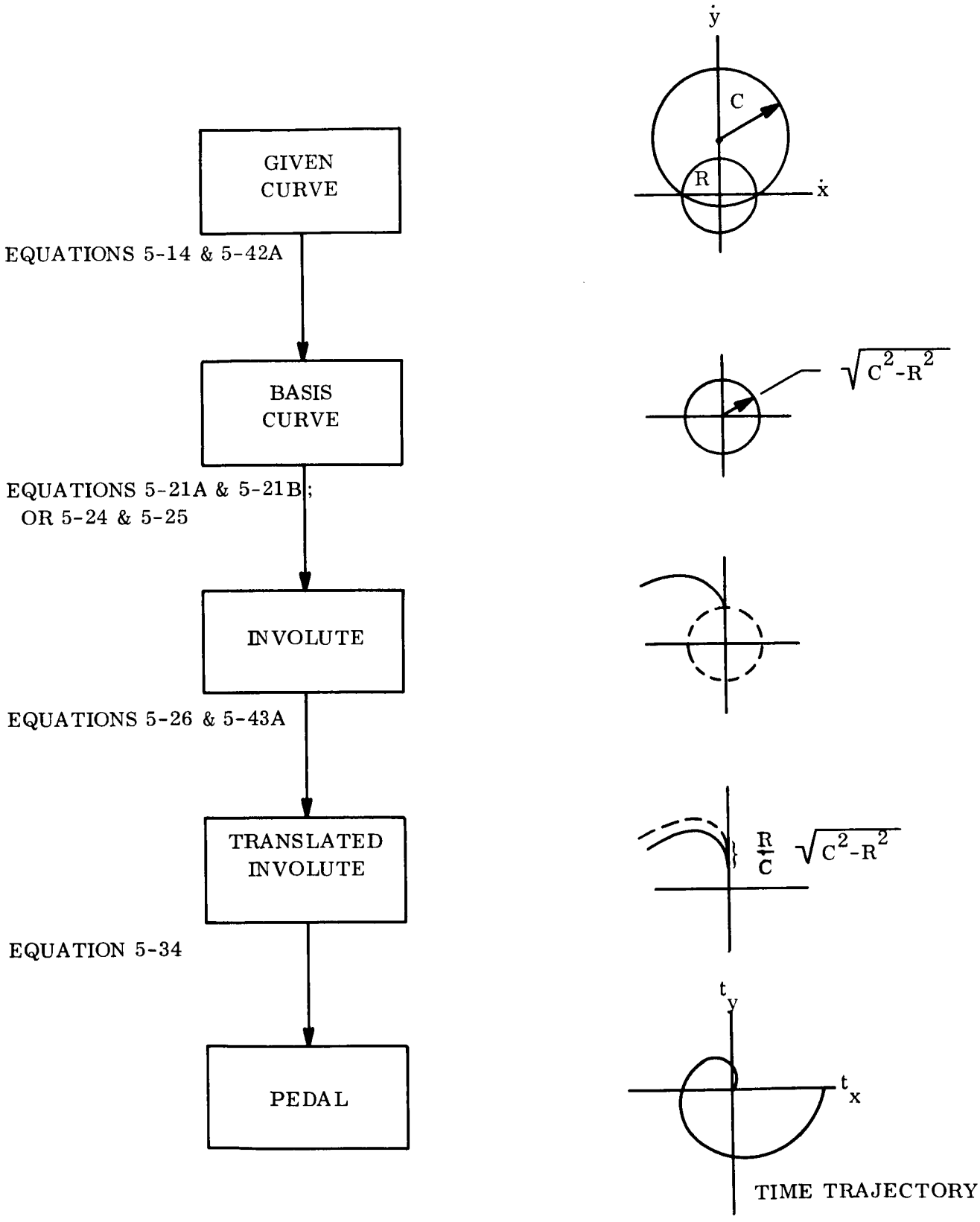

Figure 5-15. Transformation Flow Diagram

the trajectory. That is, the time locus is a complete and unique representation of the trajectory in one of the state spaces; any one locus or hodograph defines all other state loci or hodographs completely. The basic geometric parameters of the time locus are the complex time $\bar{t}$ and the slope angle α (or the polar slope $f = \tan \alpha$).

Let us assume that the given time locus is as shown in Figure 5-16A. The argument ν (referred to the t_x -axis) and scalar of the complex time $\bar{t}$ to any locus point is known, as well as the slope angle α. The parameters C, R, Ψ must be determined. The basic functional equation

$$f = \frac{\mu}{C(C+R\cos\phi)^2} \tag{5-44}$$

for $\tan \alpha$ enables determination of the apsides (consequently Ψ and ϕ) and then, the parameters C, R. Actually, two different methods to determine Ψ are possible. With the one method, Equation 5-44 provides

$$f_{\phi=\pi} = \frac{\mu}{C(C-R)^2} \tag{5-45}$$

and

$$f_{\phi=2\pi} = \frac{\mu}{C(C+R)^2} \tag{5-46}$$

for two successive apsides (apogee and perigee, respectively). The polar slope f is minimum at perigee (such as $\phi = 2\pi$) and maximum at apogee (such as $\phi = \pi$) as shown schematically in Figure 5-16B. Consequently, various radial lines through the origin may be examined until the one line providing minimum (or maximum) polar slope at the intersection of the line and time locus is identified. This radial line defines the given apse, and extension of the line in the opposite direction will define the corresponding apse at its intersection with the time locus*.

*Note that a given apse (such as perigee) is represented by a different point for each complete orbital period, since the time locus is a spiral which never closes upon itself. Extension of the radial line will pass through all such apsidal points.

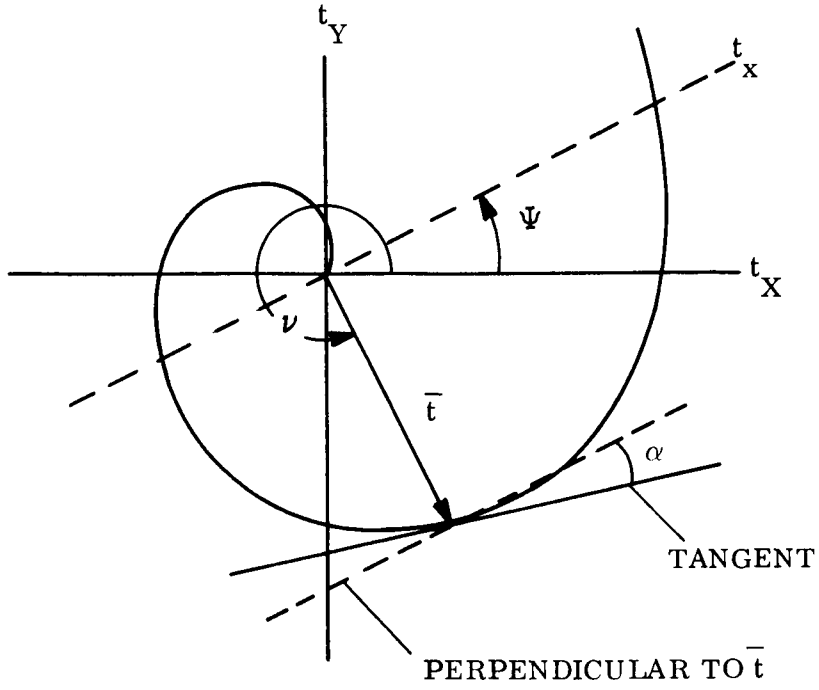

A. GIVEN TIME LOCUS

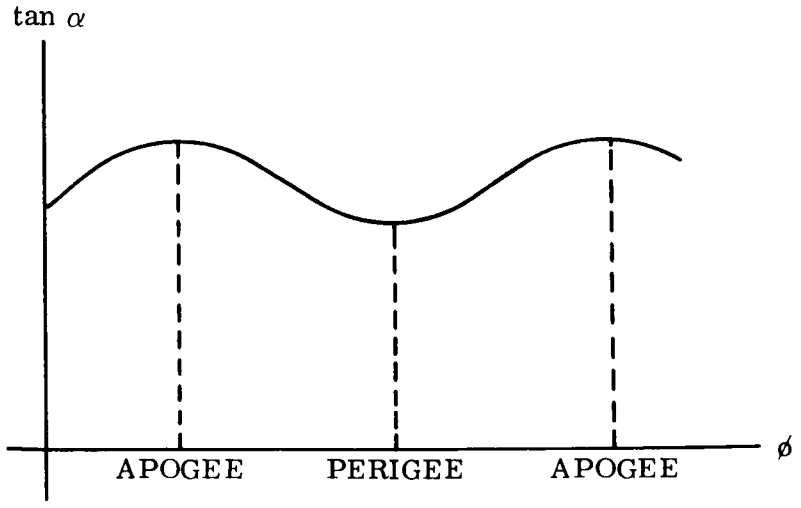

B. POLAR SLOPE CHARACTERISTIC

Figure 5-16. Apsides Determination for Any Given Time Locus

The apsidal line may be determined by another method, which employs the scalars of complex times $\bar{t}_{\pi}$ and $\bar{t}_{2\pi}$. Referring to Table 5-1, Figure 5-4B and the related discussion, it is evident that $t_{2\pi} = 2t_{\pi}$. In fact, the apsidal line is the only radial line in the time state space, which intersects the orbital time locus so that $t_{\phi+\pi} = 2t_{\phi}$. Consequently, the apsidal line can be identified by rotating a scaled line about the origin until this scalar condition is fulfilled. The apsidal points can then be identified as perigee or apogee by use of Equations 5-45 and 5-46. The smaller polar slope occurs at perigee.

Having identified the apsidal line and apsides, the parameters C, R are then determined by means of Equations 5-45 and 5-46, since the polar slopes $f_{\phi = \pi}$ and $f_{\phi = 2\pi}$ are now known. With the parameters C, R, Ψ, the position, velocity and acceleration hodographs can be immediately generated. Finally, each point on the time locus is clearly mapped over into the corresponding hodograph points in the vector spaces.

5.4 PERIMETRIC TIME CURVE

The time locus defines the orbital elapsed time from an arbitrarily selected epoch by means of a directed scalar, with direction defined by the position vector of the orbital trajectory. This definition offers unique advantages in analysis and engineering application, as discussed briefly in Subsection 5.5. However, two alternative definitions with different geometric bases are available. As noted in previous sections, orbital elapsed time can be mapped as an area in velocity vector space (Reference 13). However, orbital elapsed time can also be mapped from the orbital hodograph in acceleration vector space, as a section of the perimeter between two points of a curve which is defined by the acceleration hodograph. This perimetric time curve has special significance when considered together with the time locus.

The orbital acceleration hodograph is defined by

$$A = C\dot{\phi} = \frac{(CV_v)^2}{\mu}$$

where

$$V_v = C + R\cos\phi \tag{5-47}$$

and appears in acceleration vector space (Figure 5-1C). According to Equation 5-9

$$\dot{\phi} = \frac{CV_v^2}{\mu} \tag{5-48}$$

and

$$dt = f \cdot d\phi \tag{5-49}$$

where

$$f = \frac{\mu}{CV_v^2} \quad . \tag{5-50}$$

Viewing the transitions from Equations 5-9 to Equation 5-48 to Equations 5-49 and 5-50 as geometric transformations, the function of Equation 5-50 is obtained by geometric inversion of the acceleration hodograph with respect to a circle of radius $\sqrt{C}$ about the origin of the acceleration vector space (Reference 17). Then the orbital elapsed time between any two given points in an orbit is provided by

$$\int_{t_0}^{t} dt = \int_{\phi_0}^{\phi} f \cdot d\phi \quad . \tag{5-51}$$

The integration defined by Equation 5-51 represents the geometric process of integration along the curve defined by Equation 5-50 (namely, a section of the perimeter of the curve). This is easily seen when f is recognized as the polar ρ of the curve. Then Equation 5-46 is (in geometric terms) directly represented by

$$ds = \rho \cdot d\phi \quad . \tag{5-52}$$

The acceleration hodograph, circle of inversion and perimetric time curve are shown schematically in Figure 5-17. Several characteristics of this perimetric time curve are extremely noteworthy:

a. The curve is generated directly from the acceleration hodograph by means of a basic and simply defined transformation -- geometric inversion.

b. The orbital elapsed time is directly available as a function of the true anomaly ϕ without the intermediate use of the eccentric anomaly E.

c. The length of the tangent line which generates the involute of the perimetric time curve is the orbital elapsed time. Given an arbitrary set of orbital points for which the elapsed time is desired, the initial point will be the point of initiation of the involute and the final point will be the contact point of the curve with the tangent line to the involute.

d. The orientation of the perimetric time curve in vector space is identical with that of the acceleration vector, which is 180 degrees ahead of the position vector (Figure 5-1, A and C). Consequently, the perimetric time curve has a direct correspondence with the time locus in time state space. In essence, the perimetric time curve presents the periodic cycloidal variation of the spiral of the time locus. While the time locus always spirals outward, the perimetric time curve repeats with orbital period. For a powered trajectory, this curve will not close upon itself but will lie within a region bounded by the perimetric time curve of maximum orbital period encountered during the complete trajectory.

The state space concept and treatment of time in orbital dynamics opens many new approaches to the old and extremely complex problem of analysis of a basic state variable -- time. The

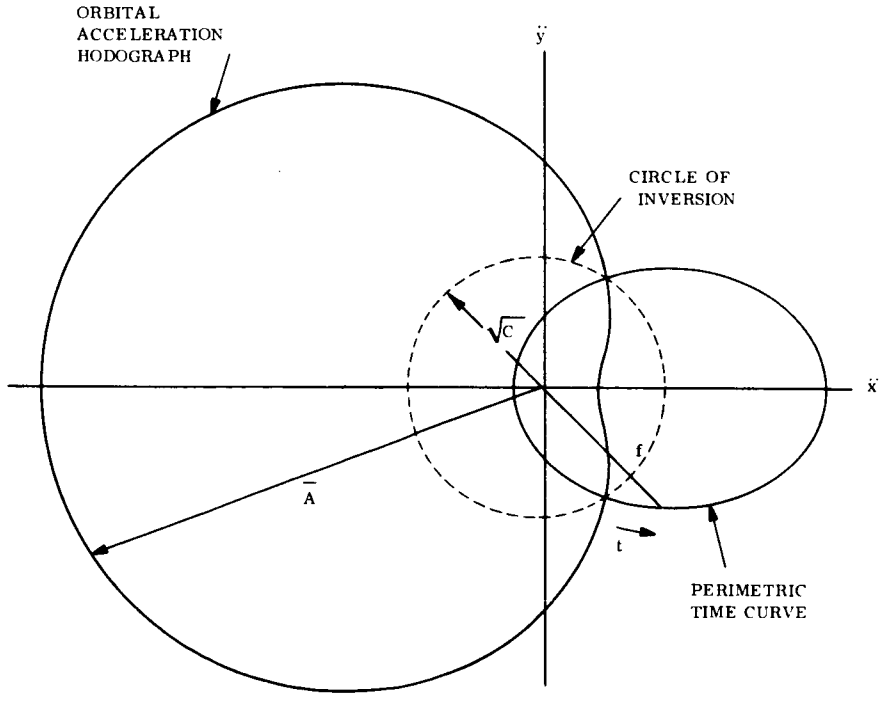

Figure 5-17. Perimetric Time Curve

time locus and the related transformations have excellent potential both for basic trajectory analysis and for system applications. A few illustrative applications are discussed briefly in the Section 5.5.

5.5 POTENTIAL APPLICATIONS

It has been shown that an orbital trajectory is completely defined by a unique locus in a time state space, which presents time as a complex variable with Cartesian coordinate reference axes and origin identical with the vector space of position, velocity and acceleration. Consequently, an orbital trajectory may be completely synthesized and analyzed in the time state space, just as in the vector spaces (that is, an orbital trajectory may be synthesized or shaped in time state space by explicit selection of the basic hodograph parameters in accordance with time constraints or conditions which may be imposed). This synthesis would directly determine the trajectory hodographs (or state loci) in all vector spaces by means of transformation between the time and vector spaces. Of course, the basic geometry of the orbital trajectory consists of a different class of curve than previously encountered in the vector space theory of Newtonian mechanics (namely, the spiral). At this point, it is interesting to summarize the characteristic forms of curve which the orbital trajectory assumes in the various state (or vector spaces):

SPACE	CHARACTERISTIC CURVE
Position	Conic
Velocity	Circle
Acceleration	Variant of Pascal's Limaçon
Time	Spiral

Note that these characteristic forms of curve are the parametric representations of any trajectory in the presence of one force center. These forms are explicitly apparent for a ballistic trajectory as shown in Figures 5-1 and 5-4. On the other hand, they are implicitly present in the instantaneous orbits of a powered trajectory, as shown in Figure 1-11 A andB of Section 1, Figure 3-7 of Section 3, and Figure 5-5 of Subsection 5.1. The utility of these

respective forms of the orbital trajectory will be dependent upon the various requirements of a given trajectory problem; for example, the thrust law (for powered orbital segments), the state variables which are subject to constraint, the observed or measured state variables, etc. Although synthesis and analysis in position vector space has been classically employed, and velocity vector space analysis is currently entering contemporary practice, acceleration vector space and time state space analysis is still in research study and application development.

When time constraints become outstanding, such as in rendezvous, time locus analysis merits special attention. Let us briefly discuss some aspects of the potential application of the time loci of trajectories, for intercept and rendezvous missions as illustrative examples. Let us first consider the conventional graphical representation of a trajectory in position vector space (Figure 5-18A). To identify the time at which each trajectory point occurs, a coding by means of point markers and corresponding time numerics is required. Such coding is not useful in direct and explicit analysis, but only as a graphical synopsis for visual examination by an engineer, analyst or astronaut. In contrast, the time locus and trajectory path shown in Figure 5-18B are well-defined in state (and vector) space so that explicit state analysis can be conducted in accordance with the analytical techniques of state (or vector) analysis* and transformation theory. Each position vector to a point of the trajectory must pass through the complex time point of the trajectory time locus as shown for points at t_1, t_2 and t_3.

Spacecraft intercept defines the simultaneous arrival of two spacecraft bodies at a given point in position vector space (Figure 5-19A). The velocity vectors may be entirely different; it is only required that

$$\left.\begin{aligned} \bar{t}_{I1} &= \bar{t}_{I2} \\ \bar{r}_{I1} &= \bar{r}_{I2} \end{aligned}\right\}$$

*Although the logic or algorithm of time state space differs from that of the vector spaces (i.e., position, velocity and acceleration), it is nevertheless a well-defined part of general vector space theory.

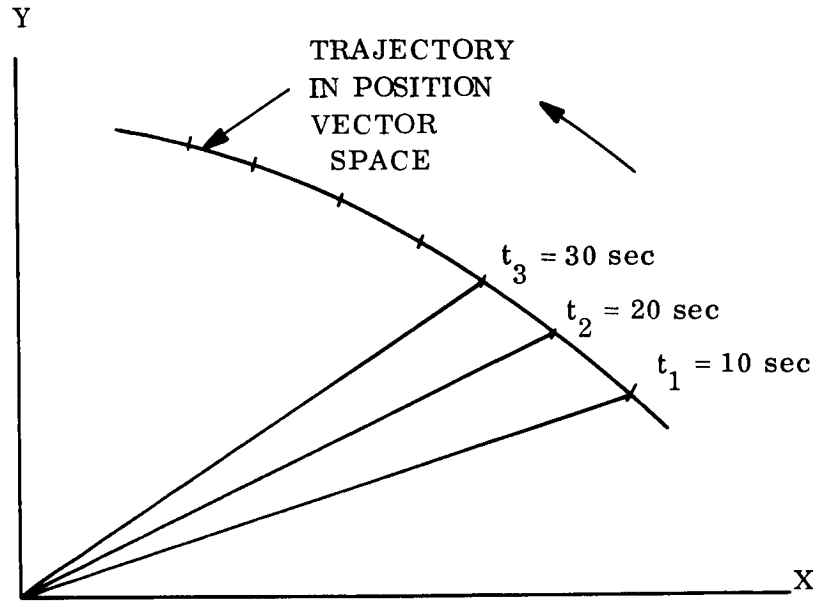

A. CONVENTIONAL GRAPH OF A TIME-REFERENCED TRAJECTORY

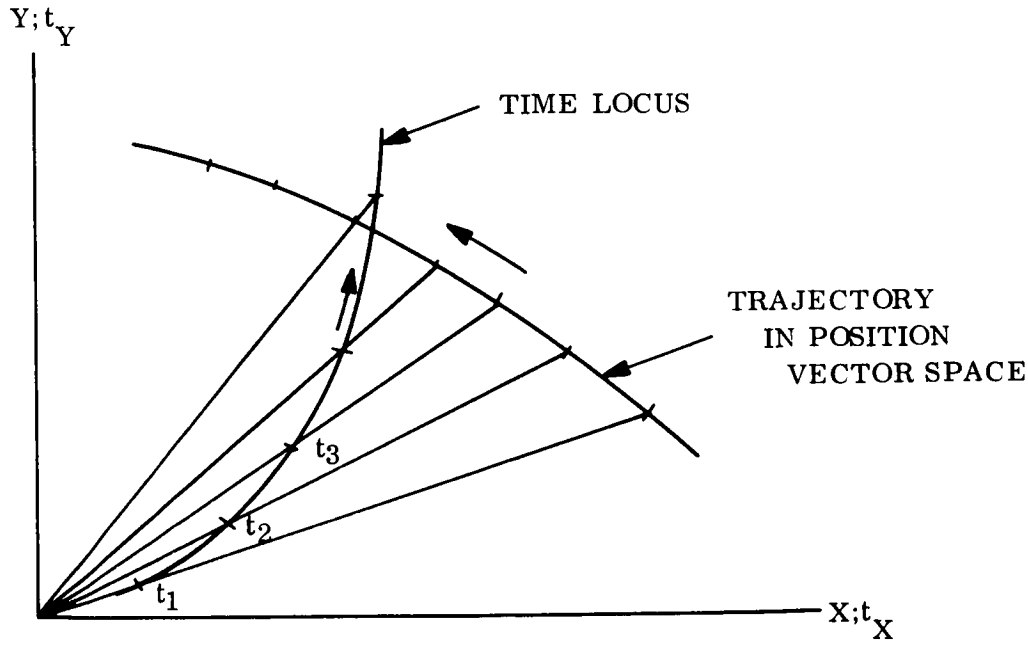

B. TIME AND POSITION LOCI OF A TRAJECTORY

Figure 5-18. Time and Position States of a Trajectory

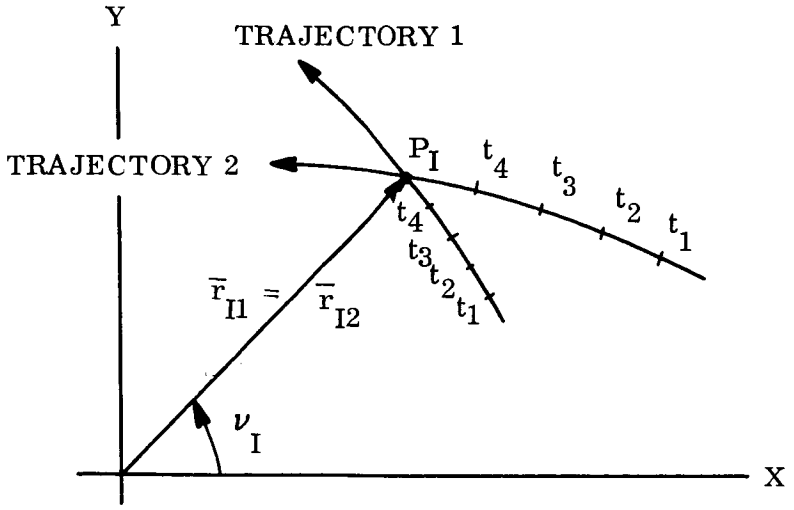

A. SUCCESSFUL INTERCEPT (CONVENTIONAL GRAPH)

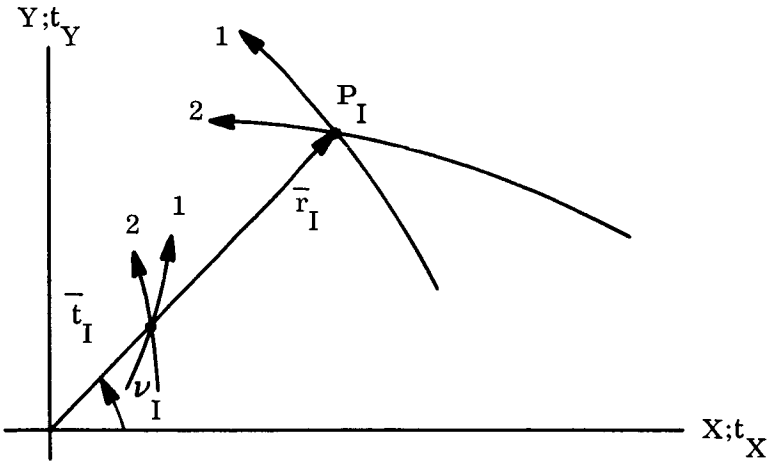

B. SUCCESSFUL INTERCEPT (STATE SPACE THEORY)

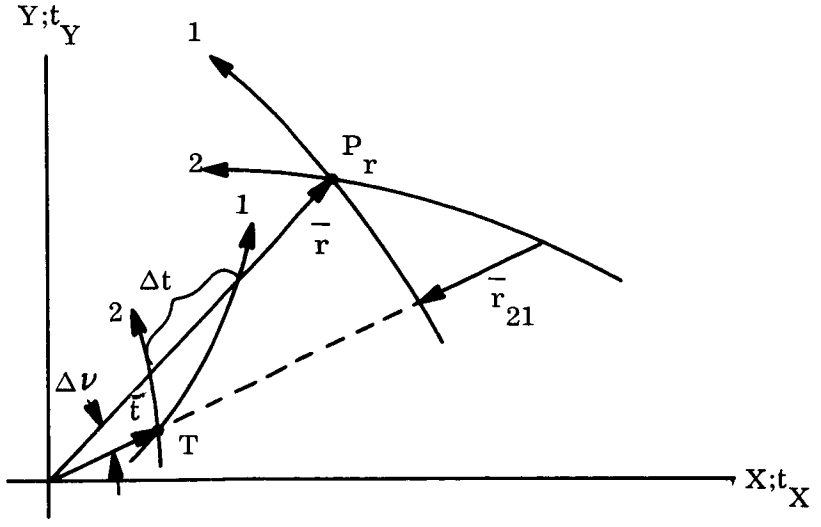

C. UNSUCCESSFUL INTERCEPT (STATE SPACE THEORY)

Figure 5-19. Spacecraft Intercept

The conventional representation of successful intercept can be replaced by the state space representation shown in Figure 5-19B. With these trajectory loci of position and complex time, successful intercept is fulfilled by the condition that the intersection of the two time loci lies at the same argument or direction angle as shown (that is, the position vector $\bar{r}_I$ coincides with the complex time $\bar{t}_I$) . Since the complete predicted trajectory loci are uniquely presented, all such points of successful intercept are directly apparent for the entire trajectory.

Unsuccessful intercept is evident when the above condition is not fulfilled (Figure 5-19C). In this case, the two spacecraft differ in arrival time at the position loci point of intersection P_r by the time difference Δt between the time loci intersections with the position vector $\bar{r}$ to the point P_r. If the complex time $\bar{t}$ to the time loci point of intersection P_t is extended to intersection with the position loci, then the directed line between the two intersection points is the relative position vector $\bar{r}_{21}$ between the two spacecraft at the time t. Although the significance of the angle between the position loci intersection (i.e., the position vector $\bar{r}$) and the time loci intersection (i.e., the complex time $\bar{t}$) is not yet understood, it is anticipated that it will prove valuable for synthesis techniques which enable reshaping of the respective spacecraft trajectories to provide successful intercept.

In general, the relative position vector at any time may be directly obtained (Figure 5-20). Assume that the position and time loci for Spacecraft 1 and 2 are given, and the relative position vector when Spacecraft 1 reaches State A is required. Consequently, the inertial position vector $\bar{r}_{A1}$ is initially specified. At the intersection point T_{A1} of the position vector $\bar{r}_{A1}$ with the corresponding Time Locus 1, construct the isochrone (i.e., a circle) as shown. At the intersection point T_{A2} of the isochrone contour with Time Locus 2, direct a radius line from the origin to intersection with Position Locus 2; the position vector $\bar{r}_{A2}$ is thereby defined. Consequently, the relative position vector $\bar{r}_{12/A}$ is obtained by the vector difference operation. If the state conditions are desired when Spacecraft 2 is at P_{B2} (i.e., with the same argument ν as before), then the comparable operations shown in Figure 5-20B identify the time and position vector for Spacecraft 1.

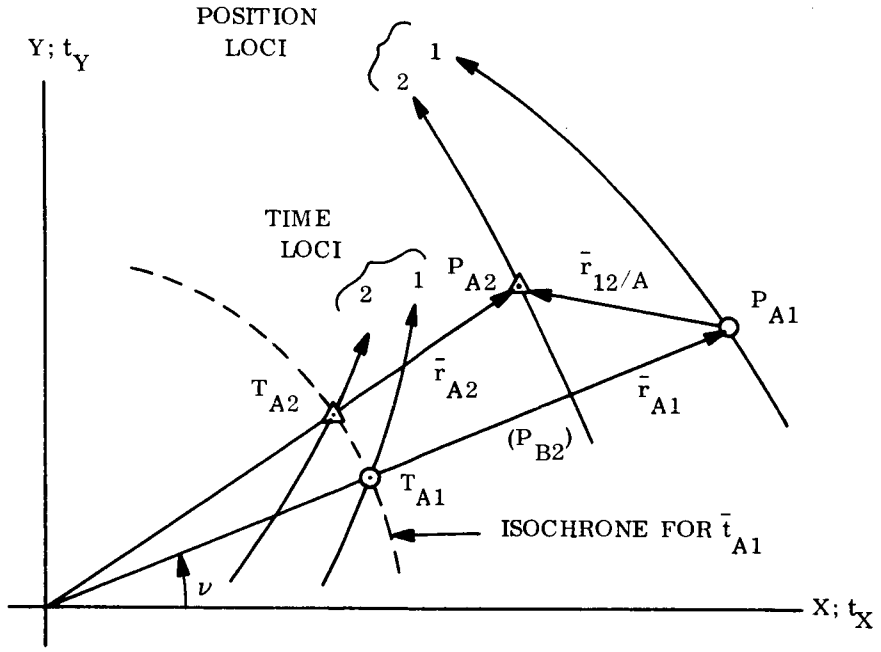

A. FOR SPACECRAFT "A" ARRIVAL AT STATE "A1" (GIVEN ν)

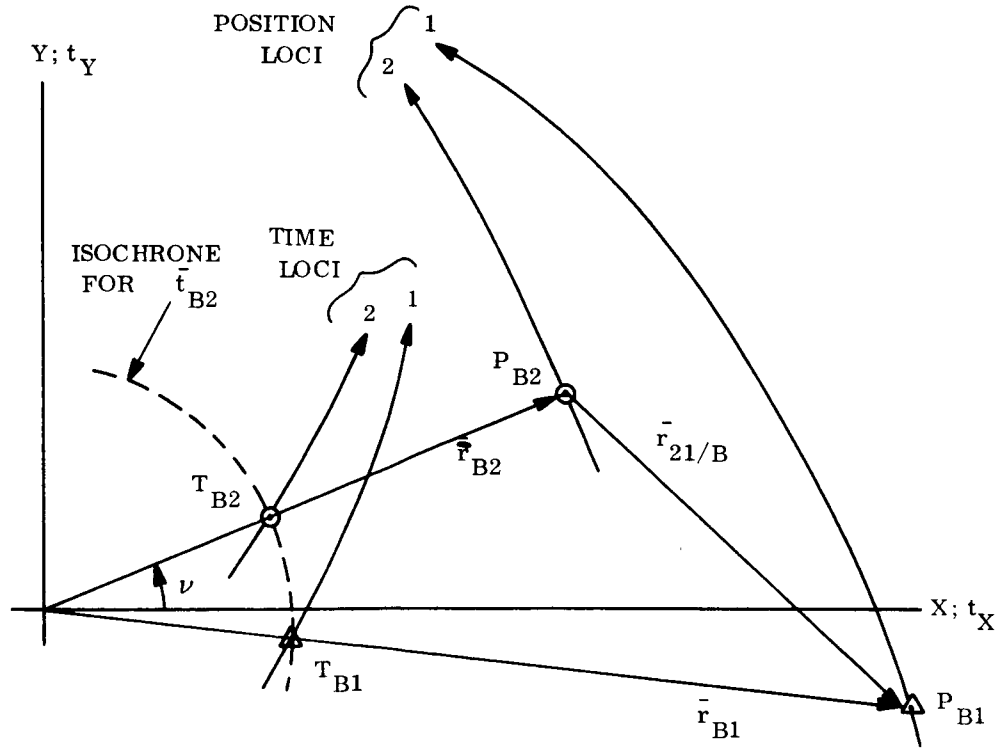

B. FOR SPACECRAFT "B" ARRIVAL AT STATE "B2" (GIVEN ν)

Figure 5-20. Relative Position Vector Between Spacecraft

The composite diagram of trajectory states may be extended to include the velocity hodographs (Figure 5-21). However, the inertial velocity vectors are not directed with the same argument ν as the position vectors. Actually, the inertial direction of the velocity vector at any trajectory point is displaced from ν by the flight path angle which exists (referred to as the instantaneous orbital hodograph, Figure 5-1B). Consequently, each absolute velocity vector must be rotated through the angle θ in order to be then directed with the position vector argument ν. If the relative velocity vector is to be presented with the correct vector magnitude and direction, it must undergo translation which is a function of θ_1, θ_2, ν_1, ν_2 so that its endpoints lie then on the radial lines defined by ν_1 and ν_2 (Figure 5-21).

Spacecraft rendezvous defines the simultaneous arrival of two spacecraft bodies at a given point in position vector space with identical velocity vectors (Figure 5-22A). The intersections of the position, velocity and time loci, respectively, must occur on one radial line. Note that the loci after intersection and passage past this radial line must reduce to one path for each state. The rendezvous shown in Figure 5-22A was obviously completed by impulsive thrust applied to Spacecraft 1 at the rendezvous point, since its state loci undergo discontinuous change at rendezvous; continuous thrust application would provide continuous curves of state loci. The velocity loci, as shown in Figure 5-22, must have been reoriented as previously described (Figure 5-21). Unsuccessful rendezvous will occur if velocity vectors, complex times or position vectors are not identical when the other two state loci coincide (Figure 5-22, B and C) for velocity vector and complex time discrepancies, respectively).

In the preceding section, it was noted that the perimetric time curve repeats with orbital period for a ballistic trajectory, or remains within a bounded area for a powered trajectory. Because of its unique properties, the perimetric time curve appears quite promising for many complex trajectory problems with time constraints. For example, the study and selection of time coincidence of multiple-period orbits for two or more orbital spacecraft becomes more tractable to analysis. Noting that

$$\rho = \frac{r}{V_\nu} \quad , \qquad (5\text{-}53)$$

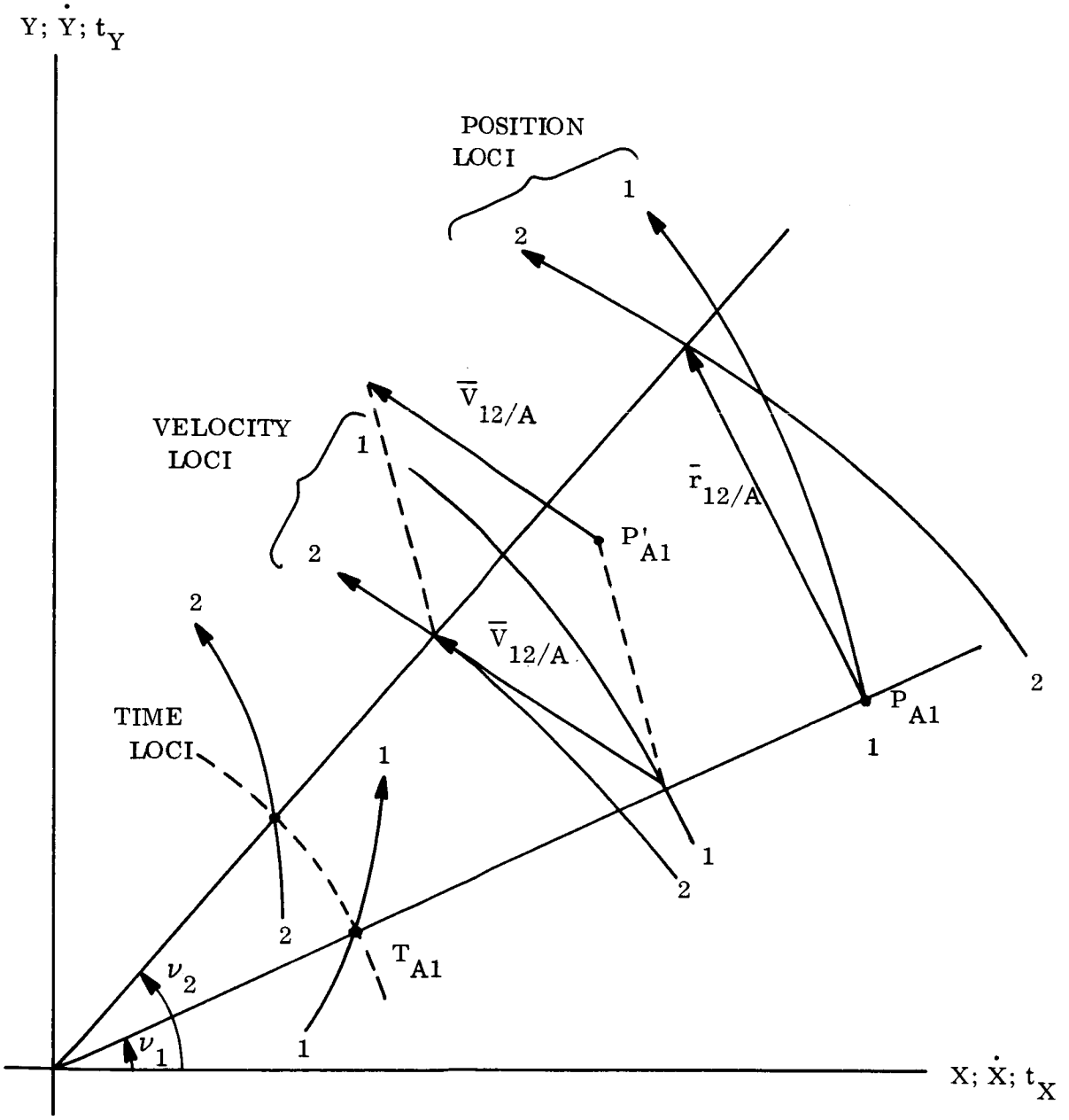

Figure 5-21. Relative Position and Velocity Vectors Between Spacecraft

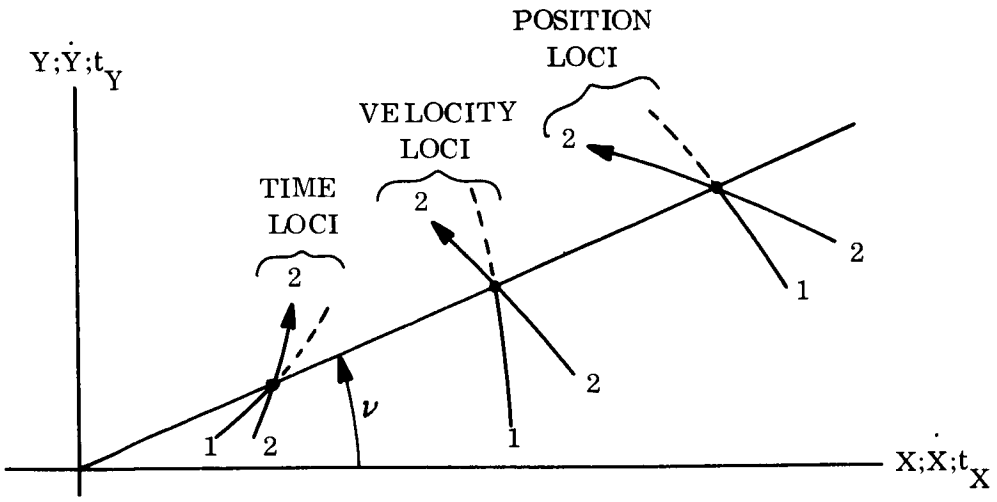

A. SUCCESSFUL RENDEZVOUS

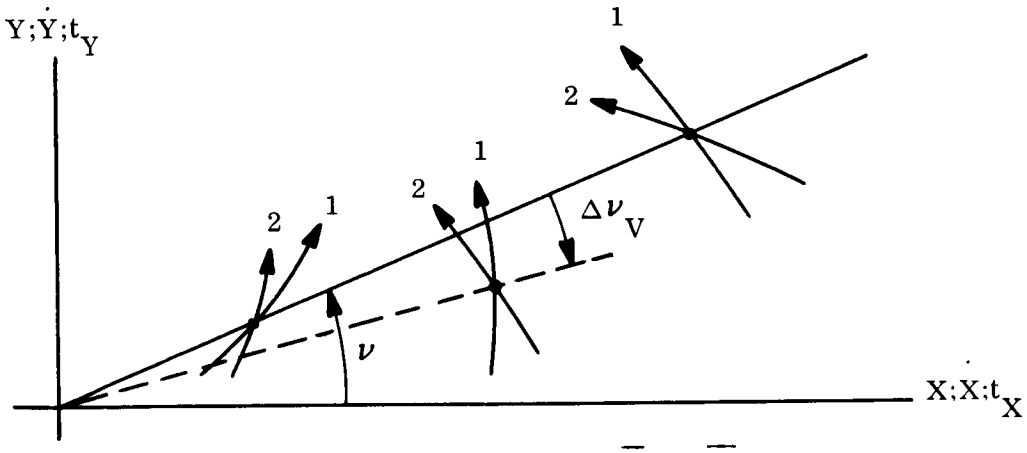

B. UNSUCCESSFUL RENDEZVOUS ($\bar{V}_{1\nu} \neq \bar{V}_{2\nu}$)

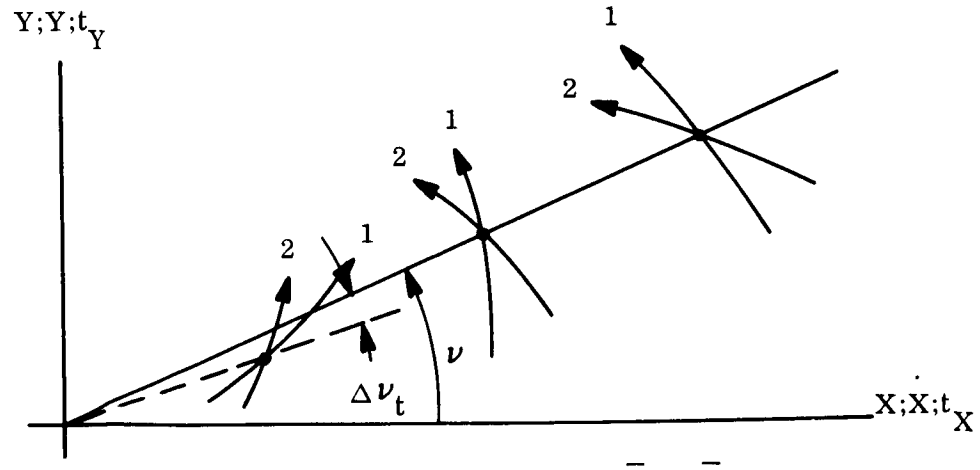

C. UNSUCCESSFUL RENDEZVOUS ($\bar{t}_{1\nu} \neq \bar{t}_{2\nu}$)

Figure 5-22. Spacecraft Rendezvous

it appears that satellite coverage problems of multisatellite networks might be more effectively treated by use of the perimetric time curve in place of the orbit in position vector space. Finally, it appears resonable that the time locus in time state space may be obtained by means of the perimetric time curve, with basic geometric transformations which do not require the use of the eccentric anomaly transform.

Although the time locus and the perimetric time curve have been developed and discussed in detail for ballistic trajectory only, the basic definitions are completely valid for powered or perturbed trajectories as well. Moreover, the parametric analysis techniques being developed in general form under both Phases IIIA and IIIB are directly applicable (as illustrated schematically in Figure 5-5). In particular, the perimetric time curve appears attractive for the detailed study of the periodic characteristics of perturbations about a basic nominal orbit. Finally, the use of complex time in the stability criterion proposed for nonlinear systems in Reference 8 might facilitate further definition and study of orbital or trajectory stability.

5.6 GENERATION OF THE ECCENTRIC ANOMALY IN VELOCITY VECTOR SPACE

Various classical and modern techniques have been devised for the geometric generation of the eccentric anomaly from the true anomaly of an orbit due to one force center. The classical form employing the "auxiliary" (or eccentric) circle in position vector space is shown in Figure 5-2A, which represents the equation

$$\tan\left(\frac{E}{2}\right) = \sqrt{\frac{1-e}{1+e}}\ \tan\left(\frac{\phi}{2}\right) \qquad (5\text{-}54)$$

In terms of the conic parameters of the elliptic orbit in position vector space, the Cartesian coordinates of a point P on the elliptic orbit and its corresponding point P_E on the auxiliary circle are related by the equations

$$a \cos E = ae + r \cos \phi \qquad (5\text{-}55)$$

$$b \sin E = r \sin \phi \qquad (5\text{-}56)$$

Also, the radius r from the force center to the given point in orbit is defined, in conic parameters, by

$$r = \frac{a(1-e^2)}{1+e\cos\phi} \quad . \tag{5-57}$$

Use of Equation 5-57 with Equations 5-55 and 5-56 provide

$$\cos E = e + \frac{(1-e^2)\cos\phi}{1+e\cos\phi} \tag{5-57A}$$

$$\sin E = \frac{\sqrt{1-e^2}\,\sin\phi}{1+e\cos\phi} \tag{5-58A}$$

Since

$$e = R/C \tag{5-59}$$

the eccentric anomaly equations are defined in velocity hodograph parameters as follows:

$$\cos E = \frac{R+C\cos\phi}{C+R\cos\phi} \tag{5-57B}$$

$$\sin E = \frac{\sqrt{C^2-R^2}\,\sin\phi}{C+R\cos\phi} \quad . \tag{5-58B}$$

Equation 5-57B suggests a geometric generation of the eccentric anomaly E from the true anomaly ϕ, in velocity vector space, as shown in Figure 5-23. Given an inertial velocity hodograph and any given hodograph point defined by the true anomaly ϕ, the successive steps for generating the eccentric anomaly E are as follows:

a. Project $\bar{C}$ on the y-axis and add this projection to $\bar{R}$ to obtain (R + C cos ϕ).

b. Project $\bar{R}$ on a line parallel to $\bar{C}$ and add this projection to a one-to-one projection of $\bar{C}$ on this line to obtain (C + R cos ϕ).

c. Erect the perpendicular to the y-axis at (R + C cos ϕ) from the origin.

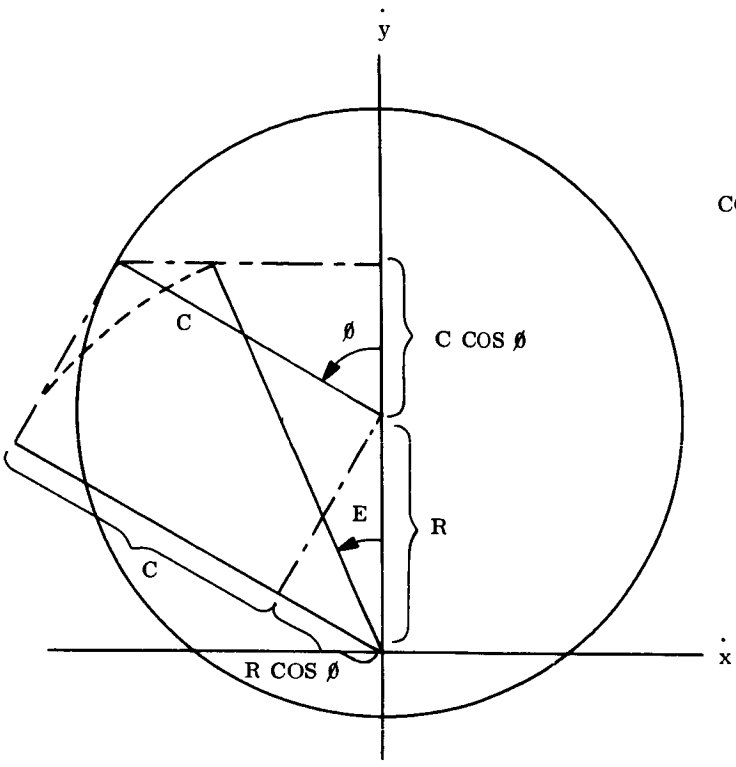

$$\cos E = \frac{R + C \cos \phi}{C + R \cos \phi}$$

Figure 5-23. Generating Eccentric Anomaly E from True Anomaly ø

d. Rotate (C + R cos ø), obtained from b, about the origin in a clockwise direction until intersection with the perpendicular in c.

e. The line from the intersection point of d to the origin forms the eccentric anomaly E with the ẏ-axis.

5.7 INVOLUTE OF A BASIS CURVE

The involute of a basis curve is the path described by the end of a flexible, non-extendable cord lying along the basis curve when unwound so that the cord remains taut and tangent to the curve (References 13, 14). Any point on the involute (Figure 5-24) is defined by the complex addition of the radius vector $\bar{z}_B$ to the tangency point P_T on the basis curve, and the tangent vector $\bar{z}_T$ from the tangency point P_T to the corresponding point on the involute (P_I); that is,

$$\bar{z}_I = \bar{z}_B + \bar{z}_T \qquad (5\text{-}59)$$

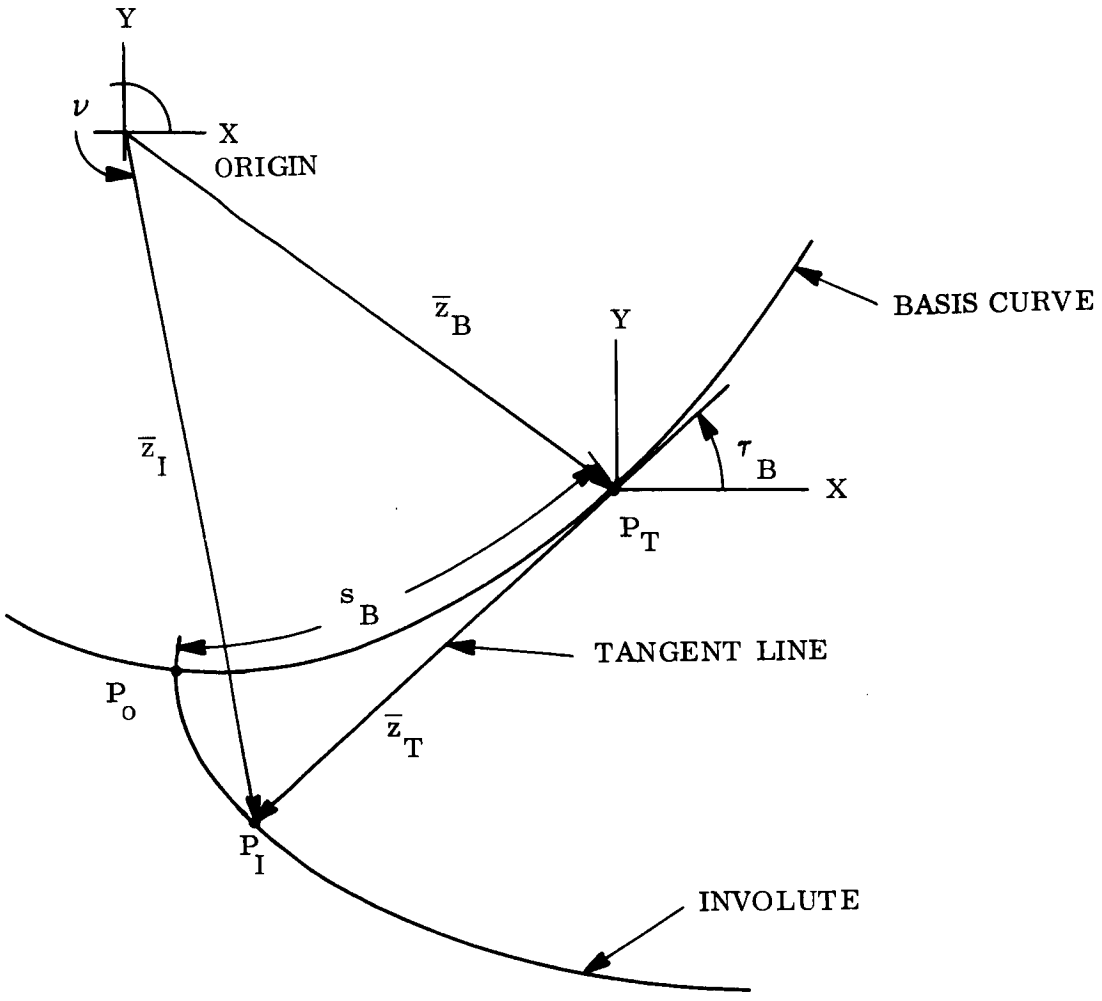

Figure 5-24. Vector Definition of the Involute

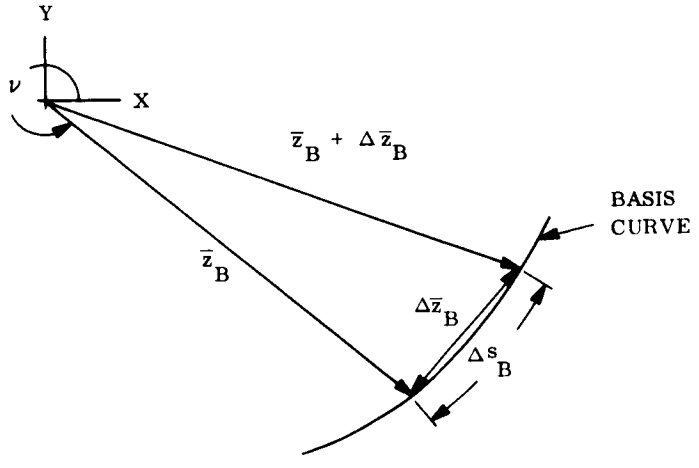

Figure 5-25. Increment of Path Length Along the Basis Curve

Assume that the radius vector $\bar{z}_B$ is defined as a function of a parameter such as the direction angle ν; that is,

$$\bar{z}_B = \bar{z}_B(\nu) \quad . \tag{5-60}$$

Then $\bar{z}_T$ and finally $\bar{z}_I$ must also be expressed as functions of the parameter ν.

According to the definition of the involute, the scalar z_T must be equal to the path length (s_B) along the basis curve between the point of initiation of the involute (P_O) and the tangency point (P_T). Consequently,

$$\bar{z}_T = s_B e^{i\xi_B} \tag{5-61}$$

where

$$\xi_B = \tau_B + \pi \quad , \tag{5-62}$$

so that

$$\bar{z}_T = s_B e^{i\tau_B} e^{i\pi} = -s_B e^{i\tau_B} \tag{5-63}$$

and

$$\bar{z}_I = \bar{z}_B - s_B e^{i\tau_B} \tag{5-64}$$

Since given basis curve is defined by the radius vector $\bar{z}_B(\nu)$, the path length s_B and tangent angle t_B must be expressed in terms of $\bar{z}_B$. Referring to Figure 5-25, it is seen that

$$\Delta s_B \doteq \left| \Delta \bar{z}_B \right| \tag{5-65}$$

so that

$$s_B = \int_{u_0}^{u} \left(\frac{ds_B}{d\nu} \right) d\nu = \int_{u_0}^{u} \left| \frac{d\bar{z}_B}{d\nu} \right| d\nu \tag{5-66}$$

In the limit,

$$d\bar{z}_B = (ds_B) e^{i\tau_B} \tag{5-67}$$

so that the argument for the tangent angle t_B can be expressed as

$$e^{i\tau_B} = \frac{d\bar{\jmath}_B}{ds_B} = \left(\frac{d\bar{\jmath}_B}{dv}\right)\left(\frac{dv}{ds_B}\right) \quad . \tag{5-68}$$

Finally,

$$\bar{\jmath}_I = \bar{\jmath}_B(v) + \bar{\jmath}_T(v) \tag{5-69}$$

in which

$$\bar{\jmath}_T(v) = \left\{\left[-\int_{u_0}^{u} \left|\frac{d\bar{\jmath}_B}{dv}\right| dv\right]\left[\left(\frac{d\bar{\jmath}_B}{dv}\right)\left(\frac{dv}{ds_B}\right)\right]\right\} \tag{5-70A}$$

or

$$\bar{\jmath}_T(v) = -s_B\left(\frac{d\bar{\jmath}_B}{ds_B}\right) \quad . \tag{5-70B}$$

References

1. Phase Work Report IIIB-1, "Genesis of the Problem (Acceleration Hodograph Analysis Powered Orbital Trajectories)" dated September 30, 1966.

2. Phase Work Report IIIB-2, "Transformation Functions of the Orbital Hodographs" dated September 30, 1966.

3. Phase Work Report IIIA-1, "Formal Presentation of the Hodographic Equations of Motion," dated January 16, 1967.

4. S.P. Altman, Orbital Hodograph Analysis, Vol. 3 AAS Science and Technology Series, Western Periodicals 1965.

5. M. Born, Einstein's Theory of Relativity, Dover Publications, 1962.

6. G. Joos, Theoretical Physics, Hafner Publishing, New York, 1950, pp. 257-258.

7. H. C. Plummer, An Introductory Treatise on Dynamical Astronomy, Dover Publications, New York, 1960.

8. Y. H. Ku and A. A. Wolf, "A Stability Criterion for Nonlinear Systems," Applications and Industry, American Institute of Electrical Engineers, July, 1959.

9. V.V. Golubev, Lectures on Integration of the Equations of Motion of a Rigid Body about a Fixed Point, Moscow, 1953 (Translation from Russian under OTS 60-21163, Monson, Jerusalem, 1960).

10. E. Leimanis and N. Minorsky, Dynamics and Nonlinear Mechanics, Some Recent Advances in the Dynamics of Rigid Bodies and Celestial Mechanics, Wiley, New York, 1958.

11. W. D. MacMillan, Statics and the Dynamics of a Particle, Dover Publications, New York, 1958.

12. F.T. Sun, "On the Hodograph Method for Solution of Orbit Problems," Proceeding of the 12th International Astronautical Congress, Academic Press, New York, 1963, pp. 879-915.

13. Phase Work Report IIIB-4, "Areal Mapping of Time in Velocity Vector Space", dated February 28, 1967.

14. R.C. Yates,Curves and Their Properties, J.W. Edwards, Ann Arbor, Michigan, 1952, p. 209.

15. C. Zwikker, The Advanced Geometry of Plane Curves and Their Applications, Dover Publications, New York, 1963. p.209.

16. "Special Curves," Encyclopedia Britannica, Vol. 6, p. 894.

17. S.P. Altman, "The Hodographic Theory of Newtonian Mechanics," Recent Developments in Space Flight Mechanics, Vol. 9, AAS Science and Technology Series, AAS Publications, Tarzana, California, 1966, pp. 45-102.

SECTION 6

AREAL MAPPING OF TIME IN VELOCITY VECTOR SPACE

AUTHOR: JOSEF S. PISTINER

SECTION 6

AREAL MAPPING OF TIME IN VELOCITY VECTOR SPACE

The analysis of the time constraints upon an orbital trajectory may be conducted in position, velocity, or acceleration vector spaces, or time state space. Time analysis in position vector space employs Kepler's equation and its graphical representation by the auxiliary circle(Reference 1). Various representations of trajectory time in velocity vector space have been developed in terms of the eccentric anomaly and the hodograph parameters C, R (Reference 2 and 3). The time locus in time state space presents trajectory time as complex time referred to an arbitrary epoch(Reference 4).

This report presents elapsed time between two points along an orbital trajectory by equations which represent an area swept out in velocity vector space, as the spacecraft proceeds in orbit. This treatment is considered a significant and complementary addition to the vector space techniques of trajectory analysis under time constraints. In particular, this areal mapping of time is directly and simply related to the velocity hodograph in a form which should be very useful in mission analysis and trajectory feasibility studies.

Kepler's equation is defined as

$$nt = E - e \sin E \tag{6-1}$$

where

n = mean orbital velocity,

t = elapsed time from perigee passage,

e = eccentricity of the orbital conic figure .

Also,

$$n = (C^2 - R^2)^{3/2}/\mu \tag{6-2}$$

and

$$E = \arcsin\left[\frac{\sin\phi\sqrt{C^2-R^2}}{C+R\cos\phi}\right] . \tag{6-3A}$$

But it can be shown that

$$\frac{\sin\phi}{C+R\cos\phi} = \left(\frac{C}{\mu}\right)y \tag{6-4}$$

so that

$$E = \arcsin\left[\left(\frac{C}{\mu}\sqrt{C^2-R^2}\right)y\right] . \tag{6-3B}$$

Consequently, since $e = R/C$,

$$nt = \arcsin\left[\left(\frac{C}{\mu}\sqrt{C^2-R^2}\right)y\right] - \left(\frac{R}{\mu}\sqrt{C^2-R^2}\right)y . \tag{6-5}$$

Equation 6-5 is a form of Kepler's equation still in position vector space, although the velocity hodograph parameters C, R have been employed rather than the conic parameters a, e. This hybrid form leads then to Kepler's equation in velocity vector space, as a function of the flight path angle θ. It can be shown that

$$\tan\theta = \left(\frac{RC}{\mu}\right)y \tag{6-6}$$

or

$$y = \left(\frac{\mu}{RC}\right)\tan\theta \tag{6-7}$$

so that

$$nt = \arcsin\left[\left(\frac{\sqrt{C^2-R^2}}{R}\right)\tan\theta\right] - \left[\left(\frac{\sqrt{C^2-R^2}}{C}\right)\tan\theta\right] . \qquad (6\text{-}8)$$

Before proceeding with development of the areal map of time in velocity vector space, a direct geometric mapping of the trajectory time in position vector space is presented. Note that the auxiliary circle for Kepler's equation, Equation 6-1, provides a graphical map only of the eccentric anomaly E, not the mean anomaly nt. The parametric equations for a curtate cycloid(References 5 and 6) are

$$x = c\delta - d\sin\delta \qquad (6\text{-}9)$$

$$y = c - d\cos\delta \qquad (6\text{-}10)$$

where $d < c$. The curtate cycloid is the locus of a point P which is located at a distance d from the center of a circle (with radius C) rolling along the x-axis. Let

$$nt = x = E - e\sin E \qquad (6\text{-}11)$$

and

$$y = 1 - e\cos E \quad ; \qquad (6\text{-}12)$$

then it is evident that Kepler's equation can be represented by a curtate cycloid in which

$$c = 1,$$
$$d = e,$$
$$\delta = E .$$

Note then that

$$y = \frac{dx}{dE} \tag{6-13}$$

$$= n \frac{dt}{dE} \quad . \tag{6-14}$$

6.1 GENERATION OF THE ECCENTRIC ANOMALY IN VELOCITY VECTOR SPACE

In Appendix A of Reference 4, the eccentric anomaly was generated in velocity vector space for corresponding points on the velocity hodograph. An alternative generating process is described here. Since it can be shown that

$$\cos E = \frac{R + C\cos\phi}{C + R\cos\phi} \quad , \tag{6-15}$$

$$\tan E = \frac{\sin\phi\sqrt{C^2 - R^2}}{R + C\cos\phi} \tag{6-16}$$

is obtained by means of Equations 6-3A and 6-15. The geometric construction of the eccentric anomaly, based upon Equation 6-16, is shown in Figure 6-1. Given an inertial velocity hodograph and any given hodograph point defined by the true anomaly ϕ, the successive steps of this construction are as follows:

a. Project $\bar{C}$ on the $\dot{y}$-axis by means of the projection line PZ and add this projection to $\bar{R}$ to obtain $(R + C\cos\phi)$;

b. Generate a circle with center identical with the hodograph center, and radius equal to the segment OT of the $\dot{x}$-axis intersected by the hodograph circle (consequently $\sqrt{C^2 - R^2}$);

c. At the intersection Q of the true anomaly radius SP with the circle generated in b, erect a line parallel with the $\dot{y}$-axis until intersection W with the projection line PZ; and

d. The line from the intersection point W to the origin forms the eccentric anomaly E with the $\dot{y}$-axis.

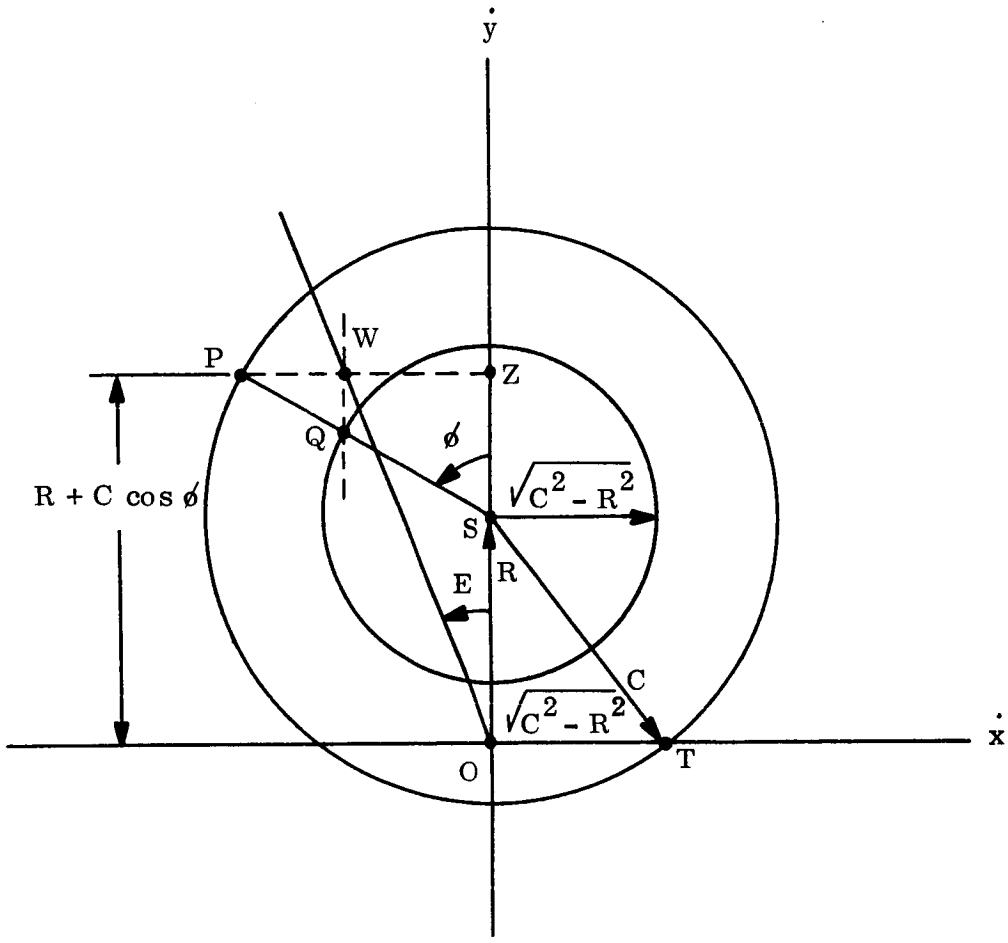

$$\tan E = \frac{\sqrt{C^2 - R^2}\sin \phi}{R + C\cos \phi} = \frac{\overline{WZ}}{\overline{OZ}}$$

Figure 6-1. Geometric Generation of the Eccentric Anomaly

With the eccentric anomaly E defined in velocity vector space, it can be easily shown that

$$(C_n)\,dt = (C - R\cos E)\,dE \quad , \tag{6-17}$$

by means of Equations 6-12 and 6-14. Let

$$\rho = C - R\cos E \quad ; \tag{6-18}$$

it is seen that the locus of points ρ is a limaçon. As shown in Figure 6-2, a point P' on the limaçon is the foot of the perpendicular from the origin O upon the tangent to the circle with radius C and center located on the $\dot{y}$-axis at (-R). The $\dot{y}$-axis is the axis of symmetry of the limaçon.

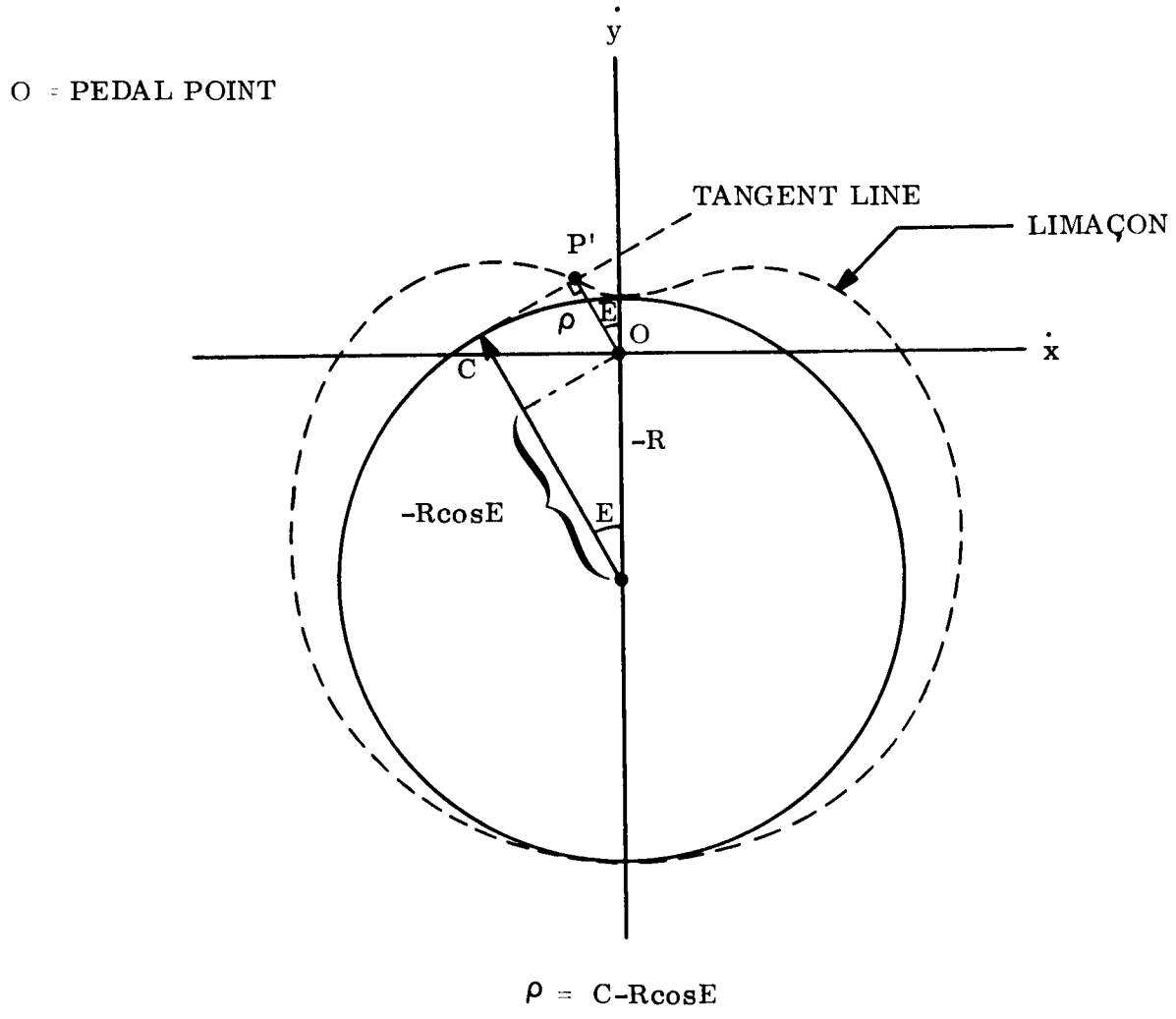

Figure 6-2. The Limaçon as the Locus of $\left[(Cn)\,dt/dE\right]$

6.2 MAP OF ELAPSED TIME AS AN AREA

Multiply both sides of Equation 6-1 by $C^2/2$ so that

$$\frac{C^2 nt}{2} = \frac{C^2 E}{2} - \frac{RC \sin E}{2} \qquad (6\text{-}19)$$

is obtained. Geometric interpretation of each term on the right-hand side of Equation 6-19 shows that

a. $(C^2E/2)$ represents the area of a circular sector with included angle E and circle radius C; and

b. (RC sinE/2) represents the area of a triangle with two sides C, R and the included angle E.

Consequently, the left-hand side of Equation 6-19 is represented by the difference between the areas of a circular sector and a triangle, as shown in Figure 6-3. Note that the eccentric anomaly E is defined in a circle with radius C and center at the origin, whereas the triangle is defined by the radius C and the line R from the origin along the $\dot{y}$-axis. The shaded area represents $(C^2nt/2)$.

Application of this areal map of orbital elapsed time in velocity vector space will require the manipulation of the two basic parameters, the angle β and line segment x', shown in Figure 6-4. That is, given the velocity hodograph parameters C, R, the areal map of time is determined by β, x'.

From the Triangle OMP,

$$x'^2 = C^2 + R^2 - 2CR\cos E \quad , \tag{6-20A}$$

or, by means of Equation 6-15,

$$x'^2 = C^2 + R^2 - 2CR\left(\frac{R + C\cos\phi}{C + R\cos\phi}\right) , \tag{6-20B}$$

so that finally

$$x' = \sqrt{C^2 - R^2}\ \sqrt{\frac{C - R\cos\phi}{C + R\cos\phi}} \tag{6-20C}$$

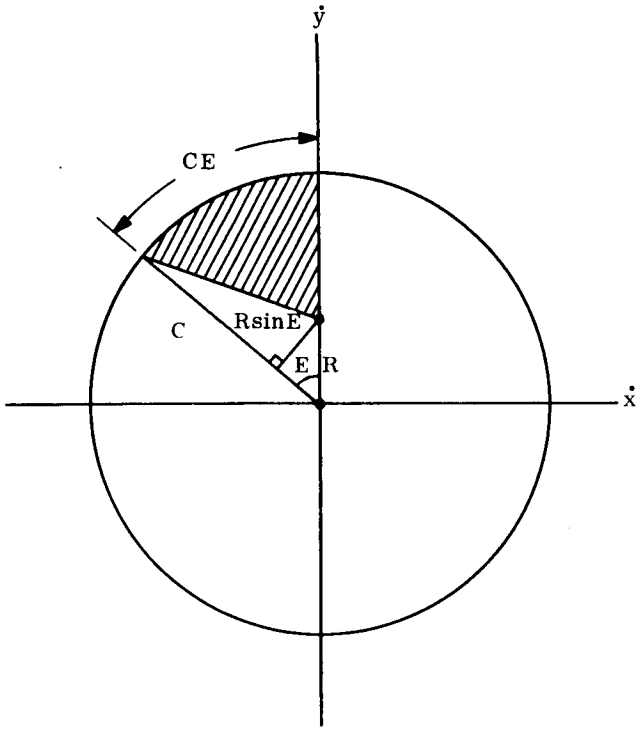

Figure 6-3. Areal Map of $(C^2nt/2)$

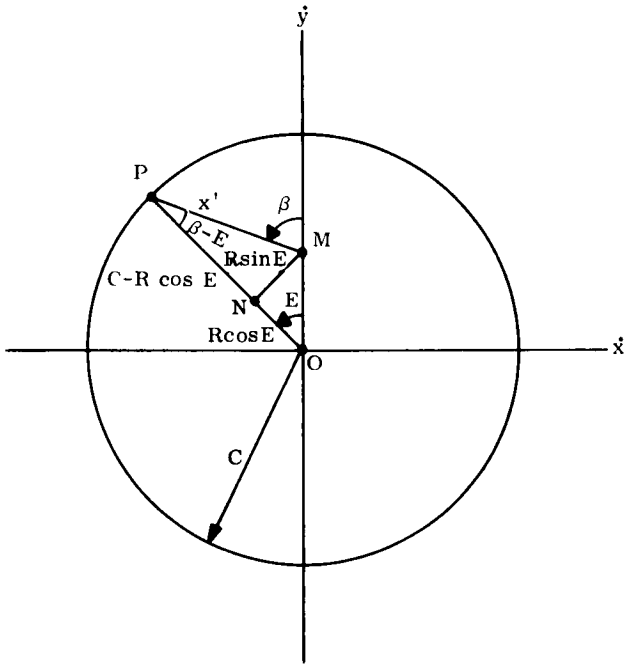

$\overline{MN}$ = R sin E
$\overline{ON}$ = R cos E
$\overline{NP}$ = C - R cos E

Figure 6-4. The Areal Mapping Parameters x', β

Also,

$$\tan(\beta - E) = \frac{R \sin E}{C - R \cos E} \tag{6-21A}$$

or, by means of Equations 6-3A and 6-15,

$$\tan(\beta - E) = \frac{R\left(\frac{\sin\phi\sqrt{C^2-R^2}}{C+R\cos\phi}\right)}{C - R\left(\frac{R+C\cos\phi}{C+R\cos\phi}\right)}, \tag{6-21B}$$

so that

$$\tan(\beta - E) = \frac{R\sin\phi}{\sqrt{C^2-R^2}} . \tag{6-21C}$$

From Equations 6-16 and 6-21C,

$$\beta = \arctan\left[\frac{R\sin\phi}{\sqrt{C^2-R^2}}\right] + \arctan\left[\frac{\sin\phi\sqrt{C^2-R^2}}{R+C\cos\phi}\right] \tag{6-22A}$$

or

$$\tan\beta = \frac{\left[\frac{R\sin\phi}{\sqrt{C^2-R^2}}\right] + \left[\frac{\sin\phi\sqrt{C^2-R^2}}{R+C\cos\phi}\right]}{1 - \left[\frac{R\sin\phi}{\sqrt{C^2-R^2}}\right]\left[\frac{\sin\phi\sqrt{C^2-R^2}}{R+C\cos\phi}\right]} \tag{6-22B}$$

so that, finally

$$\tan \beta = \frac{C \tan \phi}{\sqrt{C^2 - R^2}} \quad . \tag{6-22C}$$

Although the angle β may be computed by means of Equation 6-22C, it may be generated graphically by geometric interpretation of the alternative expression

$$\sqrt{C^2 - R^2} \tan \beta = C \tan \phi \quad . \tag{6-23}$$

Given an inertial velocity hodograph and any given hodograph point defined by the true anomaly ϕ as shown in Figure 6-5, the successive steps of this construction are as follows:

a. Construct the hodograph circle of an equal-energy circular orbit: that is, radius $= \sqrt{C^2 - R^2}$ determined by the original hodograph intercept with the $\dot{x}$-axis, and R = O;

b. Extend the true anomaly line until intercept with a line through point P parallel to the $\dot{x}$-axis;

c. Project the intersection point A parallel to the $\dot{y}$-axis until intercept with a line through point P' parallel to the $\dot{x}$-axis; and

d. The line from the intersection point B to the origin forms the angle β with the $\dot{y}$-axis.

Consequently, the areal map of elapsed time may be obtained in two alternative procedures:

a. Using the eccentric anomaly E obtained as described for Figure 6-1, generate the areal map as shown in Figure 6-3; or

b. Using the angle β obtained as described for Figure 6-5, generate the areal map as shown in Figure 6-6.

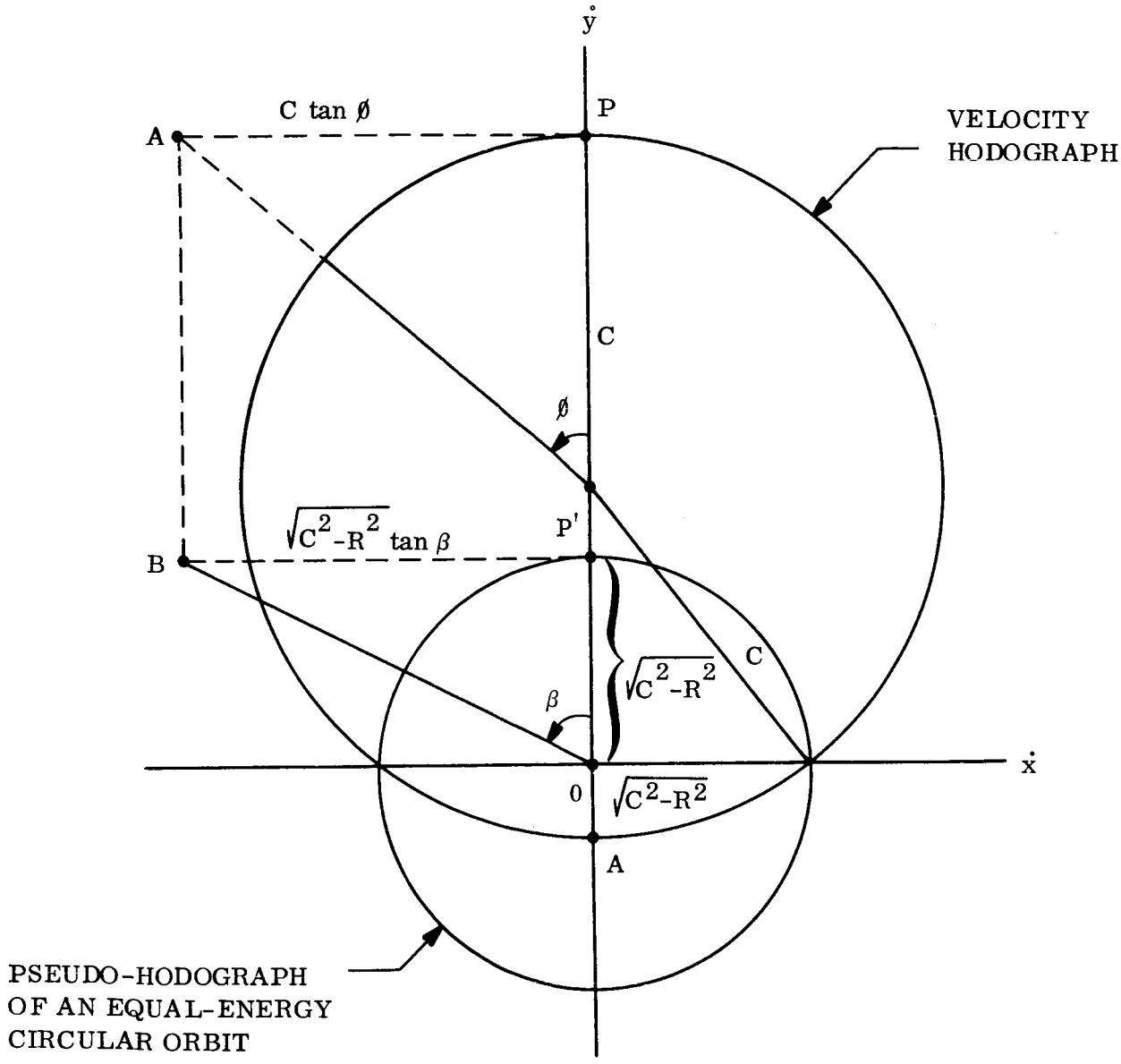

Figure 6-5. Geometric Generation of the Areal Mapping Parameter β

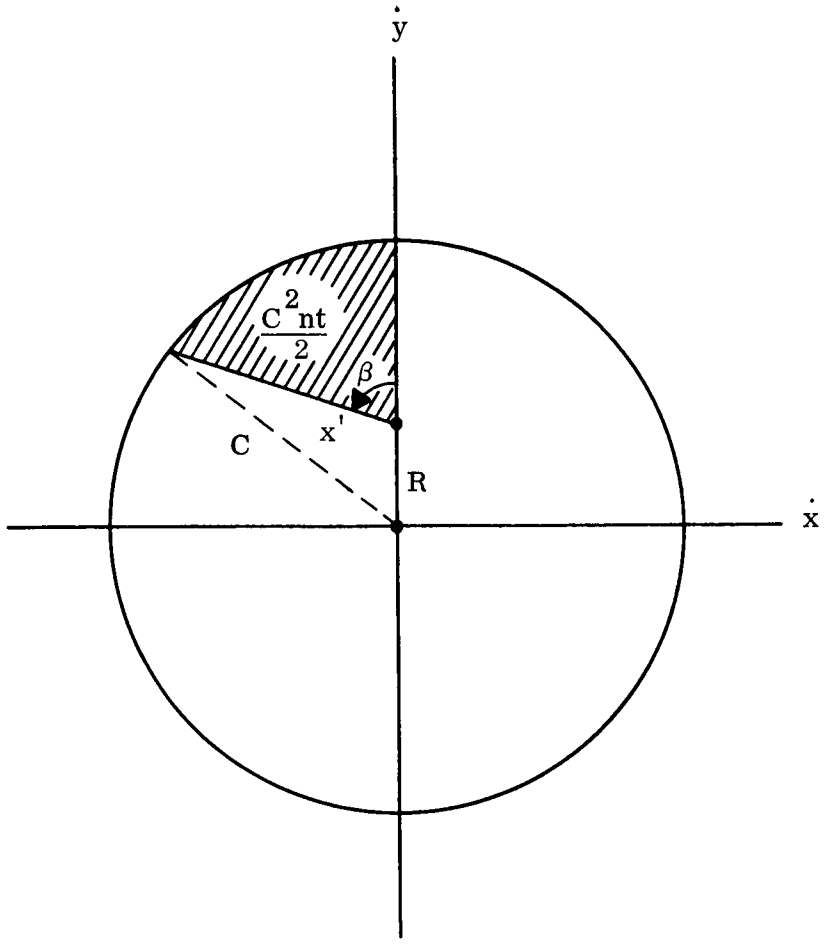

Figure 6-6. Areal Mapping by Use of the Parameter β

Upon examining Equations 6-16 and 6-22C, it is noted that the angle β and the true anomaly ϕ coincide every $(\pi/2)$, whereas the eccentric anomaly E and the true anomaly ϕ coincide only every π radians.

Some useful relations between β and ϕ, and between β and x' are summarized in Table 6-1.

Table 6-1. Additional Relationships Between β and ϕ, and β and x'

$$\cos\beta = \frac{\cos\phi\sqrt{C^2-R^2}}{\sqrt{C^2-(R\cos\phi)^2}} \tag{6-24}$$

$$\sin\beta = \frac{C\sin\phi}{\sqrt{C^2-(R\cos\phi)^2}} \tag{6-25}$$

$$\cos\phi = \frac{C\cos\beta}{\sqrt{C^2-(R\sin\beta)^2}} \tag{6-26}$$

$$\sin\phi = \frac{\sin\beta\sqrt{C^2-R^2}}{\sqrt{C^2-(R\sin\beta)^2}} \tag{6-27}$$

$$\tan(\beta-\phi) = \frac{(C-\sqrt{C^2-R^2})\tan\phi}{C\tan^2\phi+\sqrt{C^2-R^2}} \tag{6-28}$$

$$x' = \sqrt{C^2+R^2-2CR\cos E} \tag{6-29A}$$

$$x' = \sqrt{C^2-R^2}\sqrt{\frac{C-R\cos\phi}{C+R\cos\phi}} \tag{6-29B}$$

$$x' = \frac{(C^2-R^2)}{R\cos\beta+\sqrt{C^2-(R\sin\beta)^2}} \tag{6-29C}$$

$$x' = -R\cos\beta+\sqrt{C^2-(R\sin\beta)^2} \tag{6-29D}$$

6.3 TIME VARIATIONS OF x' AND β

The time variations of the parameters x', β may be useful in future research study and applications of the areal map of orbital elapsed time. The time derivative of x' is determined as follows: From equation 6-20C,

$$x'^2 = (C^2 - R^2)\left(\frac{C - R\cos\phi}{C + R\cos\phi}\right) . \tag{6-30}$$

Developing the derivative of Equation 6-30 with respect to the true anomaly ϕ,

$$2x'\,dx' = \frac{(C^2 - R^2)}{(C + R\cos\phi)^2}\left[(C + R\cos\phi)R\sin\phi - (C - R\cos\phi)(-R\sin\phi)\right] d\phi . \tag{6-31}$$

But it has been shown previously (Reference 2) that

$$\dot{\phi} = \frac{C}{\mu}(C + R\cos\phi)^2 . \tag{6-32}$$

Then Equation 6-31 provides, upon replacement of $d\phi$ by dt by means of Equation 6-32,

$$\dot{x}' = \frac{RC^2(C^2 - R^2)\sin\phi}{\mu x'} \tag{6-33A}$$

or

$$\dot{x}' = \left[\frac{RC^2\sqrt{C^2 - R^2}}{\mu}\right]\sin\phi\sqrt{\frac{C + R\cos\phi}{C - R\cos\phi}} . \tag{6-33B}$$

By use of Equation 6-2,

$$\dot{x}' = n \sin\phi \left(\frac{RC^2}{C^2-R^2} \right) \sqrt{\frac{C+R\cos\phi}{C-R\cos\phi}} \quad . \tag{6-33C}$$

The time derivative of β is determined as follows: Developing the derivative of Equation 6-22C with respect to the true anomaly ϕ,

$$\sec^2\beta \, d\beta = \frac{C}{\sqrt{C^2-R^2}} \sec^2\phi \, d\phi \quad . \tag{6-34}$$

However, according to Equation 6-24,

$$\sec\beta = \frac{\sqrt{C^2-(R\cos\phi)^2}}{\cos\phi \sqrt{C^2-R^2}} \tag{6-35}$$

so that

$$\left[\frac{C^2-(R\cos\phi)^2}{\cos^2\phi \, (C^2-R^2)} \right] d\beta = \frac{C}{\sqrt{C^2-R^2}} \sec^2\phi \, d\phi \quad . \tag{6-36}$$

Upon use of Equation 6-32 and subsequent reduction, Equation 6-36 yields

$$\dot{\beta} = \frac{C^2\sqrt{C^2-R^2}}{\mu} \left(\frac{C+R\cos\phi}{C-R\cos\phi} \right) . \tag{6-37A}$$

By means of Equation 6-30, one alternative form of Equation 6-37A is

$$\dot{\beta} = \frac{C^2 (C^2-R^2)^{3/2}}{\mu x'^2} \quad . \tag{6-37B}$$

Further, by means of Equation 6-2, a second alternative form is

$$\dot{\beta} = \frac{C^2 n}{X'^2} \quad . \tag{6-37C}$$

6.4 DISCUSSION OF THE AREAL MAP AND ITS POTENTIAL USE

It was shown, in Section 6.2, that a geometrically-defined area in velocity vector space represents the term ($C^2nt/2$), as shown in Figure 6-5. Since C and n are constant for a given orbit, this area is proportional to the orbital elapsed time t (referred to perigee passage). The mean anomaly can be directly identified on this areal map. Let

$$\alpha = e \sin E \tag{6-38}$$

so that, since e = R/C,

$$C\alpha = R \sin E \quad . \tag{6-39}$$

Then Kepler's equation (Equation 6-1) can be shown as

$$nt = E - \alpha \quad . \tag{6-40}$$

Consequently, the mean anomaly M is represented in the areal map shown in Figure 6-7, by the angle DOB. As shown previously in Figure 6-6,

$$A_1 = \frac{C^2 nt}{2} \quad . \tag{6-41}$$

But

$$A_2 = \frac{C^2 nt}{2} \tag{6-42}$$

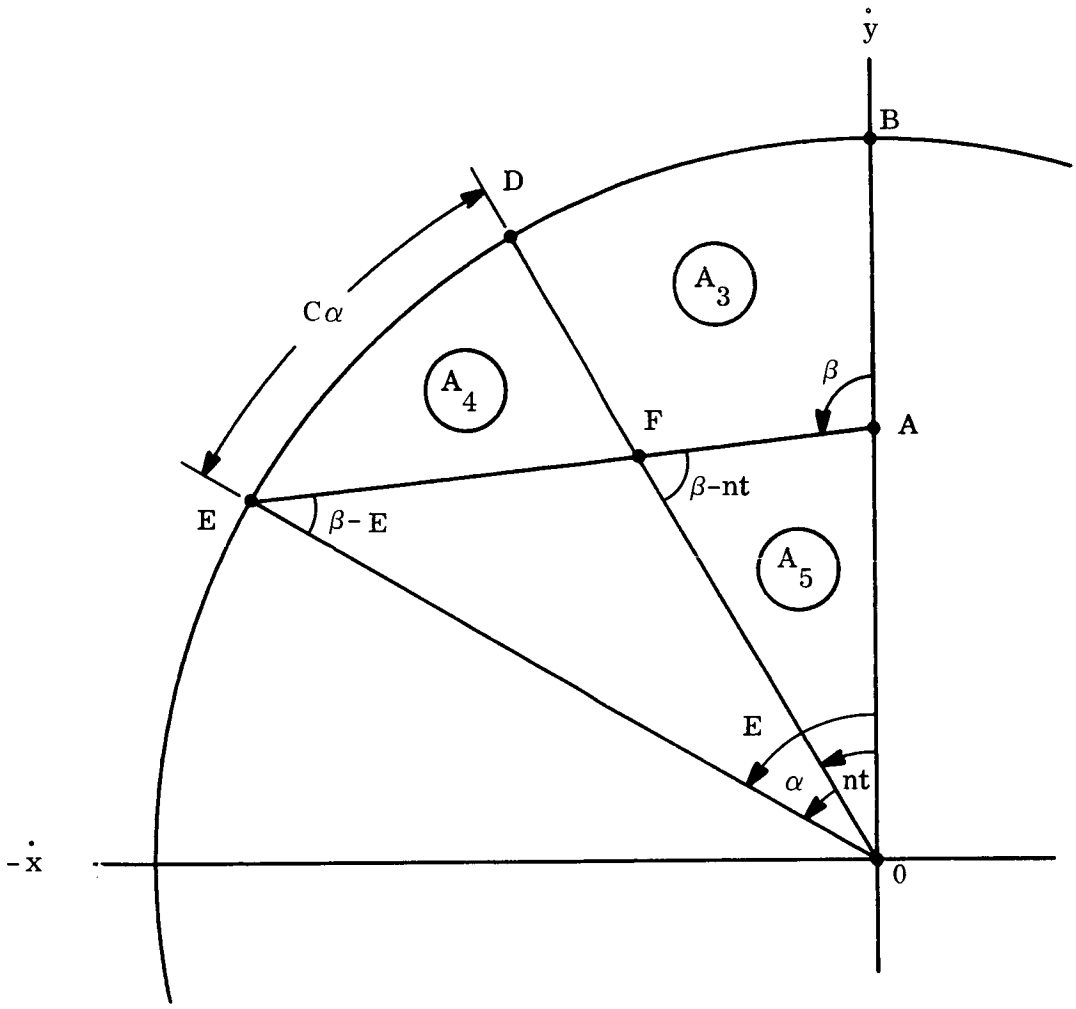

$\overline{AE} = X'$

$\overline{OA} = R$

$\overline{OE} = C$

$\overline{AB} = C-R$

$\overline{OF} \equiv S$

$\overline{AF} \equiv U$

ABEA = A_1

OBDO = A_2

ABDFA = A_3

FDEF = A_4

OAFO = A_5

Figure 6-7. The Definitive Geometry of the Areal Map

since it is a sector of a circle with radius C. Also, A_3 is common to areas A_1 (Equation 6-41) and A_2 (Equation 6-42). Consequently

$$A_4 = A_5 \tag{6-43}$$

so that it can be shown that

$$S \equiv \overline{OF} = \frac{R \sin E}{\sin \alpha + e \sin nt} \tag{6-44A}$$

or

$$S = \frac{RC \sin E}{C \sin (e \sin E) + R \sin nt} \tag{6-44B}$$

By means of the Law of Sines,

$$S = \frac{R \sin \beta}{\sin (\beta - nt)} \tag{6-45}$$

and

$$U = \frac{R \sin nt}{\sin (\beta - nt)} \tag{6-46}$$

so that

$$\frac{S}{U} = \frac{\sin \beta}{\sin nt} \tag{6-47}$$

Other useful relationships are listed in Table 6-2.

Table 6-2. Additional Relationships Between β and E

$$\tan(\beta - E) = \frac{R \sin \phi}{\sqrt{C^2 - R^2}} \tag{6-48}$$

$$= \frac{R \sin E}{C - R \cos E} \tag{6-49}$$

$$\sin(\beta - E) = e \sin \beta \tag{6-50}$$

$$\tan \beta = \frac{C \sin E}{C \cos E - R} \tag{6-51}$$

$$\frac{\tan(\beta - E)}{\tan \beta} = e \cos \phi \tag{6-52}$$

$$\cos(\beta - E) = \frac{\sin \beta (1 - e \cos E)}{\sin E} \tag{6-53}$$

$$= \frac{\cos \beta (1 - e \cos E)}{\cos E - e} \tag{6-54}$$

$$= \frac{\cos \beta}{\cos \phi} \tag{6-55}$$

$$\cos(\beta - E) = \sqrt{1 - (e \sin \beta)^2} \tag{6-56}$$

$$\tan(\beta - nt) = \frac{C \sin \alpha + R \sin nt}{C \cos \alpha - R \cos nt} \tag{6-57}$$

$$\tan(\beta - \alpha) = \frac{C \sin nt + R \sin \alpha}{C \cos nt - R \cos \alpha} \tag{6-58}$$

where

$$nt = E - \alpha \tag{6-40}$$

$$= E - e \sin E \tag{6-1}$$

The locus of point F in Figure 6-7, defined by the scalars S and U, is an oval-shaped figure such as shown in Figure 6-8. Naturally, the $\dot{y}$-axis is the axis of symmetry.

In general, the Cartesian coordinates $\dot{x}$, $\dot{y}$ of the locus point F are

$$\dot{y} = S \cos nt \tag{6-59}$$

$$\dot{x} = S \sin nt \tag{6-60A}$$

or

$$\dot{x} = \dot{y} \tan nt = \dot{y} \tan \left(E - e \sin E\right) . \tag{6-60B}$$

Since the expression (Equation 6-45) for S becomes indeterminate for nt (hence β) = O or π, these locus points ($\dot{y}_{max.}$, $\dot{y}_{min.}$) are determined by the calculus, as

$$\dot{y}_{max.} = \frac{R}{1-(1-e)^2} = \frac{C^2}{2C-R} \tag{6-61}$$

$$\dot{y}_{min.} = \frac{R}{1-(1+e)^2} = -\frac{C^2}{2C+R} . \tag{6-62}$$

Also, $\dot{x} = \dot{x}_{min.}$ when

$$2E - \varkappa = \pi$$

or

$$E = \frac{\pi}{2} + \frac{e \sin E}{2} ,$$

and $\dot{x} = \dot{x}_{max.}$ when

$$2E - \varkappa = 2\pi$$

or

$$E = \pi + \frac{e \sin E}{2} .$$

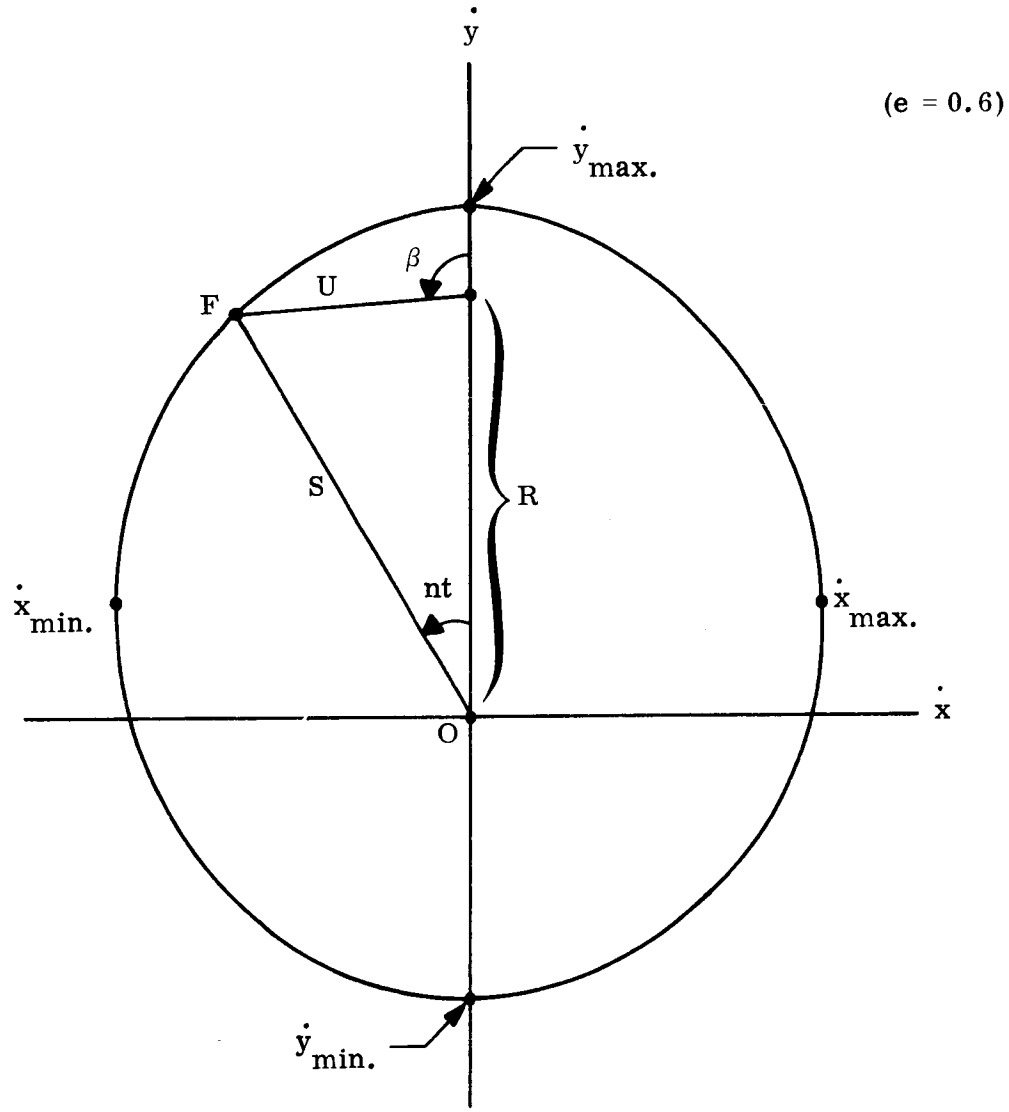

Figure 6-8. Locus of the Areal Map Point F

The oval-shaped figure shown in Figure 6-8 is the locus of the intersection point F of the areal map shown in Figure 6-7. The elapsed time t is defined by the mean anomaly M(=nt), since the mean angular velocity n is a constant for the orbit (Equation 6-2). As shown in Figure 6-8, the apex point 0 of the mean anomaly nt and the apex point A of the parameter angle β are fixed. Consequently, the variation of the coordinates of point F determines the elapsed time so that synthesis and analysis of the orbit as the result of time constraints may be provided by study of the locus of point F.

Referring to Equations 6-44 through 6-47 and 6-59 through 6-60, it would be desirable to reduce or transform the transcendental functions which determine the Cartesian coordinates $\dot{x}$, $\dot{y}$ of the locus, in order to obtain a more tractable functional form. For example, if an equivalent algebraic equation of the locus could be obtained, then direct determination of the corresponding trajectory point in position or other vector space might be carried out, without the present approximation method by series expansion. However, further research study must be conducted to explore this possibility. To date, the oval-shaped locus has not yet been identified as a simpler geometric figure; namely, neither Cartesian nor Cassinian ovals.

References

1. W.D. MacMillan, Statics and Dynamics of a Particle, Dover Publications, New York, 1958.

2. S.P. Altman, Orbital Hodograph Analysis, Vol. 3, AAS Science and Technology Series, Western Periodicals 1965.

3. F.T. Sun, "On the Hodograph Method For Solution of Orbit Problems," Proceeding of the 12th International Astronautical Congress, Academic Press, New York, 1963, pp. 879-915.

4. Phase Work Report IIIB-3, "The Complex Time Locus of an Orbital Trajectory in Time State Space," dated February 17, 1967.

5. E.H. Lockwood, A Book of Curves, Cambridge University Press, 1961, p. 146.

6. R.C. Yates, Curves and Their Properties, J.W. Edwards, Ann Arbor, Michigan, 1952, p. 65.

SECTION 7

VECTOR SPACE ANALYSIS OF ORBITAL TRAJECTORY CLASSES FOR MISSION STUDIES

AUTHOR: SAMUEL P. ALTMAN

SECTION 7

VECTOR SPACE ANALYSIS OF ORBITAL TRAJECTORY CLASSES FOR MISSION STUDIES

Trajectory synthesis and analysis is required for mission planning, space system development, and operations command and control. In operations command and control, trajectory synthesis and analysis should have been accomplished "a priori" during mission planning and/or system development; however, unforeseen operational conditions might require such trajectory reselection or reshaping "on-line". Although this situation has been avoided in most cases, future complex missions and systems may well require such action.

In any case, trajectory synthesis and analysis requires knowledgeable overall understanding of the effect of mission and system requirements upon the complete trajectory as well as upon each flight phase. In essence, synoptic rather than detailed characteristics of dynamics state variables are primary objectives of trajectory synthesis. Effective and efficient mission and system design is critically influenced by the flight envelope and the classes of trajectories which characterize all admissible trajectories within it. The vector space theory of orbital mechanics is eminently suited for this purpose, since all dynamics constraints and data are presented graphically as geometric constraints and data, with complete analytical rigor. This section summarizes and outlines basic orbital trajectory characteristics in velocity vector space, for the directed attention of and prospective use by the trajectory analyst or mission planner. Although many techniques have been developed and discussed in preceding research studies and reports, new data has been included.

7.1 SCOPE AND FORMAT OF THE TRAJECTORY CLASSES

Orbital trajectories are defined as those spacecraft trajectories which may occur in the presence of one force center. Consequently, orbital trajectories are encountered when the gravitational potential field of the sun, a major planet or major satellite (such as earth's moon) dominates the trajectory dynamics. Orbital trajectories may be divided into three categories:

a. Ballistic (i.e., orbits) subject to a spherical harmonic field only

b. Powered

c. Perturbed ballistic .

In the vector space theory, both powered flight (due to onboard thrust application) and perturbations (due to natural effects such as oblateness, triaxiality or radiation pressure) are treated analytically in similar fashion (References 1 and 2). In such treatment (still under research extension study), the characteristic effects of different classes of thrust law and perturbations are developed for subsequent detailed trajectory synthesis, and analysis of specific, individual trajectories. A mathematical discussion of this basic analytical approach is available in Reference 3; the technical discussion and detailed application will be presented later in Section 8. This section covers the ballistic trajectory (or orbit) only.

Trajectory analysis requires the concurrent evaluation and use of the trajectory state in two vector (or state) spaces, even though the trajectory locus in any one state space will define the corresponding trajectory loci in all other state spaces relevant to the orbital mechanics. For example, position and velocity vector sets ($\bar{r}$, $\bar{V}$) are commonly used in current astrodynamics and guidance study, principally because tracking and guidance system sensors (and the consequent processing logic of the required computers) are physically designed to sense such state variables. However, velocity and acceleration vector sets ($\bar{V}$, $\bar{A}$) can also be employed with equivalent analytical rigor. In fact, such vector sets are far more effective and feasible for inertial sensors which measure acceleration due to applied thrust, in order to update computer-stored data on the spacecraft trajectory. This report presents position and velocity characteristics of the ballistic trajectory in velocity vector space, in terms of inertial or polar coordinates ($\bar{V}_x$, $\bar{V}_y$ or $\bar{V}_r$, $\bar{V}_\nu$) respectively.

Since each point on the trajectory must be referred to other points on the same or other trajectories, time reference must also be provided. Consequently, the elapsed time from a time reference (or epoch) to trajectory points will be discussed.

Mission studies may require the use of state variables explicitly (i.e., $\bar{r}$, $\overline{V}$, t) or of the orbital parameters (a, e, Ψ)*. The following subsections present the characteristic space graphs of orbital trajectory classes in graphical form, for the following:

a. Vector state variables ($\bar{r}$, $\overline{V}$)

b. State variable t

c. Conic parameters (a, e, Ψ)

d. Velocity hodograph parameters (C, R, Ψ) .

Note that the parametric formulations describe the complete predicted trajectory, in implicit form. Consequently, the parametric sets are invaluable both as synoptic graphs and also for variation-of-parameters analysis.

7.2 SPACE GRAPHS (OR LOCI) OF THE VECTOR STATE VARIABLES ($\bar{r}$, $\overline{V}$)

Any given point in position vector space, defined by the position vector $\bar{r}$, will have a unique velocity vector $\overline{V}$ associated with it (as shown in Figure 7-1A) in order to trace out the orbital trajectory about the attracting force center located at the origin of the Cartesian position coordinates x, y. All points of a given trajectory will lie on a conic section in position vector space, but will lie on a circle in velocity vector space either in inertial coordinates ($\overline{V}_x$, $\overline{Y}_y$) or in polar coordinates (V_r, V_ν) as shown in Figures 7-1B and 7-1C. Although the position and velocity vector space figures of the orbital trajectory state are shown in discretely separate geometry in Figure 7-1, all such data coexists in

*Since only ballistic trajectories without perturbation are discussed here, the complete orbital motion will necessarily occur within the one orbital plane; the solid geometry equations for transition between noncoplanar orbits is well-known, thus not treated here.

complete space as shown in Figure 7-2. That is, each Figure 7-1A, B and C can be drawn on transparent overlay sheets which, when placed upon one another with common origin and properly orientated coordinate axes, will coincide with Figure 7-2. Note that, in Figure 7-1B and 7-1C, the velocity hodograph parameters become interchanged, with the direction of the circle radius reversed in relation to the positive ordinate axis (i.e., V_y or V_ν).

Although the position and velocity vectors of an elliptic orbit only are shown in Figures 7-1 and 7-2, the geometric definitions of the vector state variables at any one point of the orbital trajectory are complete and continuous in velocity vector space for all conic sections of orbit, as shown in Figure 7-3. As the conic section eccentricity increases from zero, the velocity hodograph is always a circle even though the conic section "blows up" for parabolic and hyperbolic orbits. The inertial velocity (or classical) hodograph moves up along the V_y-axis until it lies entirely in the upper halfplane, while the polar velocity (or special) hodograph drops down along the V_ν-axis until it intersects the V_r-axis.

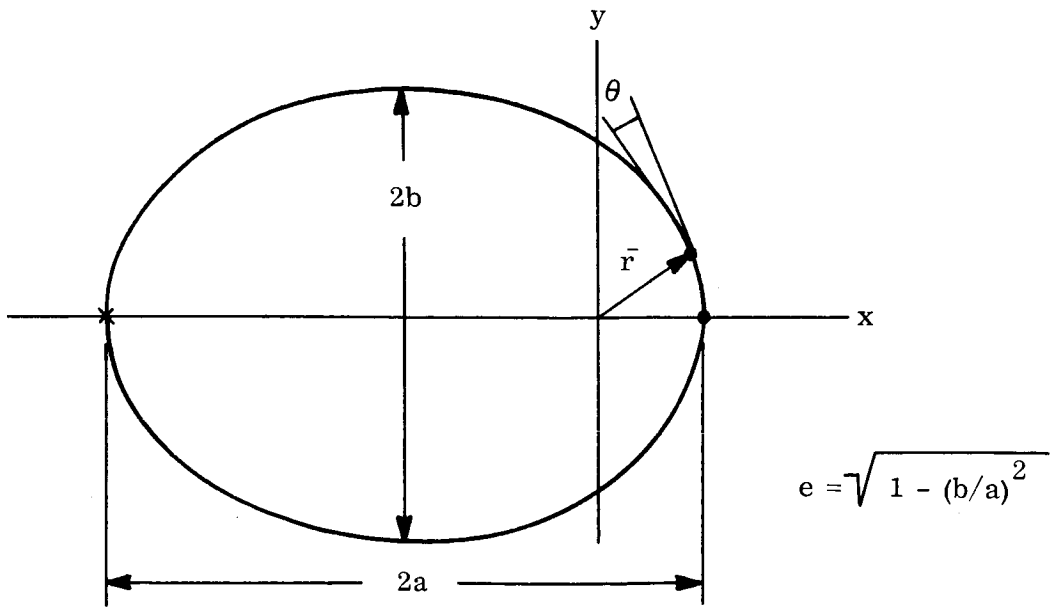

A. IN POSITION VECTOR SPACE

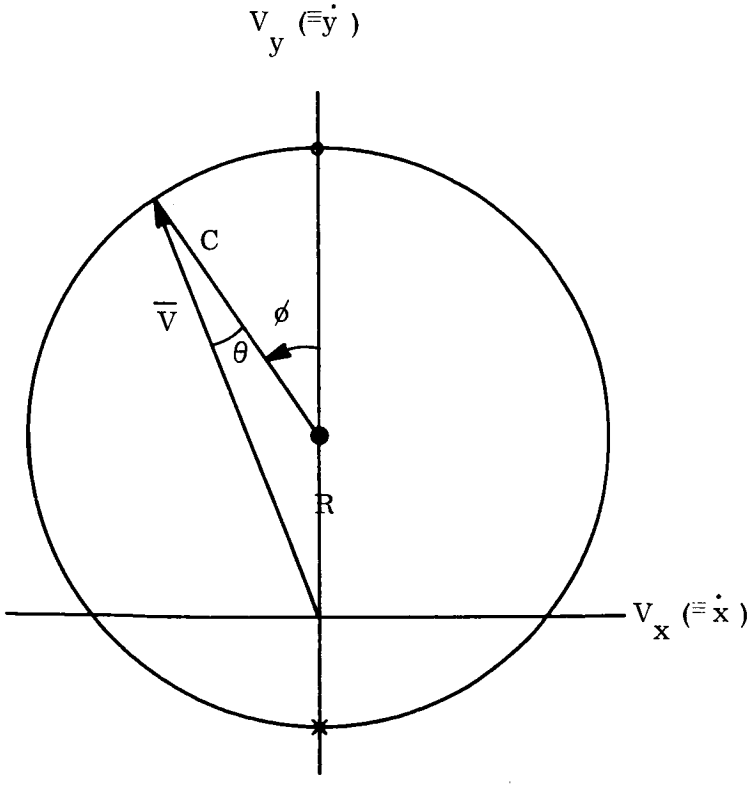

B. IN VELOCITY VECTOR SPACE
(INERTIAL COORDINATES)

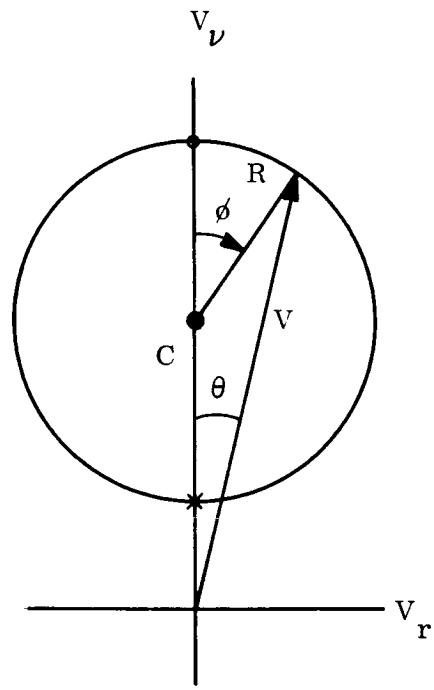

C. IN VELOCITY VECTOR SPACE
(POLAR COORDINATES)

Figure 7-1. Orbital Graphs in Position and Velocity Vector Spaces

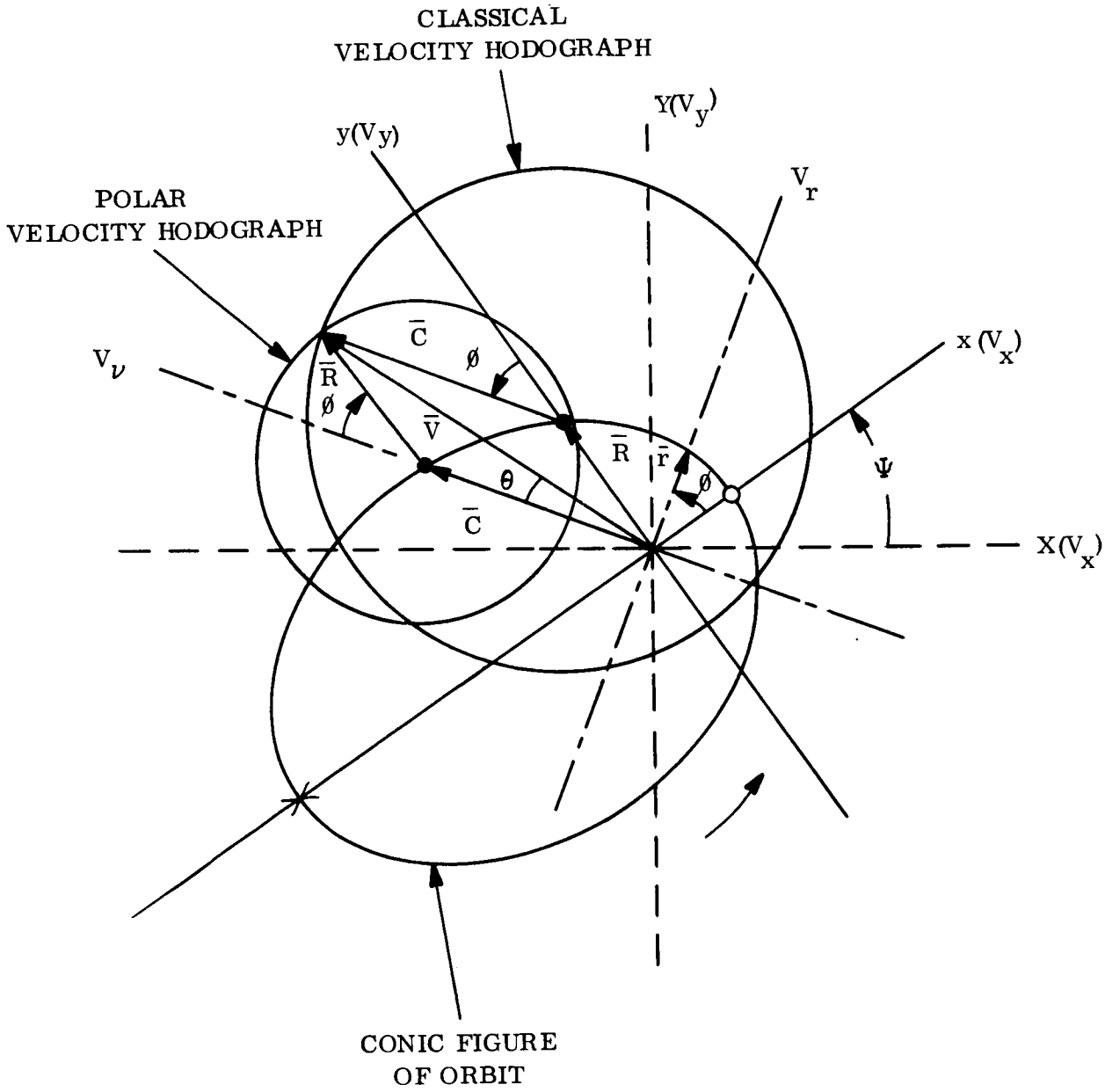

Figure 7-2. Polar and Classical (or Inertial) Velocity Hodographs of an Elliptical Orbit

	(A) CIRCULAR (e = 0)	(B) ELLIPTIC (0 < e < 1)	(C) PARABOLIC (e = 1)	(D) HYPERBOLIC (e > 1)
(I) POSITION	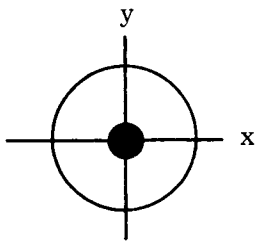	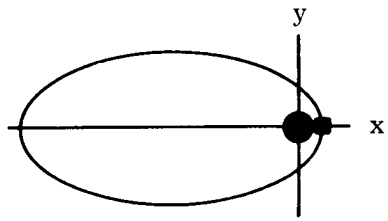	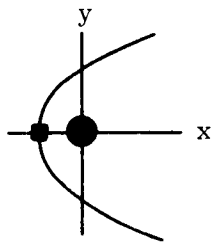	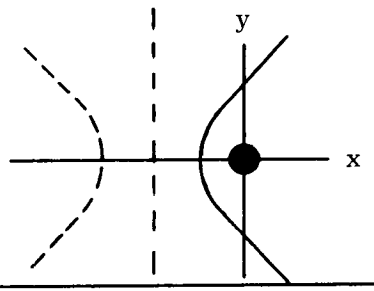
(II) VELOCITY (INERTIAL COORDINATES)	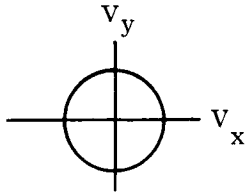 (R = 0)	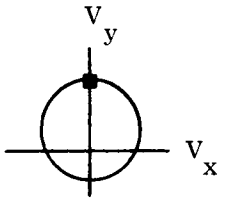 (0< R< C)	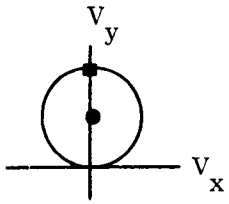 (R = C)	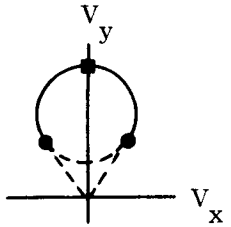 (R > C)
(III) VELOCITY (POLAR COORDINATES)	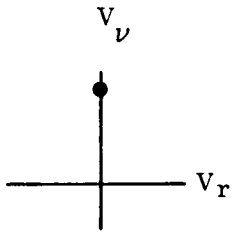	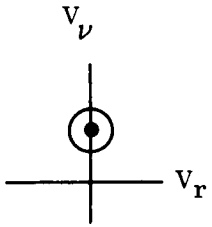	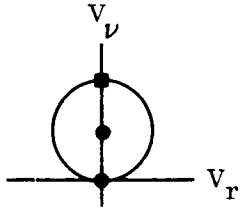	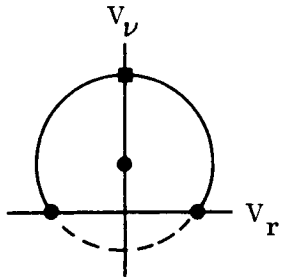

Figure 7-3. Vector Space Maps for the Conic Figures of Orbit

Space graphs of constant radius (or constant scalar magnitude of position vector) are circles in velocity vector space, as shown in Figure 7-4. These constant radius contours (i.e., circles) are related to the inertial hodograph as shown in Figure 7-4A, and to the polar hodograph as shown in Figure 7-4B. Note that only a circular orbit can be represented by a constant radius contour (see Figure 7-3 AI). Of course, space graphs of constant velocity are circles in velocity vector space, as shown in Figure 7-5. These constant velocity contours are related to the inertial hodograph as shown in Figure 7-5A, and to the polar hodograph as shown in Figure 7-5B. Here also, only a circular orbit can be represented by a constant velocity contour (see Figure 7-3 AII and 7-3 AIII).

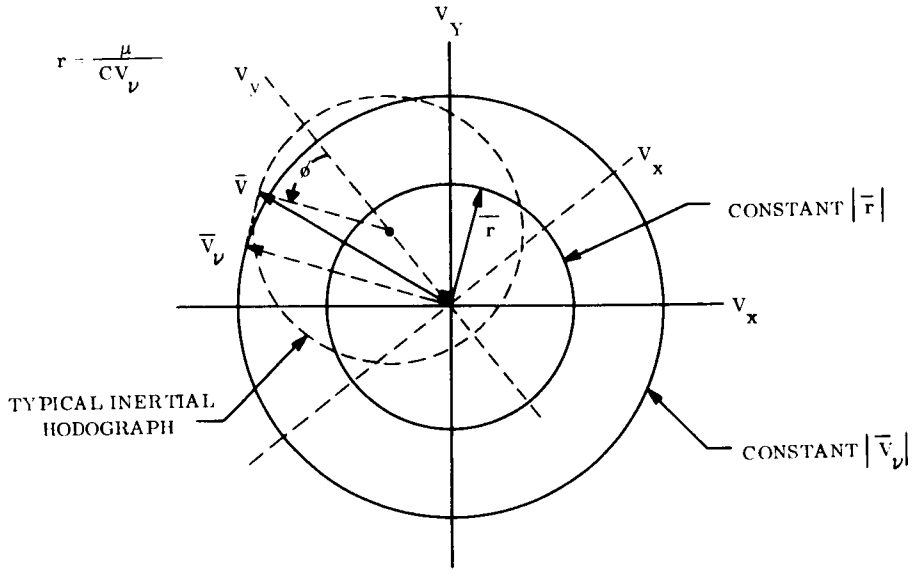

A. IN INERTIAL COORDINATES

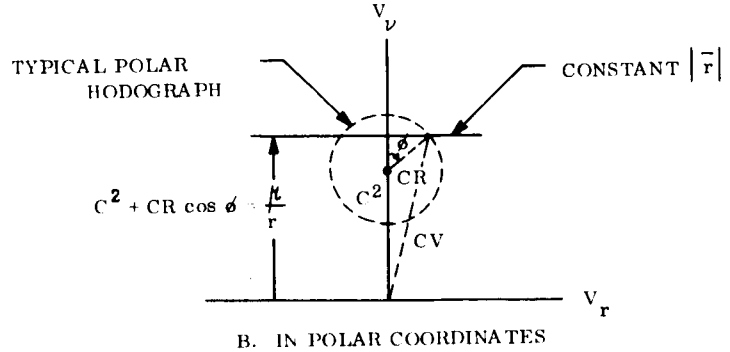

B. IN POLAR COORDINATES

Figure 7-4. Velocity Vector Space Contours of Constant Radius ($|\bar{r}|$)

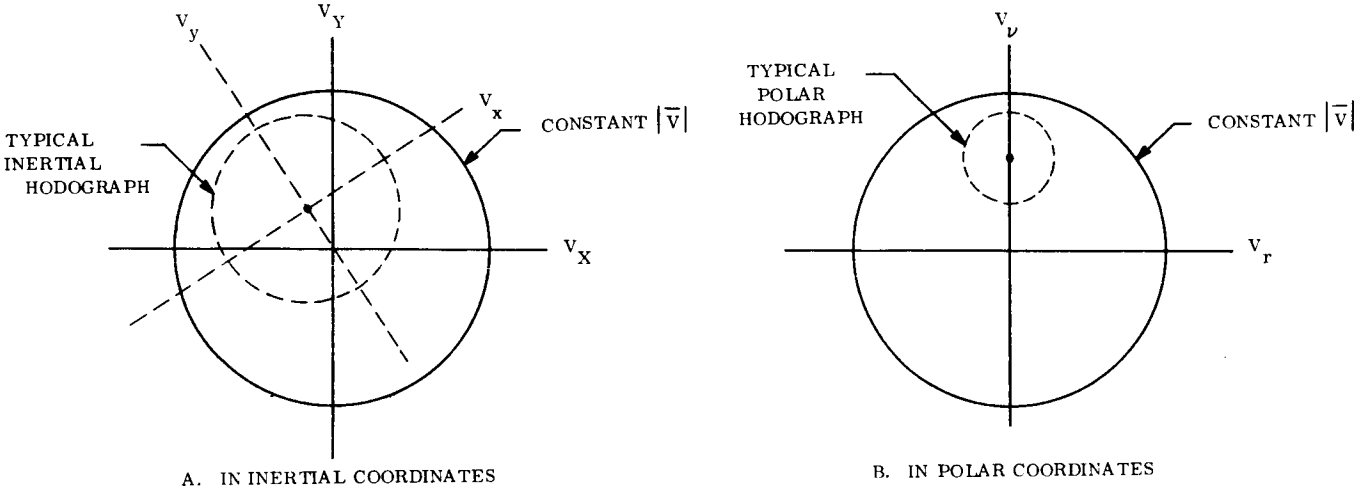

Figure 7-5. Velocity Vector Space Contours of Constant Velocity ($|\bar{V}|$)

In Figures 7-4A and 7-5A, the hodograph axes (V_x, $-V_y$) are shown disorientated from the plane-imbedded axes (V_X, V_Y). That is, the apsidal line, which defines the V_x-axis, positive in the sense of perigee passage, may, in general, not be coincident with the V_X-axis fixed in inertial space (Reference 4).

7.3 SPACE GRAPH (OR LOCUS) OF THE TIME STATE VARIABLE

The selection or constraint of the orbital time (relative to a common clock reference or epoch) is a vital part of trajectory synthesis for intercept or rendezvous with a planet or another spacecraft, or for scheduled arrival at a given point (e.g., zenith passage over a radar site at a given time of night, to provide specified communications transmission). The classical use of the eccentric anomaly E to determine orbital elapsed time by means of Kepler's equation

$$nt = E - e \sin E \qquad (7\text{-}1A)$$

or

$$C_n t = C^E - R \sin E \tag{7-1B}$$

where

n = mean orbital velocity

and

t = elapsed time from perigee passage,

is well-known. The eccentric anomaly E may be generated from the true anomaly ϕ in velocity vector space, given an inertial velocity hodograph and any given hodograph point defined by the true anomaly ϕ. Two alternative procedures* (References 5 and 6) are described in paragraph 7.6.

Although Kepler's equation (or various alternative forms which have been devised for special use) may be employed for analysis of the trajectory time conditions, the synthesis and analysis of orbital trajectories for mission feasibility and system design studies is most effectively accomplished by use of the complex time locus of the orbital trajectory in time state space (Reference 5). In special cases of satellite networks for global coverage (e.g., for communications or surveillance missions), the perimetric time curve (Reference 5) for the orbital trajectory appears quite promising as an effective presentation of the time state variable.

*Other procedures can be devised for generation of the eccentric anomaly E, by use of the polar velocity hodograph (with V_r, V_ν coordinates) rather than the inertial velocity hodograph (with V_X, V_Y coordinates).

It has been shown that time is a state variable which is represented as a complex term in time state space. The complex time $\bar{t}$ has magnitude directed identically with the position vector $\bar{r}$; that is, the complex time is directed with the angle $(\phi + \Psi)$ from the t_X-axis, or with the true anomaly ϕ from the t_x-axis. Although complex time in time state space is not governed by the algorithm of the conventional vector analysis used in mechanics, a well-defined algorithm does exist.

The time locus of a circular orbit is an Archimedes' spiral, as shown in Figure 7-6. The polar slope, defined as $\tan \alpha$, is a constant

$$\tan \alpha = \frac{dt}{d\phi} = \frac{\mu}{C^3} \quad ; \tag{7-2}$$

consequently, $t_\pi = 2t_{\pi/2}$, $t_{3\pi/2} = 3t_{\pi/2}$, $t_{2\pi} = 4t_{\pi/2}$, ...

The time locus of an elliptical (or other conic) orbit is a cycloidal variation of the Archimedes' spiral, as shown in Figure 7-7. Note that the time loci of the elliptic orbit and the circular orbit of same period coincide at apsides ($t = n\pi$). Also, the time locus of the elliptic orbit approaches the Archimedes' spiral of the circular orbit as the eccentricity approaches zero. Consequently, the time locus of the equal-period circular orbit is a first-order approximation of the time locus — even a good approximation for low-eccentricity orbits. The circular orbit of same period will have the same orbital energy. Since the orbital energy is definable in hodograph parameters by

$$\frac{2E}{m} = C^2 - R^2 \quad , \tag{7-3}$$

the hodograph parameter C* of the equal-energy circular orbit will be

$$C^* = \sqrt{C^2 - R^2} \quad , \tag{7-4}$$

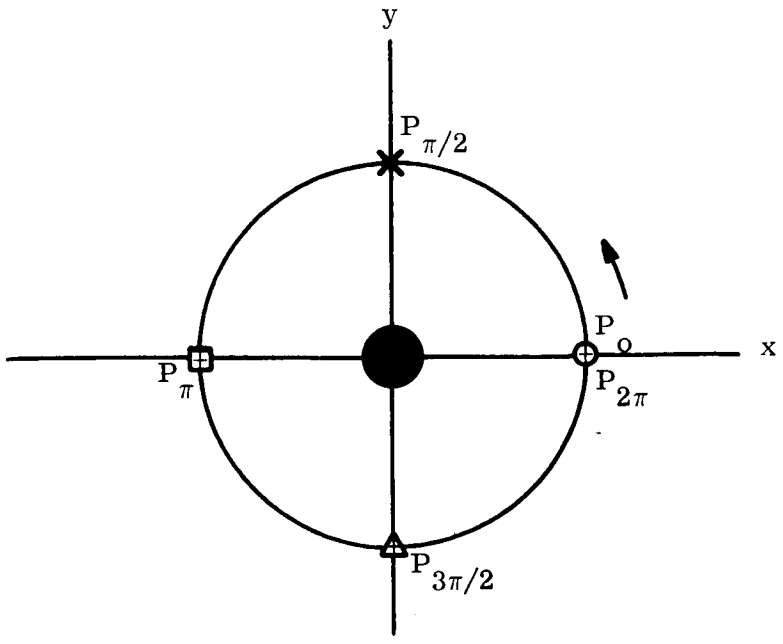

A. THE ORBIT IN POSITION VECTOR SPACE

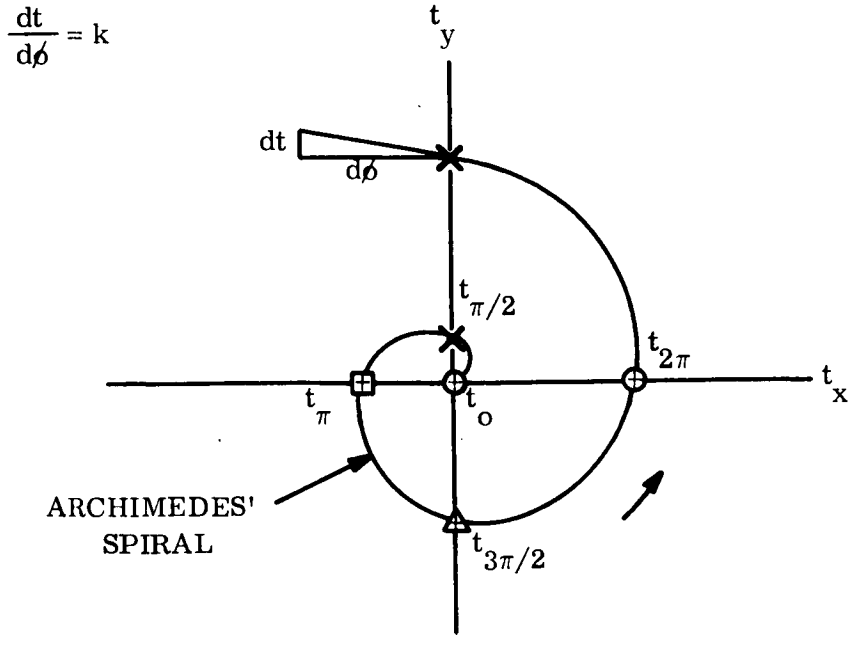

B. IN TIME STATE SPACE

Figure 7-6. Time Locus of a Circular Orbit

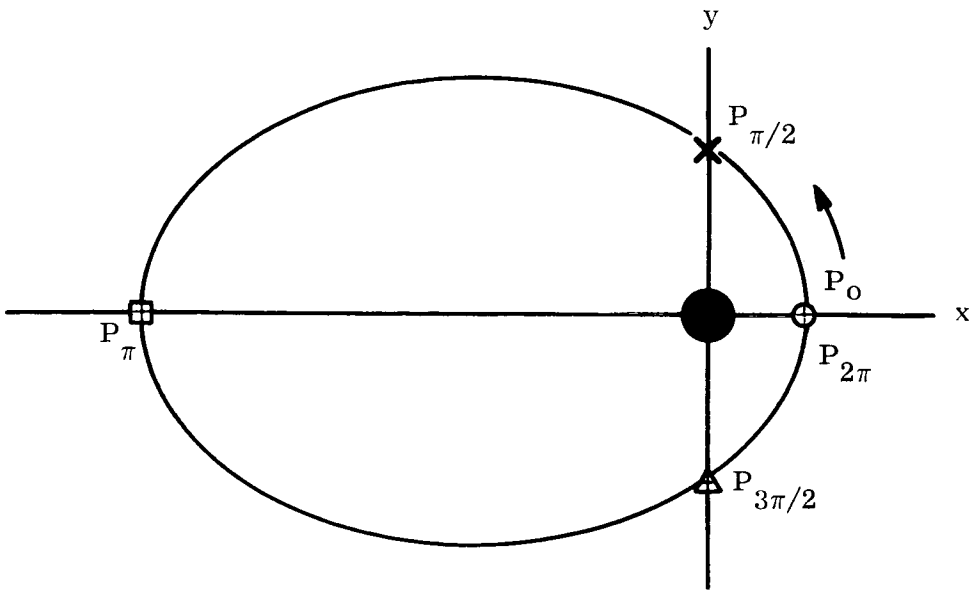

A. ORBIT IN POSITION VECTOR SPACE

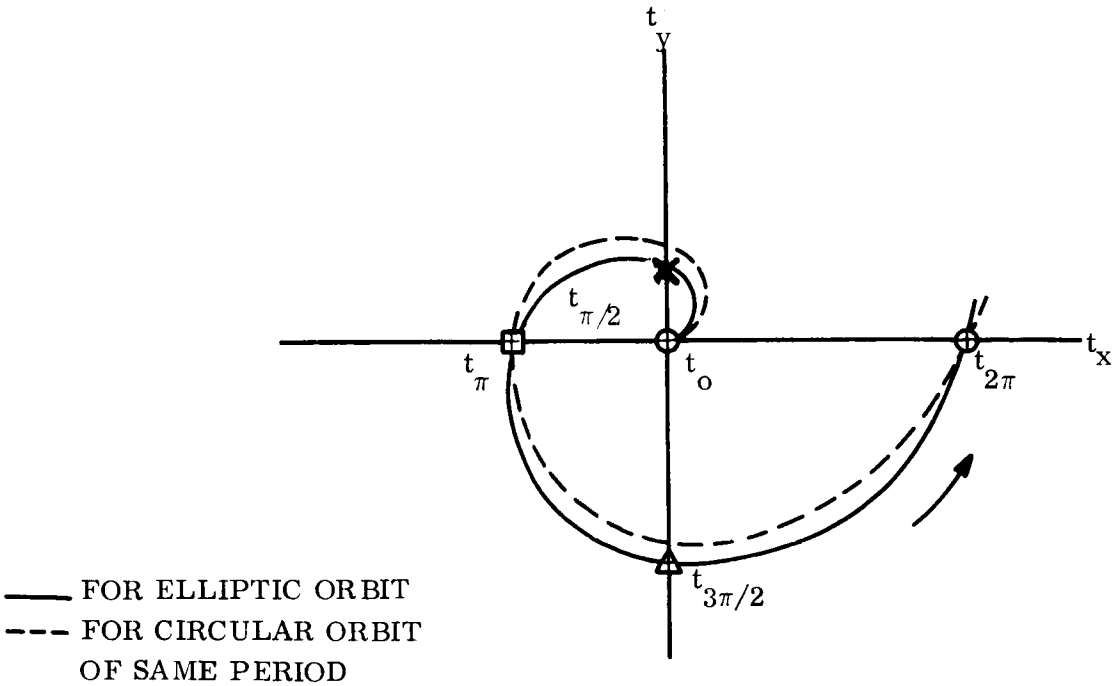

B. IN TIME STATE SPACE

Figure 7-7. Time Locus of an Elliptical Orbit

as shown in Figure 7-8. Note that the radius C* is defined by the $\dot{X}$-axis intercept of the given hodograph of the elliptic orbit.

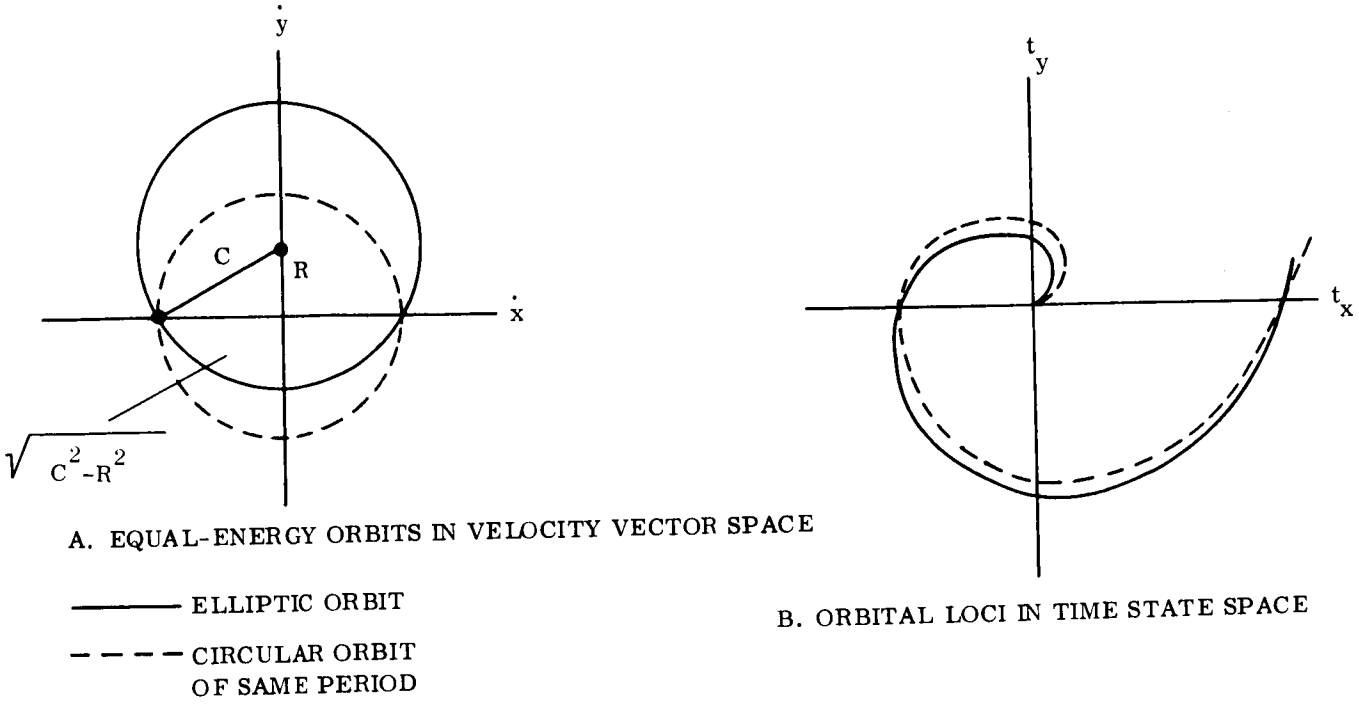

A. EQUAL-ENERGY ORBITS IN VELOCITY VECTOR SPACE

——— ELLIPTIC ORBIT

– – – – CIRCULAR ORBIT OF SAME PERIOD

B. ORBITAL LOCI IN TIME STATE SPACE

Figure 7-8. Time Loci of Equal-Energy Orbits

7.4 FAMILIES OF ORBIT, CLASSIFIED BY PARAMETERS

An orbit is defined parametrically by three parameters. For variable values of one parameter (the other two remaining fixed, or constant), an infinite family of orbits can be generated. These three families of orbits can be useful in visualizing, as well as analyzing, the tradeoffs or penalties between candidate orbits for missions. Each such family of orbits can be simply presented in velocity vector space for both conic and hodograph parameter variations, in inertial or polar hodograph format.

In position vector space, the conic parameters a, e and the apsidal line orientation Ψ (in the sense of perigee passage) comprise the definitive set of orbital parameters. The three families of elliptic orbits with conic parameter variation are shown schematically in

Figure 7-9, with the geometric constraint for each velocity vector space graph defined in Table 7-1, in direct correspondence with Figure 7-9. When the orbits are hyperbolic, the families of conic parameter variation appear as shown schematically in Figure 7-10, with the geometric constraint for each velocity vector space graph defined on Table 7-2, in direct correspondence with Figure 7-10. Each such family of orbits has a dynamics significance, as follows:

a. e = variable, (a, Ψ = fixed) — variable conic shape (fixed energy, fixed orientation)

b. a = variable, (e, Ψ = fixed) — variable energy (fixed conic shape, fixed orientation)

c. Ψ = variable, (a, e = fixed) — variable orientation (fixed energy, fixed angular momentum, fixed conic shape)

In velocity vector space, the hodograph parameters C, R and the apsidal line orientation Ψ comprise the definitive set of orbital parameters. The three families of orbits with hodograph parameter variation are shown schematically in Figure 7-11, with the geometric constraints defined in Table 7-3, in direct correspondence with Figure 7-11. Each such family of orbits has a dynamics significance, as follows:

a. R = variable, (C, Ψ = fixed) — variable bounds on radial velocity (fixed angular momentum, fixed orientation)

b. C = variable, (R, Ψ = fixed) — variable angular momentum (fixed bounds on radial velocity, fixed orientation)

c. Ψ = variable, (C, R = fixed) — variable orientation (fixed energy, fixed angular momentum, fixed conic shape)

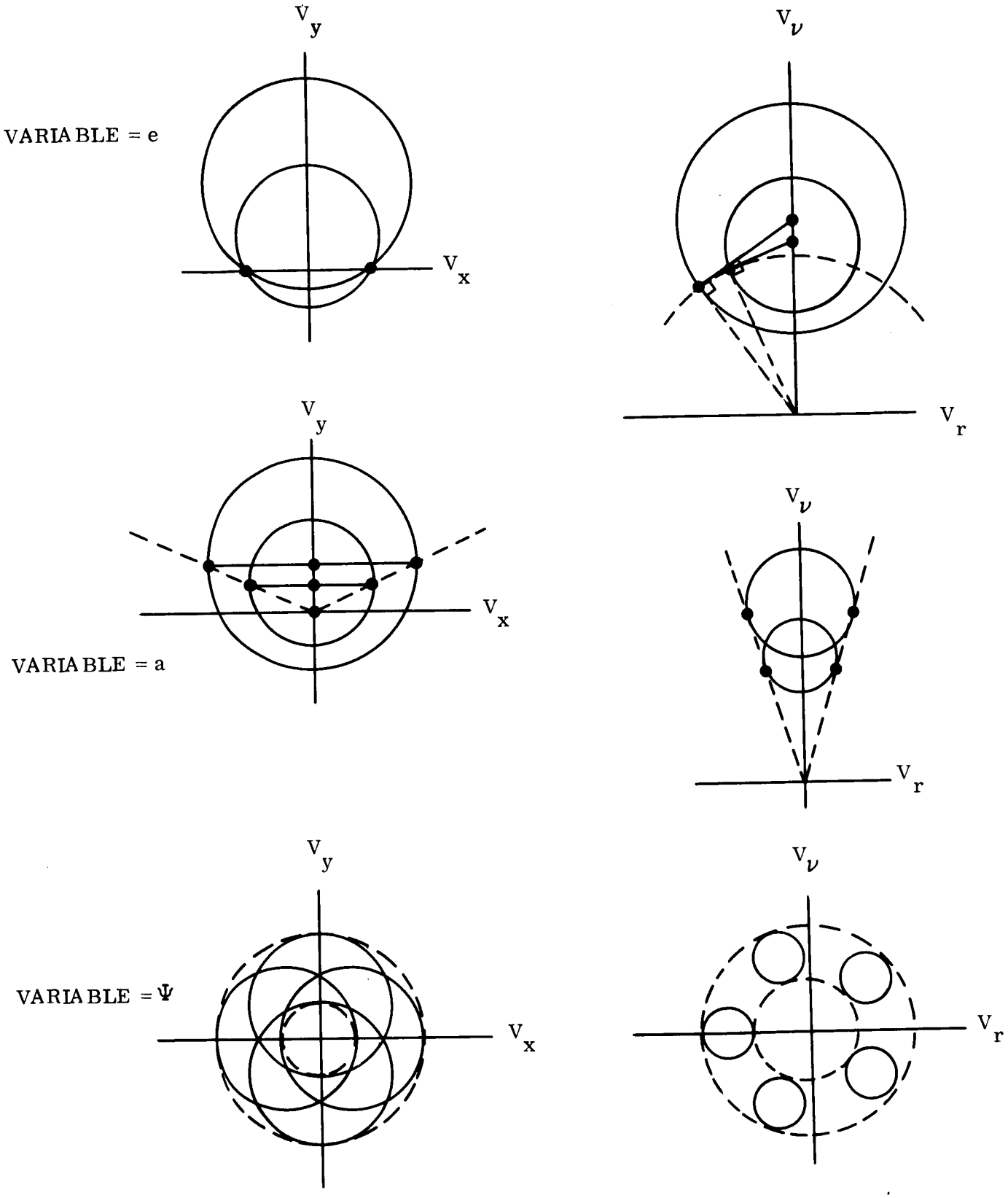

Figure 7-9. Families of Elliptic Orbits Generated by Conic Parameter Variation

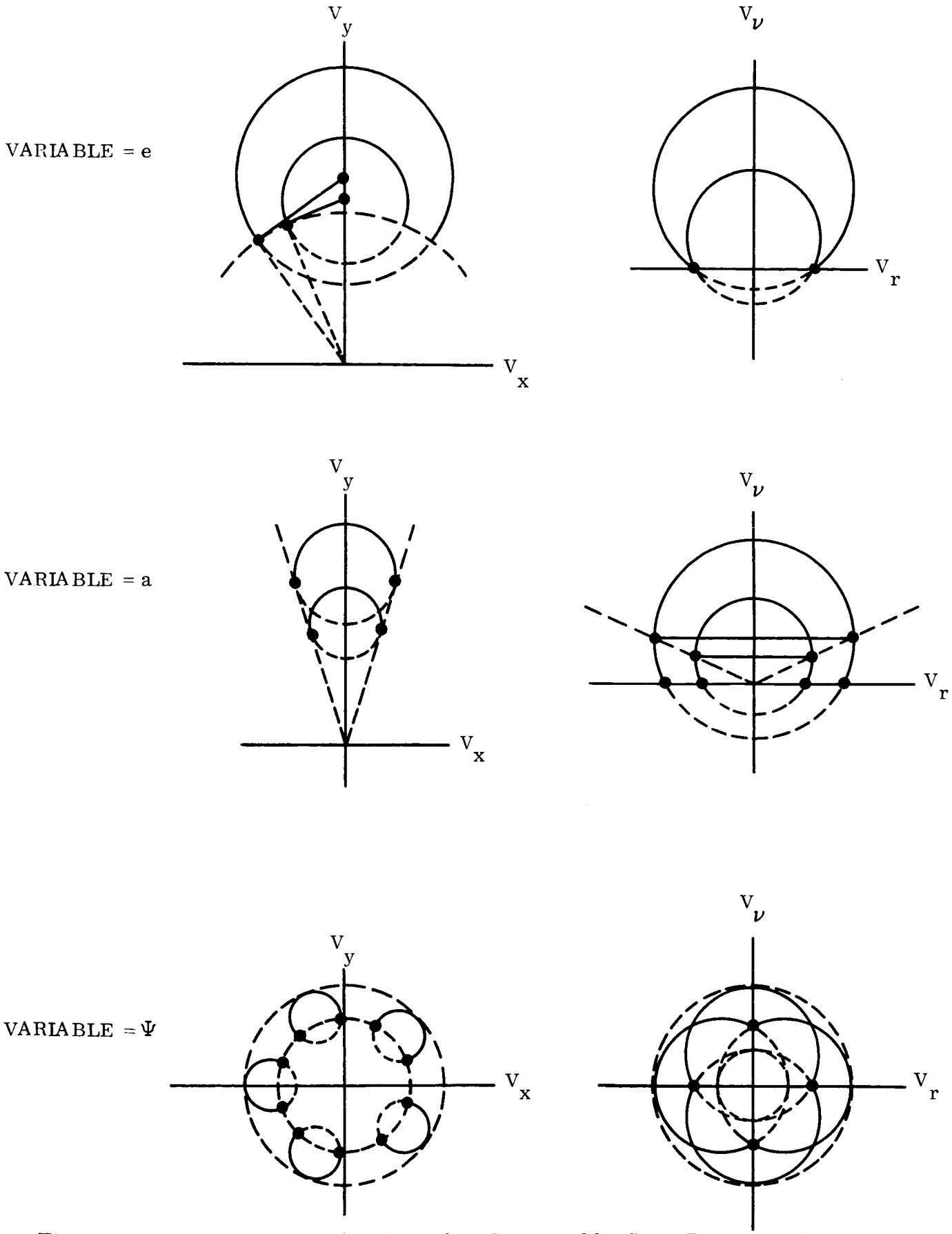

Figure 7-10. Families of Hyperbolic Orbits Generated by Conic Parameter Variation

Table 7-1. Definition of Geometric Constraints for Conic Parameter Families of Elliptic Orbits (Reference Figure 7-9)

Two common points of hodograph intersection with the V_x-axis.	All lines from origin to points of tangency with hodographs are radii of a circle.
All lines through the hodograph circle centers, directed parallel to the V_x-axis, intersect the hodographs at points on two lines (with slope $\pm m$, $m=R/C$) through the origin.	Two common lines from origin to points of tangency with hodographs, with slope $\pm m'$, $m' = (R/C) \sec \theta$ (i.e., θ = constant)
All points of hodograph intersection with the Ψ-axis (i.e., the line of apsides) through the origin lie on fixed inner and outer circles about the origin; or All hodographs have the same radius length, with centers lying on a circle about the origin.	All points of hodograph intersection with the Ψ-axis (i.e., the line of apsides) through the origin lie on fixed inner and outer circles (about the origin) which comprise envelopes about the hodographs; or All hodographs have the same radius length, with centers lying on a circle about the origin.

Table 7-2. Definition of Geometric Constraints for Conic Parameter Families of Hyperbolic Orbits (Reference Figure 7-10)

All lines from origin to points of tangency with hodographs are radii of a circle.	Two common points of hodograph intersection with the V_x-axis.
Two common lines from origin to points of tangency with hodographs, with slope $\pm m'$, $m'=(R/C) \sec \theta$ (i.e., θ = constant)	All lines through the hodograph circle centers, directed parallel to the V_x-axis, intersect the hodographs at points on two lines (with slope $\pm m$, $m=R/C$) through the origin.
All points of hodograph intersection with the Ψ-axis (i.e., the line of apsides) through the origin lie on fixed inner and outer circles (about the origin) which comprise envelopes about the hodographs. or All hodographs have the same radius length, with centers lying on a circle about the origin.	All points of hodograph intersection with the Ψ-axis (i.e., the line of apsides) through the origin lie on fixed inner and outer circles about the origin. or All hodographs have the same radius length, with centers lying on a circle about the origin.

Table 7-3. Definition of Geometric Constraints for Hodograph Parameter Families of Orbits (Reference Figure 7-11)

All hodographs have the same radius lengths, with centers lying on the V_y-axis; consequently bounded by two lines parallel to the V_y-axis.	All hodograph centers at one common point on the V_ν-axis.
All hodograph centers at one common point on the V_ν-axis.	All hodographs have the same radius lengths, with centers lying on the V_ν-axis; consequently bounded by two lines parallel to the V_ν-axis.
All points of hodograph intersection with the Ψ-axis (i.e., the line of apsides) through the origin lie on fixed inner and outer circles about the origin. or All hodographs have the same radius length, with centers lying on a circle about the origin.	All points of hodograph intersection with the Ψ-axis (i.e., the line of apsides) through the origin lie on fixed inner and outer circles (about the origin) which comprise envelopes about the hodographs. or All hodographs have the same radius length, with centers lying on a circle about the origin.

Note that the same geometric figures and constraints apply both to elliptic and hyperbolic orbits in Figure 7-11. Of course, the limiting conditions for the hyperbolic hodograph sequent which represents the branch about the filled focus will govern, just as in Figure 7-10.

Obviously, transformation between the conic and hodograph parameters may be useful. Table 7-4 summarizes the basic definitions of hodograph parameters, hodograph equations and transformation equations.

7.5 SUGGESTED WORK AIDS FOR GRAPHICAL SYNTHESIS OF TRAJECTORIES

The salient features of hodographic synthesis and analysis of orbits have been summarized in this subsection, in order to call attention to their potential application in mission feasibility and system design studies. Although all equations are uniquely and inherently suited for graphical synthesis, it is emphasized that they are completely well-defined and analytically

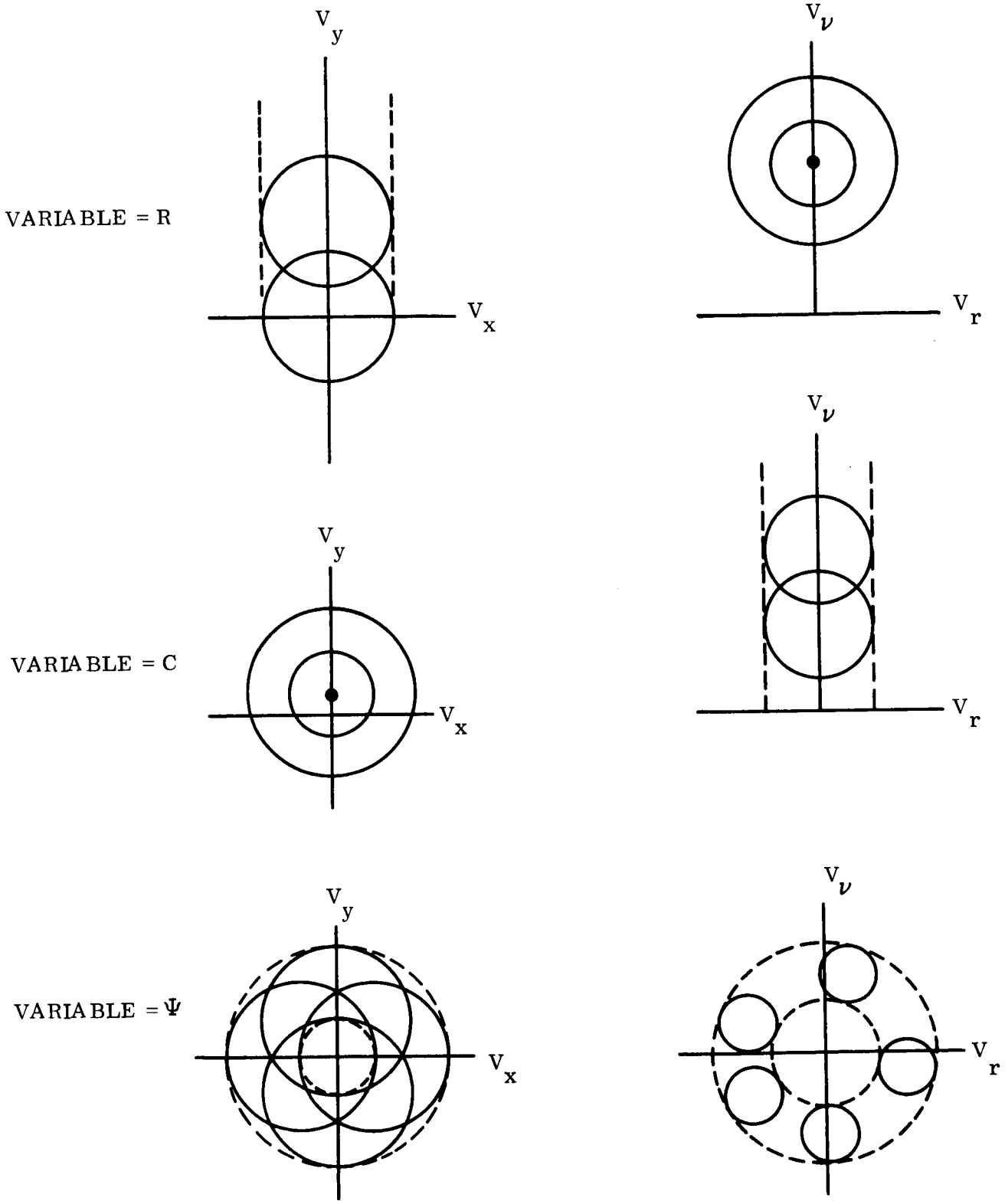

Figure 7-11. Families of Orbits Generated by Hodograph Parameter Variations

Table 7-4. Basic Velocity Hodograph Equations and Conic Variable Transformations

A. Hodograph Parameters

$$C = \frac{\mu}{r V_v} = \frac{\mu}{r^2 \dot{v}}$$

$$R = \sqrt{\frac{2E}{m} + C^2}$$

B. The Hodograph Equations

$$V_x = -C \sin \phi$$

$$V_y = R + C \cos \phi$$

$$V_r = R \sin \phi$$

$$V_v = C + R \cos \phi$$

C. Transformation Equations (Hodograph/Conic Parameters)

$$e = \frac{R}{C}$$

$$a = \frac{\mu}{C^2 - R^2}$$

$$n = \frac{(C^2 - R^2)^{3/2}}{\mu}$$

$$p = a(1 - e^2) = \frac{\mu}{C^2}$$

rigorous, so that direct use with computer programs is obvious. Whereas synthesis and analysis in position vector space (as in conventional practice) encounters serious or irksome obstacles in concurrent shaping or selection of position, velocity and time state conditions, the use of hodographic techniques in velocity vector space, together with time state space, provides a rapid and remarkably accurate methodology for trajectory synthesis. All graphical synthesis can be directly converted into basic routines of computer programs. In fact, a CRT or solid-state input-output access display, for "communications" between analyst and computer, is an immediately realizable possibility.

For graphical synthesis or analytical aid, a set of three basic transparent sheets is suggested, as shown in Figures 7-12 and 7-14. Each sheet might be color coded, for ease of visual differentiation between lines and circles of Figures 7-12 and 7-13 respectively. The use of a transparent plastic sheet with light frosting on one side is recommended for temporary or permanent retention of a trajectory synthesis, recorded

by pen, pencil or stylus. Figures 7-12 and 7-13 are identical r-θ polar coordinate plots, whereas Figure 7-14 consists of various scales of Archimedes' spiral. Although only one spiral will be required for a given family of orbits with equal energy, the alternative scales of spiral can be used if a scale change is desirable. A Cartesian grid sheet may also be used, if Cartesian components of the state variables are repeatedly required.

Figures 7-12 and 7-13 are rotated and/or translated in problem application, whereas Figure 7-14 is only rotated about its origin. If Figure 7-12 is chosen to represent inertial space (i.e., origin and axes represent the inertial vector and state space origins and axes), then the origins of Figures 7-12 and 7-14 may be pinned together, thereby enabling only relative rotation.

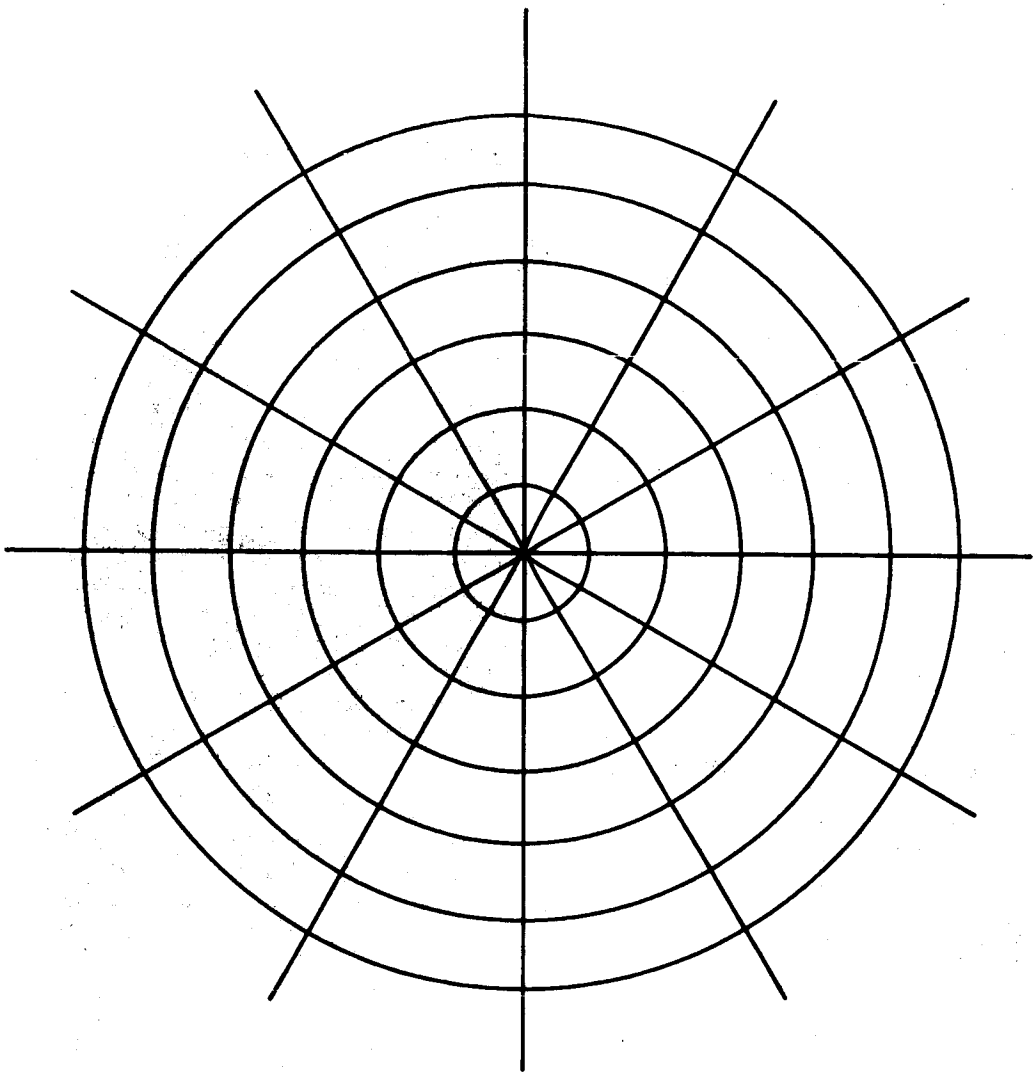

Figure 7-12. Euclidean Space Matrix (Position)

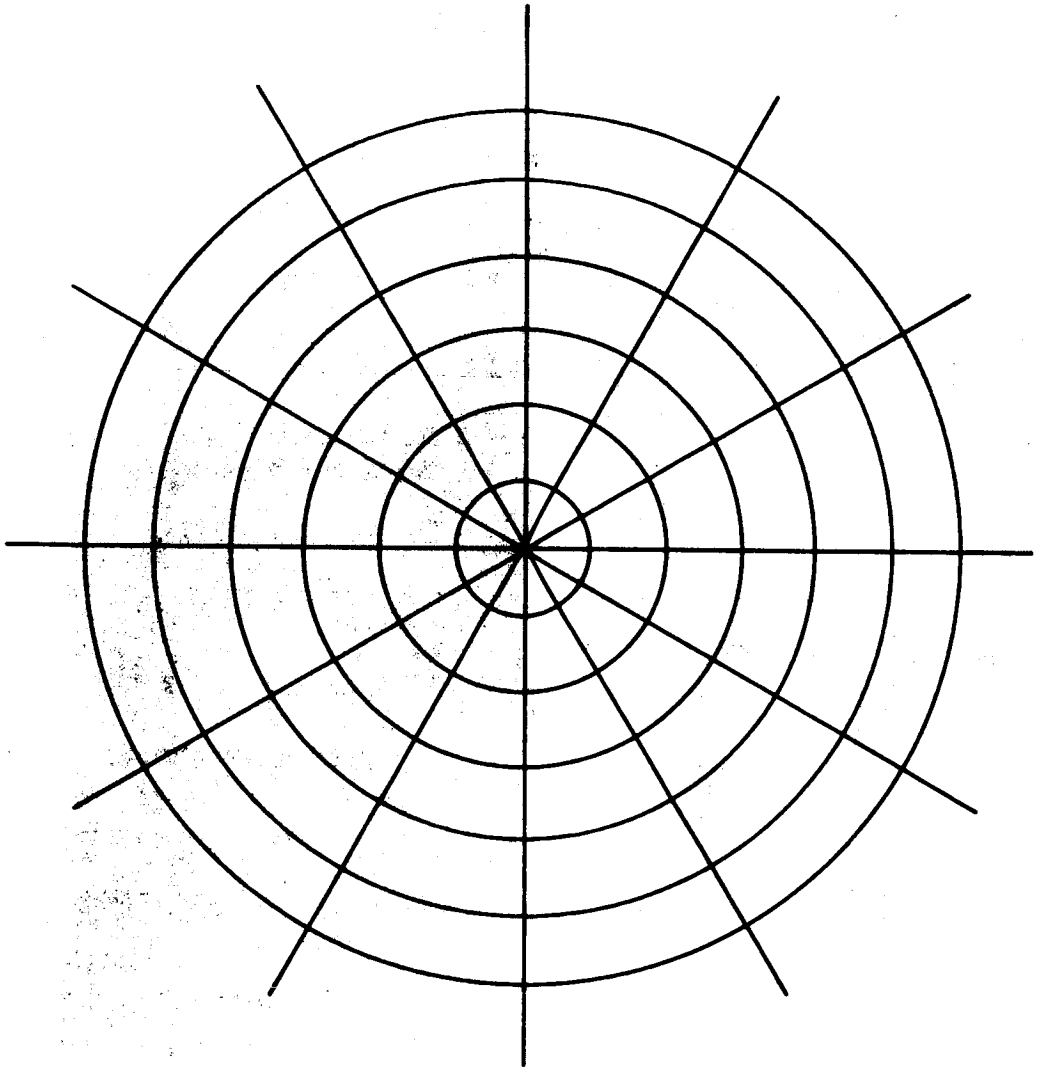

Figure 7-13. Hodograph Matrix (Velocity)

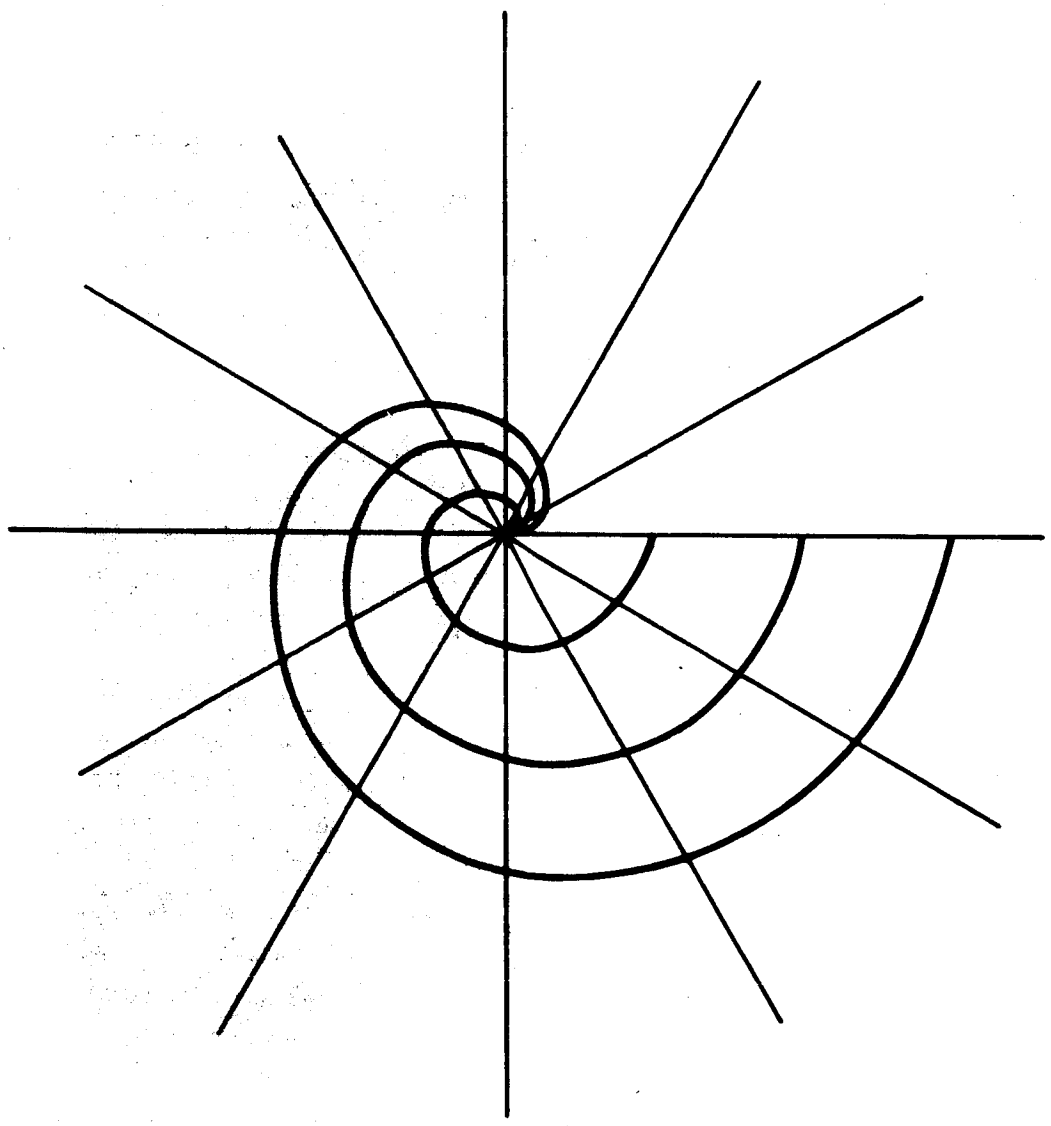

Figure 7-14. Spiral Matrix (Time)

The discussion of Potential Applications in Reference 5 may suggest some problem applications. Without providing detailed instructions or examples, exploitation of these trajectory synthesis techniques and aids is left to the analyst's understanding, imagination and interest.

7.6 GENERATION OF THE ECCENTRIC ANOMALY IN VELOCITY VECTOR SPACE

The eccentric anomaly E can be generated from the true anomaly ϕ in velocity vector space. Two alternative procedures are presented here, based upon a given inertial velocity hodograph and any given hodograph point defined by the true anomaly ϕ.

One procedure, based upon the relation

$$\cos E = \frac{R + C\cos\phi}{C + R\cos\phi} \quad , \tag{7-5}$$

consists of the following set of successive steps of geometric construction, as shown in Figure 7-15:

a. Project $\overline{C}$ on the $\dot{y}$-axis and add this projection to $\overline{R}$, to obtain $(R + C \cos \phi)$;

b. Project $\overline{R}$ on a line parallel to $\overline{C}$ and add this projection to a one-to-one projection of $\overline{C}$ on this line, to obtain $(C + R \cos \phi)$;

c. Erect the perpendicular to the $\dot{y}$-axis at $(R + C \cos \phi)$ from the origin;

d. Rotate $(C + R \cos \phi)$ obtained from b above about the origin in a clockwise direction until intersection with the perpendicular in c above;

e. The line from the intersection point of d above to the origin forms the eccentric anomaly E with the $\dot{y}$-axis.

The other procedure, based upon the relation

$$\tan E = \frac{\sin\phi\sqrt{C^2 - R^2}}{R + C\cos\phi} \quad , \tag{7-6}$$

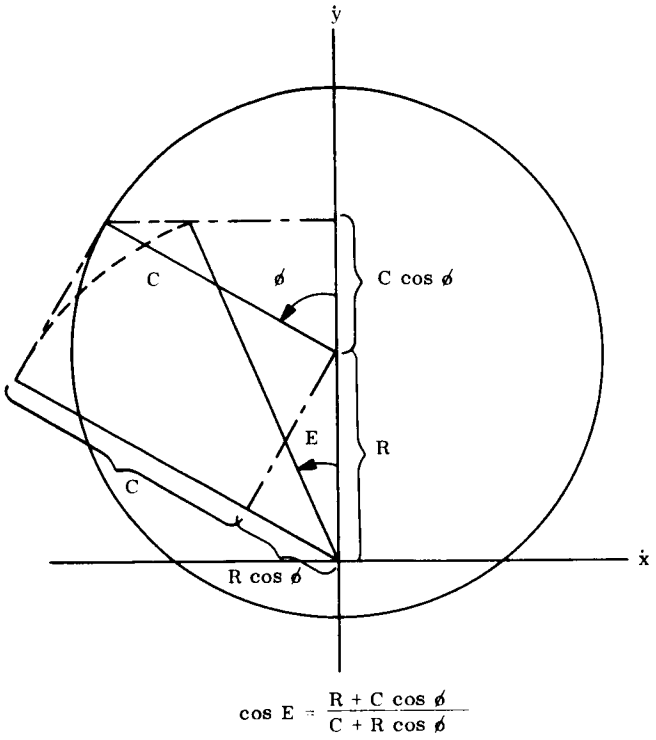

Figure 7-15. Generating Eccentric Anomaly E from True Anomaly ø

consists of the following set of successive steps of geometric construction, as shown in Figure 7-16:

a. Project $\overline{C}$ on the ẏ-axis by means of the projection line PZ and add this projection to $\overline{R}$, to obtain (R + C cos ø);

b. Generate a circle with center identical with the hodograph center, and radius equal to the segment OT of the ẋ-axis intersected by the hodograph circle (consequently $\sqrt{C^2 - R^2}$);

c. At the intersection Q of the true anomaly radius SP with the circle generated in b, erect a line parallel with the ẏ-axis until intersection W with the projection line PZ; and

d. The line from the intersection point W to the origin forms the eccentric anomaly E with the ẏ-axis.

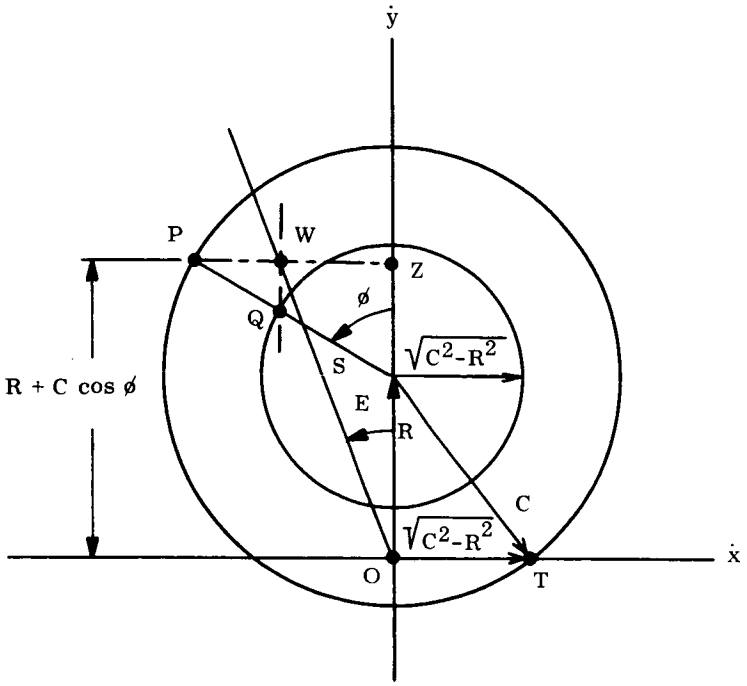

$$\tan E = \frac{\sqrt{C^2-R^2}\sin\phi}{R + C\cos\phi} = \frac{\overline{WZ}}{\overline{OZ}}$$

Figure 7-16. Geometric Generation of the Eccentric Anomaly

REFERENCES

1. S P. Altman, Orbital Hodograph Analysis, Vol. 3, AAS Science and Technology Series, Western Periodicals, 1965.

2. S.P. Altman, "The Hodographic Theory of Newtonian Mechanics," Recent Developments in Space Flight Mechanics, Vol. 9, AAS Science and Technology Series, AAS Publications, Tarzana, California, 1966, pp. 45-102.

3. E. Kasner, "Differential Geometric Aspects of Dynamics," American Mathematical Society Colloquium Series, Vol. 3, 1913.

4. Phase Work Report IIIA-1, "Formal Presentation of the Hodographic Equations of Motion," dated January 16, 1967.

5. Phase Work Report IIIB-3, "The Complex Time Locus of an Orbital Trajectory in Time State Space," dated February 17, 1967.

6. Phase Work Report IIIB-4, "Areal Mapping of Time In Velocity Vector Space," dated February 28, 1967.

SECTION 8

THE DIFFERENTIAL GEOMETRY OF ORBITAL TRAJECTORY FIELDS IN ACCELERATION VECTOR SPACE

AUTHORS: S. P. ALTMAN
Y. H. KU
W. F. MACKEY

SECTION 8

THE DIFFERENTIAL GEOMETRY OF ORBITAL TRAJECTORY FIELDS IN ACCELERATION VECTOR SPACE

An orbital trajectory is represented in acceleration vector space by its acceleration hodograph (Reference 1). Consequently, trajectory synthesis and analysis may be accomplished in the acceleration vector space, for ballistic or perturbed flight -- with natural, high-thrust or low-thrust perturbations. In the present case, the orbital trajectory occurs in the presence of one inverse-square attracting force center.

Acceleration vector space analysis is based upon knowledge and manipulation of the characteristic fields of trajectory hodographs, by use of its differential geometry. That is, differential variation of the dynamics of the instantaneous orbits, produced by applied thrust, is expressed in terms of the hodograph parameters C, R, Ψ. This parametric treatment is both analytically rigorous and realizable in engineering practice because the variations of these parameters are complete differentials in one vector space. Thus, the method of "variation of parameters" (Reference 2) is employed directly upon the trajectory as represented by its acceleration hodograph in acceleration vector space. However, the new concept of the state space theory of astrodynamics* enables the study, development and use of the characteristic properties of the geometric figure of the acceleration hodograph, by means of the differential geometry (References 3 and 4). By means of the hodographic or other state transformations (References 5 and 6), the acceleration hodograph may be mapped into any other state space -- without formal integration by quadratures -- to obtain any other "basic state variables"** of the trajectory as required (e.g., for specification of constraints, observations or control). All such transformations are invariant, of algebraic form, and conformal.

---

* In this case, the state space is the acceleration vector space. The term "vector space" without designation is reserved exclusively to describe the Newtonian vector spaces of position, velocity, acceleration, ... The term "state space" is most general, including the "vector space" as a subclass in which the conventional algorithm of "vector analysis" defines the logical operations in the space. However, any state space will be bound by an invariant algorithm of operations within that space, even though different in logic from other state spaces (e.g., time state space vs. position vector space).

** The "basic state variables" are defined as: position, velocity, acceleration (i.e., in vector spaces); time and mass (in state spaces).

In this analytical approach, all dynamic constraints (either natural or imposed by applied thrust) are completely presentable as geometric constraints in a state space. Consequently, the differential geometry of the fields of orbital trajectory hodographs which are generated by applied thrust acceleration will identify the powered orbital trajectory and all characteristic properties of dynamic behaviour. Moreover, the theory of geodesics (i.e., extremals of the geometry), can then be applied directly to trajectory optimization. Thus, for the first time, an alternative formal procedure of optimization (other than the variational calculus) becomes available, and complete correlation between solutions obtained by means of the geodesics theory and of the variational calculus must then be possible. As Hilbert and Cohn-Vossen (Reference 7) note:

> "Thus differential geometry and the calculus of variations proceed in opposite directions: In differential geometry we begin with properties affecting the vicinity of a point on a surface and deduce properties governing the overall structure of the figure under consideration; in the calculus of variations we deduce local properties from properties relating to the overall structure."

The application of the general theory of differential geometry as presented in this section is concisely described by Laugwitz (Reference 3), in terms of the curvature κ, torsion λ and path length s of a space curve:

> "Since κ (s) and λ(s) can be assigned independently of each other, these two functions even constitute a complete system of independent invariants. Therefore all geometric properties of a curve are completely determined by this pair of functions; in other words, the geometry of the curve is completely known if its natural (or intrinsic) equations $\kappa = \kappa$ (s), $\lambda = \lambda$(s) are given. At the same time, we can recognize a general method for solving problems in the differential geometry of space curves, in the following procedure: Write down all of the hypotheses, express all vectors occurring in them in terms of those of the moving trihedron, and replace the higher derivatives by using Frenet's formulas. In this manner the hypotheses can be transformed into relations involving only the vectors of the moving trihedron and the functions κ (s), λ(s) (along with their derivatives). The solution can then, in general, be accomplished by comparing corresponding coefficients of the vectors of the moving trihedron and solving the resulting differential equations for κ (s), λ(s)."

This section presents the definitive theory for acceleration vector space analysis of all orbital trajectories by use of the differential geometry, in the following subsections:

Subsection

8.1 The Trajectory Field

8.2 The Trajectory Equations

8.3 The Vector Formulas and Alternative Sets

8.4 Variations of the Parameters of the Orbital Trajectory Field

8.5 Criteria of Optimization in Acceleration Vector Space

8.6 Concluding Remarks.

For ease of initial development and presentation, trajectory motion in two-dimensional space only is explored, so that the space curve torsion $\lambda = 0$. Nevertheless, extension of the analytical procedure to three-dimensional trajectories will be clearly indicated.

8.1 THE TRAJECTORY FIELD

As shown schematically in Figure 8-1, a trajectory may be defined as the locus or hodograph of the state vectors in position, velocity or acceleration vector spaces. In particular, the orbital acceleration hodograph implicitly defines the position and velocity hodographs in accordance with the following equations:

Acceleration		Velocity		Position	
modulus $\bar{\rho}$	$=$	$\dfrac{(CV_v)^2}{\mu}$	$=$	$\dfrac{\mu}{r^2}$	(8-1, 8-2)
argument $\bar{\rho}$	$=$	$\phi_w + \dfrac{\pi}{2} + \theta$	$=$	$\phi + \pi$	(8-3, 8-4)
θ'	$=$	$\arctan\left(\dfrac{2V_r}{V_v}\right)$	$=$	$\arctan(2\tan\theta)$.	(8-5, 8-6)

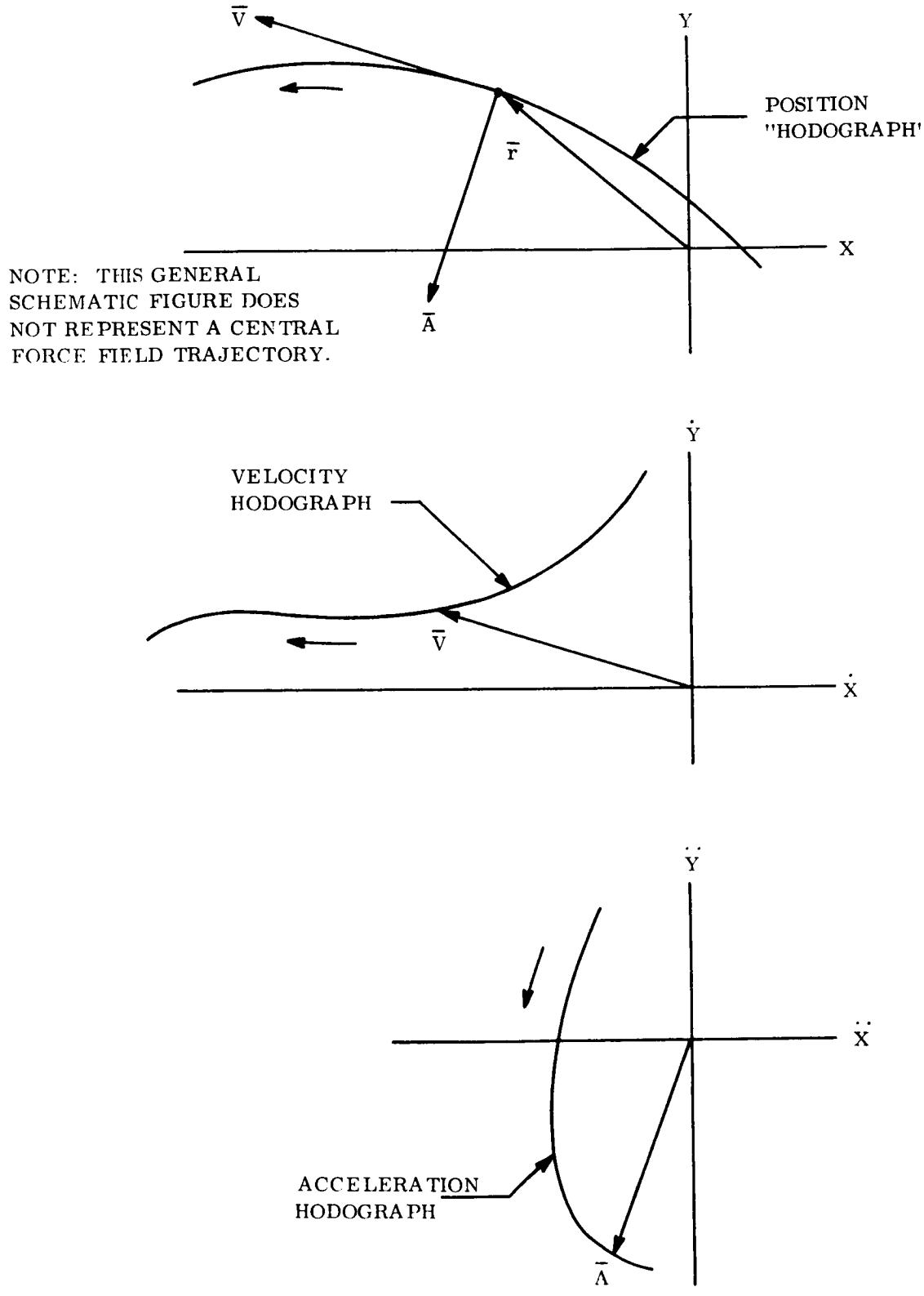

Figure 8-1. Corresponding Trajectory Hodographs of State Vectors

The orbital acceleration hodograph is a figure resembling the limaçon (References 8 and 9), as shown schematically in Figure 8-2. Note that the acceleration polar $\bar{\rho}$ in Figure 8-2 is identically the acceleration vector $\bar{A}$ in Figure 8-1. (The change in notation is intended to delineate the difference in analytical procedure with the differential geometry of the trajectory hodograph, and the classical dynamics of motion in the physical sense.) The polar vector $\bar{\rho}$ (defined by modulus and argument) generates the hodograph, whereas the polar angle θ' defines the direction of the tangent line to the hodograph, referred to the perpendicular of the polar $\bar{\rho}$. The polar $\bar{\rho}$ and the polar angle θ' are definable as functions of the velocity and position vectors, by the relations shown in Figure 8-2. Noting Equations 8-1 through 8-6,

$$V_r = R \sin \phi \tag{8-7}$$

$$V_v = C + R \cos \phi \quad , \tag{8-8}$$

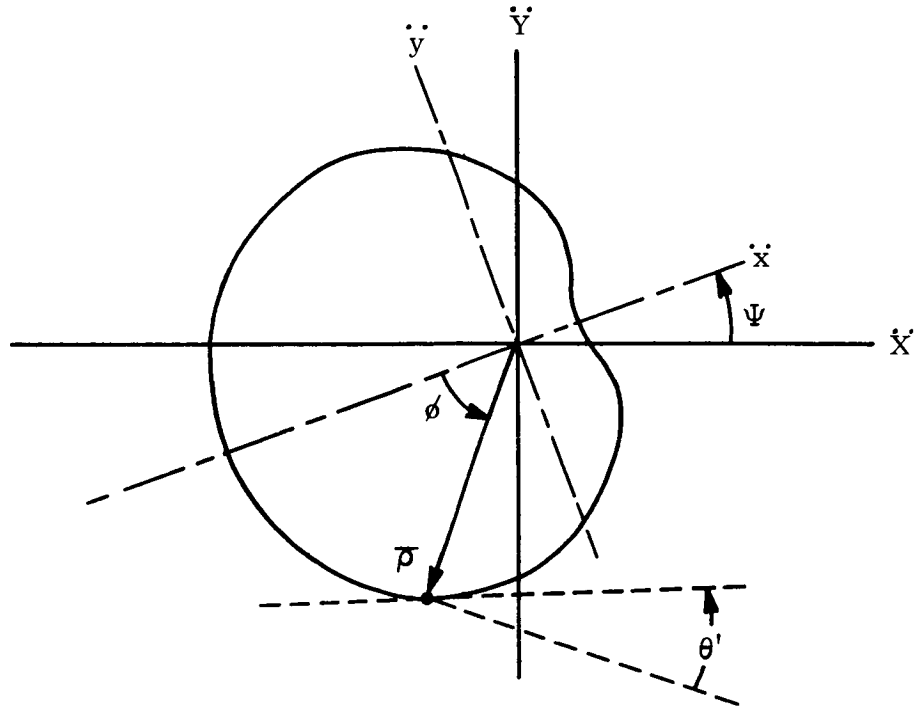

Figure 8-2. Orbital Acceleration Hodograph

it is seen that all dynamics conditions of position and velocity at a point of the instantaneous orbit are fulfilled when ($\bar{\rho}$, θ') are specified. Consequently, the parameter set (C, R, Ψ) is also determined. Note that the orientation of the acceleration hodograph in inertial coordinates is defined by the apsidal line direction angle Ψ (Figure 8-2).

Since a point in the acceleration vector space and the tangent to the hodograph figure at that point defines the complete state conditions*, then endpoint conditions of a powered trajectory are fulfilled when the terminal sets of point and tangent line are achieved by terminal hodographs of the continuum of instantaneous acceleration hodographs, as shown schematically in Figure 8-3. The powered trajectory hodograph (References 1 and 10) is the locus of successive points on the hodographs of the instantaneous orbits (i.e., on the instantaneous ballistic hodographs) in the acceleration vector space.

Each powered trajectory hodograph (as shown in Figure 8-3) is one of a field of such hodographs which may be provided by a thrust program and a given set of initial conditions. The field can be generated by variation of the control parameters or coefficients of the thrust program. For example, assume that a thrust law is programmed as follows:

> Whenever applied, the thrust vector will always be directed opposite to the instantaneous velocity vector.

If the endpoint conditions are specified, then two control parameters are available:

a. The time of thrust application (i.e., the duration interval and its location along the complete trajectory between endpoints).

b. The magnitude of the thrust vector.

---

* In any state space, a point and the hodograph tangent to the space curve at the point define the trajectory state completely. Consequently, the hodograph transformations of Reference 3 require only such state data for determination of all other vector states. Note that this is independent of the choice of coordinate systems.

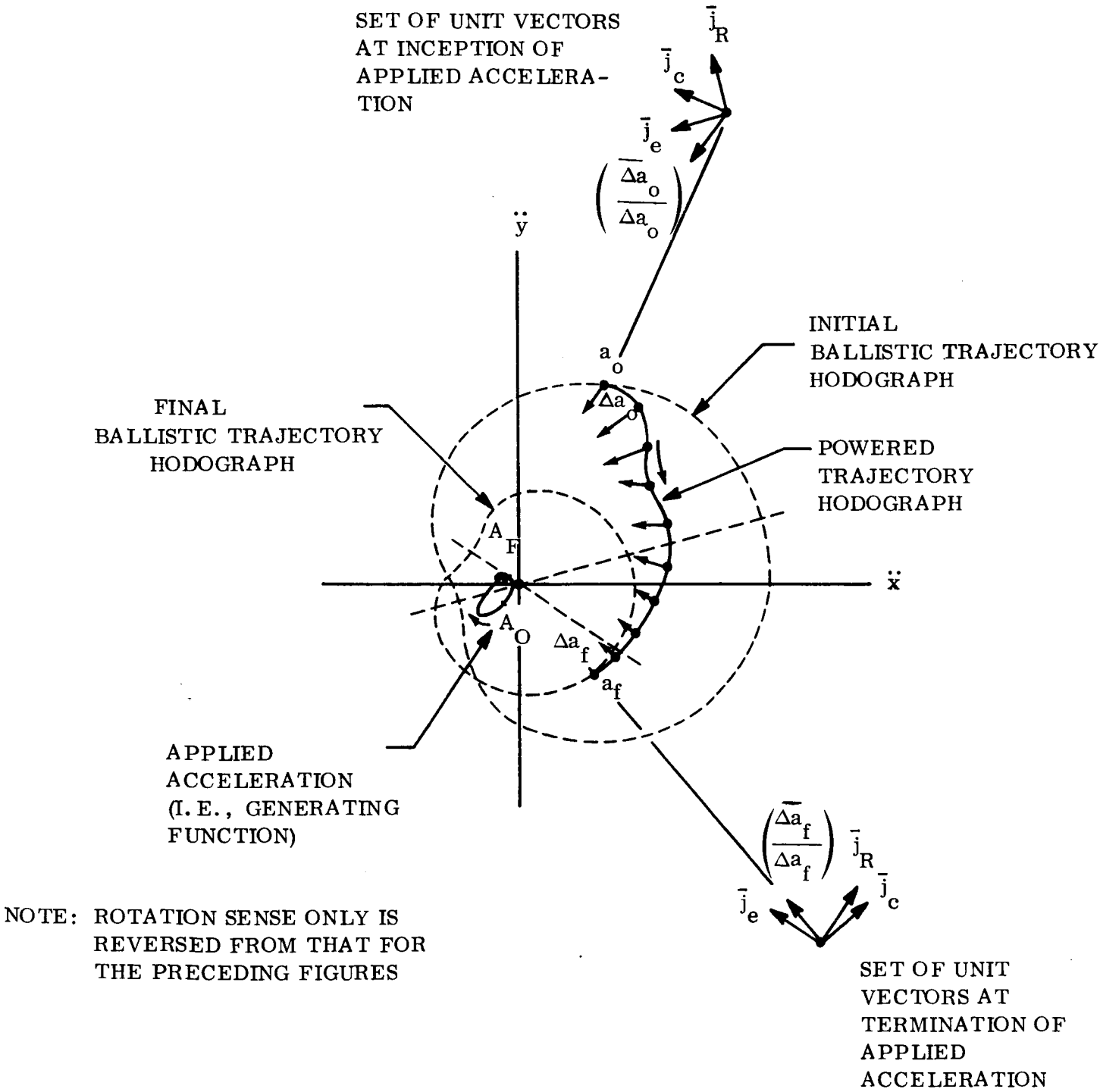

NOTE: ROTATION SENSE ONLY IS REVERSED FROM THAT FOR THE PRECEDING FIGURES

Figure 8-3. Acceleration Hodograph of a Powered Trajectory

Various values of these control parameters will generate a field of alternative realizable trajectories, as shown schematically in Figure 8-4*. Noting that the terminal states I and F are defined by the points, and tangents to the space curve at the points, in the acceleration vector space, the characteristic fields of hodograph solution may occur as follows:

a. No single powered trajectory hodograph of the realizable field may fulfill the endpoint conditions (Figure 8-4A),

b. Only one powered trajectory hodograph of the realizable field will fulfill the endpoint conditions (Figure 8-4B), or

c. Multiple admissible solutions of powered trajectory hodographs are available (Figure 8-4C).

If the given thrust program cannot fulfill the given endpoint conditions**, then it is totally useless in fulfilling the spacecraft mission. In general, any reasonably valuable and realizable thrust program will provide at least one solution within a bounded admissible region. If the spacecraft vehicle remains within this admissible region, the case of Figure 8-4A will not arise; however, if the spacecraft leaves this region (i.e., enters a catastrophic abort condition), then the one admissible solution which the thrust program can provide would no longer be useful.

At least one admissible solution will be imbedded within the field of realizable powered trajectory hodographs, as shown in Figure 8-4B, for most thrust programs devised for a given region of solution. The existence of only one unique admissible solution means that only one set of values of the control parameters can provide solution. This highly restrictive situation (from the system engineer's viewpoint) is rarely encountered in practice, fortunately, since physical systems require a range or band of useful control variation.

* In general, a simple geometric field such as shown schematically in Figure 8-4 will usually occur for variation of any one parameter alone.

** Of course, such conditions will include time and mass state constraints, if desired, as well as the vector space constraints which are completely defined in Figure 8-4.

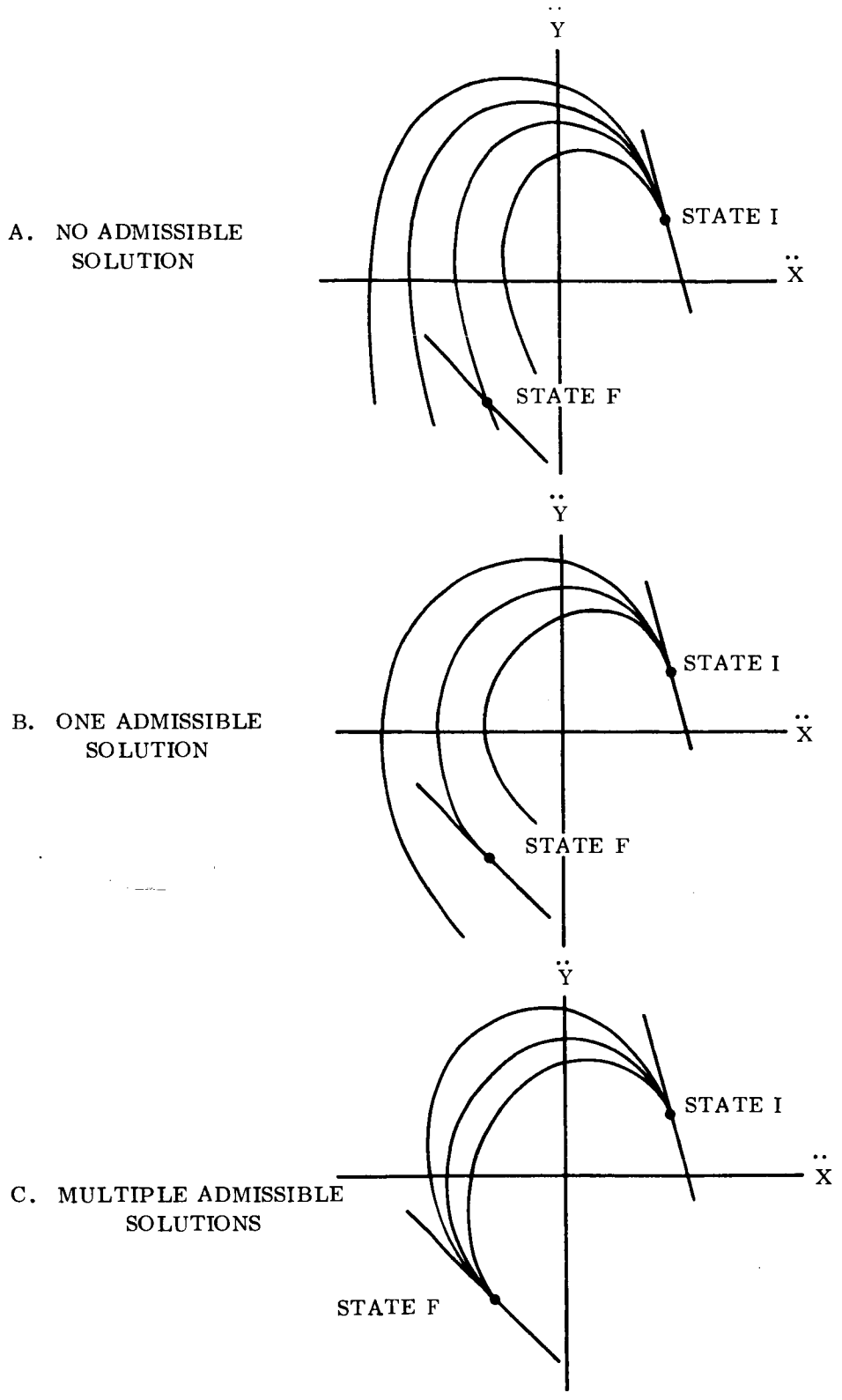

Figure 8-4. Fields of Powered Trajectory Hodographs in Acceleration Vector Space (for Specified Endpoint Conditions)

However, most useful thrust programs have multiple admissible solutions (Figure 8-4C). In fact, at least one infinite set of admissible solutions is usually available; consequently, the trajectory analyst must then resort to criteria for preferred selection of some few solutions of merit. Trajectory optimization is intended to provide additional criteria or constraints to identify these few solutions. As is well-known (at least among analysts in astrodynamics), the analytical definition of such solutions is quite difficult. Moreover, a means of analytical classification of the characteristic properties or merits of the large region of remaining admissible solutions would be extremely useful and even essential for the system designer, especially for anticipated space operations in which the few desirable solutions may become unattainable due to unforeseeable deterioration in the trajectory capabilities of the spacecraft system. It is intended that the geodesics theory of differential geometry may at least complement the variational calculus to provide useful engineering methods and criteria.

8.2 THE TRAJECTORY EQUATIONS

The hodographic equations of motion determine the trajectory hodograph (powered or ballistic) in acceleration vector space. In powered flight, the thrust vector $\overline{T}$, which is defined by two control variables (γ, m), will cause variation of the space curve of the powered trajectory hodograph in accordance with the equations of motion. That is, the thrust scalar is proportional to the rate of fuel mass expended in propulsion, and the thrust direction defined by the angle γ between the thrust vector $\overline{T}$ and the local horizon in the sense of the flight direction (positive for clockwise rotation). The hodograph space curve can then be expressed in terms of its moving trihedron, by means of the curvature κ and torsion λ.

It is shown in References 1 and 10 that the hodographic equations of motion, with time t as the independent variable, are

$$A_x = -\dot{C}\sin\phi - R\dot{\Psi} - C\dot{v}\cos\phi \qquad (8\text{-}9)$$

$$A_y = \dot{C}\cos\phi + \dot{R} - C\dot{v}\sin\phi \qquad (8\text{-}10)$$

or

$$A_r = \dot{R}\sin\phi - R\dot{\Psi}\cos\phi - C\dot{\upsilon} \tag{8-11}$$

$$A_\upsilon = \dot{R}\cos\phi + R\dot{\Psi}\sin\phi + \dot{C} \quad , \tag{8-12}$$

where

$$-\dot{\Psi} = \frac{\dot{C}}{C}\left[\frac{V_\upsilon + C}{V_r}\right] + \frac{\dot{R}}{R}\left[\frac{V_\upsilon - C}{V_r}\right] \quad , \tag{8-13}$$

and

$$\dot{\upsilon} = \dot{\Psi} + \dot{\phi} \tag{8-14}$$

since

$$\upsilon = \Psi + \phi \quad .$$

Also,

$$\frac{T_x}{m} = -\dot{C}\sin\phi - R\dot{\Psi} \tag{8-15}$$

$$\frac{T_y}{m} = \dot{C}\cos\phi + \dot{R} \tag{8-16}$$

or

$$\frac{T_r}{m} = \dot{R}\sin\phi - R\dot{\Psi}\cos\phi \tag{8-17}$$

$$\frac{T_v}{m} = \dot{R}\cos\phi + R\dot{\Psi}\sin\phi + \dot{C} \; ; \qquad (8\text{-}18)$$

also, the term $C\dot{\nu}$ represents the ballistic acceleration due to gravitational attraction. Only two control variables (γ, m) are available, since the thrust scalar T is itself a function of the mass rate change ($-V_e \dot{m}$)*. Consequently, the control variables (γ, m) cause direct variation of $\dot{C}$, $\dot{R}$, and consequently the dependent parametric terms Ψ and ϕ

The vector space locus of the total instantaneous acceleration is defined by

$$(A_x + R\dot{\Psi})^2 + (A_y - \dot{R})^2 = (\dot{C})^2 + (-C\dot{\nu})^2 \qquad (8\text{-}19)$$

or

$$(A_r + C\dot{\nu})^2 + (A_v - \dot{C})^2 = (\dot{R})^2 + (R\dot{\Psi})^2 \; , \qquad (8\text{-}20)$$

which are graphically presented as shown schematically in Figure 8-5. The vector space locus of the thrust acceleration is defined by

$$\left(\frac{T_x}{m} + R\dot{\Psi}\right)^2 + \left(\frac{T_y}{m} - \dot{R}\right)^2 = (\dot{C})^2 \qquad (8\text{-}21)$$

or

$$\left(\frac{T_r}{m}\right)^2 + \left(\frac{T_v}{m} - \dot{C}\right)^2 = (\dot{R})^2 + (R\dot{\Psi})^2 \; , \qquad (8\text{-}22)$$

which are graphically presented as shown schematically in Figure 8-6. Note that the two loci shown in Figures 8-5 and 8-6 differ only by the presence of the ballistic acceleration vector $\overline{C\dot{\nu}}$ in the total instantaneous acceleration locus of Figure 8-5, and its absence in the thrust acceleration locus of Figure 8-6.

* In three-dimensional space, an additional control variable will be available, for thrust direction referred to the instantaneous orbital plane.

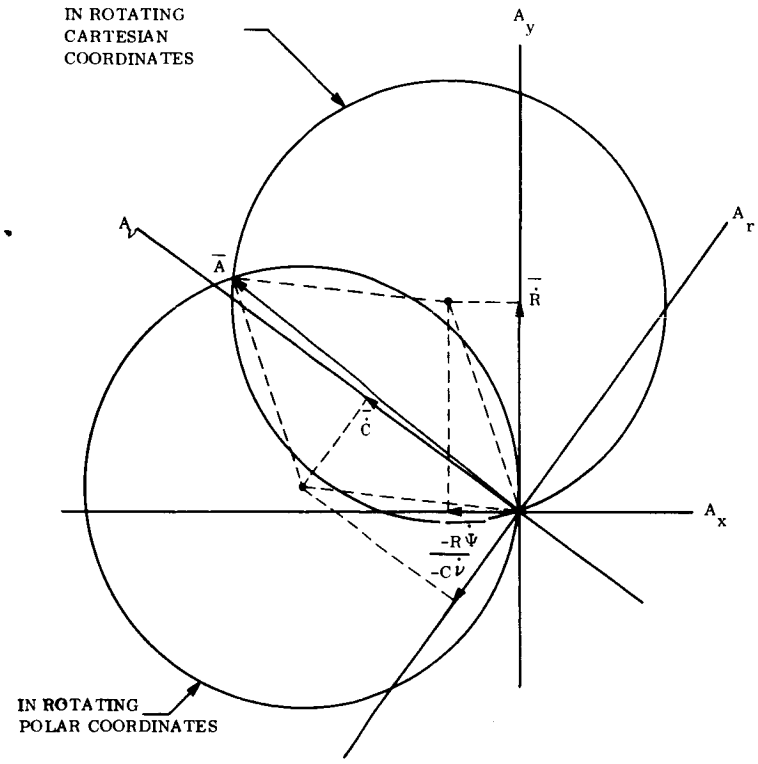

Figure 8-5. Total Instantaneous Acceleration Locus

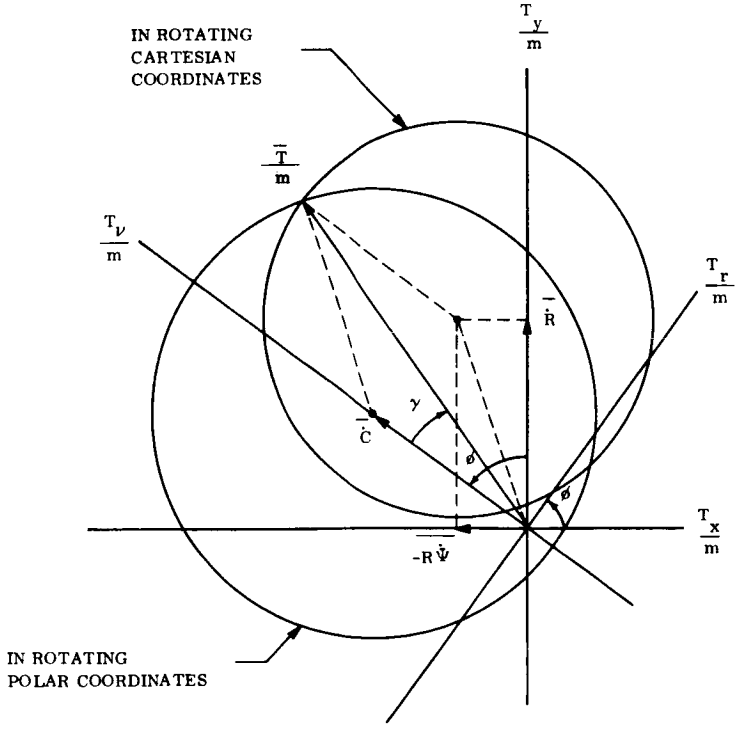

Figure 8-6. Thrust Acceleration Locus

In trajectory synthesis and analysis, the thrust program is devised and subsequent investigation and operational use assigns useful values to the available control parameters. Consequently, the hodographic parameter variations ($\dot{C}$, $\dot{R}$) and the associated dependent parameter variation Ψ should be expressed explicitly as functions of the instantaneous state parameters (C, R, ϕ) and the control parameters (γ, m).

As shown in Figure 8-5,

$$\frac{T_r}{m} = \frac{T}{m} \sin \gamma \tag{8-23}$$

$$\frac{T_v}{m} = \frac{T}{m} \cos \gamma \tag{8-24}$$

or

$$\frac{T_x}{m} = -\frac{T}{m} \sin (\phi - \gamma) \tag{8-25}$$

$$\frac{T_y}{m} = \frac{T}{m} \cos (\phi - \gamma) \tag{8-26}$$

Consequently, it can be shown that

$$\frac{T}{m} = \frac{\dot{R} + \dot{C} \cos \phi}{\cos (\phi - \gamma)} \tag{8-27}$$

Then

$$\dot{C} = -\left(\frac{T}{m}\right) \left(\frac{C}{C + R \cos \phi}\right) \cos \gamma \tag{8-28}$$

$$\dot{R} = \left(\frac{T}{m}\right) \left[\cos (\phi - \gamma) + \left(\frac{C}{C + R \cos \phi}\right) \cos \phi \cos \gamma\right] \tag{8-29}$$

and

$$R\dot{\Psi} = \left(\frac{T}{m}\right) \left[\sin (\phi - \gamma) + \left(\frac{C}{C + R \cos \phi}\right) \sin \phi \cos \gamma\right] . \tag{8-30}$$

Note that the parameter variation $\dot{\Psi}$ is a dependent function of $\dot{C}$ and $\dot{R}$ as shown by Equation 8-13. The hodographic acceleration state vectors are presented schematically in isometric view in Figure 8-7, in relation to the instantaneous position hodograph, for ease of recognition.

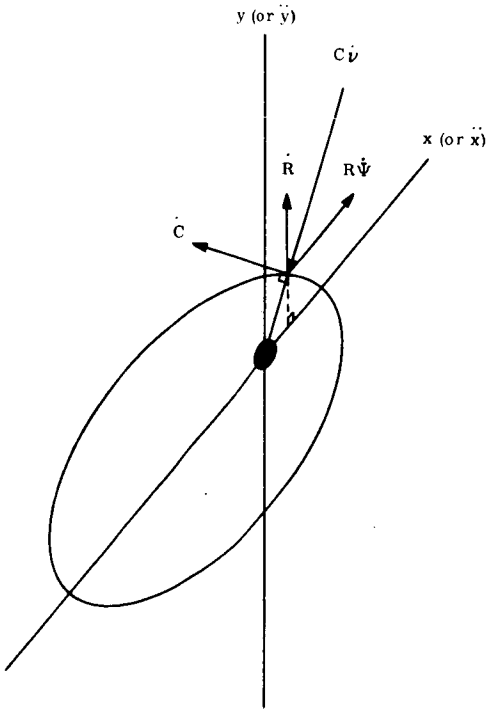

Figure 8-7. Acceleration Hodograph State Vectors

It is conventionally assumed that a thrust force $\overline{T}$ must necessarily be expressed in trajectory analysis in terms of a mass flow rate (dm/dt). Although this is a valid alternative form of Newton's second law for the actual physical process of energy conversion at a rocket or propulsion chamber, this approach does not reflect awareness of the state of contemporary propulsion system technology. The guidance command is directed to a feedback control subsystem of the complete propulsion system. Consequently, fuel flow is no longer controlled directly (as in primitive or older designs of space propulsion) but thrust force or a measurable parameter which is predictable and responsive to the effective thrust force is employed as a control feedback. As a result, thrust force variation need no longer be specified by the trajectory analyst in terms of commanded fuel flow rate. In fact, this present practice imposes most severe demands upon the propulsion control subsystem,

without taking advantage of the inherent capabilities of feedback controls. That is, it is suggested that thrust force control command to the propulsion feedback control as a function of a trajectory space variable, rather than the fuel flow rate, can provide superior spacecraft system trajectory control. In this way, two advantages may accrue:

a. The propulsion control design will not be subjected to severe high-frequency response requirements.

b. The actual spacecraft system performance (not an arbitrary guidance law and its immediate implementation) will determine the required thrust force.

If desired, the trajectory equations for the acceleration hodograph may be used for acceleration vector space analysis, with time t as the independent variable, just as presented to this point. However, the complete and rigorous state space theory indicates that a space variable (such as ϕ) should be employed as the independent variable, rather than time t. Then time becomes a dependent state variable, expressed as a trajectory time locus in time state space (Reference 1). Since

$$\frac{T}{m} = -V_e\left(\frac{\dot{m}}{m}\right) \quad , \tag{8-31}$$

then

$$\frac{T_x}{m}^{\circ} = V_e \sin(\phi-\gamma)\left(\frac{m^{\circ}}{m}\right) = -C^{\circ}\sin\phi - R\dot{\Psi}^{\circ} \tag{8-32}$$

$$\frac{T_y}{m}^{\circ} = -V_e \cos(\phi-\gamma)\left(\frac{m^{\circ}}{m}\right) = C^{\circ}\cos\phi + R^{\circ} \tag{8-33}$$

or

$$\frac{T_r}{m}^{\circ} = -V_e \sin\gamma\left(\frac{m^{\circ}}{m}\right) = R^{\circ}\sin\phi - R\dot{\Psi}^{\circ}\cos\phi \tag{8-34}$$

$$\frac{T_v}{m}^{\circ} = -V_e \cos\gamma\left(\frac{m^{\circ}}{m}\right) = R^{\circ}\cos\phi + R\dot{\Psi}^{\circ}\sin\phi + C^{\circ} \tag{8-35}$$

where

$$T_{(\,)}^{\circ} \equiv -V_e \dot{m}^{\circ}\Big|_{(\,)} = T_{(\,)}\left[\frac{dt}{d\phi}\right] \tag{8-36}$$

$$\dot{m}^{\circ} \equiv \frac{d\dot{m}}{d\phi}$$

$$C^{\circ} \equiv \frac{dC}{d\phi}$$

$$R^{\circ} \equiv \frac{dR}{d\phi}$$

$$\Psi^{\circ} \equiv \frac{d\Psi}{d\phi} \quad .$$

As before, the hodographic parameter variations can be expressed explicitly as functions of the instantaneous state parameters and control parameters, as follows:

$$C^{\circ} = -\left(\frac{T^{\circ}}{m}\right)\left(\frac{C}{C+R\cos\phi}\right)\cos\tau \tag{8-37}$$

$$R^{\circ} = \left(\frac{T^{\circ}}{m}\right)\left[\cos(\phi-\tau) + \left(\frac{C}{C+R\cos\phi}\right)\cos\phi\cos\tau\right] \tag{8-38}$$

$$R\Psi^{\circ} = \left(\frac{T^{\circ}}{m}\right)\left[\sin(\phi-\tau) + \left(\frac{C}{C+R\cos\phi}\right)\sin\phi\cos\tau\right] . \tag{8-39}$$

Thus, the thrust (or applied) acceleration scalar (T/m) may be programmed, as a function of the space variable ϕ, by the direct input command to the propulsion control system for $d\dot{m}/d\phi$ rather than the customary $d\dot{m}/dt$. Then the variation of mass and time, as a function of the space variable ϕ, is apparent as the mass and time loci in mass and time state spaces respectively (References 1 and 6). The time locus (Reference 6) will provide $dt/d\phi$ as a function of the parameters C, R, ϕ. Although the mass locus has not yet been subjected to

intensive study, an interesting form of the mass state equation is presented in Subsection 8.7 for future study of the mass locus in mass state space.

8.3 THE VECTOR FORMULAS AND ALTERNATIVE SETS

The "formulas of Frenet" or the "Serret-Frenet formulas" define any three-dimensional space curve by means of three orthogonal vectors of the moving trihedron. As shown schematically in Figure 8-8, the "moving trihedron" of the three unit vectors $\bar{j}_T$, $\bar{j}_K$, $\bar{j}_Z$ associated with a point on the space curve will rotate in orientation with the curve as the point moves along the curve. Moreover, it is eminently desirable that the equations of the space curve be independent of the choice of a coordinate system; that is, all variables be intrinsic properties of the curve alone. Consequently, the Serret-Frenet vector formulas are "natural" or "intrinsic" equations, as follows:

$$\left.\begin{aligned} \frac{d\bar{j}_T}{ds} &= K\bar{j}_K \\ \frac{d\bar{j}_K}{ds} &= -K\bar{j}_T + \lambda\bar{j}_Z \\ \frac{d\bar{j}_Z}{ds} &= -\lambda\bar{j}_K \end{aligned}\right\} \qquad (8\text{-}40)$$

where the curvature $K = K(s)$ and the torsion $\lambda = \lambda(s)$. The path length s extends along the space curve identically. Also,

$$(\bar{\rho}')^2 = 1 \qquad (8\text{-}41)$$

$$\bar{j}_T = \bar{\rho}' \qquad (8\text{-}42)$$

PLANE	THROUGH	VECTORS
OSCULATING		TANGENT $\bar{j}_T$ PRINCIPAL NORMAL $\bar{j}_K$
RECTIFYING		BINORMAL $\bar{j}_Z$ TANGENT $\bar{j}_T$
NORMAL		PRINCIPAL NORMAL $\bar{j}_K$ BINORMAL $\bar{j}_Z$

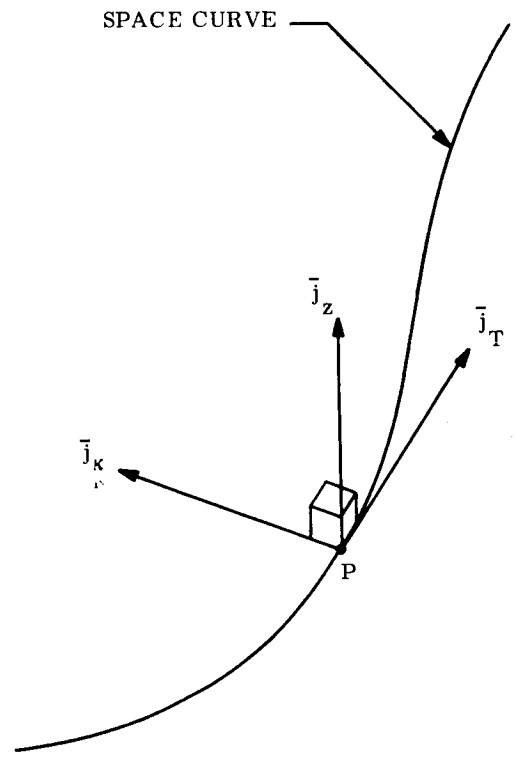

Figure 8-8. Moving Trihedron

$$\bar{J}_K = \frac{\bar{\rho}''}{|\bar{\rho}''|} \tag{8-43}$$

$$K = |\bar{\rho}''| = \frac{\mathrm{Im}\left[(\bar{\rho}')^* \bar{\rho}''\right]}{|\bar{\rho}'|^3} = \frac{1}{2j} \frac{(\bar{\rho}')^* \bar{\rho}'' - \bar{\rho}'(\bar{\rho}'')^*}{\left[\bar{\rho}'(\bar{\rho}')^*\right]^{3/2}} \tag{8-44}$$

$$\lambda = \left(\frac{d\bar{J}_K}{ds}\right) \bar{J}_Z = \frac{\bar{\rho}'\,\bar{\rho}''\,\bar{\rho}'''}{(\bar{\rho}'')^2} \tag{8-45}$$

$$s = \int \left|\frac{d\bar{\rho}}{d\phi}\right| d\phi = \int \left[\rho^2 + \left(\frac{d\rho}{d\phi}\right)^2\right]^{\frac{1}{2}} \tag{8-46}$$

where

$$\bar{\rho}' = \frac{d\bar{\rho}}{ds}$$

$$\bar{\rho}'' = \frac{d^2\bar{\rho}}{ds^2}$$

$$\bar{\rho}''' = \frac{d^3\bar{\rho}}{ds^3}$$

and ( )* denotes the complex conjugate of ( ).

Referring to the trajectory equations of the preceding subsection, we see that the independent variable is the space variable ϕ rather than the path length s. Although the immediately available equations of motion are expressed as functions of ϕ, the use of path length s is obviously attractive for direct use of the Serret-Frenet formulas in the basic form of Equation 8-40. Moreover, it appears that the trajectory flight time is an inverse function of the path length of the acceleration hodograph; that is, the longer the path length of the acceleration hodograph (for given endpoint conditions), the shorter will be the elapsed flight time. (This property will be briefly discussed in a later subsection.) Consequently, the study encompasses the planned use of the Serret-Frenet vector formulas in continuing research and applications. However, the space variable ϕ will be retained at least as the coordinate reference between the moving trihedron and the state spaces.

The following three sets of unit vectors will be employed in subsequent acceleration space analysis of fields of powered trajectory hodographs:

a. The hodographic set.

b. The polar set.

c. The geometric set.

These sets of unit vectors are shown schematically in Figure 8-9, together with the "position polar" set ($\bar{j}_r$, $\bar{j}_\nu$, $\bar{j}_z$) which is referred to the position vector $\bar{r}$. Note that the "position

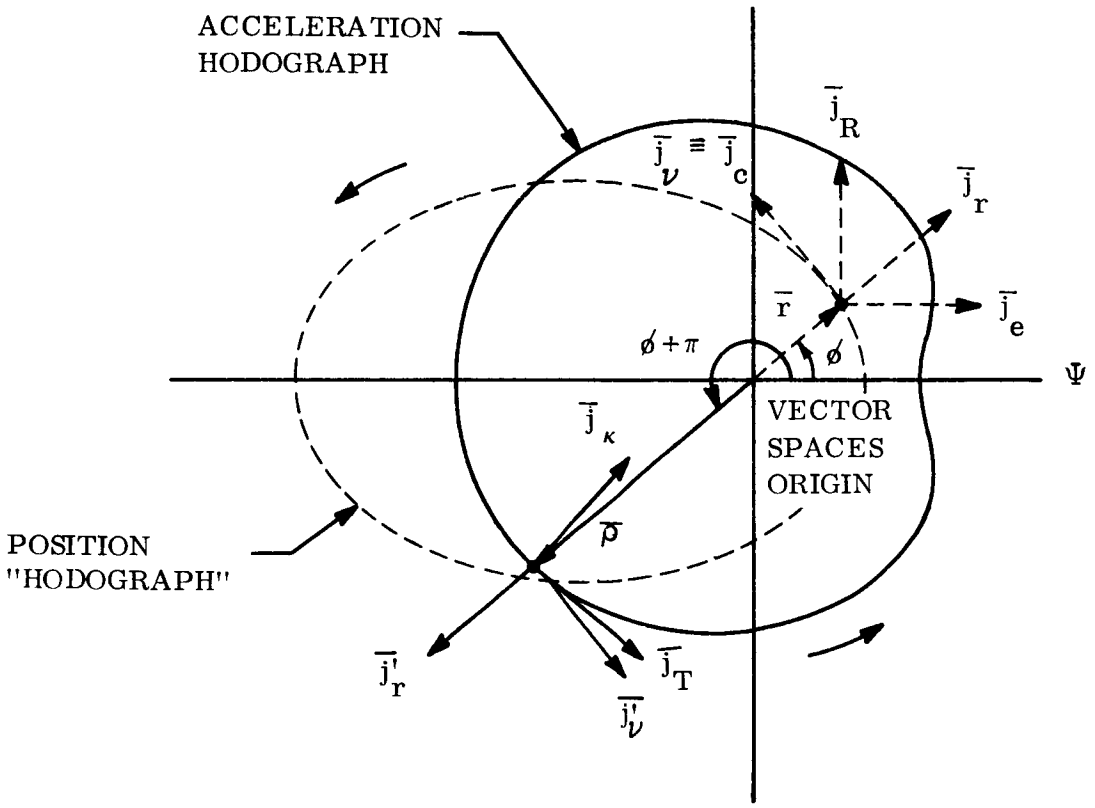

VECTOR SET	UNIT VECTORS			
HODOGRAPHIC	$\bar{J}_C$	$\bar{J}_R$	$\bar{J}_e$	$\bar{J}_z$
GEOMETRIC		$\bar{J}_T$	$\bar{J}_K$	$\bar{J}_z$
POLAR		$\bar{J}_r'$	$\bar{J}_\upsilon'$	$\bar{J}_z'$
POSITION POLAR		$\bar{J}_r$	$\bar{J}_\upsilon$	$\bar{J}_z$

orthogonal sets
(or subset)

NOTE: $\bar{J}_r' = -\bar{J}_r$

$\bar{J}_\upsilon' = -\bar{J}_\upsilon$

$\bar{J}_\upsilon \equiv \bar{J}_C$

Figure 8-9. Unit Vector Sets for Acceleration Vector Space Analysis

polar" set is referred to the position "hodograph" or trajectory figure, the hodographic set to the velocity hodograph, and the polar as well as geometric set to the acceleration hodograph. The latter three sets are shown in Figure 8-10, referred to the instantaneous point on the acceleration space curve of a powered trajectory hodograph. The hodographic set ($\bar{j}_C$, $\bar{j}_R$, $\bar{j}_e$, $\bar{j}_z$) yields natural or intrinsic equations of orbital mechanics, with the position "hodograph" (or "Keplerian orbit") and velocity hodograph defined implicitly. The polar set ($\bar{j}'_r$, $\bar{j}'_\nu$, $\bar{j}'_z$) yields polar equations of orbital mechanics in acceleration vector space, with the position vector (rather than the Keplerian orbit) defined implicitly. Since $\bar{j}'_\nu = -\bar{j}'_\nu$, then $\bar{j}_C \equiv \bar{j}_\nu = -\bar{j}'_\nu$; also, $\bar{j}'_r = -\bar{j}_r$, $\bar{j}'_z \equiv \bar{j}_z$. The primary utility of the polar set is for definition of the geometric figure of the state space curve of the acceleration hodograph, prior to definition and use of the intrinsic parameters (κ, s). That is, its use is intermediate between the hodographic set for the differential geometry of the state curve. The geometric set ($\bar{j}_T$, $\bar{j}_\kappa$, $\bar{j}_z$) yields natural or intrinsic equations of the differential geometry of the state space curve of the acceleration hodograph.

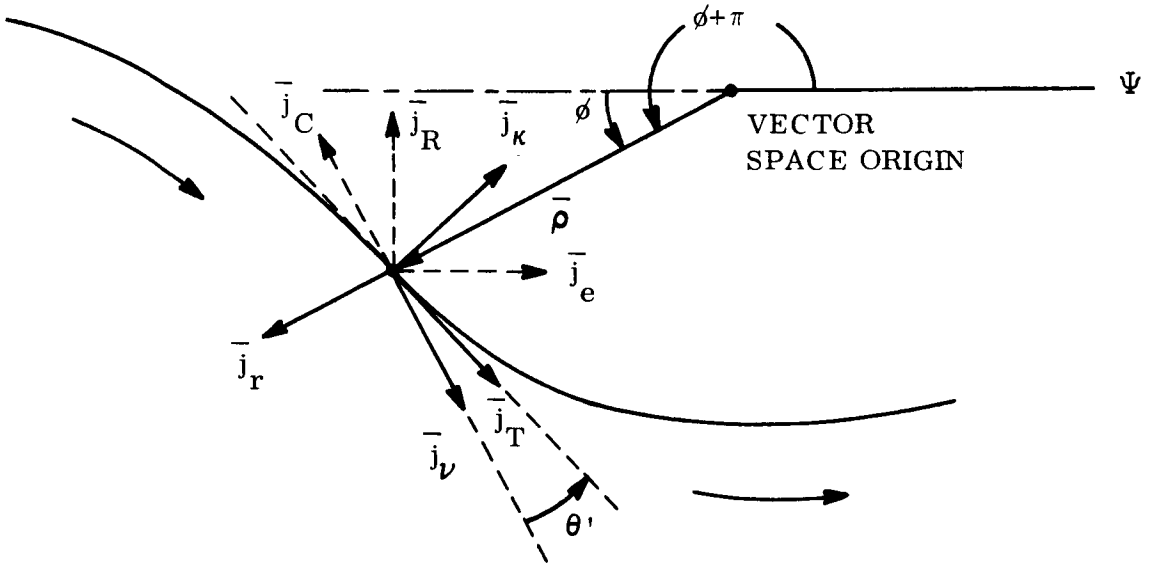

Figure 8-10. Unit Vector Sets Referred to a Powered Trajectory Hodograph

The transformation matrices between these three sets of unit vectors are as follows:

$$\begin{Bmatrix} \bar{J}_T \\ \bar{J}_K \\ 0 \end{Bmatrix} = \begin{bmatrix} -\cos(\phi+\theta') & -\cos\theta' & \sin(\phi+\theta') \\ \sin(\phi+\theta') & \sin\theta' & \cos(\phi+\theta') \\ 0 & 0 & 0 \end{bmatrix} \begin{Bmatrix} \bar{J}_R \\ \bar{J}_c \\ \bar{J}_e \end{Bmatrix} \tag{8-47}$$

$$\begin{Bmatrix} \bar{J}_T \\ \bar{J}_K \end{Bmatrix} = \begin{bmatrix} -\sin\phi & \cos\theta' \\ -\cos\phi & -\sin\theta' \end{bmatrix} \begin{Bmatrix} \bar{J}_r' \\ \bar{J}_v' \end{Bmatrix} \tag{8-48}$$

$$\begin{Bmatrix} \bar{J}_r' \\ \bar{J}_v' \\ 0 \end{Bmatrix} = \begin{bmatrix} -\sin\phi & 0 & -\cos\phi \\ -\cos\phi & 1 & \sin\phi \\ 0 & 0 & 0 \end{bmatrix} \begin{Bmatrix} \bar{J}_R \\ \bar{J}_c \\ \bar{J}_e \end{Bmatrix} . \tag{8-49}$$

The curvature κ has been developed, in Subsection 8.8, as a function of the geometric variables ρ, ϕ and θ' of the space curve of the acceleration hodograph, as follows:

$$K = \frac{\cos^3\theta'}{\rho}\left(1 + \cot\phi\tan\theta' + \frac{3}{2}\tan^2\theta'\right) . \tag{8-50}$$

The torsion λ will be determined by the cross-plane component of the perturbing thrust or force. Since the unique nonlinear mechanics of orbital motion in an inverse-square central force field are experienced dominantly in the instantaneous orbital plane, the torsion will be essentially independent of the orbital mechanics. Perturbations due to oblateness or triaxiality terms of the gravitational potential can be analyzed in terms of an effective torsion λ upon the trajectory curve. However, in two-dimensional motion, the Serret-Frenet formulas reduce to

$$\left.\begin{aligned} \frac{d\bar{J}_T}{ds} &= K\bar{J}_K \\ \frac{d\bar{J}_K}{ds} &= -K\bar{J}_T \end{aligned}\right\} \qquad (8\text{-}51)$$

since $\lambda_{2D} = 0$.

8.4 VARIATIONS OF THE PARAMETERS OF THE ORBITAL TRAJECTORY FIELD

The basic relations between the orbital mechanics (ballistic or powered) and the trajectory state in acceleration vector space in the form of a space curve are now available for variational analysis of the orbital trajectory field of such curves. These equations, summarized in Table 8-1, are classed as the hodographic equations of thrust perturbation, polar equations and intrinsic equations of the acceleration space curve. To demonstrate the inter-relation of these sets of equations, the functional flow diagram of Figure 8-11 relates the sets or "blocks" of variational equations which comprise the medium for variational analysis of the trajectory field. Block "B" equations

$$\delta\rho = \rho_C \delta C + \rho_R \delta R + \rho_\phi \delta\phi \qquad (8\text{-}52)$$

$$\delta\theta' = \theta'_C \delta C + \theta'_R \delta R + \theta'_\phi \delta\phi \qquad (8\text{-}53)$$

transform the acceleration state parameters (C, R) into the polar geometric parameters, whereas the successive Block "C" equations

$$\delta K = K_\rho \delta\rho + K_{\theta'} \delta\theta' + K_\phi \delta\phi \qquad (8\text{-}54)$$

Table 8-1. Basic Differential-Geometric Equations of Orbital Trajectory Fields

Ⓐ HODOGRAPHIC EQUATIONS OF THRUST PERTURBATION

$$C^\circ = -\frac{T^\circ}{m}\left(\frac{C}{C+R\cos\phi}\right)\cos\tau = -\frac{T^\circ}{m}\left(\frac{C}{V_v}\right)\cos\tau \qquad (8\text{-}37)$$

$$R^\circ = \frac{T^\circ}{m}\left[\cos(\phi-\tau)+\left(\frac{C}{C+R\cos\phi}\right)\cos\phi\cos\tau\right] = \frac{T^\circ}{m}\left[\cos(\phi-\tau)+\left(\frac{C}{V_v}\right)\cos\phi\cos\tau\right] \qquad (8\text{-}38)$$

$$R\Psi^\circ = \frac{T^\circ}{m}\left[\sin(\phi-\tau)+\left(\frac{C}{C+R\cos\phi}\right)\sin\phi\cos\tau\right] = \frac{T^\circ}{m}\left[\sin(\phi-\tau)+\left(\frac{C}{V_v}\right)\sin\phi\cos\tau\right] \qquad (8\text{-}39)$$

Ⓑ POLAR EQUATIONS OF ACCELERATION SPACE CURVE

$$\rho = \frac{C^2}{\mu}\left(C^2+R\cos\phi\right)^2 = \frac{(CV_v)^2}{\mu} \qquad (8\text{-}1)$$

$$\theta' = \arctan\left(\frac{2R\sin\phi}{C+R\cos\phi}\right) = \arctan\left(\frac{2V_r}{V_v}\right) \qquad (8\text{-}5)$$

Ⓒ INTRINSIC EQUATIONS OF ACCELERATION SPACE CURVE

$$K = \frac{\cos^3\theta'}{\rho}\left(1+\cot\phi\tan\theta'+\frac{3}{2}\tan^2\theta'\right) \qquad (8\text{-}50)$$

$$s = \int\left|\frac{d\bar{\rho}}{d\phi}\right|d\phi = \int\left[\rho^2+\left(\frac{d\rho}{d\phi}\right)^2\right]^{\frac{1}{2}}d\phi \qquad (8\text{-}46)$$

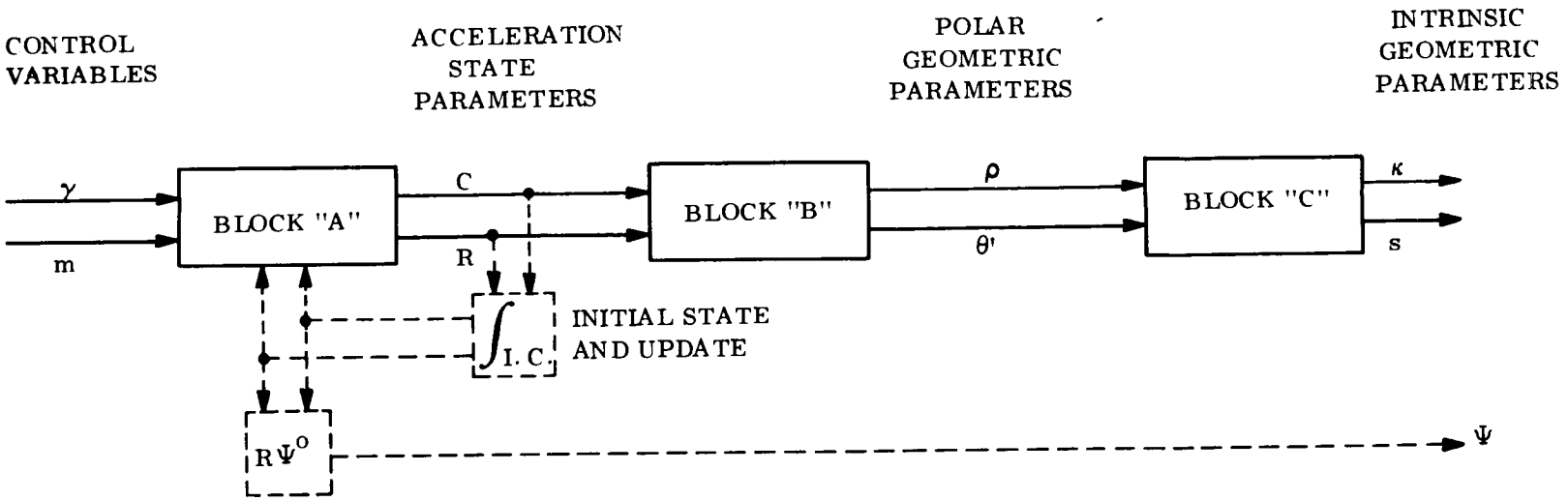

BLOCK "A"
HODOGRAPHIC EQUATIONS OF THRUST PERTURBATION (SEE TABLE 8-1)

BLOCK "B"
POLAR EQUATIONS 8-52, 8-53

BLOCK "C"
INTRINSIC EQUATIONS 8-54, 8-55

NOTE: SEE TABLES 8-2 AND 8-3 FOR PARTIAL DERIVATIVES OF BLOCKS "B" AND "C"

Figure 8-11. Functional Flow Diagram for Variational Analysis of Trajectory State

$$\delta s = \left[(\delta\rho)^2 + (\rho\delta\phi)^2 \right]^{\frac{1}{2}} \qquad (8\text{-}55)$$

transform the polar geometric parameters into the intrinsic geometric parameters. Note that the hodographic equations of thrust perturbation (listed in Table 8-1) are identically the variational equations for the hodograph parameters in response to the control variables of thrust. The complete hodographic equations of motion include this set as a sub-class (References 1 and 10).

In Figure 8-11, the update of the hodograph parameters C, R and the apsidal line direction angle Ψ is indicated in dotted outline and flow in order to indicate a direct and obvious computation logic which might be desirable. Although the differential-geometric equations of the powered trajectory hodograph may be employed, in theory, to carry out this update process, it appears that computation time and accuracy will be improved by direct update of the hodograph parameters, as shown. However, this procedure does not detract from the vital use of the differential geometry as a means of definitive study of the characteristic properties of the trajectory field, or its use (both in theory and application) for trajectory selection and optimization.

At this point, attention is called to the implied use of the space variable ϕ as the independent variable of computation (Figure 8-11). However, the functional flow diagram and variational analysis technique is valid for any desired selection of the independent variable. The trajectory hodograph in acceleration vector space is independent of the choice of the independent variable for analysis or computation. As an example of this analytical freedom of variable selection, subsequent study and exploratory application might suggest the use of the space variable ν as the independent variable. Since

$$\upsilon = \Psi + \phi$$

is the direction angle defining the spacecraft orientation in inertial space, it undergoes only continuous variation under thrust perturbation whereas both Ψ and consequently ϕ may experience discontinuous variation -- at least in theory. In practice, the gradient of

variation for ν will often be significantly less than the gradient of variation for ϕ in powered flight. As another example, time t could also be employed as the independent variable, although its treatment as a dependent state variable appears most useful in practice and theory. Moreover, maps and criteria for the evaluation as well as optimization of elapsed time in acceleration vector space appear attainable with further research study on complex time as a state variable in the state space theory.

The partial derivatives (Equations 8-56 through 8-72) required for Block B and C equations in Figure 8-11 are listed in Tables 8-2 and 8-3, respectively. Although the partials have been presented as functions of the parameters of the immediately preceding state representation (see the functional flow diagram of Figure 8-11), these equations may be converted to equivalent functions of other parameter sets [e.g., $\rho_c = f(\rho, \theta', \phi)$] . Note that the alternative sets of velocity state parameters (C, R) or (V_r, V_ν) may be used for the polar geometry variations; the former (i.e., hodographic) set is parametric whereas the latter (i.e., polar) is coordinate-bound.

The Block C equations define the intrinsic geometric parameters (κ, s) in terms of the polar geometric parameters (ρ, θ'), for the unique acceleration space curve due to one inverse-square attracting force center. However, a fundamental and completely general set of partials can be specified, which are valid for any space curve. This fundamental set consists of the following equations:

$$\frac{\partial s}{\partial \rho} = -\csc \theta' \qquad (8\text{-}73A)$$

$$\frac{\partial s}{\partial \phi} = \rho \sec \theta' \qquad (8\text{-}74A)$$

$$\frac{\partial K}{\partial \rho} = -\frac{K}{\rho} \qquad (8\text{-}75A)$$

Table 8-2. Partial Derivatives for Block "B" Equations
(Polar Geometric Variations)

PARTIAL TERM	$= f(C, R, \phi)$	$= f(V_r, V_v, \phi)$	EQUATION NO.
$\rho_C \equiv \frac{\partial \rho}{\partial C}$	$\frac{2C}{\mu}(2C+R\cos\phi)(C+R\cos\phi)$	$\frac{2V_v}{\mu}(2V_v - V_r\cot\phi)(V_v - V_r\cot\phi)$	8-56, 8-57
$\rho_R \equiv \frac{\partial \rho}{\partial R}$	$\frac{2C^2}{\mu}\cos\phi\,(C+R\cos\phi)$	$\frac{2V_v}{\mu}\cos\phi\,(V_v - V_r\cot\phi)^2$	8-58, 8-59
$\rho_\phi \equiv \frac{\partial \rho}{\partial \phi}$	$-\frac{2C^2}{\mu}(R\sin\phi)(C+R\cos\phi)$	$-\frac{2V_v}{\mu}V_r(V_v - V_r\cot\phi)^2$	8-60, 8-61
$\theta_C' \equiv \frac{\partial \theta'}{\partial C}$	$-\frac{2R\sin\phi}{(C+R\cos\phi)^2+(2R\sin\phi)^2}$	$-\frac{2V_r}{V_v^2+(2V_r)^2}$	8-62, 8-63
$\theta_R' \equiv \frac{\partial \theta'}{\partial R}$	$\frac{2C\sin\phi}{(C+R\cos\phi)^2+(2R\sin\phi)^2}$	$\frac{2(V_v\sin\phi - V_r\cos\phi)}{V_v^2+(2V_r)^2}$	8-64, 8-65
$\theta_\phi' \equiv \frac{\partial \theta'}{\partial \phi}$	$\frac{2R(R+C\cos\phi)}{(C+R\cos\phi)^2+(2R\sin\phi)^2}$	$\frac{2V_r(V_r+V_v\cot\phi)}{V_v^2+(2V_r)^2}$	8-66, 8-67

Table 8-3. Partial Derivatives for Block "C" Equations
(Intrinsic Geometric Variations)

PARTIAL TERM	$= f(\rho, \theta', \phi)$	EQUATION NO.
$K_\rho \equiv \frac{\partial K}{\partial \rho}$	$-\frac{\cos^3\theta'}{\rho^2}\left(1+\cot\phi\tan\theta'+\frac{3}{2}\tan^2\theta'\right)$	8-68
$K_{\theta'} \equiv \frac{\partial K}{\partial \theta'}$	$\frac{\cos\theta'}{\rho}\left[\cot\phi\left(1-3\sin^2\phi\right)+3\sin^2\theta'\left(\tan\theta'-\frac{3}{2}\right)\right]$	8-69
$K_\phi \equiv \frac{\partial K}{\partial \phi}$	$-\frac{\sin\theta'\cos^2\theta'\csc^2\phi}{\rho}$	8-70
$S_\rho \equiv \frac{\partial s}{\partial \rho}$	$-\csc\theta'$	8-71
$S_\phi \equiv \frac{\partial s}{\partial \phi}$	$\rho\sec\theta'$	8-72

Moreover, the analogous general form of Equations 8-60 and 8-61 is obtainable directly by means of Equation 8-73A and 8-74A, as follows:

$$\frac{\partial \rho}{\partial \phi} = -\rho \tan \theta' \quad . \tag{8-76}$$

The differential form of Equations 8-73A through 8-75A can be compactly presented as

$$\boxed{\frac{dK}{K} = -\frac{d\rho}{\rho} = \frac{ds}{\rho \csc \theta'} = \frac{d\phi}{\cot \theta'}} \quad . \tag{8-73B;8-74B;8-75B}$$

Although the Block "C" equations for the orbital acceleration hodograph are indispensable for specific solutions as well as continuing research and application studies, the general equations can be invaluable as signposts calling attention to characteristic properties which might otherwise be obscured by the functional complexity of the specialized and detailed equations for the trajectory curve. For example, Equation 8-73 calls attention directly to a remarkable simple yet useful property: namely, the ratio of the differential of the curvature to the curvature itself is equal in magnitude (but of inverse slope or negative sign) to the ratio of the differential of the polar to the polar itself (i.e., the instantaneous ballistic acceleration). On the other hand, this property is not obviously evident as represented by the specialized form of Equation 8-68.

8.5 CRITERIA OF OPTIMIZATION IN ACCELERATION VECTOR SPACE

The orbital trajectory field and its constituent paths in acceleration space may be generated in accordance with the definitive equations presented in the preceding subsection. Being able to generate all admissible trajectory paths (or hodographs), those paths which are optimal with respect to a useful criteria should be definable for mission analysis, operations plans, and system design. This analytical process of trajectory optimization in astrodynamics has been (and continues to be) dominated by the use of the variational calculus almost exclusively*. However, as presented at the beginning of this section, the differential

*As an historical footnote, trajectory optimization in the modern sense -- by the variational calculus -- developed a little over two decades ago, stemming principally from the pioneering work by Cicala (Italy) and Behrbohm (Sweden).

geometry can attain the same objectives by a different or converse approach. In particular, this differential-geometric optimization of orbital trajectories may offer new and cogent approaches to those analytical obstacles that impede further advances with the variational calculus, by use and extension of the geodesics theory of surfaces. Ironically, much of the classical theory of advanced dynamics has been based upon differential-geometric principles of space curves, although such work has not been advanced since Kasner (Reference 11) about 1910. The state space theory of Newtonian mechanics formalizes the trajectory "state history" in state spaces so that precise and complete analysis by differential geometry (and its related fields of tensors and non-Euclidean geometry) is feasible and attainable in the immediate future.

To conduct trajectory optimization in acceleration vector space, a desired criterion of optimization must first be analytically defined or interpreted in that state space. For example, referring to the powered trajectory hodograph shown in Figure 8-3, what unique geometric property of this curve can represent a desired optimal condition for this trajectory -- contrasted with all admissible trajectories under the given control law? Although definitive work in future state space study is required to establish these optimal criteria and their application to trajectory optimization itself, some preliminary thoughts and observations (based upon the developments ot the state space theory) are presented in this subsection, both for demonstration of the differential-geometric approach to optimization and also to serve as a "point of departure" for future study.

Two optimizations are of immediate and outstanding interest in trajectory analysis: (1) minimum fuel and (2) minimum time of trajectory flight. Different problem statements for these optimizations are encountered. In essence, such problems reflect different specifications of state conditions at the trajectory endpoints or along the anticipated actual path between the endpoints. Some aspects of the classical theory -- together with the state space theory in this section -- suggest two differential-geometric criteria for minimum fuel in acceleration vector space. The state space theory on the complex time locus (Reference 6) suggests a differential-geometric criterion for minimum time. Considered together, some provocative speculations arise on their mathematical inter-relation.

The "least-curvature" principle of Gauss and Hertz (Reference 12) states: "Of all paths consistent with the constraints (which are supposed to do no work), the actual trajectory is that which has the least curvature." In this usage, "curvature" refers to the square root of the function

$$\sum m \left\{ \left(\ddot{X} - \frac{F_x}{m} \right)^2 + \left(\ddot{Y} - \frac{F_Y}{m} \right)^2 + \left(\ddot{Z} - \frac{F_z}{m} \right)^2 \right\}$$

where

X, Y, Z = the coordinates of the particle system along any admissible path for which the position and velocity vectors at a given instant are the same as in some actual trajectory.

F_x, F_Y, F_z = components of the external force acting on the particle system.

Consequently, the actual trajectory is that one path for which the "curvature" function is least or minimal. When the active "external force" is due to the gravitational force center, then the principle of least curvature identifies the ballistic trajectory which must be actually generated. When the active external force consists of thrust force in addition to the gravitational force, then the principle of least curvature identifies a powered trajectory which (consistent with the constraint of the thrust control law) minimizes the "curvature" function. A minimum "curvature" function for a powered trajectory implies that the smallest amount of propulsion energy (or fuel) will be required. Although the immediate fruitful use of the principle of least curvature in powered trajectory synthesis and analysis is not directly apparent, it does identify a minimum fuel trajectory. Note that, if the actual trajectory happens to be a ballistic path, then the force components F_X, F_Y, F_Z will be identically zero even though the propulsion force is physically available upon command.

Speculating upon the possible geometric interpretation of the principle of least curvature, Silver (Reference 13) contemplated the statement of the least curvature principle in the literal sense; that is, that the term "curvature" can refer (with equal validity) to the curva-

ture κ of the geometric figure of the trajectory in position vector space*. Consequently, Silver proposed that "of all paths between two terminals, the path requiring the least acceleration is the path of least curvature." In this case, the least curvature is defined by

$$\delta \int |K| \, ds = 0 \quad . \tag{8-77}$$

That is, the integral (including the endpoints) of the absolute value of the geometric curvature must be minimized. Silver's proposition was not proven or analytically related to the principle of least curvature. However, let us now assume that the geometric curvature in question is the curvature of the acceleration space curve (or acceleration hodograph) of the trajectory state, rather than the curvature of the position space curve. Then, as shown by the differential relation between the curvature K and polar ρ of the acceleration space curve,

$$\frac{dK}{K} = - \frac{d\rho}{\rho} \quad , \tag{8-73B}$$

a direct relation exists between the hodograph curvature and the hodograph acceleration at each point (or time) of the trajectory. But the hodograph acceleration is, in fact, the state variable with which the "curvature" function (shown previously) of the principle of least curvature is directly concerned. Consequently, the differential-geometric relations of the acceleration space curve are the means for complete analytical investigation of the validity of a theorem relating minimal geometric curvature to minimal propulsion energy. If it were demonstrated that minimal curvature, in the definitive sense of Equation 8-[redacted]77, of the powered acceleration hodograph is a characteristic property of a trajectory which required minimal fuel expenditure, then the state space theory (together with Kasner's theorem** on transformations of natural families of curves) would relate this characteristic

* It is apparent that the term "curvature" applied by Hertz to the subject function was not accidental or casual, but deliberate. The geometric aspects of fields and dynamics were basic means of theoretical advances not only by Hertz, but by many other classical investigators.

** Ref. 11, p. 81: "Every natural system on one surface becomes by the conformal representation a natural system on the other." Conversely, "the only point transformations (in any space) which convert every natural family into a natural family are the conformal."

property of the acceleration hodograph curvature to the path curvature in position vector space. At this point, all analytical theory and evidence indicates strong likelihood that Silver's proposition is valid. However, rigorous and complete analytical investigation must be completed before this optimization criterion is accepted for subsequent trajectory optimization.

Another speculation on the characteristic properties of the trajectory hodograph in acceleration vector space becomes strengthened, for further investigation, by the strong likelihood of least curvature providing a minimum-fuel powered trajectory. That is, the least curvature condition (Equation 8-77) suggests an equivalent geometric interpretation as an area integral in acceleration vector space. Consider the powered trajectory hodograph (Figure 8-12) initiated at Point I on the initial ballistic trajectory hodograph and terminated at Point F on the final ballistic trajectory hodograph. If the spacecraft had proceeded in ballistic flight over the identical central angle $\Delta\nu$, its terminal point would then be Point F'. Curve 1, together with the powered trajectory hodograph curve, forms a closed envelope or area about the continuum of thrust acceleration vectors due to propulsion thrust (also see Figure 8-3). Note that this area bounds line elements of acceleration vector which are not collinear or otherwise bound to one another (such line elements do not fill the area so that it is "everywhere dense"). Consequently, the bounding volume cannot be an integral of the applied acceleration. However, consider the area (1FF') between the powered trajectory hodograph and the initial hodograph segment (1F). The area 1FF' represents the continuous change in ballistic state, due to thrust acceleration, so that it is filled "everywhere dense" with the acceleration line elements. It is suggested that this area is a direct function of the total thrust energy or fuel expenditure. If so, then minimization of area 1FF' would be an optimization criteria for minimum fuel. Since this area is generated by the changes in path curvature along the powered trajectory hodograph, it is directly related to the geometric curvature integral (Equation 8-76) and the least curvature. Again, strong likelihood exists that this proposition may be valid.

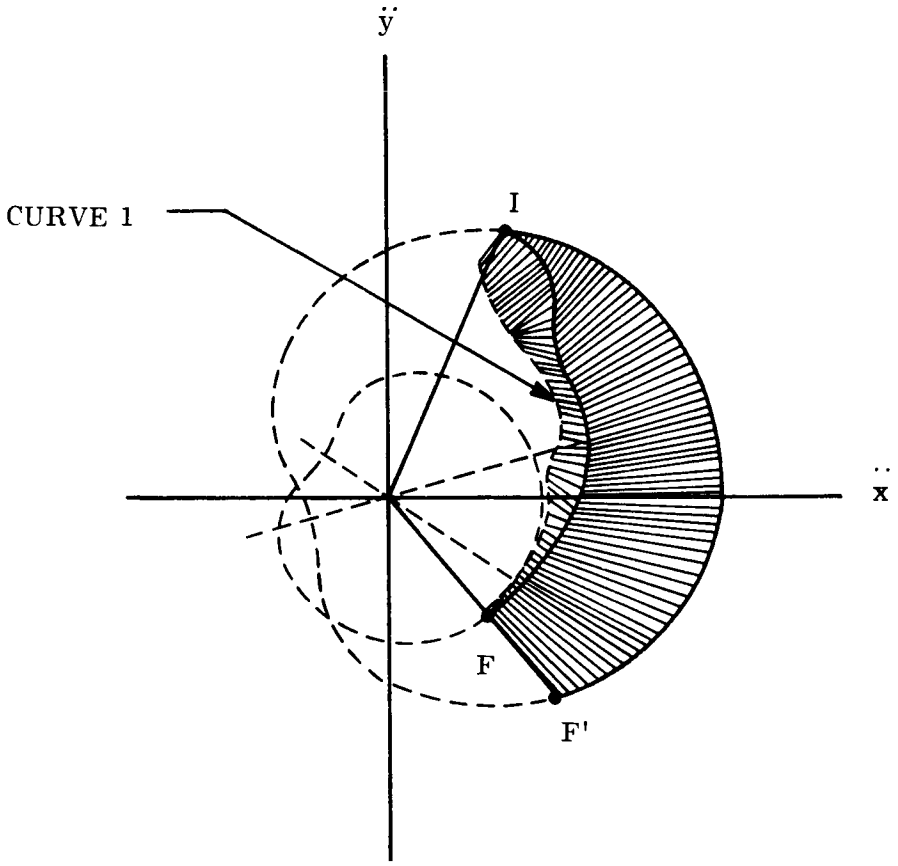

Figure 8-12. Characteristic Velocity Increment as an Area Integral in Acceleration Vector Space

The other outstanding optimization criterion of immediate interest is minimum time of trajectory flight. Actually, "minimum flight time" is not meaningful unless the attendant constraints (both in dynamic state and available fuel) of the problem statement are specified. Obviously, large velocities will yield minimal flight time. However, the fuel penalty would be extremely prohibitive. Although contemporary trajectory optimization by means of the variational calculus does necessarily treat time constraints, the analytic relation and tradeoffs between minimum time and minimum fuel solutions has not been adequately explored or understood.

Initial exploratory study of the orbital acceleration hodograph indicated that geometric inversion of this acceleration space curve defined the trajectory flight time (Reference 9). Subsequent definitive study (Reference 6) of the complex time locus in time state space identified the result of this geometric transformation as a curve in acceleration space -- the path length representing the trajectory time. This perimetric time curve of an orbital

acceleration hodograph is shown schematically in Figure 8-13. Since the trajectory of the figure is an orbit (i.e., ballistic), the perimetric time curve is a closed figure. The perimetric time curve for a powered trajectory hodograph will not, in general, be a closed figure. Based upon this geometric transformation, relating the path length of the acceleration hodograph and the path length (representing time) of the perimetric time curve, it can be shown that the longer the hodograph path length, the shorter the time curve path length*. Consequently, maximum path length of the powered trajectory hodograph characterizes (or implies) minimum time of flight along the powered trajectory. Referring to Figure 8-12, minimum flight time will be provided by a powered trajectory with the longest path length of its acceleration hodograph (i.e., hodograph path length between Points I and F), compared with all other admissible trajectories in the trajectory field for the given control law and trajectory constraints.

Let us consider the geometric properties of the powered acceleration hodograph, which are proposed candidates as optimization criteria for minimum fuel and minimum time trajectory solutions. As shown in Figure 8-14A, the flight time (Δt) is minimized by the maximum line integral along the powered acceleration hodograph, whereas the characteristic velocity increment ΔV (or fuel expenditure) is minimized by the minimum area integral between the initial orbital hodograph segment and the powered trajectory hodograph**. The area is closed by the segment of the terminal polar ρ_F extended to the initial orbital hodograph segment. For a given set of endpoint conditions, all elements of the geometry are fixed except the space curve of the powered trajectory hodograph itself. This space curve must be imbedded within the trajectory field for the given control law and specified constraints, as shown schematically in Figure 8-14B. It is apparent, then, that the tradeoff

* Since the radius of the circle of inversion is the square root of the hodograph parameter C, the circle of inversion as well as the hodograph polar will change continually for the powered acceleration hodograph. Nevertheless, the above statement is valid for powered flight also.

** Note that these two stated criteria do not imply -- as casual glance at the figure might lead one to presume -- that minimum fuel and minimum time must be provided jointly by one trajectory solution.

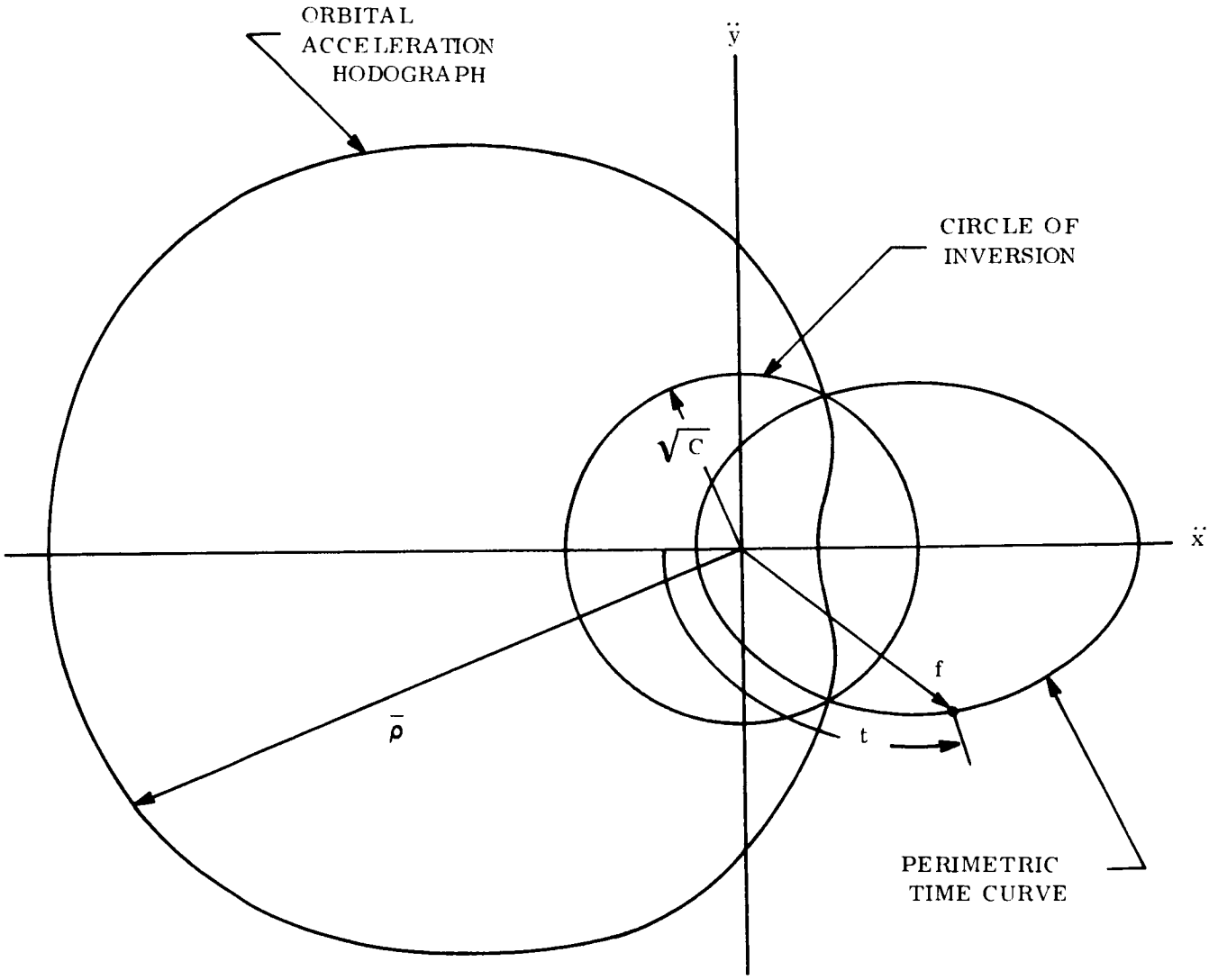

Figure 8-13. Perimetric Time Curve of an Orbit

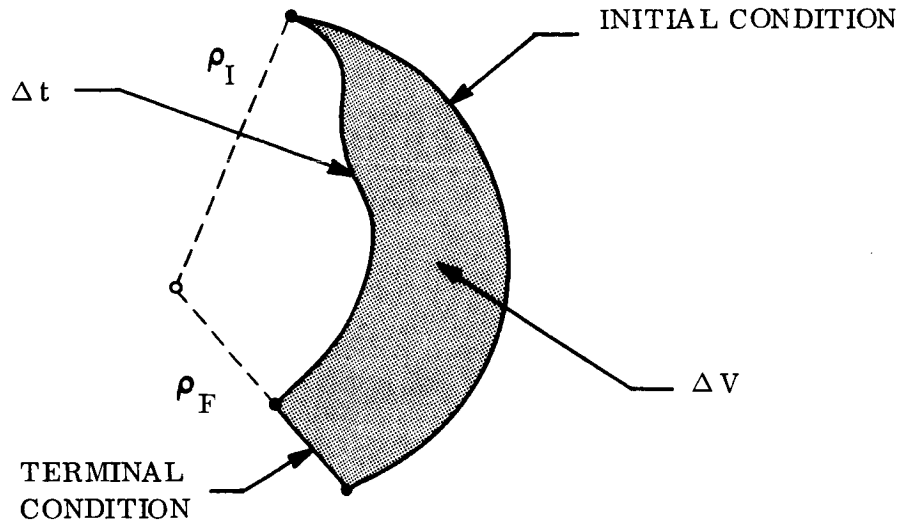

A. LINE AND AREA INTEGRALS

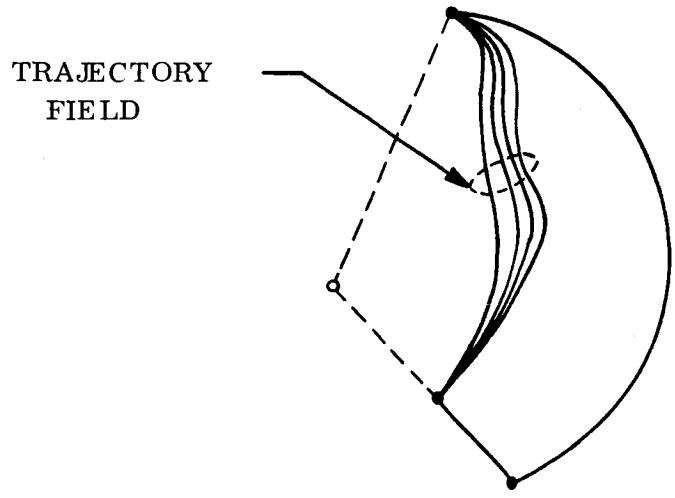

B. TRAJECTORY FIELD CONSTRAINT

Figure 8-14. Optimization Criteria in Acceleration Vector Space

between fuel and time optimization is influenced by the geometric properties of the trajectory field. These unique geometric properties, together with fundamental theorems on the analytic relations between the line and area integrals, would not only enable the determination of the minimum time and minimum fuel solutions, but also provide parameters for tradeoff evaluation. Of course, alternative problem statements which allow free selection of one or more endpoint conditions would vary the boundary conditions of the area, as well as influence the geometric properties of the trajectory field, with the same control law.

8.6 CONCLUDING REMARKS

This report provides the definitive theory and equations for the differential geometry of the acceleration space curves of individual paths in any orbital trajectory field. The trajectory field itself is generated by a given control law, in accordance with the variational equations. Within the trajectory field, the presence and nature of optimal paths (defined according to specified optimization criteria) should be identified for engineering evaluation and application. However, the optimization criteria of trajectory dynamics must first be expressed as geometric criteria of the acceleration vector space, for subsequent use of the geodesics theory of the differential geometry in obtaining the optimal solutions. Immediate, future study should be directed to analytic development of the geometric criteria for minimum fuel and minimum time solutions, based upon the approaches suggested in the preceding subsection.

At the same time, the conventional trajectory optimization calculus can be employed concurrently, based upon the definitive work of Phase IIIA. Such work would serve two purposes:

a. Advance the use of the variational calculus in optimizing trajectories by means of a complete and natural parametric formulation of the equations of motion.

b. Provide a means for analytic correlation between the methods of the differential geometry and the variational calculus.

As far as is known, no other optimization technique is currently available to check (or correlate with) trajectory solutions obtained by the variational calculus. From the viewpoint of theory, the differential geometry and the calculus-of-variations should provide complementary solutions so that major significant advances in trajectory optimization, especially for effective engineering application, should then be attained.

Specifically, the following body of theory has been presented in this report:

a. Hodographic equations of motion in acceleration vector space, in inertial and polar coordinates, with time t as the independent variable.

b. Hodographic equations of motion, with the space variable ϕ as the independent variable.

c. Intrinsic equations of the acceleration vector space curve of the powered (or ballistic) trajectory

d. The optimization criterion for minimum elapsed time Δt along a trajectory identified as the maximum line integral along the space curve of the trajectory acceleration hodograph

e. The optimization criterion for minimum fuel (or characteristic velocity increment ΔV) identified as the minimum area integral over the area formed by the trajectory acceleration hodograph and two curves of boundary conditions, one initial and the other terminal.

The hodographic equations with time t as the independent variable (i.e., a above) can be employed for trajectory analysis in accordance with conventional contemporary practice and techniques, including trajectory optimization by means of the variational calculus. The hodographic equations with the space variable ϕ as the independent variable (i.e., b above) is suitable also for use of the conventional contemporary techniques. However, direct guidance command of the propulsion control subsystem as a function of the immediate state variables of the trajectory is then possible, to attain more effective closed-loop guidance system performance with existing technology. The intrinsic equations of the acceleration space curve (i.e., c above) can be employed for orbital trajectory analysis by means of the differential geometry. In particular, trajectory selection and optimization can now be accomplished by use of the geodesics theory of surfaces. As the result of preliminary study

on optimization criteria in acceleration vector space, a minimum time criterion (i.e., d above) and minimum fuel criteria (i.e., e above) have been proposed for subsequent trajectory optimization in acceleration vector space. These criteria may enable the future derivation of the direct relation between minimum time and minimum fuel solutions, and the consequent tradeoff penalties. In particular, the minimum fuel criteria may provide a modern state-space interpretation of the classical principal of least curvature in advanced dynamics.

Attention is called to Kasner's unique work (Reference 11) on "differential geometric aspects of dynamics." This general theory can prove valuable in future research study on the differential geometry of trajectories. However, its objectives and scope must be clearly understood to appreciate its limitations. Kasner deals chiefly with the differential geometry of systems of trajectories. As he emphasizes: "It is essential to observe that the properties considered relate not to the individual curves, but to the infinite systems of curves." Since we are concerned not only with individual trajectories, but trajectories in the presence of a specific force field (i.e., the inverse-square attracting central force field), the analysis of orbital trajectories is highly specialized from the viewpoint of Kasner's work. However, since the orbital trajectories are subclasses of the general systems of trajectories treated by Kasner, many valuable theorems are available without restrictions (other than specified in his work). For example, Kasner employs the normal and tangential components of the force vector, and relates it to a Cartesian coordinate set (these components can be immediately described by the unit vector set of the intrinsic geometric parameters). However, Kasner has not directed his work to the analysis of trajectory paths in state space other than position. Obviously, the state space concept as a foundation for analytical theory of dynamics was not yet available to him. Consequently, much of his work is devoted to discussion of space curves in position vector space only and consequently restricted from direct application to complete trajectory analysis.

8.7 THE MODULUS OF THE ORBITAL MASS STATE

In trajectory synthesis, two alternative but converse procedures may be employed:

a. Specify the trajectory path so that the required mass rate will subsequently be determined

b. Specify the mass rate which provides the propulsive thrust so that the subsequent trajectory path is obtained.

In accordance with the state space theory, procedure a defines direct transformation from acceleration vector space to mass state space, whereas procedure b defines inverse transformation from mass state space to acceleration vector space.

With procedure b, a specified control law will define the functional variation of the propulsive thrust

$$T = -V_e \dot{m} \tag{8-78}$$

or

$$T = -V_e m^{\circ} \quad . \tag{8-79}$$

Subsequent use of Equations 8-78 or 8-79 as discussed in subsection 8.2 will generate the trajectory field of admissible solutions. This procedure is most usual in conventional practice.

With procedure a, an arbitrary specified trajectory or field of trajectories will necessitate direct transformation to the mass state space to determine the propulsion subsystem design characteristics implied by such trajectories. The following equation, based upon Equation 8-27 in subsection 8.2, can be used to obtain the required mass rate:

$$-V_e\left(\frac{dm}{m}\right) = \frac{dR + dC(\cos\phi)}{\cos(\phi - \tau)} \tag{8-80}$$

With time t as the independent variable,

$$-V_e\left(\frac{m^\circ}{m}\right) = \frac{\dot{R} + \dot{C}\cos\phi}{\cos(\phi - \gamma)} \quad ; \tag{8-81}$$

with the space angle ϕ as the independent variable,

$$-V_e\left(\frac{m^\circ}{m}\right) = \frac{R^\circ + C^\circ \cos\phi}{\cos(\phi - \gamma)} \quad . \tag{8-82}$$

Then, for example, integration of Equation 8-80 provides

$$-V_e \ln m = \int \sec(\phi - \gamma)\, dR + \int \cos\phi \sec(\phi - \gamma)\, dC \tag{8-83A}$$

or

$$\boxed{-V_e \ln m = \int \sec(\phi - \gamma)\left[dR + dC(\cos\phi)\right]} \quad . \tag{8-83B}$$

The functional relation of Equation 8-83B is shown schematically in the vector diagram of Figure 8-15.

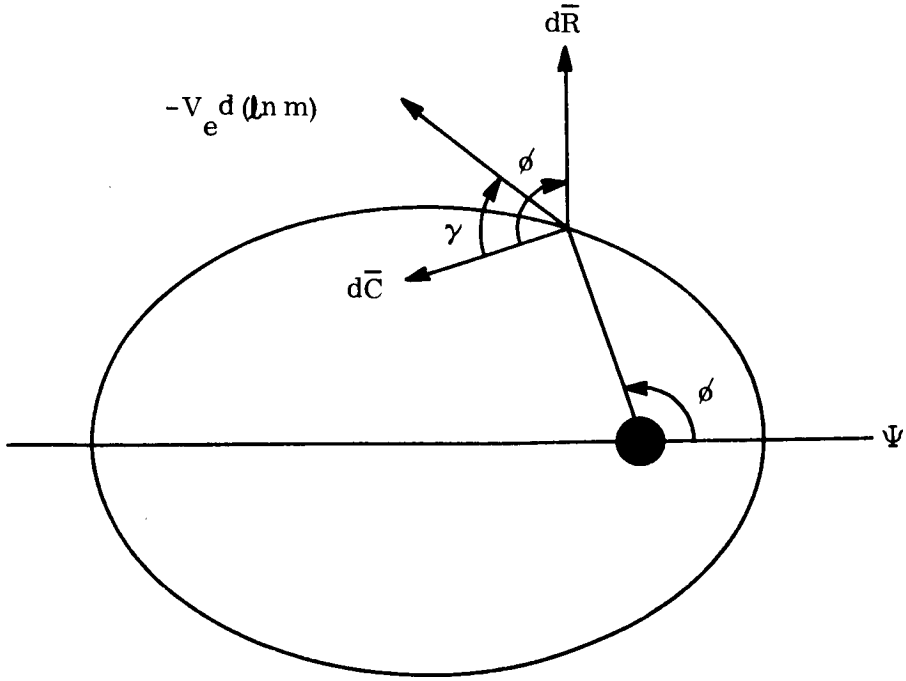

Figure 8-15. Relation Between Mass Variation and Hodograph Parameter Differentials

An alternative form of the modulus of the orbital mass state may prove useful in future work on the orbital mass locus.

$$\frac{T_r}{m} = \dot{R}\sin\phi - R\dot{\Psi}\cos\phi \tag{8-84}$$

$$\frac{T_v}{m} = \dot{R}\cos\phi + R\dot{\Psi}\sin\phi + \dot{C} \quad . \tag{8-85}$$

Since

$$\dot{\Psi} = -\dot{v} - \dot{\phi} \quad , \tag{8-86}$$

we obtain, upon substitution of Equation 8-86 in Equation 8-84,

$$\frac{T_r}{m} = \dot{R}\sin\phi + R\dot{\phi}\cos\phi - R\dot{v}\cos\phi \quad . \tag{8-87}$$

But

$$\dot{R}\sin\phi + R\dot{\phi}\cos\phi = \frac{d}{dt}(R\sin\phi) \tag{8-88}$$

so that Equation 8-87 becomes

$$\frac{T_r}{m} = \frac{d}{dt}(R\sin\phi) - R\dot{v}\cos\phi \quad . \tag{8-89}$$

Similarly, Equation 8-85 can be reduced to

$$\frac{T_v}{m} = \frac{d}{dt}(C + R\cos\phi) + R\dot{v}\sin\phi \quad . \tag{8-90}$$

Then

$$\left(\frac{T_r}{m}\right)dt = d(R\sin\phi) - (R\cos\phi)\,dv \tag{8-91}$$

and

$$\left(\frac{T_v}{m}\right) dt = d(C + R\cos\phi) + (R\sin\phi)\, d\upsilon \qquad (8\text{-}92)$$

so that, upon integration,

$$-V_e \sin\gamma \ln m = R\sin\phi - \int (R\cos\phi)\, d\upsilon \qquad (8\text{-}93)$$

and

$$-V_e \cos\gamma \ln m = (C + R\cos\phi) + \int (R\sin\phi)\, d\upsilon \; . \qquad (8\text{-}94)$$

Then, in complex notation, Equations 8-93 and 8-94 combine to provide

$$-V_e \ln m = iC + R(\sin\phi + i\cos\phi) - \int R(\cos\phi - i\sin\phi)\, d\upsilon \qquad (8\text{-}95A)$$

or

$$-V_e \ln m = Ce^{i\left(\frac{\pi}{2}\right)} + Re^{i\left(\phi - \frac{\pi}{2}\right)} - \int Re^{-i\phi} d\upsilon \qquad (8\text{-}95B)$$

so that

$$-V_e \ln m = Ce^{i\left(\frac{\pi}{2}\right)} + Re^{i\left(\phi - \frac{\pi}{2}\right)} - \int (Re^{-i\phi})\upsilon^{\circ} d\phi \qquad (8\text{-}96C)$$

where

$$\upsilon^{\circ} = \frac{d\upsilon}{d\phi} = 1 + \Psi^{\circ} \; .$$

With Equation 8-96C, the mass rate modulus ($-V_e$ ln m) is expressed as a function of C, R, ϕ and ν. Since the direction angle ν is defined in inertial coordinates, Equation 8-96C provides a direct relation between the mass rate modulus and the observable ν. Note that, if $\Psi^{\circ} = 0$, $\nu^{\circ} \equiv 1$; that is, $\nu \equiv \phi$ so that, in Equation 8-96C,

$$\int (Re^{-i\phi})v^{\circ}\,d\phi\Big|_{\Psi^{\circ}=0} = \int Re^{-i\phi}\,d\phi \ .$$

8.8 THE CURVATURE κ OF THE BALLISTIC ACCELERATION HODOGRAPH

The curvature κ of the ballistic acceleration hodograph, shown schematically in Figure 8-2, is defined by the general equation

$$K = \frac{\mathrm{Im}\left[(\bar{\rho}')^{*}\,\bar{\rho}''\right]}{|\bar{\rho}'|^{3}} \tag{8-97}$$

where

$$\bar{\rho}' = \frac{d\bar{\rho}}{ds}$$

$$\bar{\rho}'' = \frac{d^{2}\bar{\rho}}{ds^{2}}$$

$$(\bar{\rho}')^{*} = \text{complex conjugate of } \bar{\rho}' \ .$$

In complex notation, the polar vector $\bar{\rho}$ of the acceleration hodograph is

$$\bar{\rho} = \frac{C^{2}(C+R\cos\phi)^{2}}{\mu}\, e^{i(\phi+\pi)} \tag{8-98}$$

so that

$$\bar{\rho}' = \frac{C^{2}}{\mu}(C+R\cos\phi)^{2}\, ie^{i(\phi+\pi)} - \frac{C^{2}}{\mu}\left[2R\sin\phi(C+R\cos\phi)\right] e^{i(\phi+\pi)}, \tag{8-99}$$

$$(\bar{\rho}')^* = -\frac{C^2}{\mu}(C+R\cos\phi)^2 i e^{-i(\phi+\pi)} - \frac{C^2}{\mu}\left[2R\sin\phi(C+R\cos\phi)\right]e^{-i(\phi+\pi)} \quad (8\text{-}100A)$$

or

$$(\bar{\rho}')^* = -\frac{C^2}{\mu}e^{-i(\phi+\pi)}\left\{\left[2R\sin\phi(C+R\cos\phi)\right] + i\left[(C+R\cos\phi)^2\right]\right\}, \quad (8\text{-}100B)$$

and

$$\bar{\rho}'' = -\frac{C^2}{\mu}(C+R\cos\phi)^2 e^{i(\phi+\pi)} - \frac{C^2}{\mu}\left[2R\sin\phi(C+R\cos\phi)\right] i e^{i(\phi+\pi)} -$$

$$-\frac{C^2}{\mu}\left[2R\sin\phi(C+R\cos\phi)\right] i e^{i(\phi+\pi)} - \frac{C^2}{\mu}\left[2Re^{i(\phi+\pi)}\right]\left[\cos\phi(C+R\cos\phi) - k\sin^2\phi\right] \quad (8\text{-}101A)$$

or

$$\bar{\rho}'' = -\frac{C^2}{\mu}e^{i(\phi+\pi)}\left\{\left[(C+R\cos\phi)^2 + 2R\cos\phi(C+R\cos\phi) - 2R^2\sin^2\phi\right] + \right.$$

$$\left. + i\left[4R\sin\phi(C+R\cos\phi)\right]\right\} . \quad (8\text{-}101B)$$

Consequently,

$$\mathrm{Im}\left[(\bar{\rho}')^*\bar{\rho}''\right] = \frac{C^4}{\mu^2}\left\{(C+R\cos\phi)^2\left[(C+R\cos\phi)^2 + 2R\cos\phi(C+R\cos\phi) - \right.\right.$$

$$\left.\left. - 2R^2\sin^2\phi\right] + \left[8R^2\sin^2\phi(C+R\cos\phi)^2\right]\right\} \quad (8\text{-}102A)$$

or

$$\mathrm{Im}\left[(\bar{\rho}')^*\bar{\rho}''\right] = \frac{C^4}{\mu^2}(C+R\cos\phi)^2\left[(C+R\cos\phi)^2 + 2R\cos\phi(C+R\cos\phi) + \right.$$

$$\left. + 6R^2\sin^2\phi\right] , \quad (8\text{-}102B)$$

and

$$|\bar{\rho}'| = \frac{C^2}{\mu}\left[(C+R\cos\phi)^4 + 4R^2\sin^2\phi\,(C+R\cos\phi)^2\right]^{\frac{1}{2}} \qquad (8\text{-}103A)$$

or

$$|\bar{\rho}'| = \frac{C^2}{\mu}(C+R\cos\phi)\left[(C+R\cos\phi)^2 + 4R^2\sin^2\phi\right]^{\frac{1}{2}} \qquad (8\text{-}103B)$$

so that

$$|\bar{\rho}'|^3 = \frac{C^6(C+R\cos\phi)^3}{\mu^3}\left[(C+R\cos\phi)^2 + 4R^2\sin^2\phi\right]^{\frac{3}{2}}. \qquad (8\text{-}104)$$

Then

$$K = \frac{\mu}{C^2(C+R\cos\phi)}\,\frac{\left[(C+R\cos\phi)^2 + 2R\cos\phi(C+R\cos\phi) + 6R^2\sin^2\phi\right]}{\left[(C+R\cos\phi)^2 + 4R^2\sin^2\phi\right]^{\frac{3}{2}}} \qquad (8\text{-}105A)$$

or

$$K = \frac{\mu}{C^2 V_v}\,\frac{\left[V_v^2 + 2V_v R\cos\phi + 6V_r^2\right]}{\left[V_v^2 + 4V_r^2\right]^{3/2}} \qquad (8\text{-}105B)$$

$$K = \frac{\mu}{(CV_v)^2}\left[\frac{1 + \frac{2R\cos\phi}{V_v} + 6\left(\frac{V_r}{V_v}\right)^2}{\left\{1 + \left(\frac{2V_r}{V_v}\right)^2\right\}^{3/2}}\right] \qquad (8\text{-}106C)$$

$$K = \frac{1}{\rho}\left[\frac{1 + \frac{2V_r \cot\phi}{V_v} + \frac{3}{2}\left(\frac{2V_r}{V_v}\right)^2}{(1+\tan^2\theta')^{3/2}}\right] \qquad (8\text{-}106D)$$

$$K = \frac{1}{\rho}\left[\frac{1 + \cot\phi \tan\theta' + \frac{3}{2}\tan^2\theta'}{\sec^3\theta'}\right] \qquad (8\text{-}106E)$$

so that, finally,

$$K = \frac{\cos^3\theta'}{\rho}\left(1 + \cot\phi \tan\theta' + \frac{3}{2}\tan^2\theta'\right). \qquad (8\text{-}106F)$$

REFERENCES

1. Phase Work Report IIIB-1, "Genesis of the Problem (Acceleration Hodograph Analysis of Powered Orbital Trajectories)" dated September 30, 1966.

2. F. R. Moulton, Differential Equations, Dover Publications, New York, 1958.

3. D. Laugwitz, Differential and Riemannian Geometry, translated by F. Steinhardt, Academic Press, New York, 1965.

4. D. J. Struik, Differential Geometry, Addison-Wesley, Reading Massachusetts, 1961.

5. Phase Work Report IIIB-2, "Transformation Functions of the Orbital Hodographs" dated September 30, 1966.

6. Phase Work Report IIIB-3, "The Complex Time Locus of an Orbital Trajectory in Time State Space," dated February 17, 1967.

7. D. Hilbert and S. Cohn-Vossen, Geometry and the Imagination, Translated by P. Nemenyi, Chelsea Publishing Co., New York, 1956, p. 190.

8. S. P. Altman, Orbital Hodograph Analysis, Vol. 3, AAS Science and Technology Series, Western Periodicals, 1965.

9. S. P. Altman, "The Hodographic Theory of Newtonian Mechanics," Recent Developments in Space Flight Mechanics, Vol. 9, AAS Science and Technology Series, 1966, pp. 45-102.

10. Phase Work Report IIIA-1, "Formal Presentation of the Hodographic Equations of Motion," dated January 16, 1967.

11. E. Kasner, "Differential Geometric Aspects of Dynamics", American Mathematical Society Colloguium Series, Vol. 3, 1913.

12. E. T. Whittaker, A Treatise on the Analytical Dynamics of Particles and Rigid Bodies, Cambridge University Press, 1964, pp. 254-261.

13. M. Silver, "The Principle of Least Curvature," informal internal (GE-MSD) communication to S. P. Altman, circa June 1966.